NASA Technical Memorandum 89020

Low-Speed Aerodynamic Characteristics of a Wing-Canard Configuration With Underwing Spanwise Blowing on the Trailing-Edge Flap System

Daniel W. Banks and John W. Paulson, Jr.

JANUARY 1987

NASA

NASA Technical Memorandum 89020

Low-Speed Aerodynamic Characteristics of a Wing-Canard Configuration With Underwing Spanwise Blowing on the Trailing-Edge Flap System

Daniel W. Banks and John W. Paulson, Jr.
Langley Research Center
Hampton, Virginia

National Aeronautics
and Space Administration

**Scientific and Technical
Information Branch**

1987

SUMMARY

An investigation of the effects of spanwise blowing applied to the lower surface of a trailing-edge flap system on a wing-canard configuration has been conducted in the Langley 4- by 7-Meter Tunnel. The investigation studied spanwise-blowing angles of 30°, 45°, and 60° measured from a perpendicular to the body centerline. The test conditions covered a range of free-stream dynamic pressures up to 50 psf for thrust coefficients up to 2.1 over a range of angles of attack from -2° to 26°. Model height above the wind tunnel floor was varied from a height-to-span ratio of 1.70 down to 0.20 (a representative wheel touchdown height).

The results from the investigation indicated that blowing angles of 30° and 45° increased the induced-lift increment produced by spanwise blowing on the lower surface of a trailing-edge flap system. Increasing the blowing angle to 60°, in general, produced little further improvement.

INTRODUCTION

The runway field length required for current-technology high-performance aircraft is generally limited by the landing ground roll distance rather than take-off distance because the high installed thrust of the aircraft provides for take-off performance far in excess of landing performance. Various methods have been investigated to take advantage of this thrust to reduce landing distance by the use of thrust-induced lift (resulting in lower approach speeds) and by the use of thrust reversing to provide greater deceleration once the aircraft is on the runway. These methods have met with various degrees of success, depending on the effectiveness of the particular concept in producing high lift and the complexity of actually producing and maintaining the physical hardware involved. One promising concept which is successful at generating high induced lift, and which appears to be relatively simple to implement on an operational aircraft, is the use of spanwise blowing on the trailing edge of a flap system (ref. 1). This concept allows all or part of the engine exhaust to be directed in the spanwise direction by use of a secondary nozzle on the side of an engine nacelle. This spanwise flow mixes with and is turned chordwise by the free-stream flow; it is then deflected down by the trailing-edge flap system. The resulting increased downwash generates induced lift in a manner similar to an externally blown flap, but without the complexity of having the engines located under the wing as in, for example, the YC-15 STOL transport concept.

A previous investigation (ref. 1) tested spanwise-blowing angles, measured from a perpendicular to the body centerline, of -30°, 0°, and 30° (i.e., 0° was perpendicular to the body centerline). The data of reference 1 showed that the highest lift increments occurred when the chordwise angle of the secondary flow (that which blows under the flap) was directed rearward parallel to the flap hinge line. At that blowing angle some of the flow was not turned by the flap, and it was therefore proposed that still higher lift increments could be obtained for blowing angles directed even more rearward.

The present investigation was conducted in the Langley 4- by 7-Meter Tunnel with the model of reference 1. The spanwise-blowing nozzles were tested at an angle of 30° (to repeat the data of ref. 1) and at two additional angles of 45° and 60°.

Thrust coefficients up to 2.1 were studied, and the model was tested in the approach and landing configuration both in and out of ground effect. The range of free-stream dynamic pressures was 0 to 50 psf.

SYMBOLS

All data have been reduced to coefficient form and are presented in the stability-axis system. Symbols in parentheses are used on the computer-generated figures.

b	(B)	wing span, ft
C_A		axial-force coefficient, $F_A/q_\infty S$
$C_{A,T}$		static-thrust axial-force coefficient, $[(F_{A,S}/p_a)p_\infty]/q_\infty S$
$C_{A,TR}$		thrust-removed axial-force coefficient, $C_A - C_{A,T}$
C_D	(CD)	drag coefficient, $C_A \cos \alpha + C_N \sin \alpha$
$C_{D,TR}$	(CDTR)	thrust-removed drag coefficient, $C_{A,TR} \cos \alpha + C_{N,TR} \sin \alpha$
C_L	(CL)	lift coefficient, $C_N \cos \alpha - C_A \sin \alpha$
$C_{L,TR}$	(CLTR)	thrust-removed lift coefficient, $C_{N,TR} \cos \alpha - C_{A,TR} \sin \alpha$
C_m	(CM)	pitching-moment coefficient, $M_Y/q_\infty S\bar{c}$
$C_{m,T}$		static-thrust pitching-moment coefficient, $[(M_{Y,S}/p_a)p_\infty]/q_\infty S\bar{c}$
$C_{m,TR}$	(CMTR)	thrust-removed pitching-moment coefficient, $C_m - C_{m,T}$
C_N		normal-force coefficient, $F_N/q_\infty S$
$C_{N,T}$		static-thrust normal-force coefficient, $[(F_{N,S}/p_a)p_\infty]/q_\infty S$
$C_{N,TR}$		thrust-removed normal-force coefficient, $C_N - C_{N,T}$
C_μ	(CT)	ideal thrust coefficient for total configuration, $\dot{m}V_j/q_\infty S$
$\bar{c}$		wing mean aerodynamic chord, ft
F_A		axial force, $F_{A,B} - F_{A,PT} - F_{A,FT}$, lbf
F_N		normal force, $F_{N,B} - F_{N,PT} - F_{N,FT}$, lbf
h	(H)	height above tunnel floor, ft
L/D		lift-drag ratio, C_L/C_D
M_Y		pitching moment, $M_{Y,B} - M_{Y,PT} - M_{Y,FT}$, ft-lbf
$\dot{m}$		measured nozzle mass-flow rate, slugs/sec

p_a	ambient barometric pressure, lbf/ft^2
p_∞	free-stream static pressure, lbf/ft^2
q_∞	free-stream dynamic pressure, lbf/ft^2
S	wing surface area, ft^2
V_j	ideal jet velocity, ft/sec
α	angle of attack, deg
δ_f	inboard/outboard-flap deflection $\delta_{f,in}/\delta_{f,out}$, positive for trailing edge down, deg (e.g., 45°/26° signifies an inboard-flap deflection of 45° and an outboard-flap deflection of 26°)
Λ_C	cascade vector (spanwise-blowing) angle, positive for outer edge aft, deg (0° is perpendicular to the body centerline)

Subscripts:

B	balance measurement
FT	flowing tare
in	inboard
out	outboard
PT	pressure tare
S	static data

Abbreviations:

F.S.	fuselage station, in.
W.L.	waterline, in.

MODEL DESCRIPTION

The tests were conducted on the wing-canard model of reference 1 equipped with new secondary cascade (spanwise-blowing) nozzles. The cascade nozzles are shown in figure 1 and were designed to be similar to the "alternate" nozzles of reference 1, but with cascade vector angles of 30°, 45°, and 60°. The cascade nozzles protruded slightly from the nacelle side, as shown in figure 1(b). The main exhaust nozzle was a two-dimensional design vectored 45° down and was used throughout the test. The ratio of the cascade-nozzle area to the main-exhaust-nozzle area was 0.60. Since the flow was assumed to be choked, the flow split according to the area. High-pressure air used to simulate jet flow was routed into the model through the sting support system. The trailing-edge flap system was comprised of independent inboard and outboard sections. The flap deflections δ_f are denoted as the inboard deflection over

the outboard deflection (i.e., $\delta_{f,in}/\delta_{f,out}$). Complete details of the model are available in reference 1.

TEST CONDITIONS

The investigation was conducted in the Langley 4- by 7-Meter Tunnel. The tunnel was utilized in the closed-test-section mode. The free-stream dynamic pressure was varied from 0 (static) to 50 psf. The angle-of-attack range was from -2° to 26°. Sideslip angle was held constant at 0°. Thrust coefficient was varied from 0 to 2.1. For ground-effect studies the ratio of model height to wing span h/b was varied from tunnel centerline (h/b = 1.70) to a nominal wheel touchdown height (h/b = 0.20).

To be able to distinguish between the direct-thrust effects and the thrust-induced effects, a static ($q_\infty = 0$) thrust calibration was performed prior to the wind-on ($q_\infty > 0$) tests. The calibration was conducted as was done in reference 1.

PRESENTATION OF RESULTS

The results of the investigation are presented in three sections, corresponding to the grouping of the data obtained. Where appropriate, each figure is divided into two parts: part (a) presents the overall configuration aerodynamic characteristics and part (b) presents the thrust-removed aerodynamic characteristics (ref. 1). The data obtained in this investigation are grouped as follows:

	Figures
The longitudinal aerodynamic characteristics at various angles of attack for four selected thrust coefficients (C_μ = 0, 0.19, 0.60, and 1.07)	2 to 25
The longitudinal aerodynamic characteristics at various thrust coefficients for three selected angles of attack (α = 8°, 12°, and 16°)	26 to 43
The longitudinal aerodynamic characteristics at various nondimensional heights above the floor (h/b) at the approach angle of attack (α = 14°) to determine ground-induced changes	44 to 67

For each group of figures, data are presented for the configuration with each of the three spanwise-blowing angles (30°, 45°, and 60°) and with each of the three combinations of flap deflection angle (26°/26°, 45°/26°, and 45°/45°).

DISCUSSION OF RESULTS

Effect of Angle of Attack on Longitudinal Aerodynamic Characteristics

The longitudinal aerodynamic characteristics as a function of angle of attack are presented in figures 2 to 25. The power-off data of figure 2 show no effects attributable to the cascade vector angle; this result was expected since the cascade vector angle had only a small effect on the external geometry. The changes in power-off longitudinal characteristics due to flap deflection (shown in fig. 14) were indicative of trailing-edge separation for $\delta_f > 26°/26°$. Trailing-edge separation is

characterized by lift losses (or negligible increases) accompanied by nose-up pitching-moment changes as flap deflection angle (or angle of attack) is increased.

With $\Lambda_C = 30°$ and $C_\mu = 0.19$ (fig. 3), the longitudinal characteristics increased compared with the power-off configuration (i.e., lift increased, pitching moment became more nose down, and drag shifted toward the negative). When Λ_C was increased from 30° to 45°, the lift increased and nose-down pitching-moment increases occurred for the configuration with $\delta_f = 26°/26°$. No additional benefit was realized by increasing the angle from $\Lambda_C = 45°$ to 60°. As was the case for most of these configurations, some of the force and moment changes were due to direct thrust, whereas the remainder are considered to have been induced by the secondary flow. The thrust-removed data ($C_{D,TR}$, $C_{L,TR}$, and $C_{m,TR}$) show a slight decrease in lift and pitching moment relative to the thrust-included data. Since the level of the thrust-removed data is slightly less than the thrust-included data and still greater than the power-off data, it can be deduced that much of the effect is thrust induced. The secondary flow for $\Lambda_C = 60°$ affected a smaller area on the inboard flap and did not result in any additional thrust-induced effects compared with the case for $\Lambda_C = 45°$. The angle $\Lambda_C = 60°$ indicated that the flow would not be likely to affect the outboard flap. There was also a much larger direct-thrust component, as shown by the thrust-removed data being much closer to the power-off data.

Increasing the thrust to $C_\mu = 0.60$ (fig. 4) further increased the lift and nose-down moment; as was the case for $C_\mu = 0.19$, there was an increase in lift when Λ_C was changed from 30° to 45°, but in general little additional benefit obtained by increasing Λ_C from 45° to 60°. The thrust-removed data indicated that the lower blowing angles (30° to 45°) resulted in much more induced lift than did $\Lambda_C = 60°$.

The results for $C_\mu = 1.07$ (fig. 5) were similar to the cases with lower blowing rates, except there were more significant direct-thrust components in the data. This indicates that there was little additional increase in induced effects as thrust was increased from $C_\mu = 0.60$ to 1.07.

Deflecting the inboard flap to 45° and leaving the outboard section at 26° resulted in a small lift loss but increased nose-up pitching moment compared with the 26°/26° flap for the power-off case, indicating trailing-edge flow separation on the flaps (i.e., center of lift shifting forward with lift loss). The longitudinal aerodynamic characteristics for $\delta_f = 45°/26°$ with power applied were similar to those for $\delta_f = 26°/26°$ and in some cases (e.g., fig. 23) had lift losses compared with the 26°/26° case. In most cases for $\delta_f = 45°/26°$, increasing the blowing angle from 45° to 60° had no benefit aerodynamically, and the only clear difference was the increase in the direct-thrust vector. The aerodynamic benefits (i.e., lift increases and drag decreases) of the 45°/26° flap were small compared with the 26°/26° flap case. This was true even when the high-thrust data for the 45°/26° flap (fig. 9) were compared with the low-thrust data for the 26°/26° flap (fig. 3). The more highly deflected flaps created an adverse pressure gradient that could not be maintained, and there was significant flow separation. A flap with gap and overhang such that it would behave more like an externally blown flap configuration would be able to take advantage of higher turning angles by using some of the secondary flow to maintain attached flow on the flap. Deflecting the outboard flap to 45° ($\delta_f = 45°/45°$, fig. 10) actually improved the lift characteristics over those for $\delta_f = 45°/26°$ and came close to the level of lift performance for $\delta_f = 26°/26°$,

although there was much higher drag which resulted in lower L/D. The ineffectiveness of the 45°/26° flap setting appeared to be primarily due to interference in the region of the spanwise segmentation of the inboard and outboard flaps; for δ_f = 45°/26°, that interference caused additional separation and venting of the undersurface of the wing as was shown in reference 1. In all cases, increasing flap deflection resulted in an increase in drag.

Effect of Thrust Coefficient on Longitudinal Aerodynamic Characteristics

The longitudinal aerodynamic characteristics as a function of thrust coefficient are presented in figures 26 to 43. In all cases the addition of thrust and the subsequent increase in thrust coefficient C_μ resulted in an increase in configuration lift, a decrease in overall drag, and an increase in nose-down pitching moment. For thrust coefficients greater than 0.60, the changes in aerodynamic characteristics were primarily due to direct-thrust components resulting from the jet being turned downward by the flap. At the lower thrust coefficients these changes were predominantly due to thrust-induced effects, although at each thrust coefficient both effects were present. It is shown in the thrust-removed data that at lower thrust coefficients the incremental lift increases were predominant and that, in some cases at very high thrust coefficients (C_μ > 0.80), there were actually small incremental lift losses. These results indicate that the lift enhancement potential of this concept is much greater at lower values of thrust, considering the amount of thrust required to obtain a given lift increment.

This spanwise-blowing concept is sensitive to the combination of flap deflection and spanwise-blowing angle as well as to thrust level. As mentioned previously, the largest lift increments were realized at moderate thrust coefficients (C_μ = 0.40) and were predominantly due to thrust-induced effects. This would have been the condition for which the largest area on the flap sections was affected with just enough flow to generate induced lift without significant thrust deflection. Further gains in lift become increasingly costly in terms of thrust, and the aircraft becomes impossible to trim or to control with even the most powerful aerodynamic controls, requiring that some additional control mechanism be provided.

Effect of Model Height on Longitudinal Aerodynamic Characteristics

The longitudinal aerodynamic characteristics as a function of model height are presented in figures 44 to 67. All ground-effect cases were run at a simulated approach angle of attack of 14°. The data show little effect until the model height was less than a semispan above the tunnel floor (i.e., h/b < 0.5). Even below h/b = 0.5 the lift increases because of ground effect were fairly small, the greatest being approximately 0.1 for C_μ = 0 and δ_f = 45°/45°. In some cases (e.g., δ_f = 45°/45°, Λ_C = 60°, and C_μ = 1.07), there were lift losses and drag decreases because of the jet sheet being constrained by the floor resulting in decreased jet deflection angle. Likewise, changes in drag and pitching-moment coefficient because of ground effect were also fairly small.

The data show that most configurations benefitted from ground effect, although the magnitudes were small. The configurations which experienced lift loss in ground effect were those which were operating at high thrust coefficients (C_μ = 1.07), at high blowing angles (Λ_C = 60°), and at large flap deflections (δ_f = 45°/45°).

SUMMARY OF RESULTS

A wind tunnel test has been conducted on the concept of spanwise blowing on the trailing-edge flap system of a wing-canard configuration. This investigation was an extension of earlier work and was conducted to study the effect of increased rearward deflection of the spanwise-blowing jet. The results of the test are summarized as follows:

1. Spanwise-blowing angles (cascade vector angles) of 30° and 45° produced the largest lift increments. For a blowing angle of 60°, the lift increments were, for the most part, small compared with those of the lower angles; in some cases, the lift remained the same or decreased when blowing angle was increased to 60°.

2. The longitudinal aerodynamic characteristics of configurations with spanwise segmented flaps (inboard/outboard deflection of 45°/26°) were generally worse than those of configurations with full-span flaps (deflections of 26°/26° or 45°/45°).

3. In general, those configurations with lower thrust coefficients (<0.60) had much better thrust-induced aerodynamic characteristics, whereas the configurations with higher thrust coefficients (>0.60) were dominated by direct-thrust effects.

4. Most of the configurations tested benefitted from ground effect, although all aerodynamic coefficient increments were reduced with increasing thrust coefficient for configurations in ground effect.

5. Lift benefits were better at moderate thrust coefficients both in and out of ground effect.

NASA Langley Research Center
Hampton, Virginia 23665-5225
November 19, 1986

REFERENCE

1. Paulson, John W., Jr.; Quinto, P. Frank; and Banks, Daniel W.: Investigation of Trailing-Edge-Flap Spanwise-Blowing Concepts on an Advanced Fighter Configuration. NASA TP-2250, 1984.

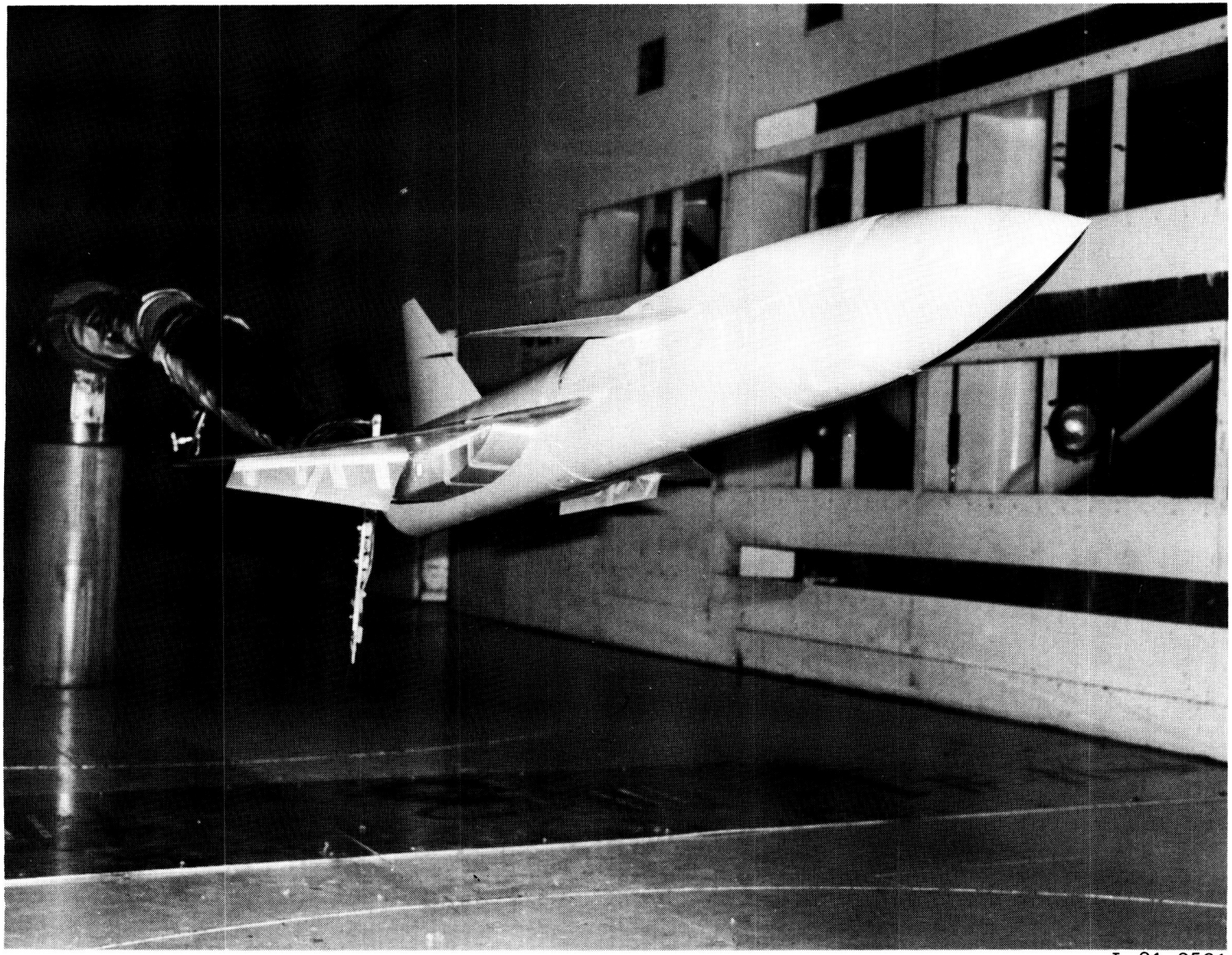

L-81-8581

(a) Model in Langley 4- × 7-Meter Tunnel.

Figure 1.- Modified NASA wing-canard model with underwing spanwise blowing on trailing-edge flap.

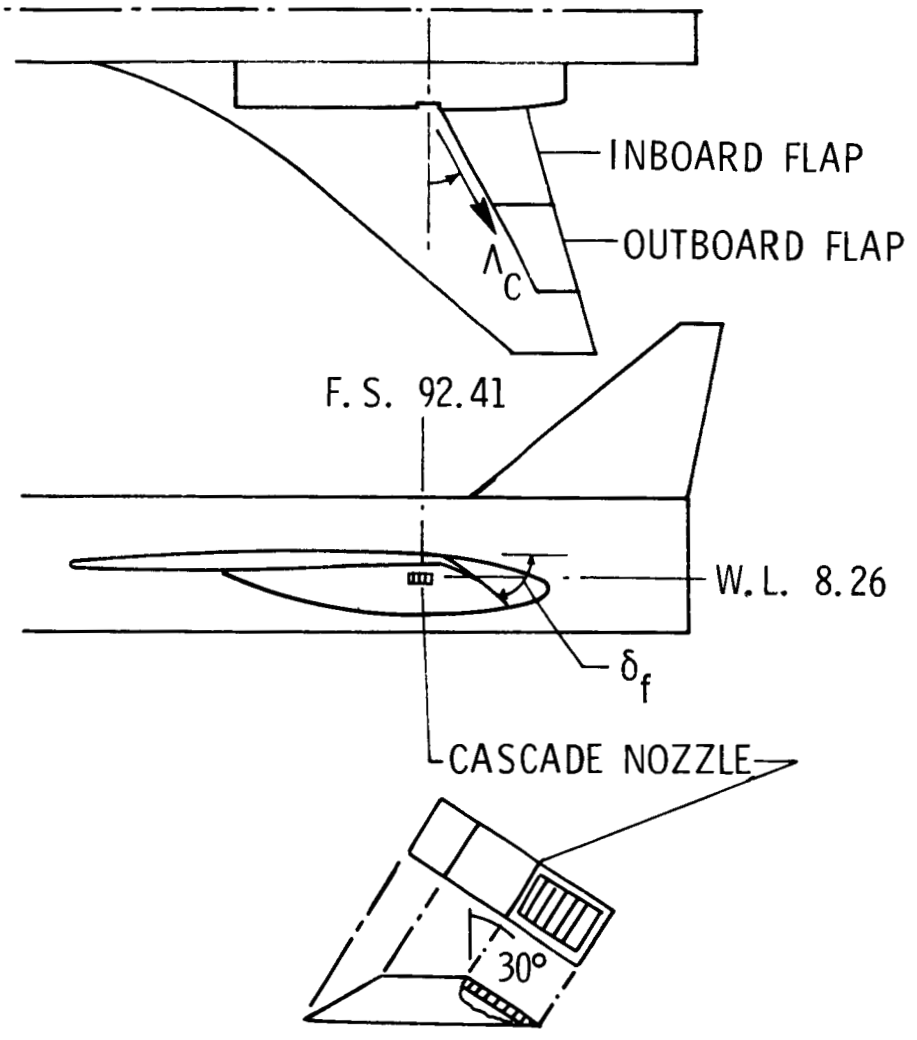

(b) Location of cascades under trailing-edge flap system.

Figure 1.- Continued.

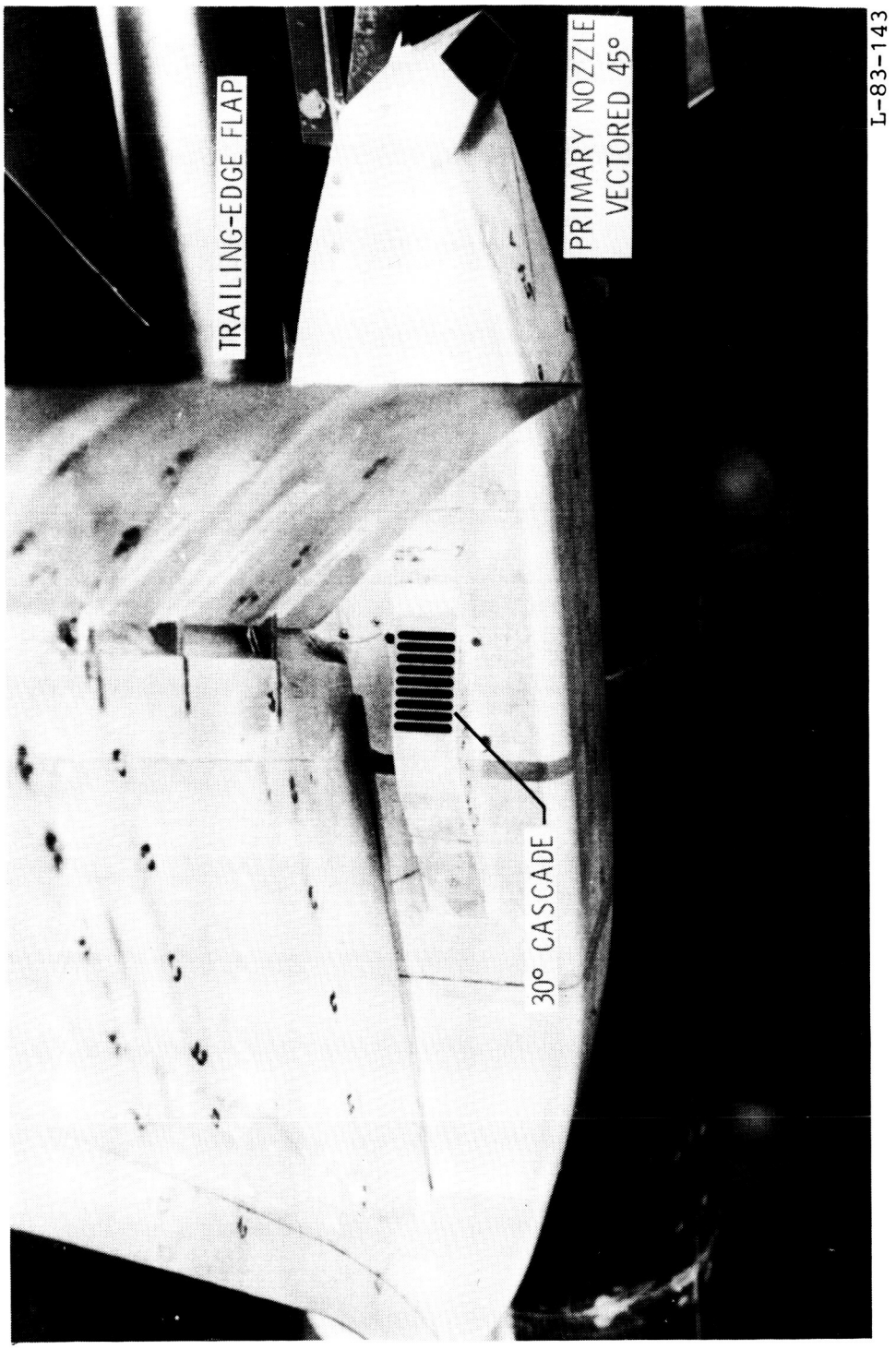

(c) Location of cascade.

Figure 1.- Concluded.

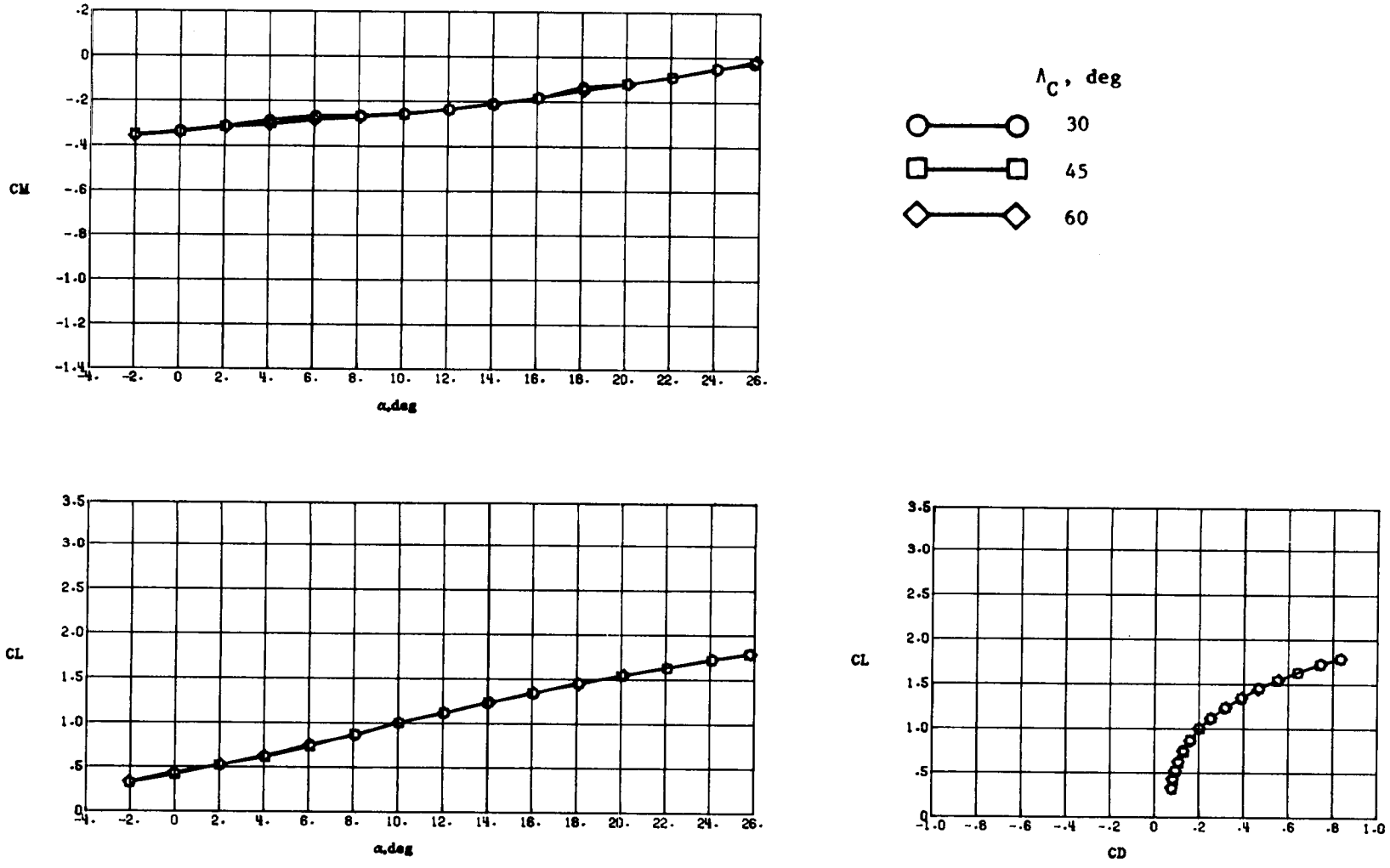

Figure 2.- Effect of cascade vector angle on longitudinal aerodynamic characteristics with $C_\mu = 0$ and $\delta_f = 26°/26°$.

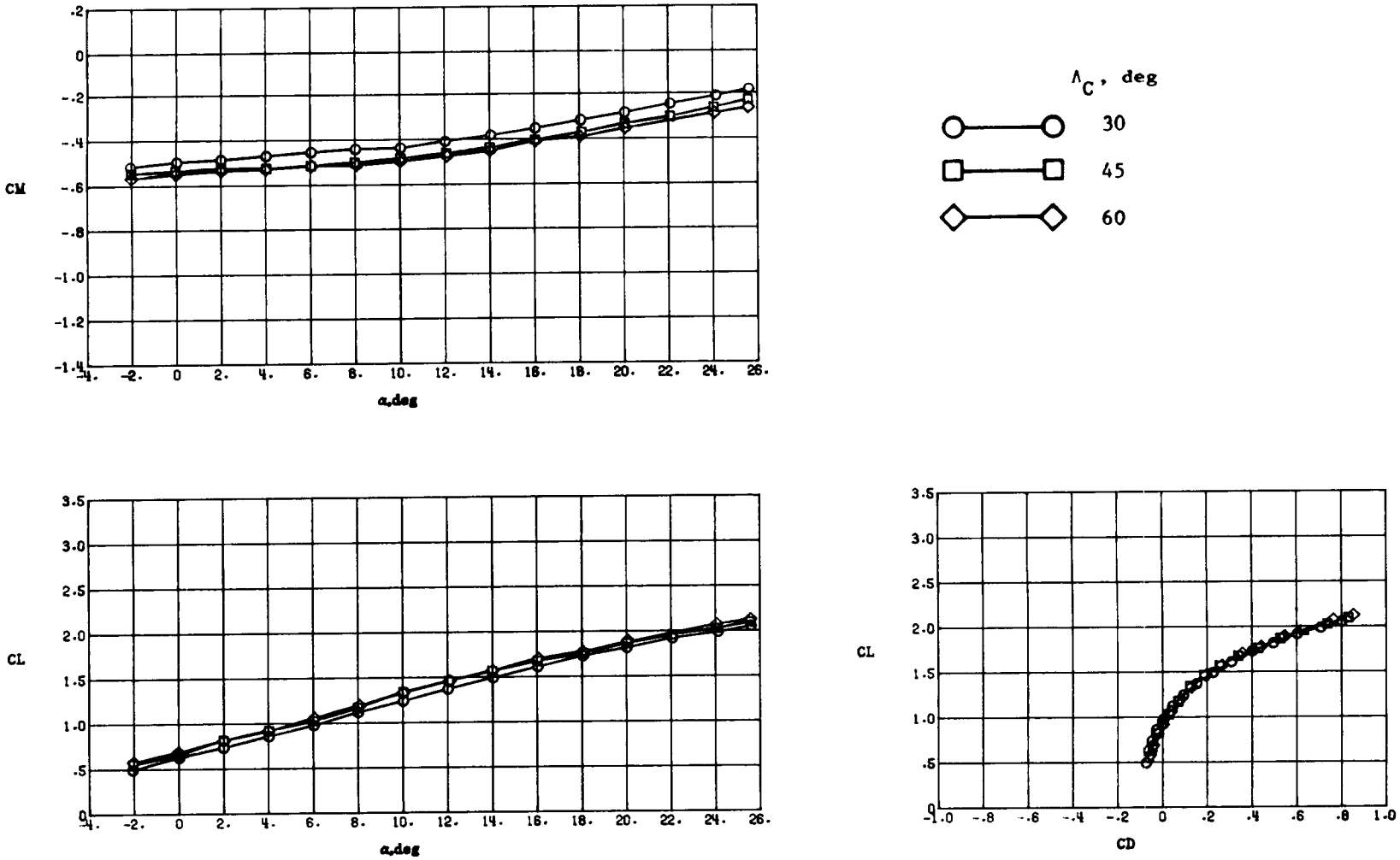

(a) Thrust included.

Figure 3.- Effect of cascade vector angle on longitudinal aerodynamic characteristics with $C_\mu = 0.19$ and $\delta_f = 26°/26°$.

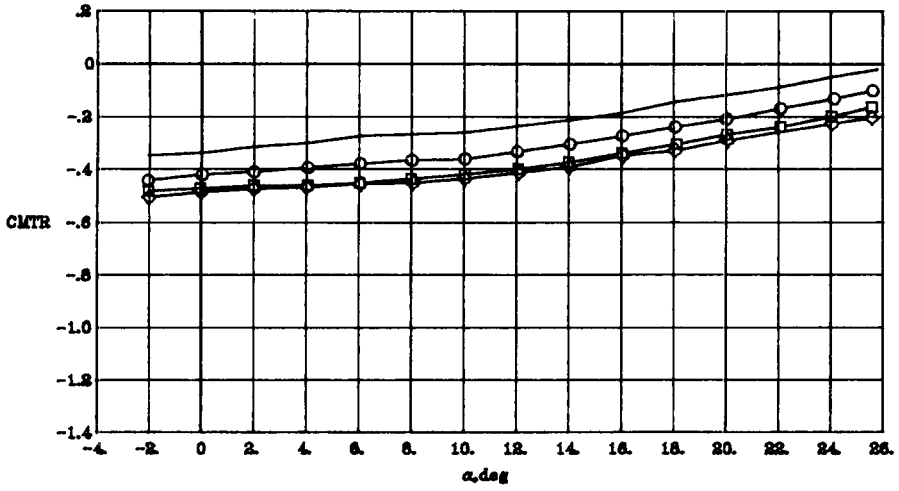

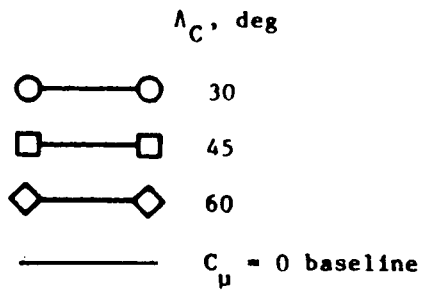

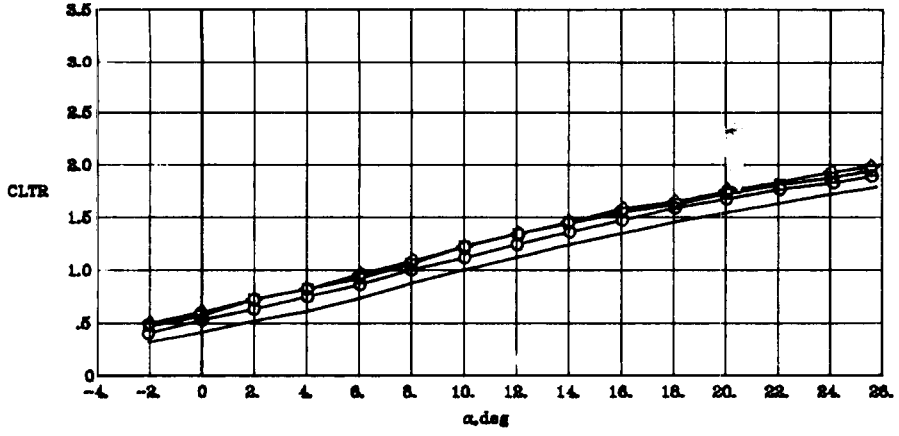

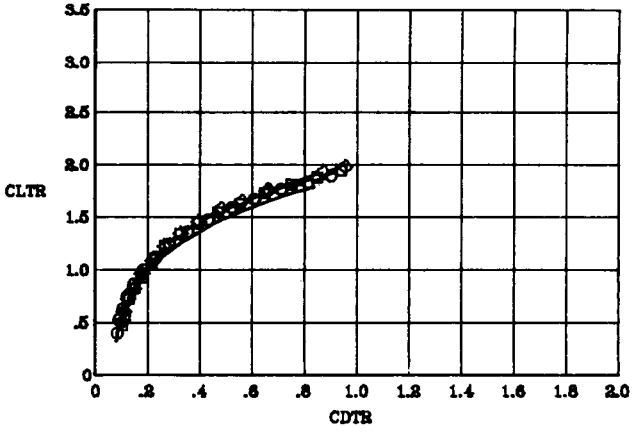

(b) Thrust removed.

Figure 3.- Concluded.

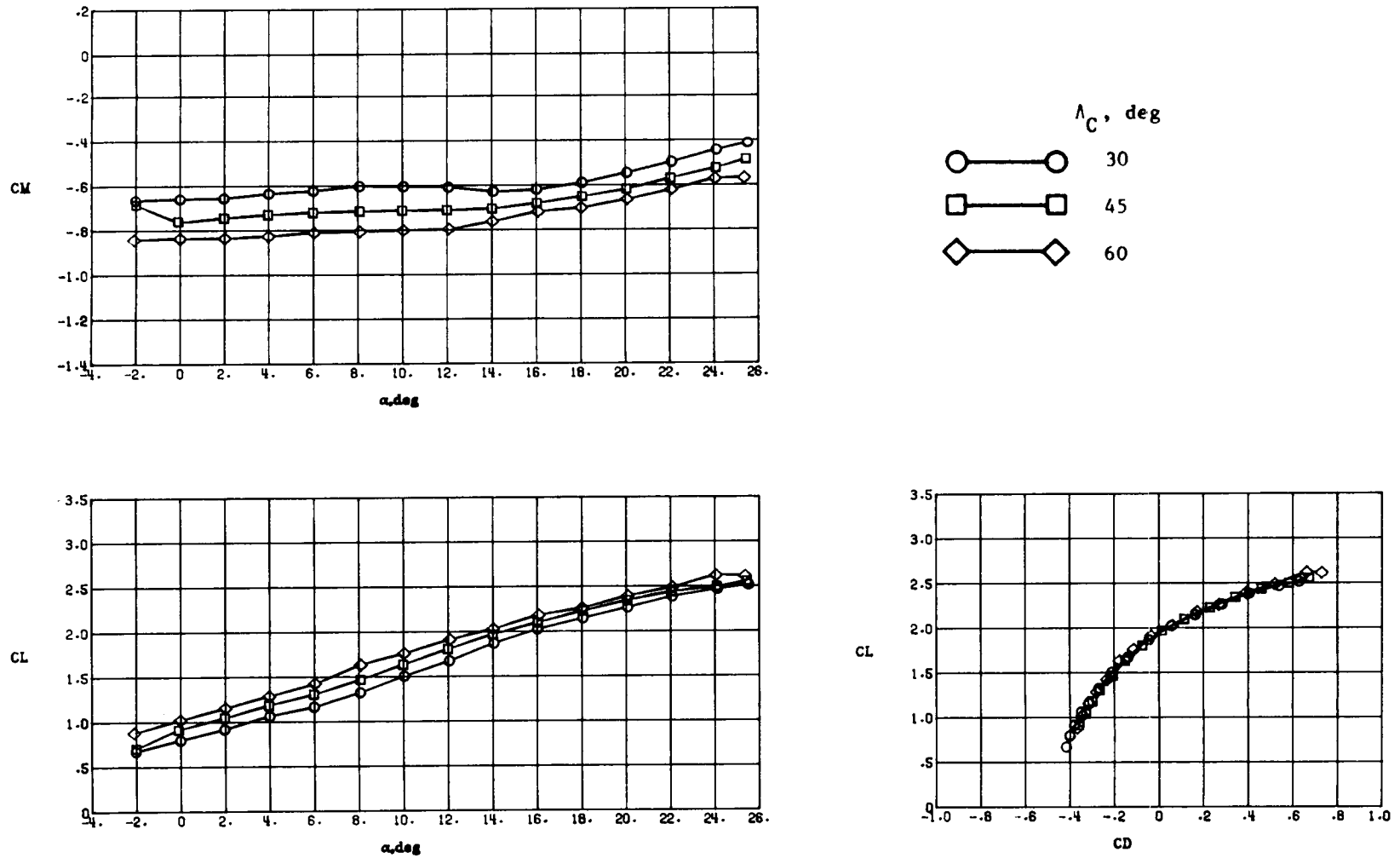

(a) Thrust included.

Figure 4.- Effect of cascade vector angle on longitudinal aerodynamic characteristics with $C_\mu = 0.60$ and $\delta_f = 26°/26°$.

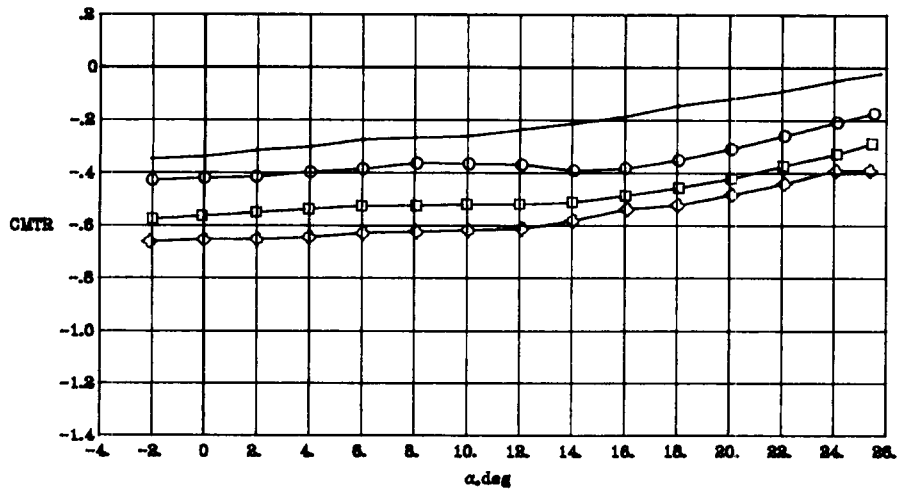

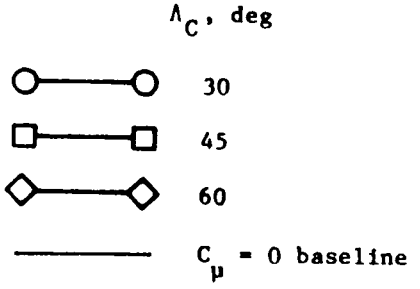

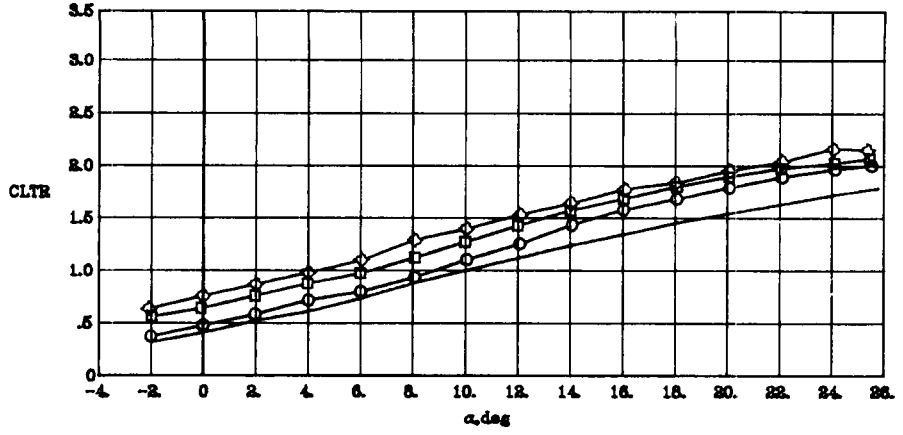

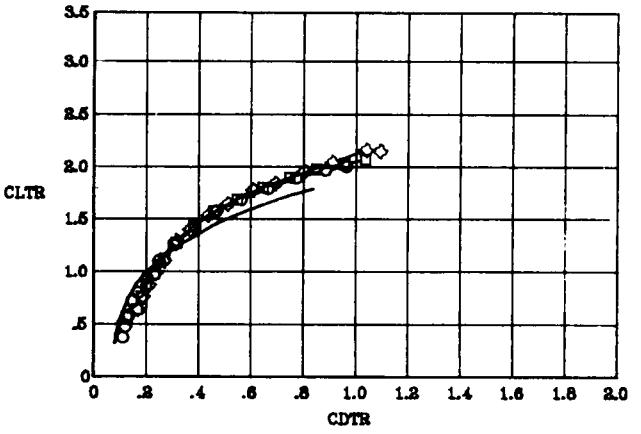

(b) Thrust removed.

Figure 4.- Concluded.

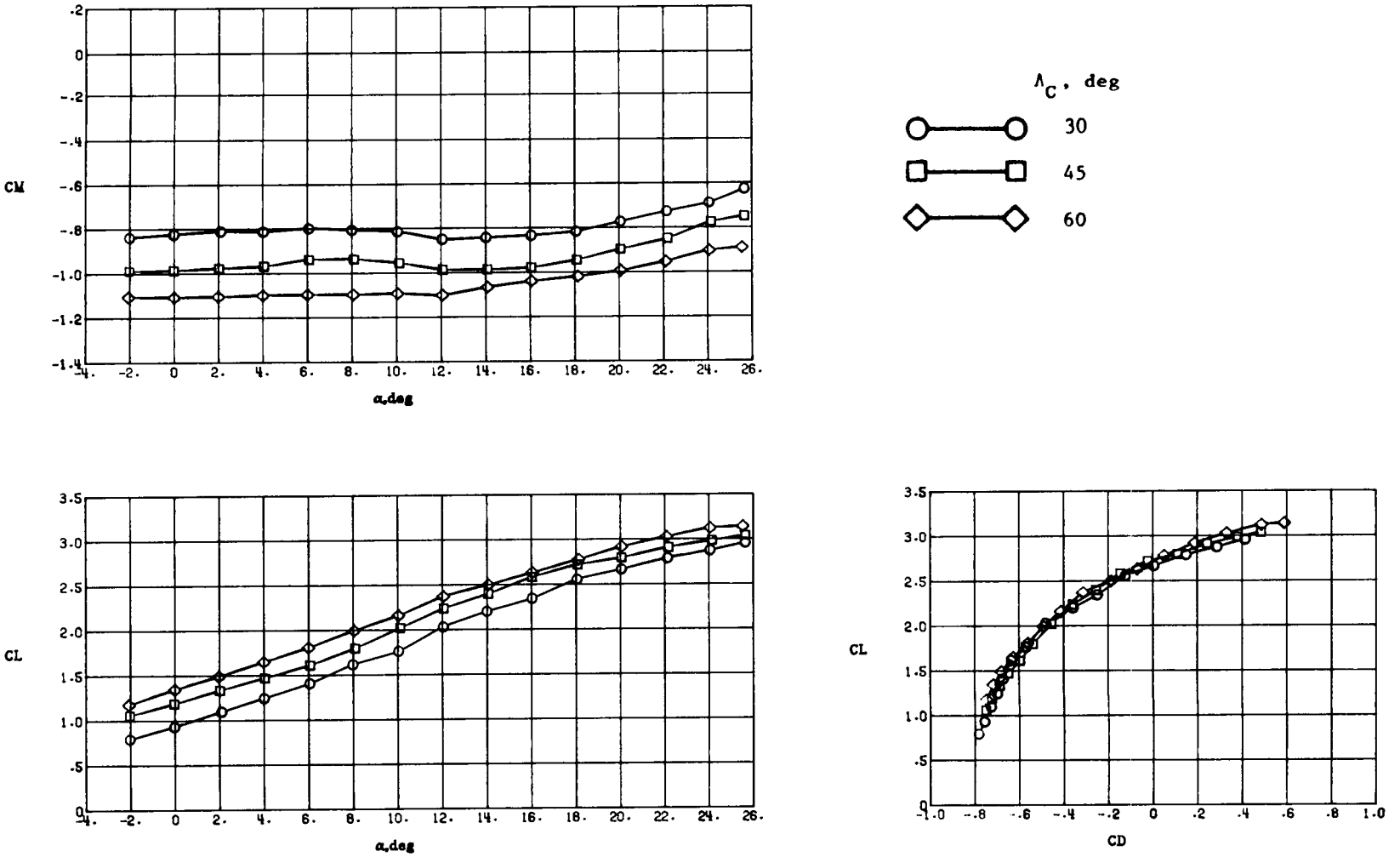

(a) Thrust included.

Figure 5.- Effect of cascade vector angle on longitudinal aerodynamic characteristics with $C_\mu = 1.07$ and $\delta_f = 26°/26°$.

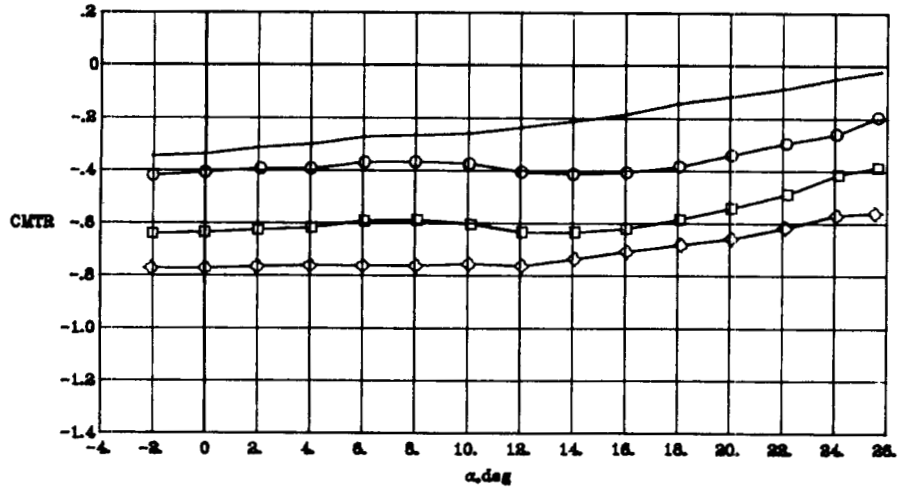

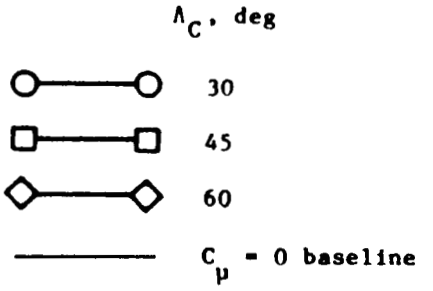

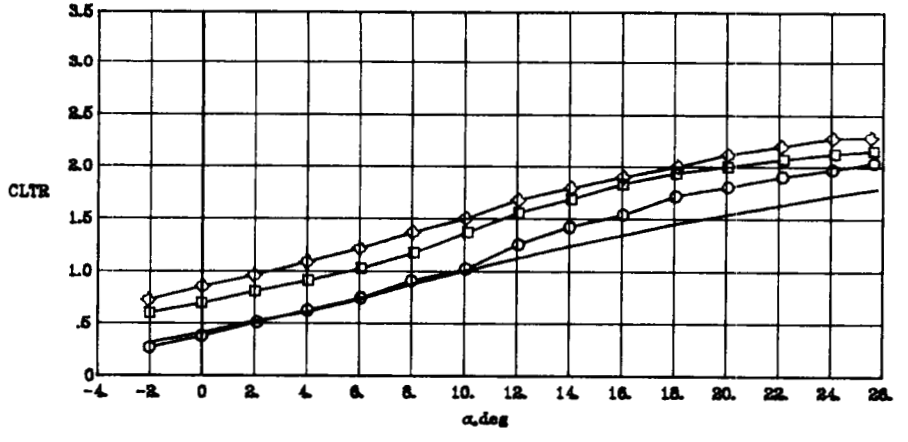

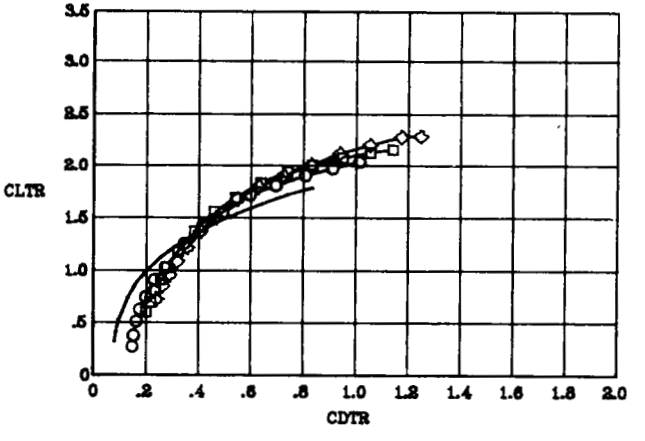

(b) Thrust removed.

Figure 5.- Concluded.

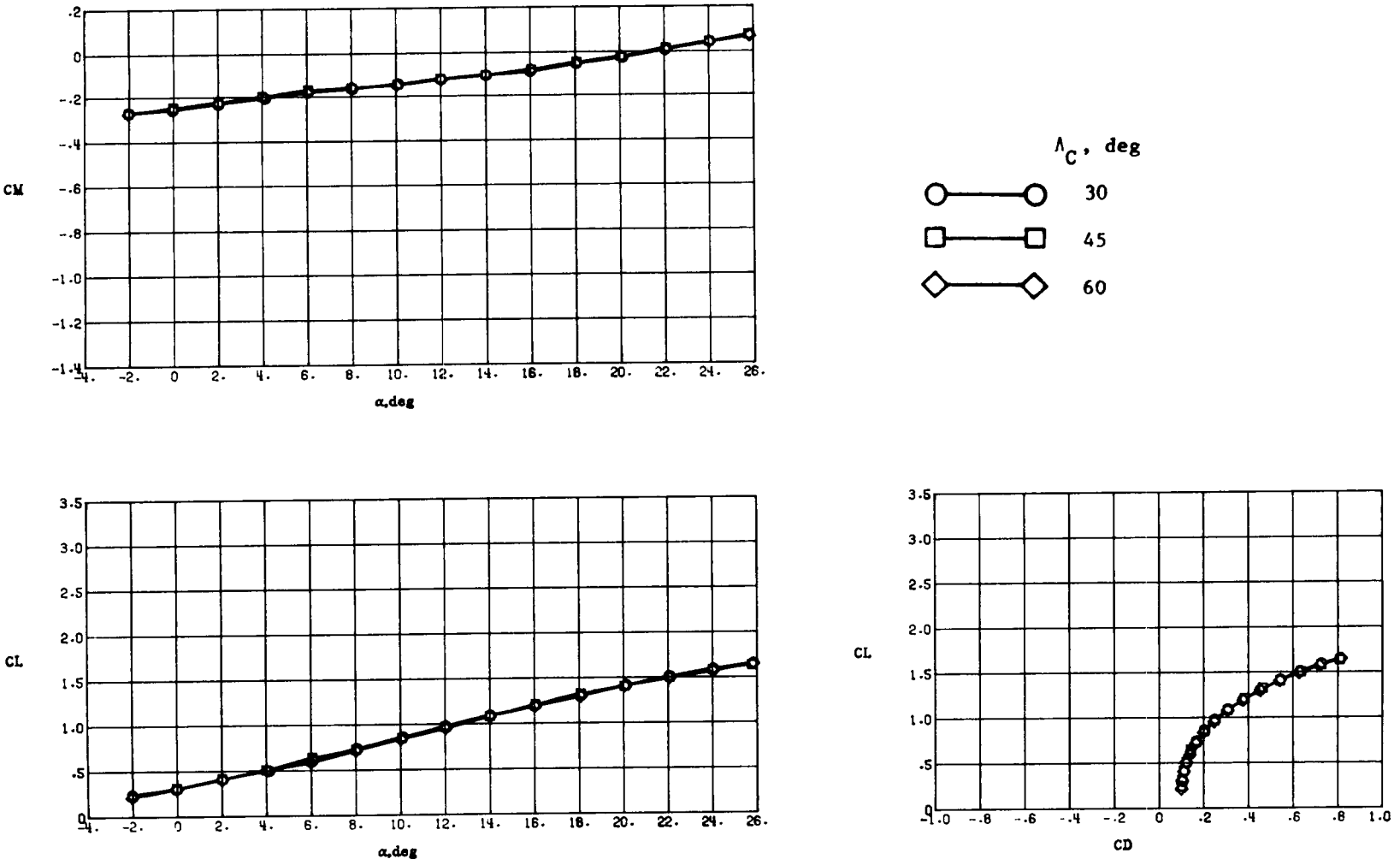

Figure 6.- Effect of cascade vector angle on longitudinal aerodynamic characteristics with $C_\mu = 0$ and $\delta_f = 45°/26°$.

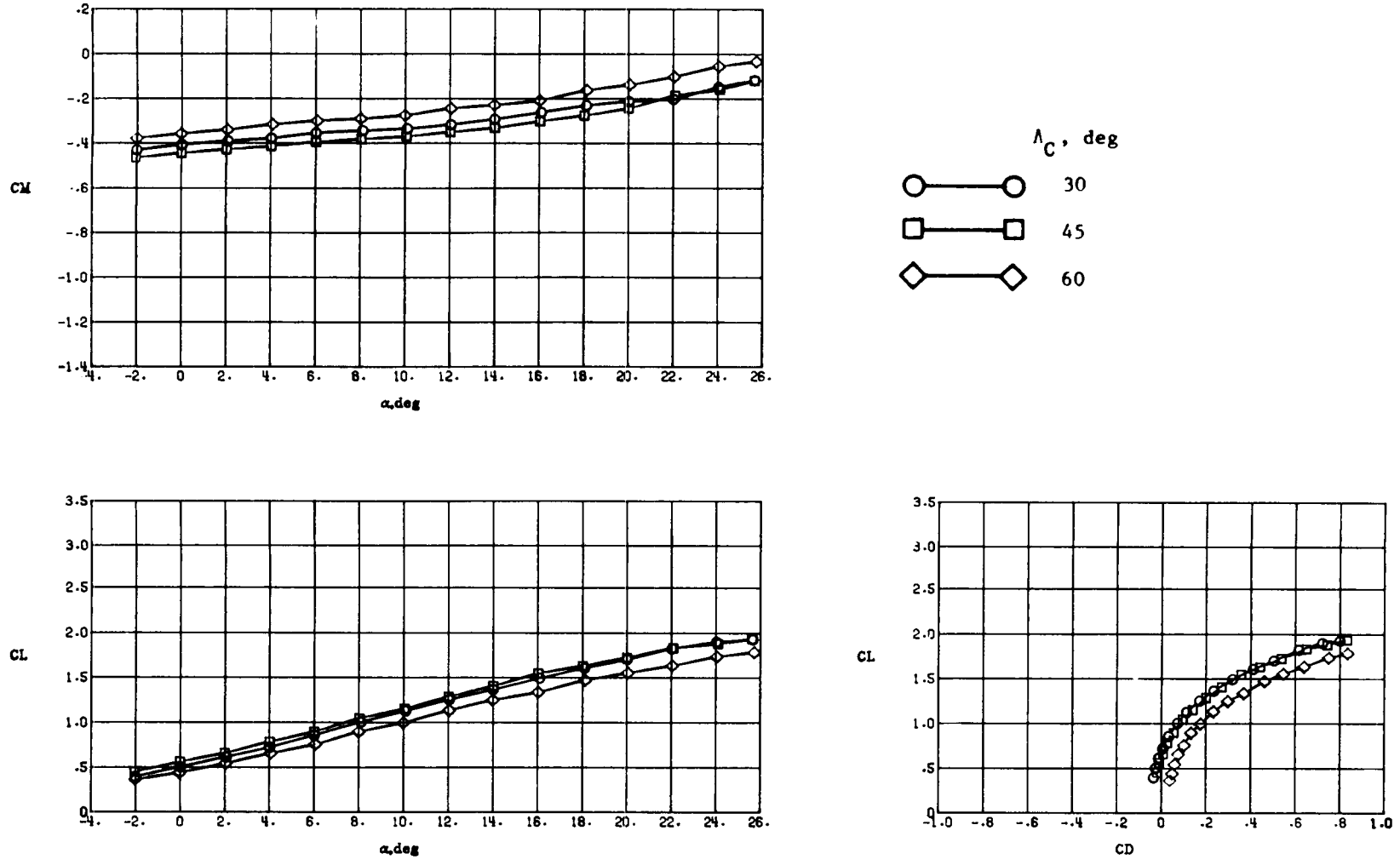

(a) Thrust included.

Figure 7.- Effect of cascade vector angle on longitudinal aerodynamic characteristics with $C_\mu = 0.19$ and $\delta_f = 45°/26°$.

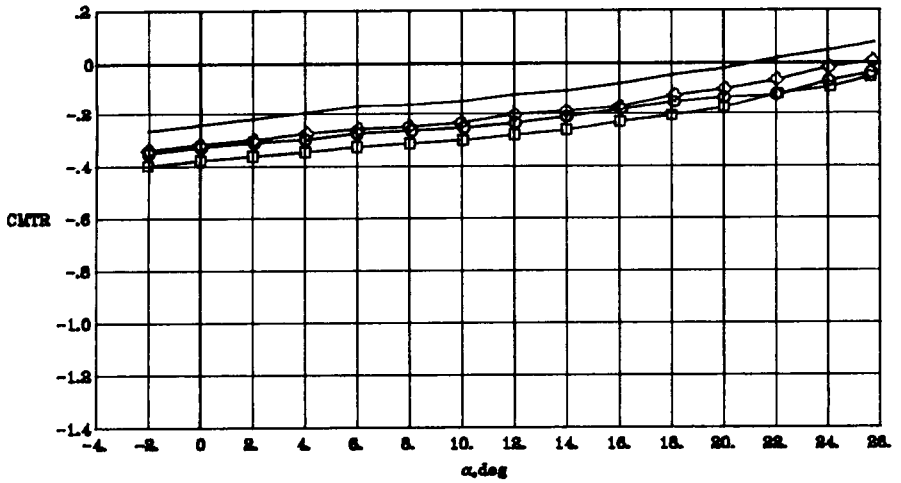

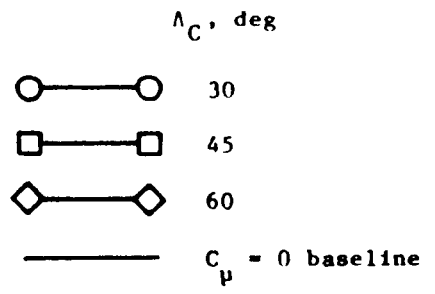

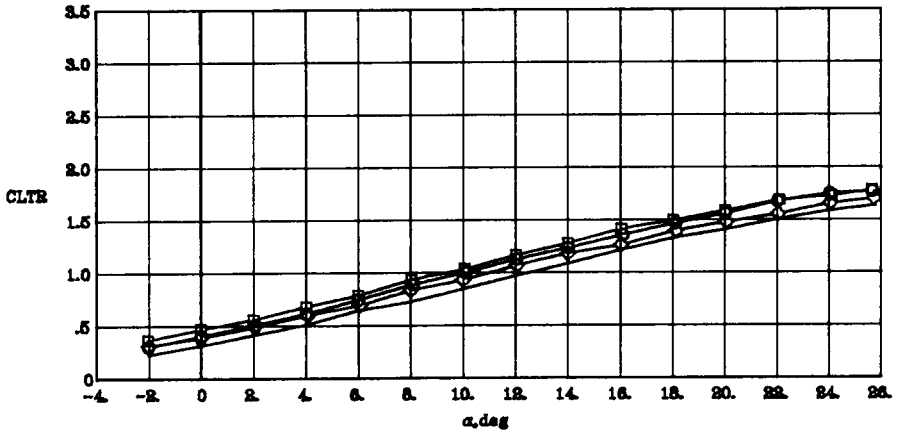

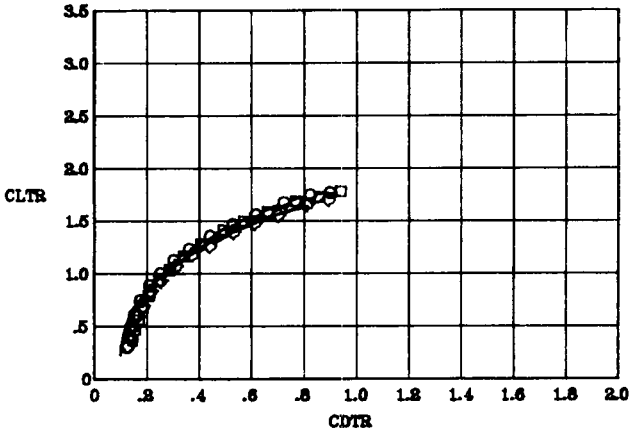

(b) Thrust removed.

Figure 7.- Concluded.

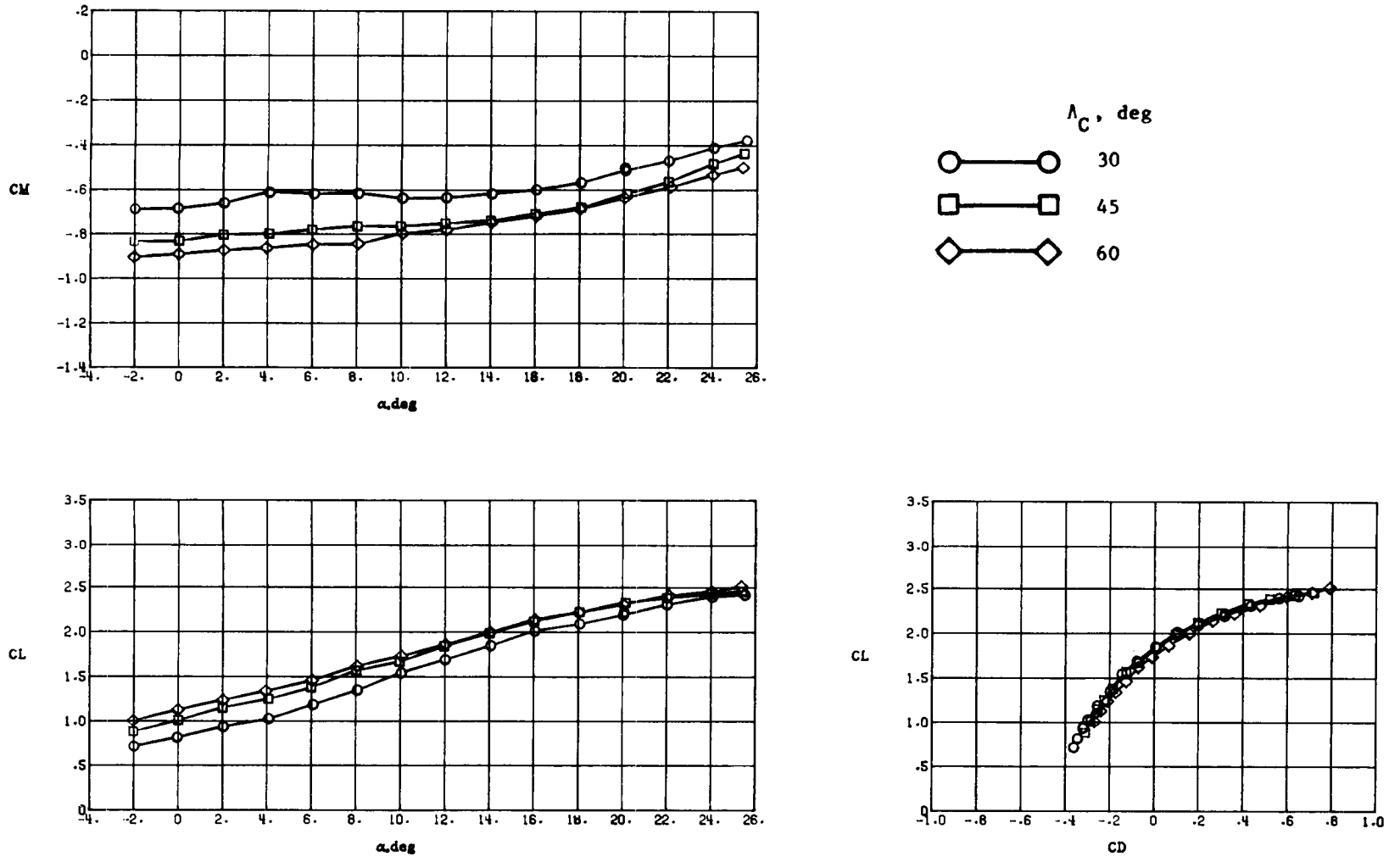

(a) Thrust included.

Figure 8.- Effect of cascade vector angle on longitudinal aerodynamic characteristics with $C_\mu = 0.60$ and $\delta_f = 45°/26°$.

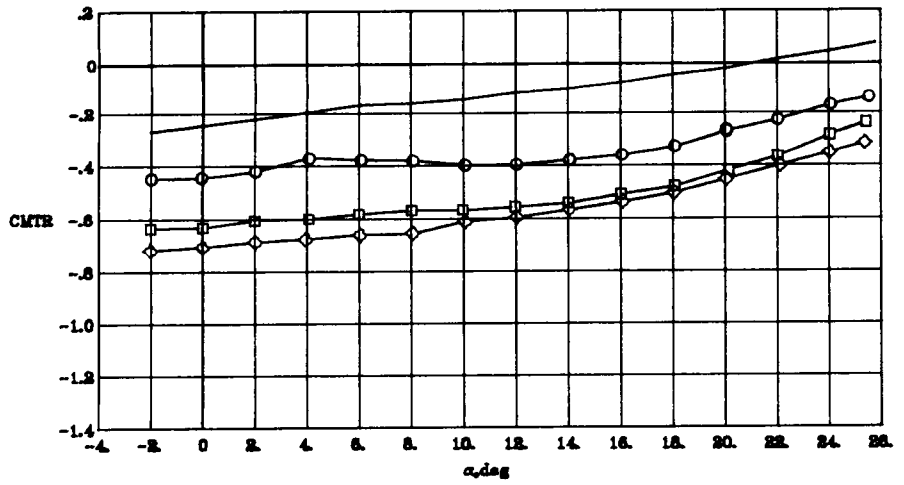

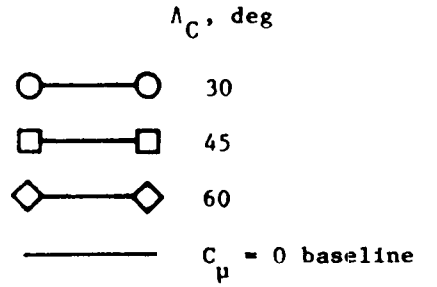

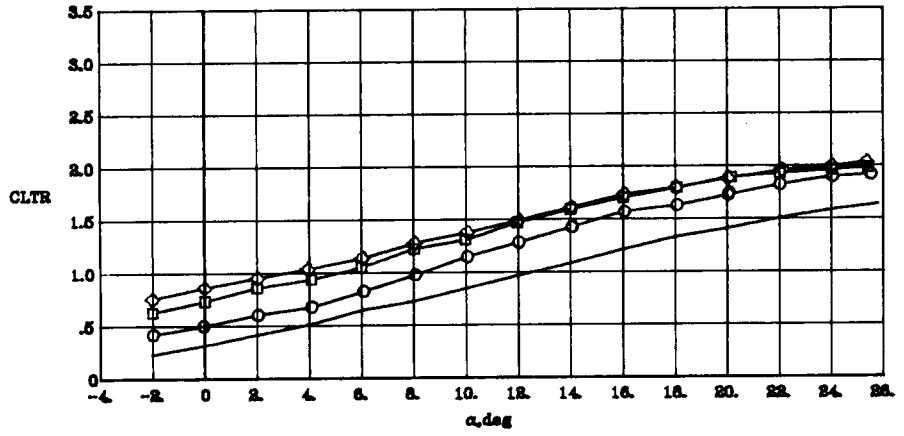

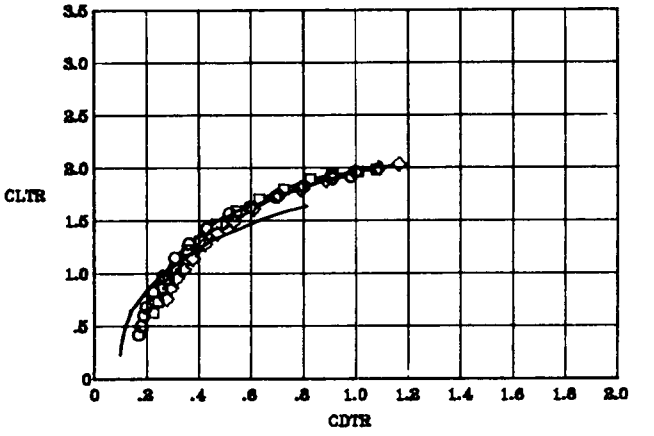

(b) Thrust removed.

Figure 8.- Concluded.

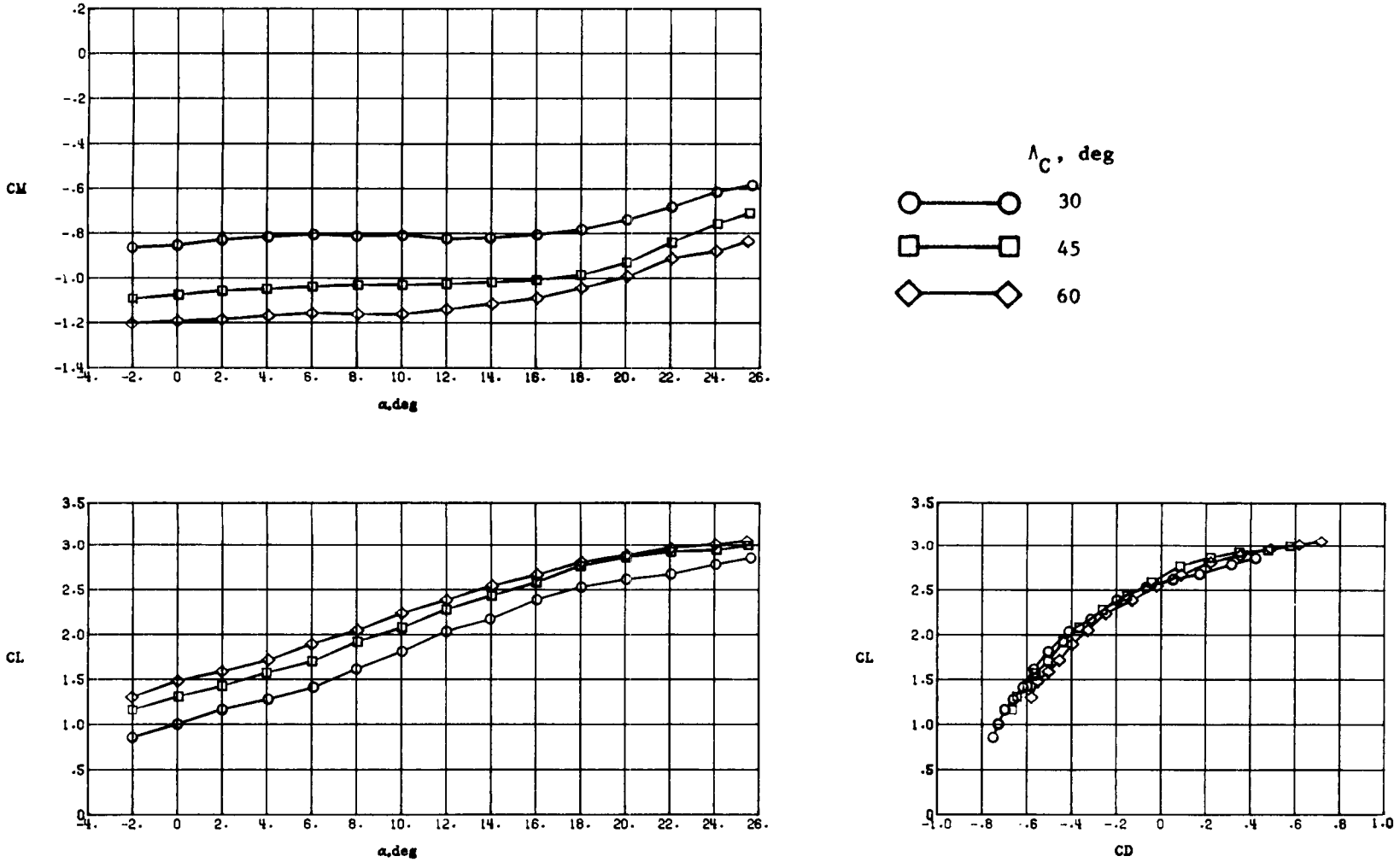

(a) Thrust included.

Figure 9.- Effect of cascade vector angle on longitudinal aerodynamic characteristics with $C_\mu = 1.07$ and $\delta_f = 45°/26°$.

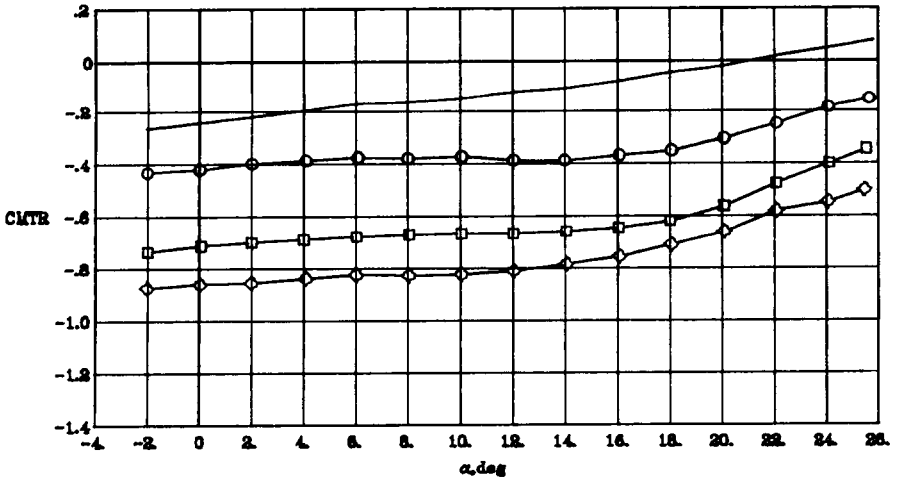

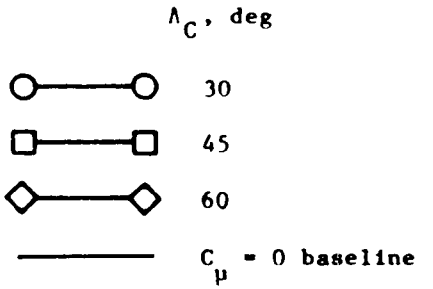

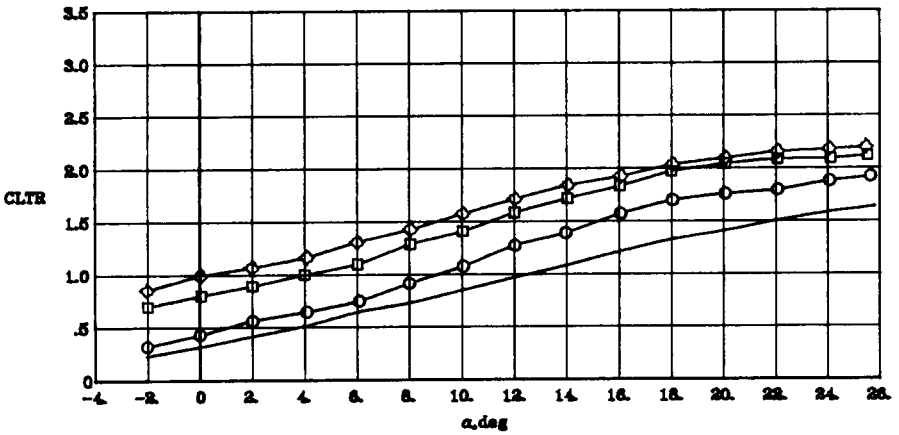

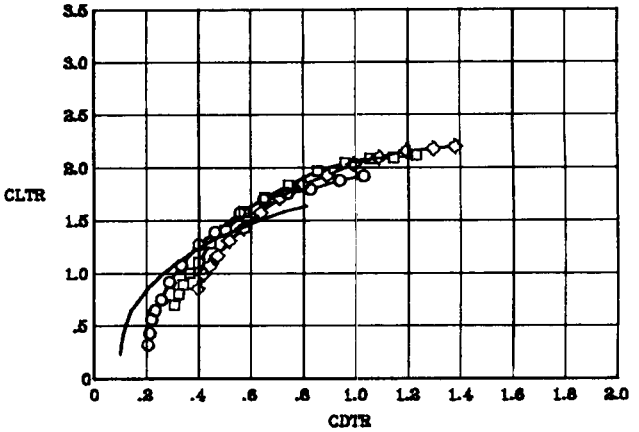

(b) Thrust removed.

Figure 9.- Concluded.

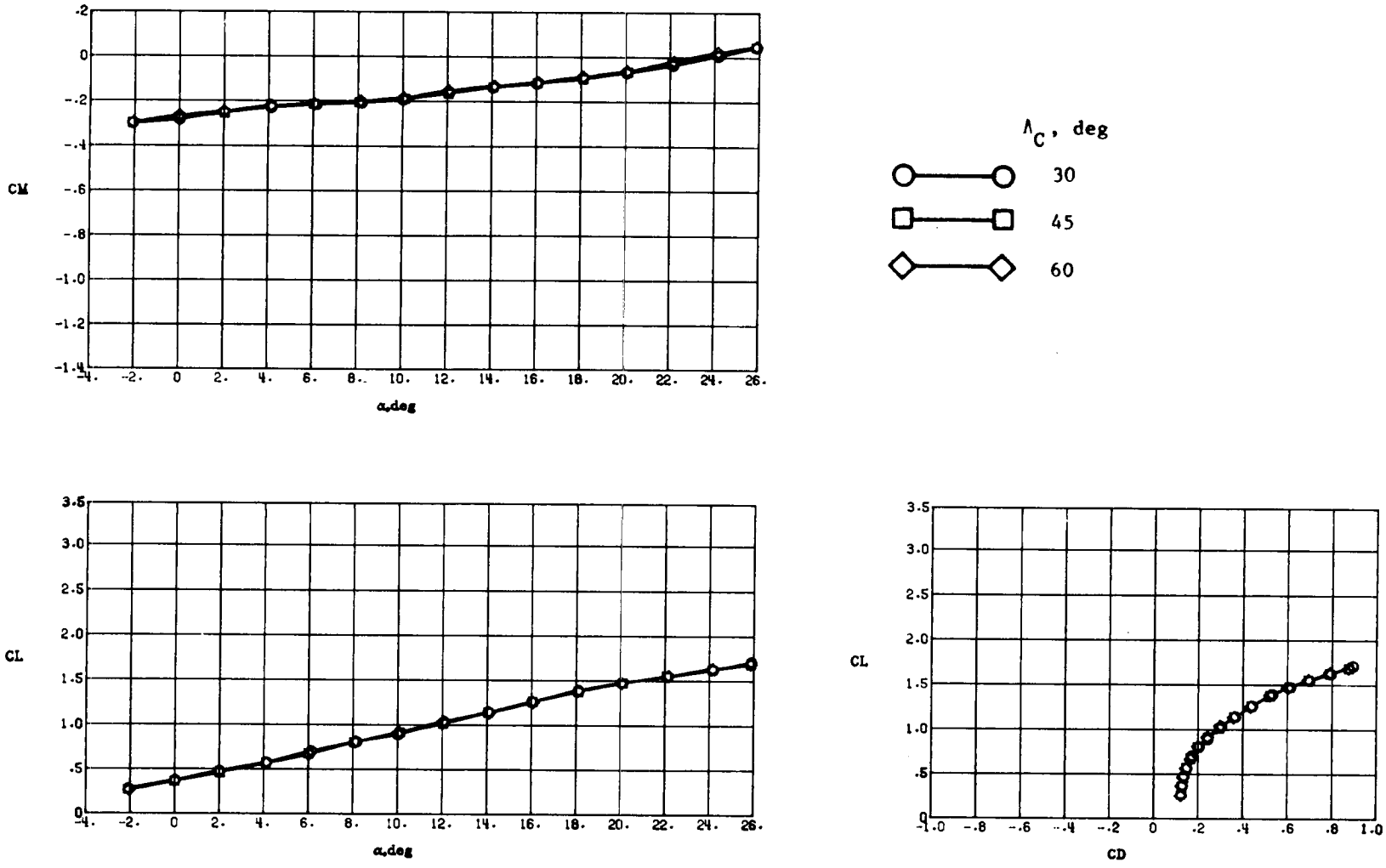

Figure 10.- Effect of cascade vector angle on longitudinal aerodynamic characteristics with $C_\mu = 0$ and $\delta_f = 45°/45°$.

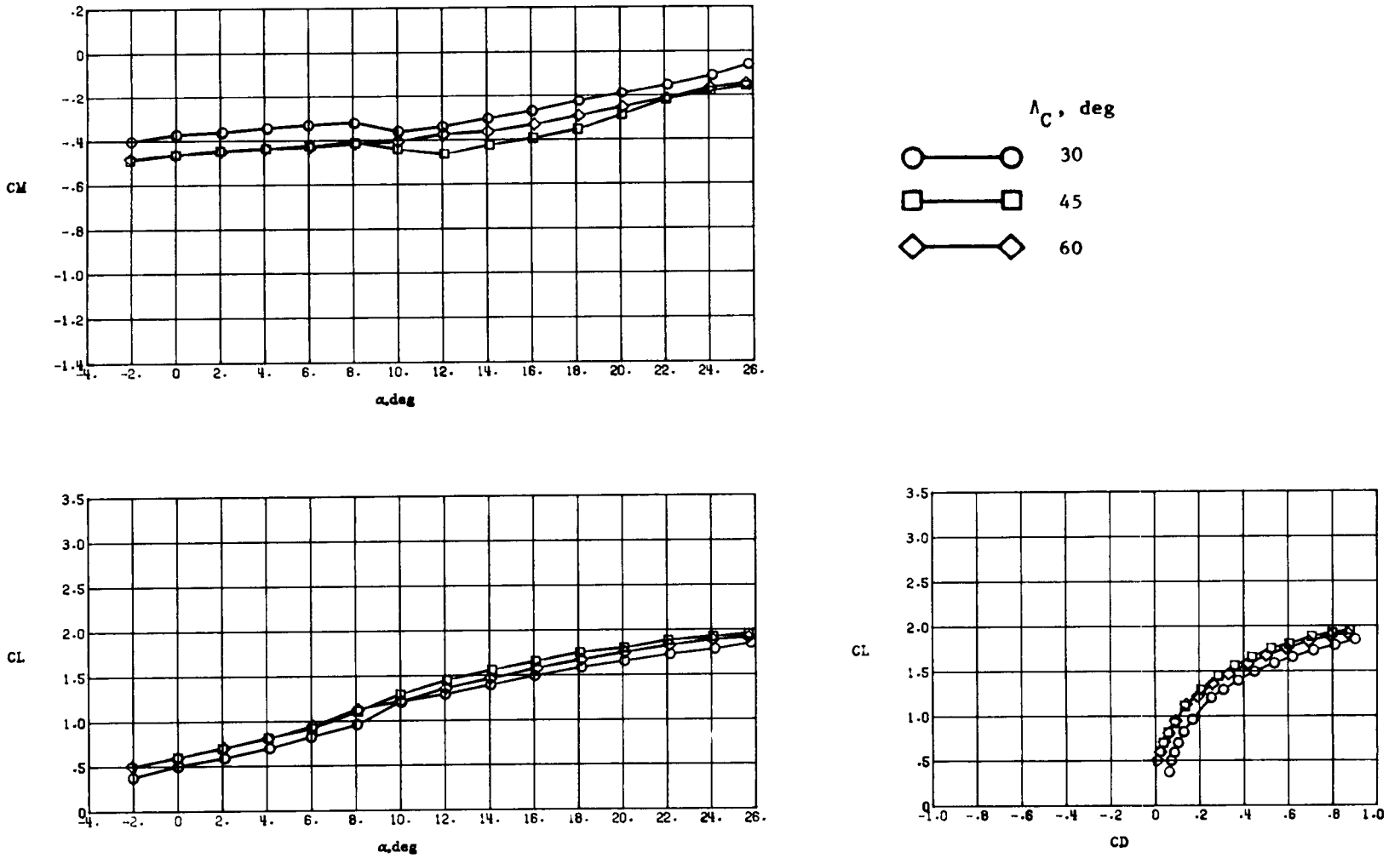

(a) Thrust included.

Figure 11.- Effect of cascade vector angle on longitudinal aerodynamic characteristics with $C_\mu = 0.19$ and $\delta_f = 45°/45°$.

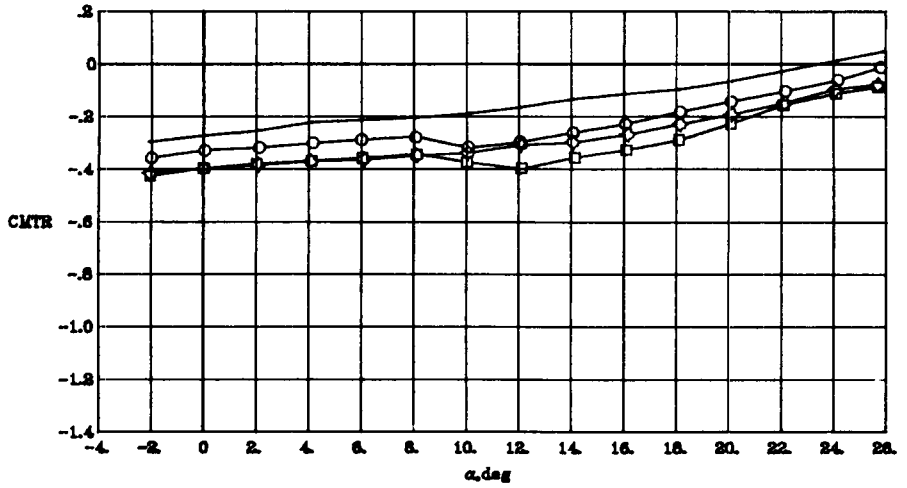

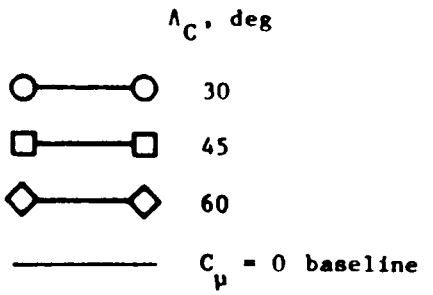

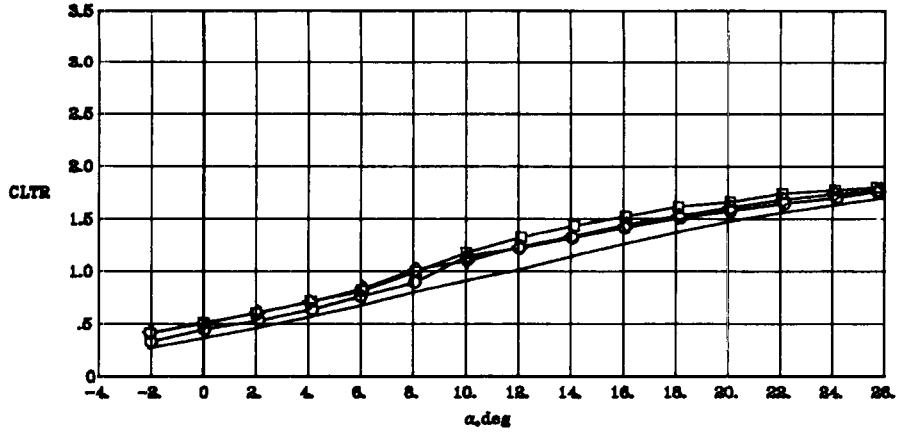

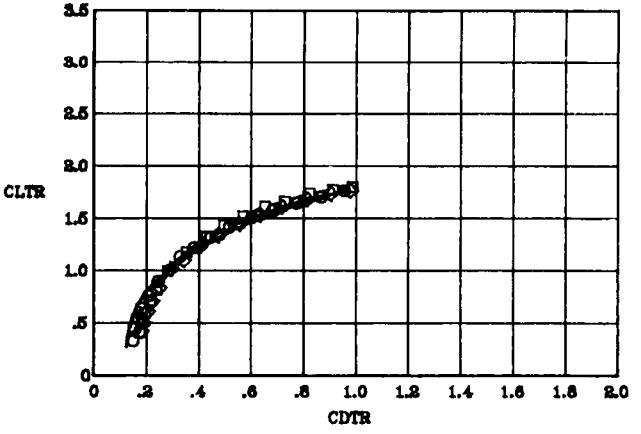

(b) Thrust removed.

Figure 11.- Concluded.

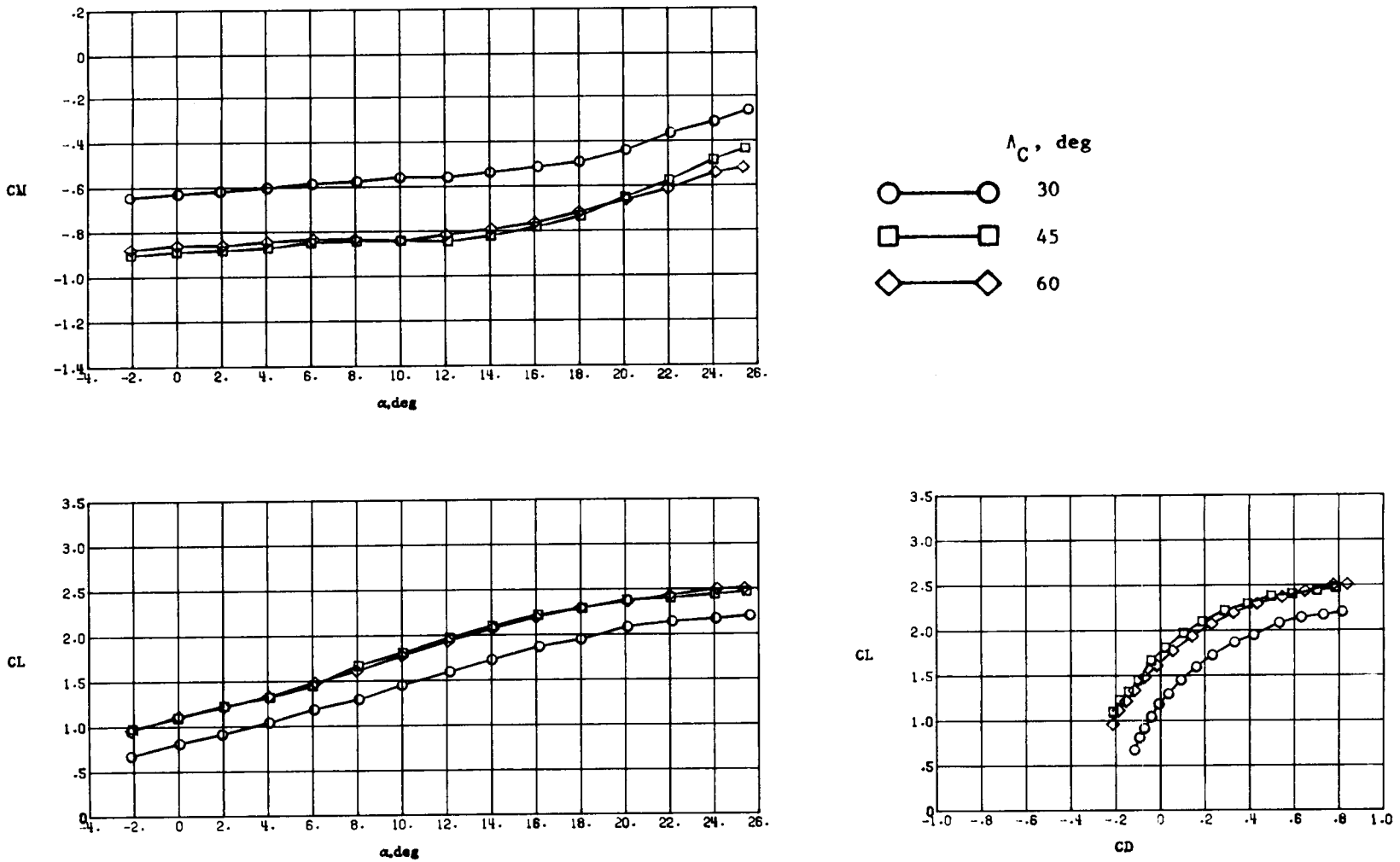

(a) Thrust included.

Figure 12.- Effect of cascade vector angle on longitudinal aerodynamic characteristics with $C_\mu = 0.60$ and $\delta_f = 45°/45°$.

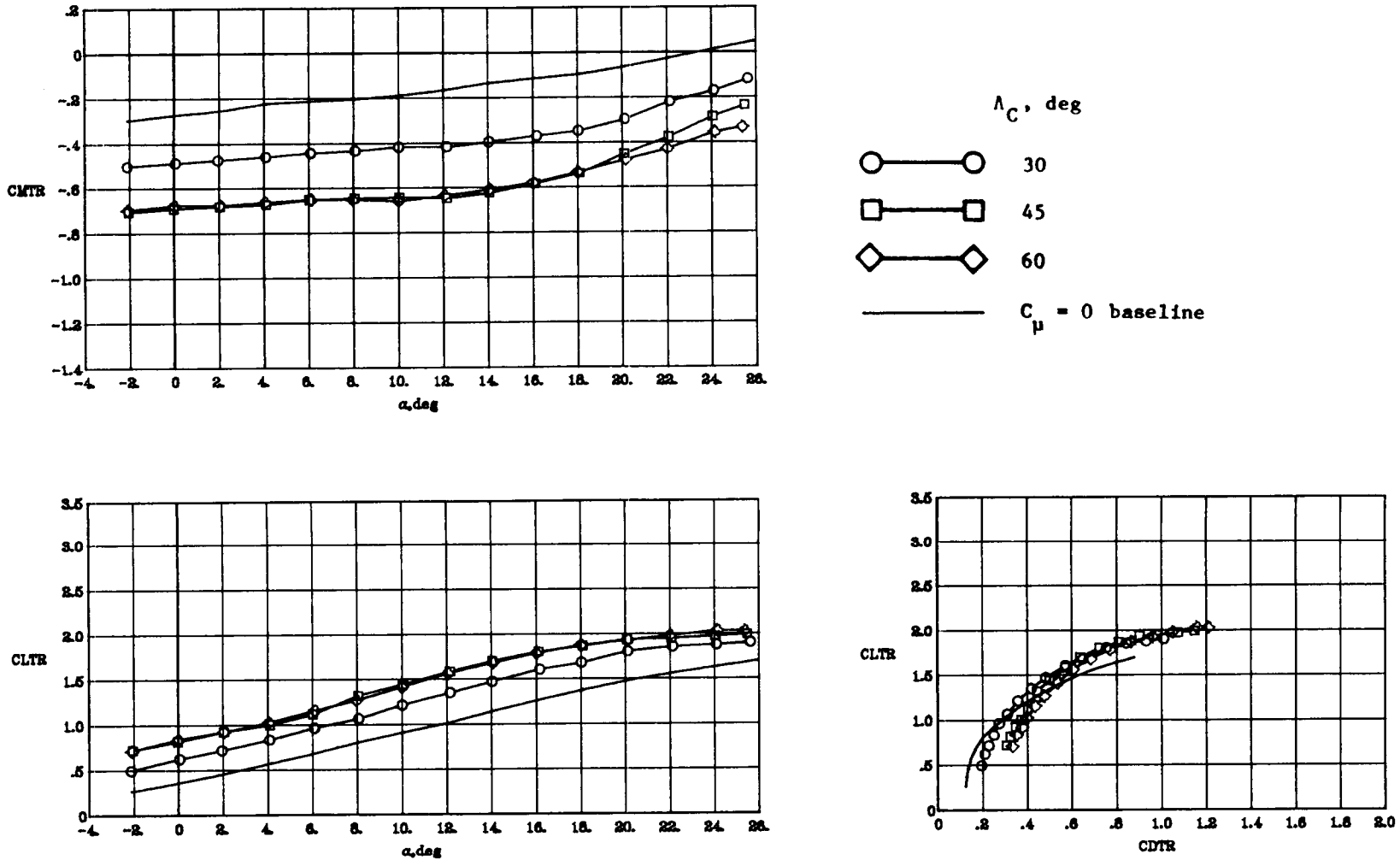

(b) Thrust removed.

Figure 12.- Concluded.

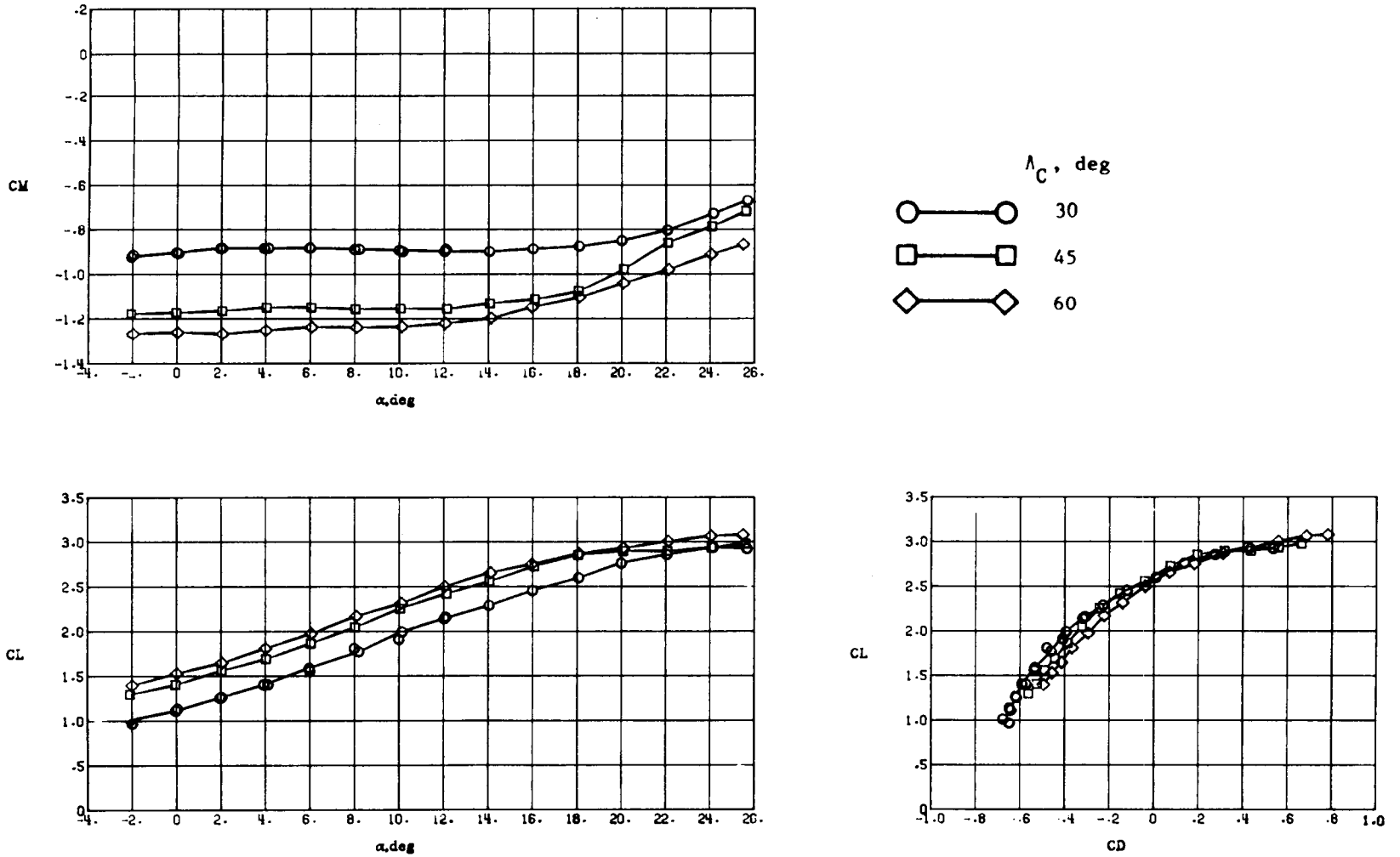

(a) Thrust included.

Figure 13.- Effect of cascade vector angle on longitudinal aerodynamic characteristics with $C_\mu = 1.07$ and $\delta_f = 45°/45°$.

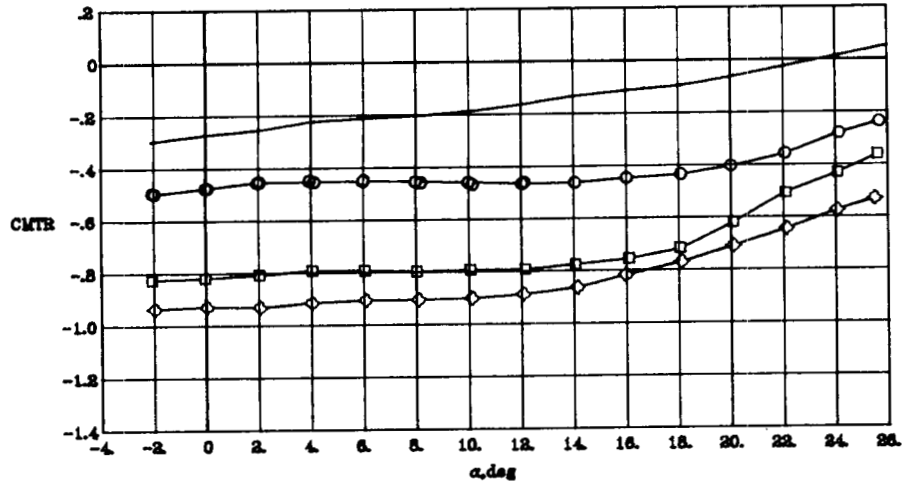

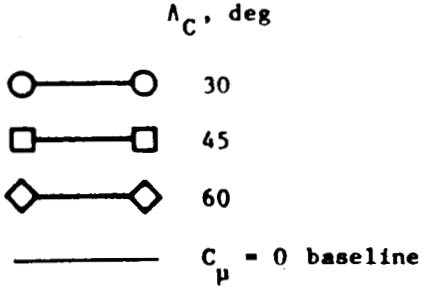

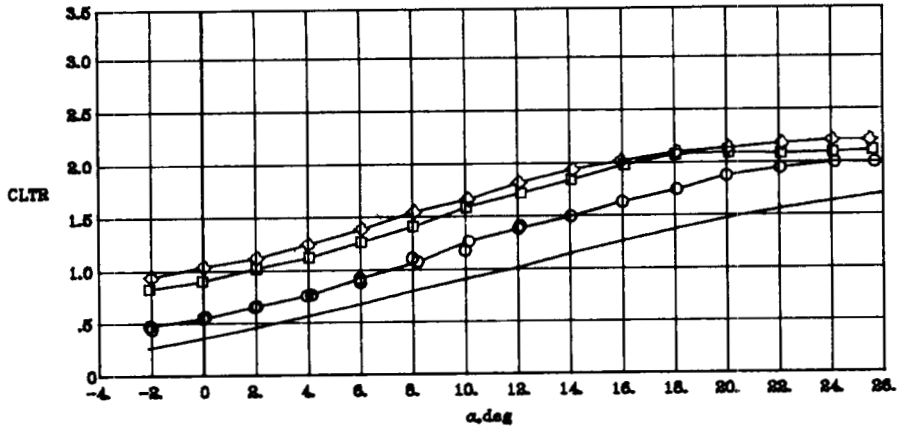

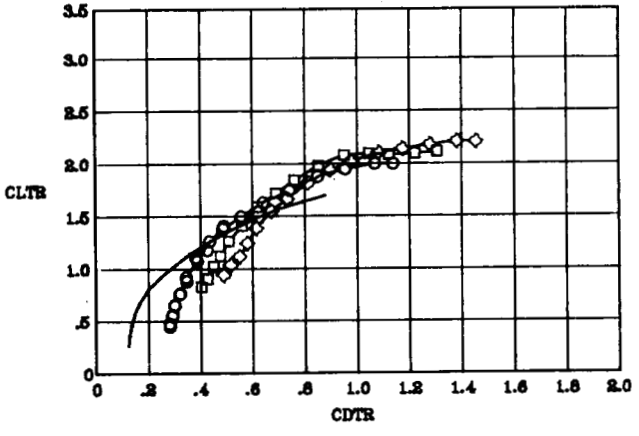

(b) Thrust removed.

Figure 13.- Concluded.

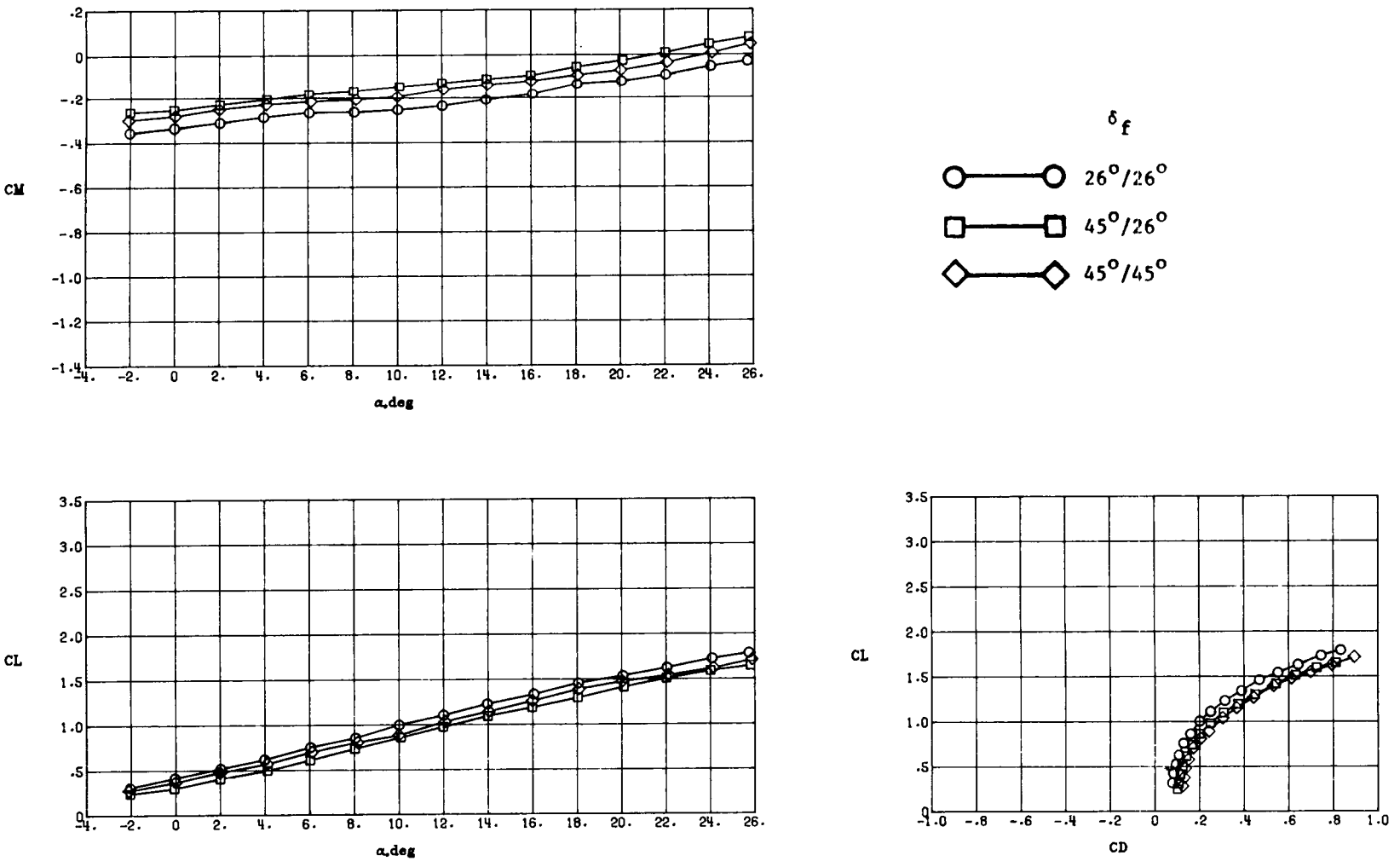

Figure 14.- Effect of flap deflection angle on longitudinal aerodynamic characteristics with $C_\mu = 0$ and $\Lambda_C = 30°$.

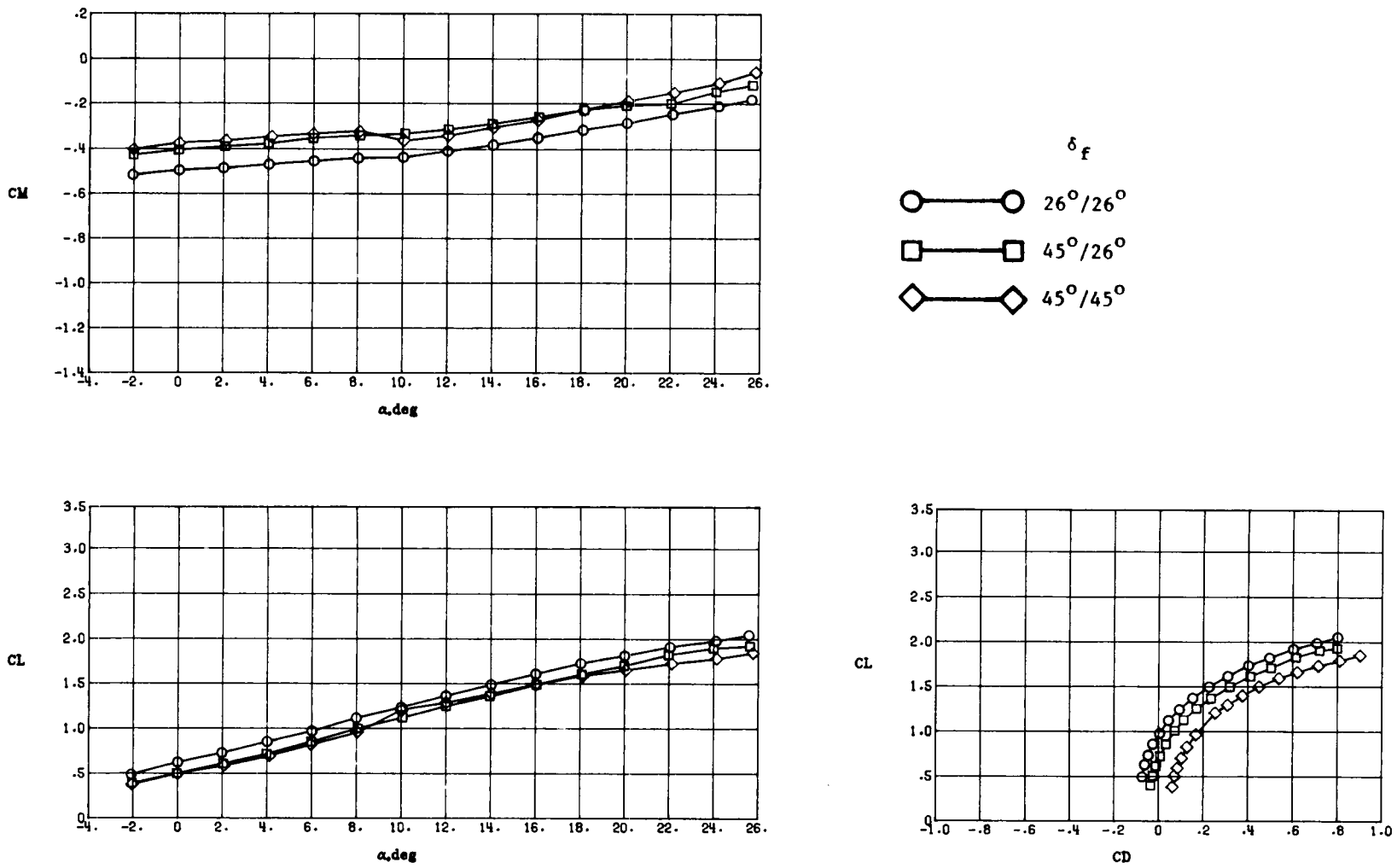

(a) Thrust included.

Figure 15.- Effect of flap deflection angle on longitudinal aerodynamic characteristics with $C_\mu = 0.19$ and $\Lambda_C = 30°$.

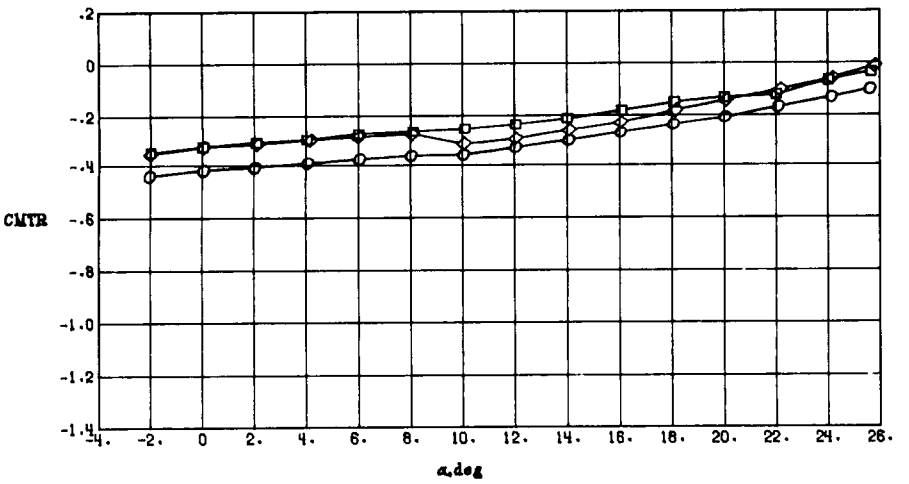

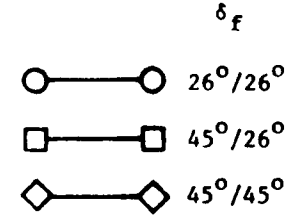

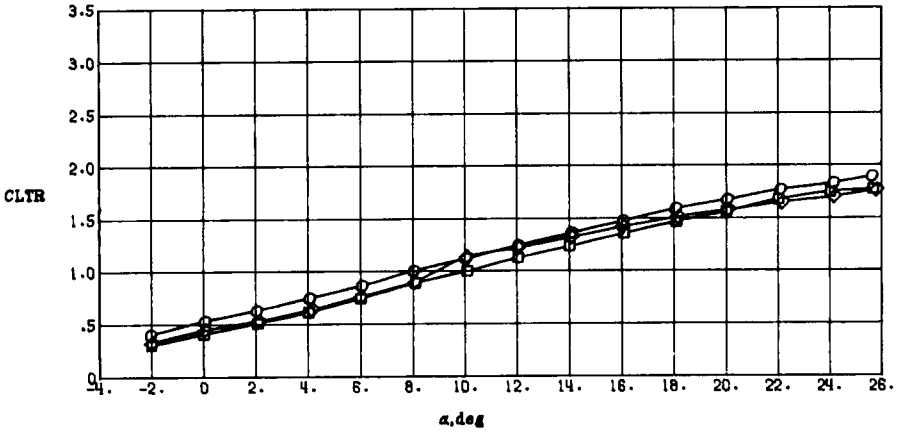

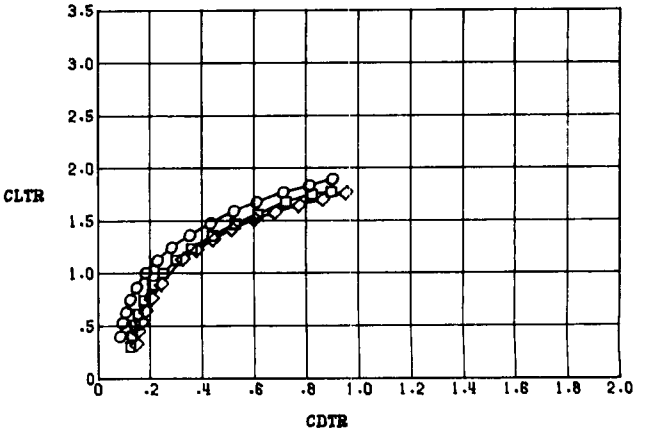

(b) Thrust removed.

Figure 15.- Concluded.

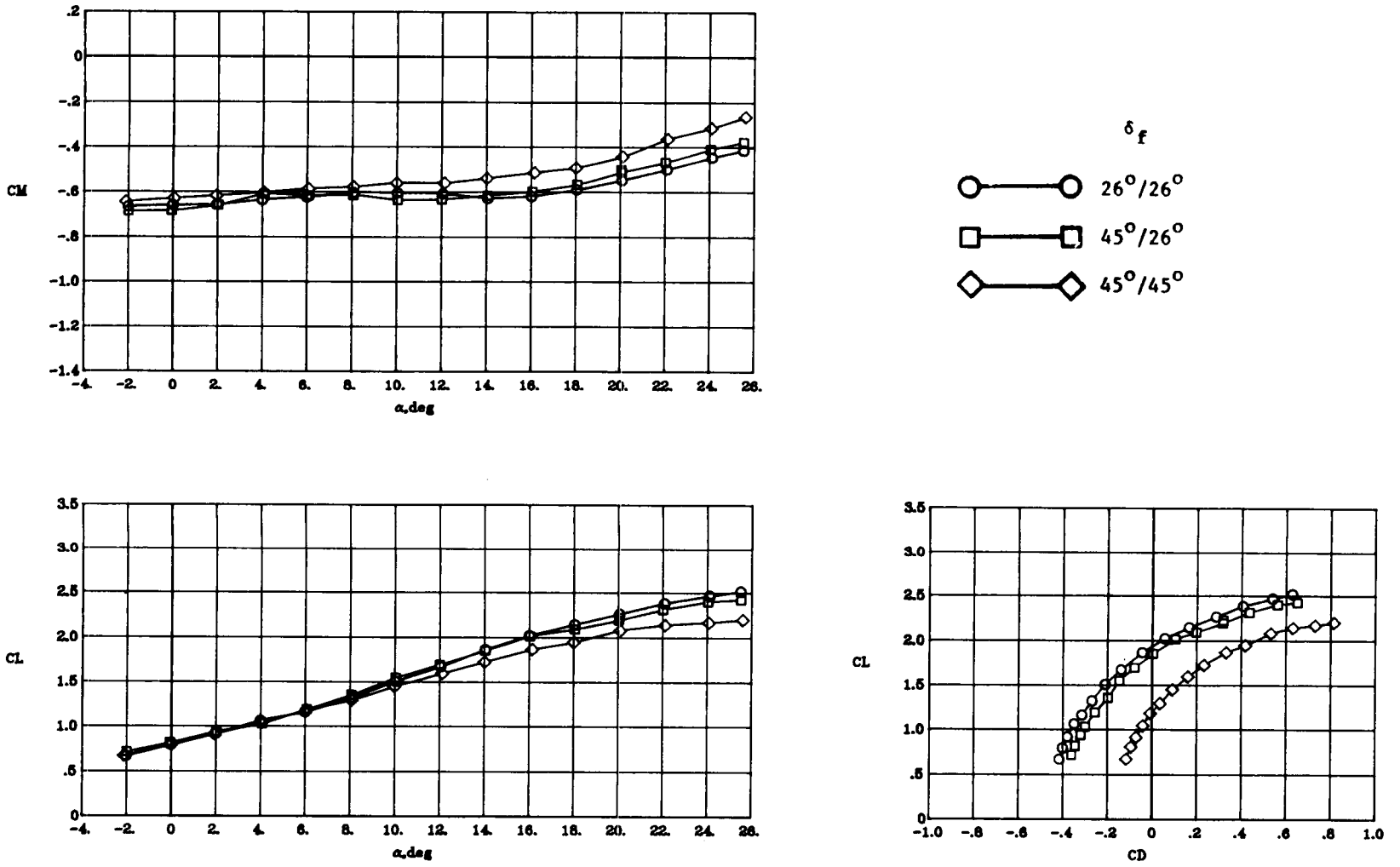

(a) Thrust included.

Figure 16.- Effect of flap deflection angle on longitudinal aerodynamic characteristics with $C_{\mu} = 0.60$ and $\Lambda_C = 30°$.

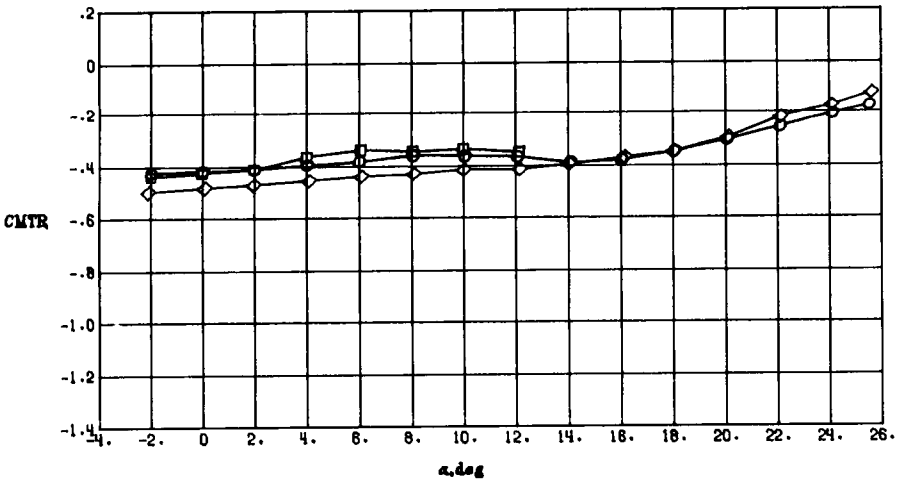

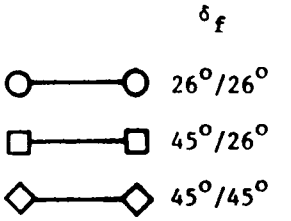

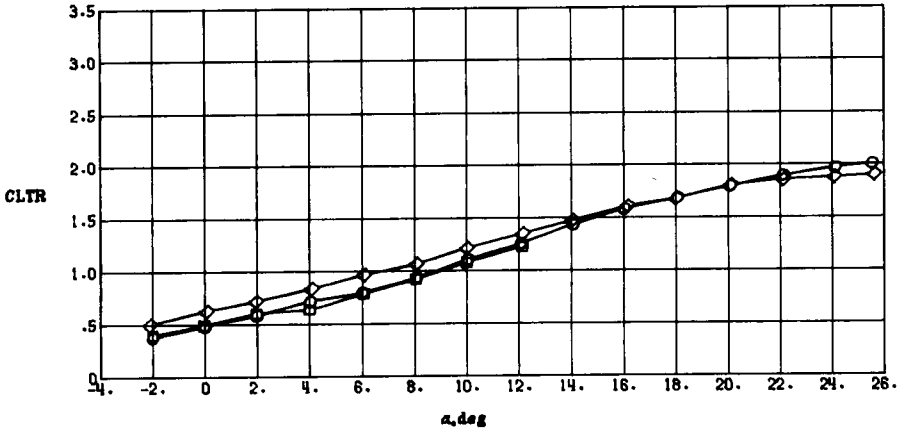

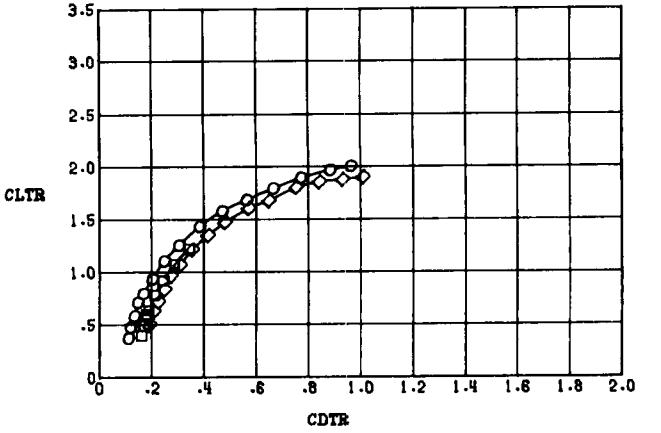

(b) Thrust removed.

Figure 16.- Concluded.

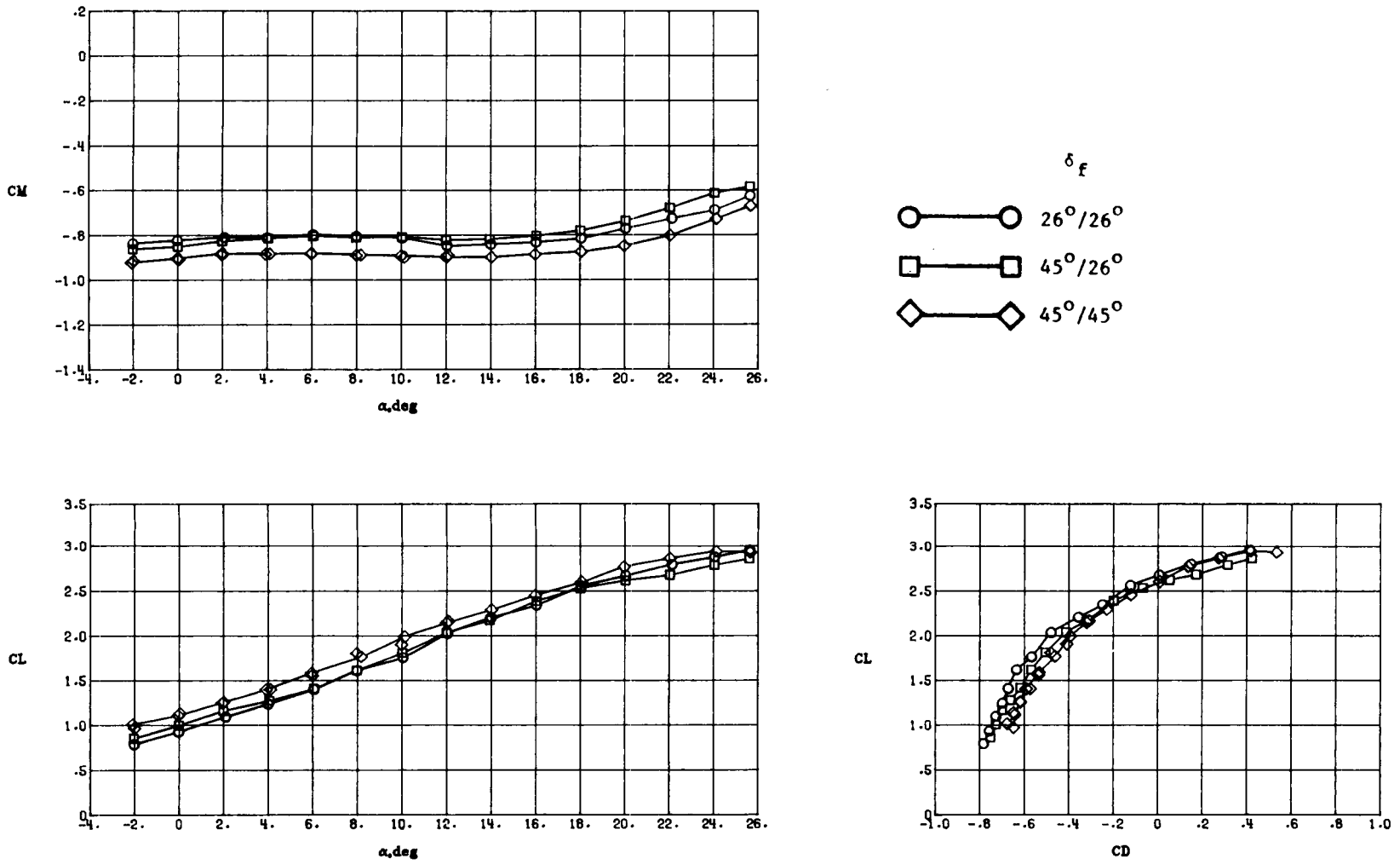

(a) Thrust included.

Figure 17.- Effect of flap deflection angle on longitudinal aerodynamic characteristics with $C_{\mu} = 1.07$ and $\Lambda_C = 30°$.

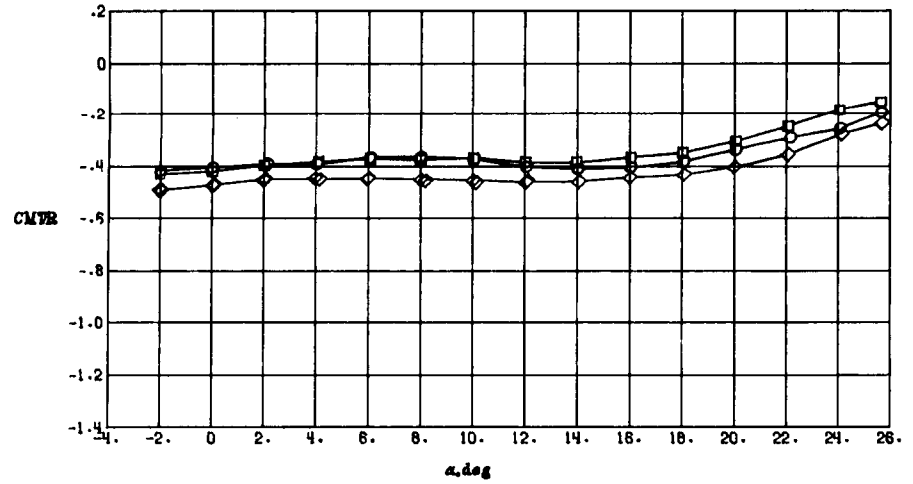

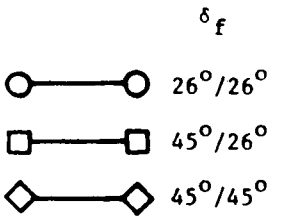

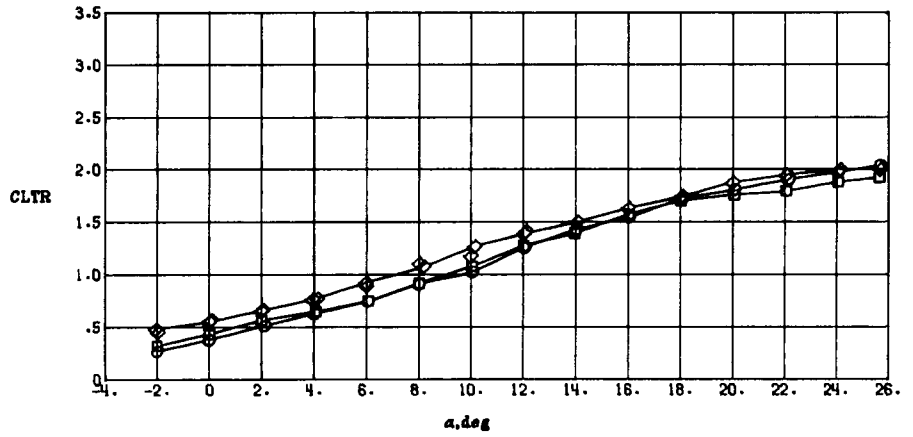

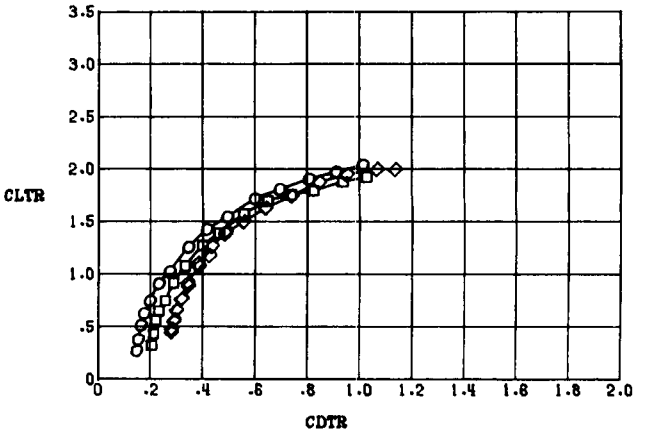

(b) Thrust removed.

Figure 17.- Concluded.

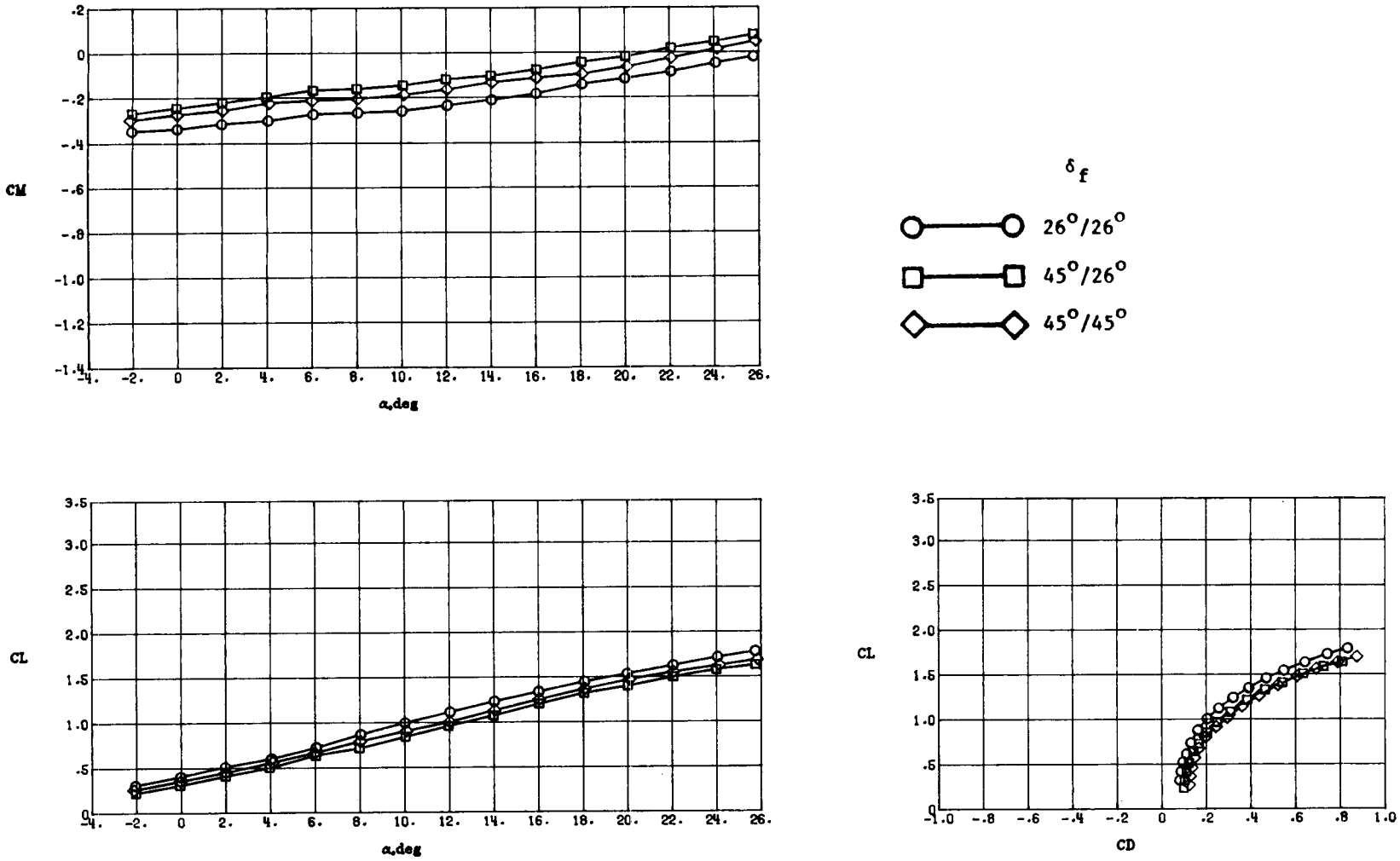

Figure 18.- Effect of flap deflection angle on longitudinal aerodynamic characteristics with $C_\mu = 0$ and $\Lambda_C = 45°$.

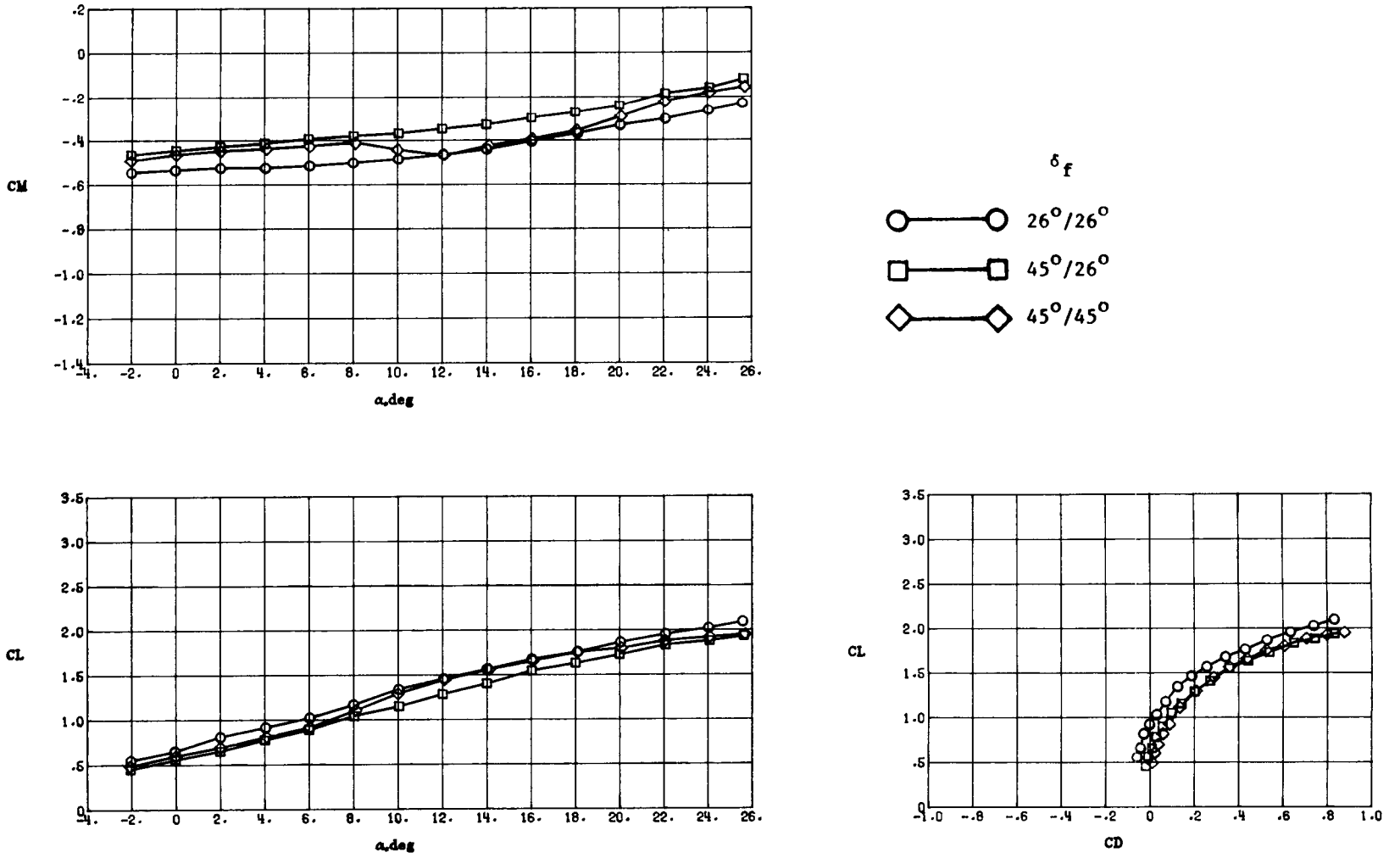

(a) Thrust included.

Figure 19.- Effect of flap deflection angle on longitudinal aerodynamic characteristics with $C_\mu = 0.19$ and $\Lambda_C = 45°$.

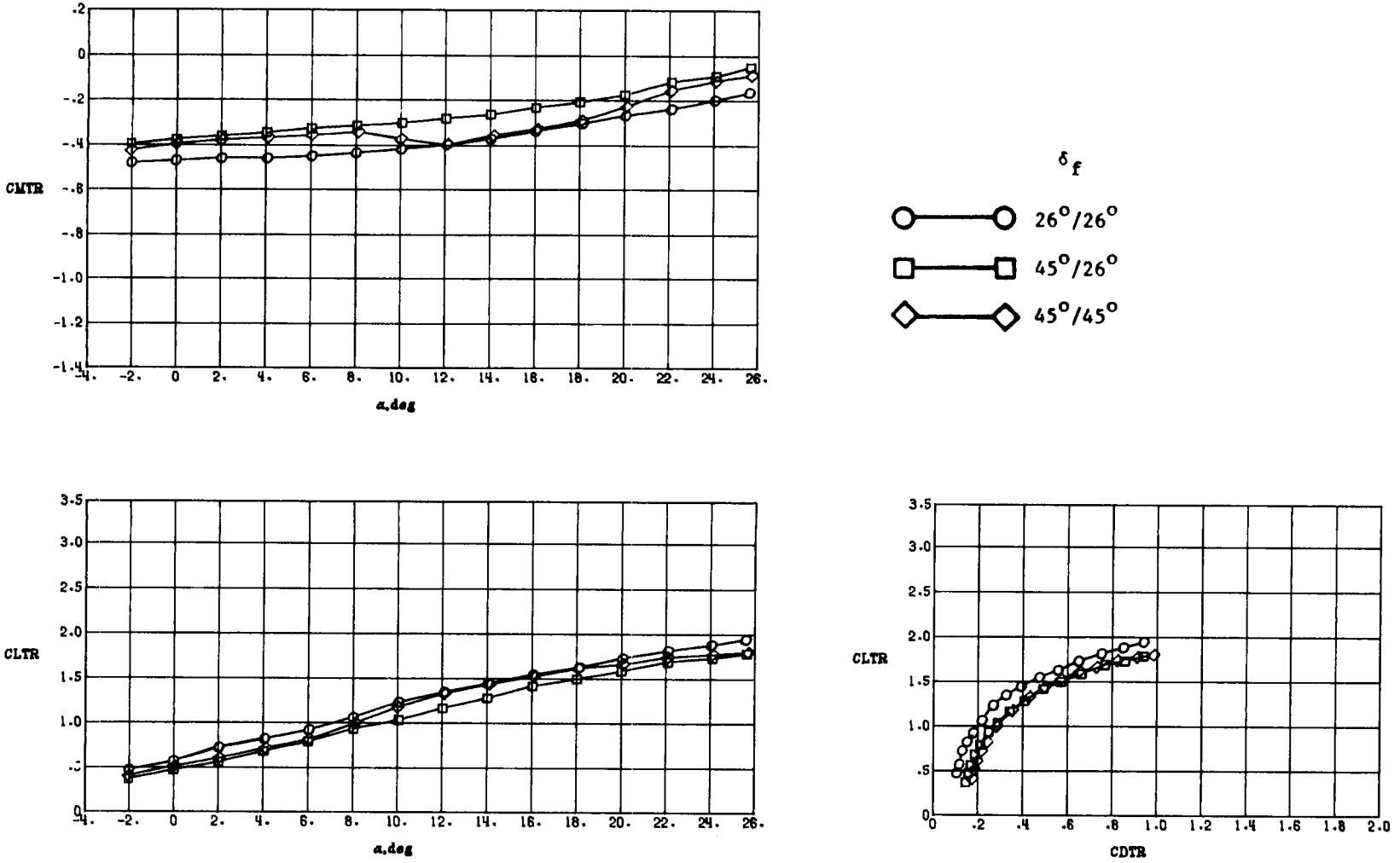

(b) Thrust removed.

Figure 19.- Concluded.

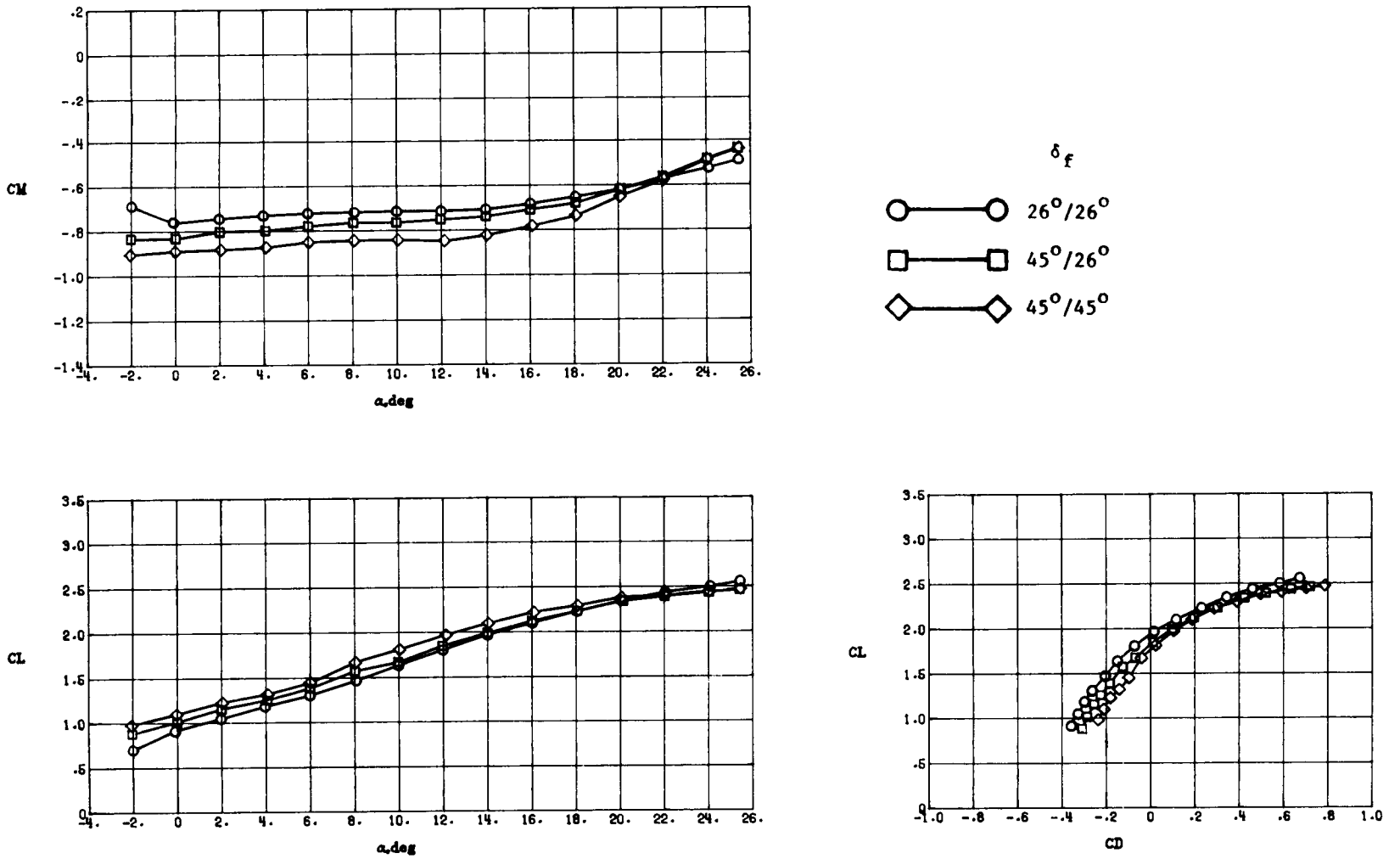

(a) Thrust included.

Figure 20.- Effect of flap deflection angle on longitudinal aerodynamic characteristics with $C_\mu = 0.60$ and $\Lambda_C = 45°$.

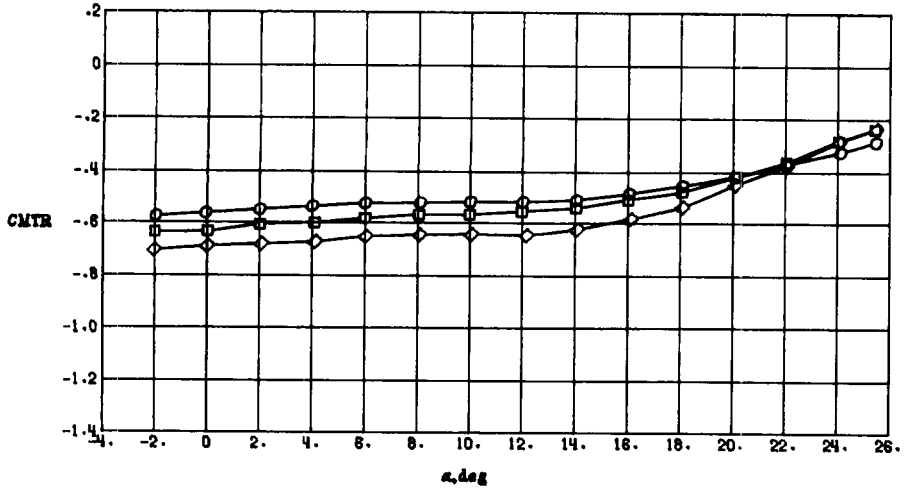

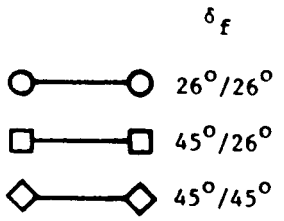

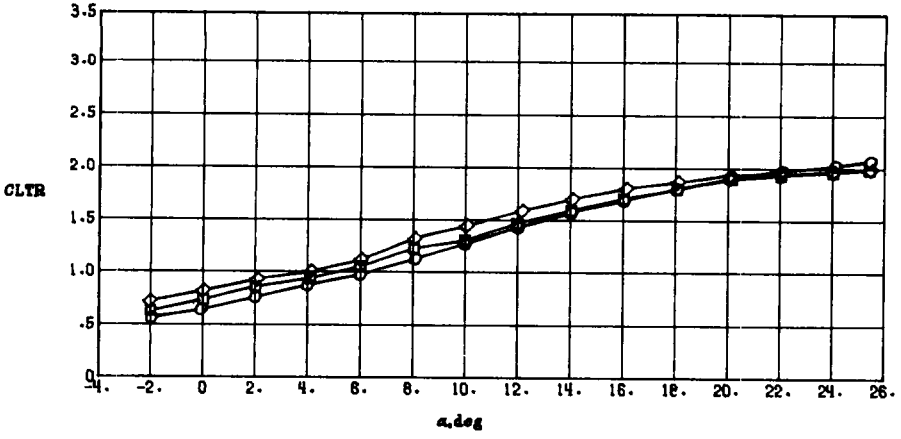

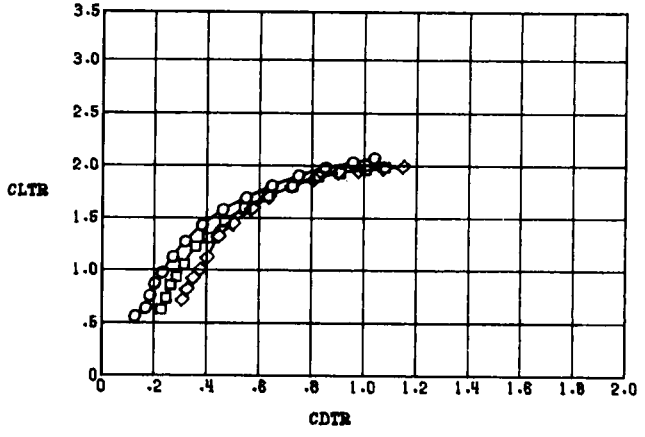

(b) Thrust removed.

Figure 20.- Concluded.

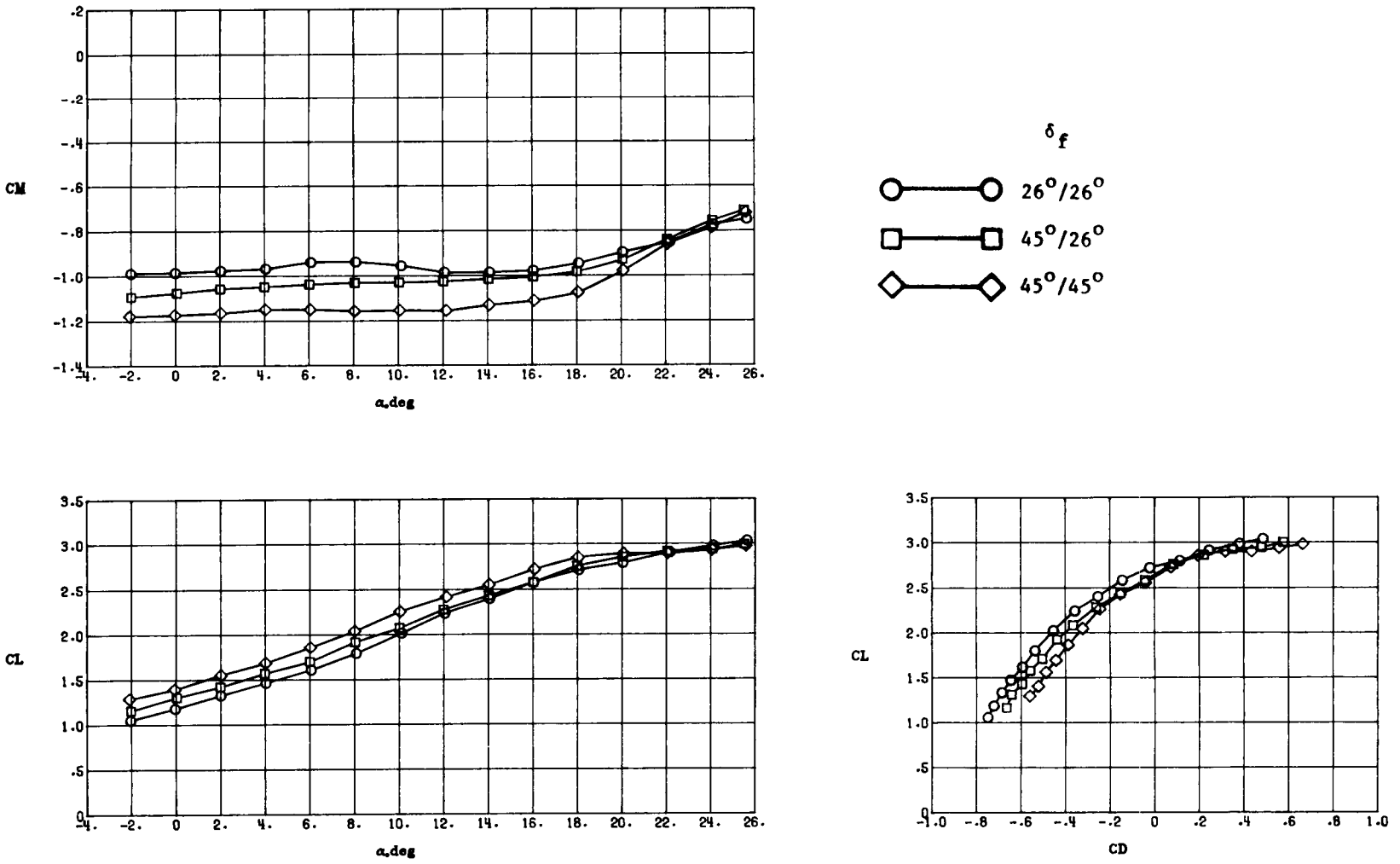

(a) Thrust included.

Figure 21.- Effect of flap deflection angle on longitudinal aerodynamic characteristics with $C_\mu = 1.07$ and $\Lambda_C = 45°$.

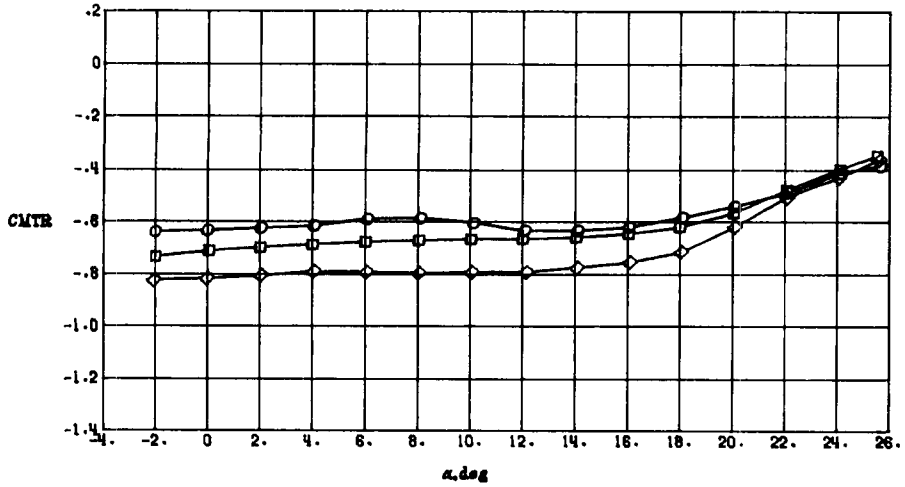

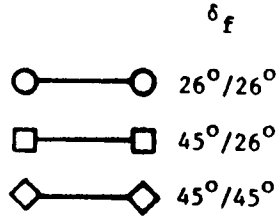

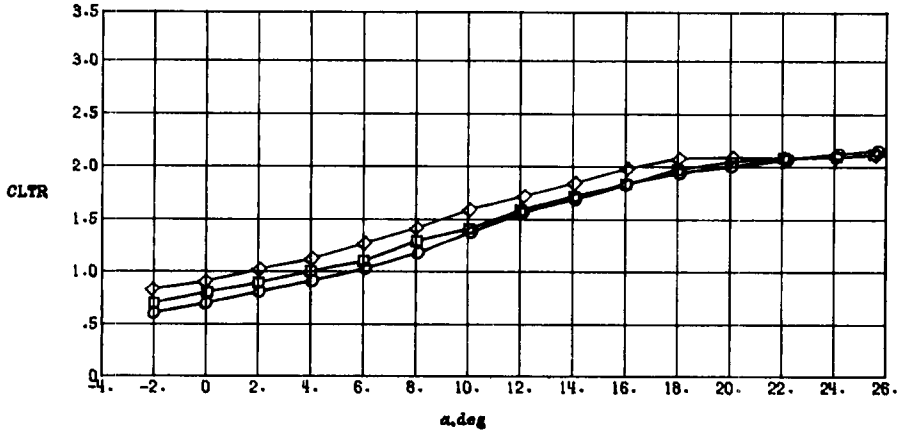

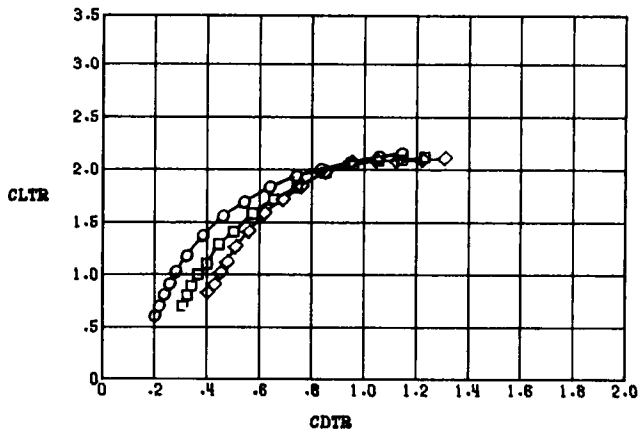

(b) Thrust removed.

Figure 21.- Concluded.

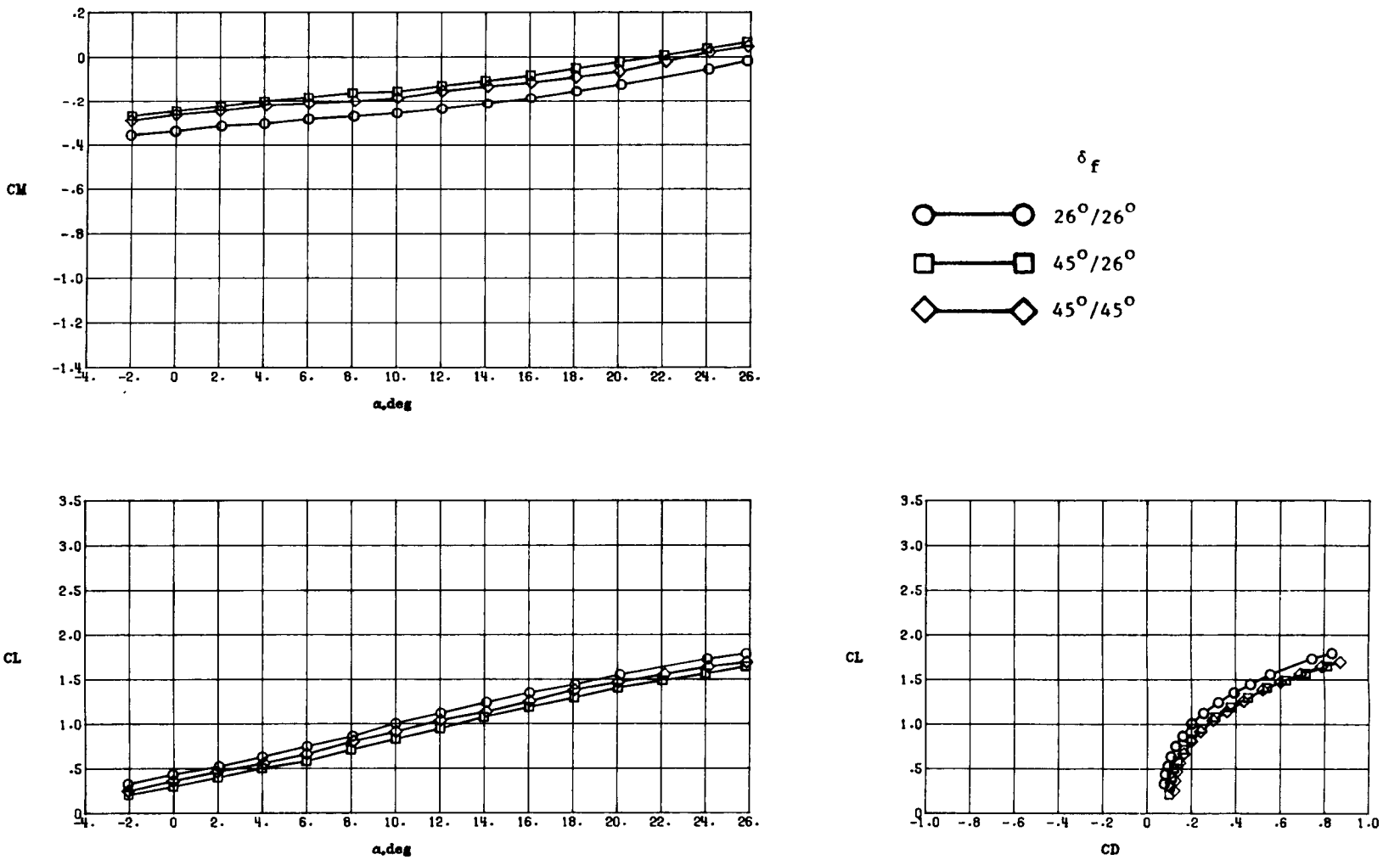

Figure 22.- Effect of flap deflection angle on longitudinal aerodynamic characteristics with $C_\mu = 0$ and $\Lambda_C = 60°$.

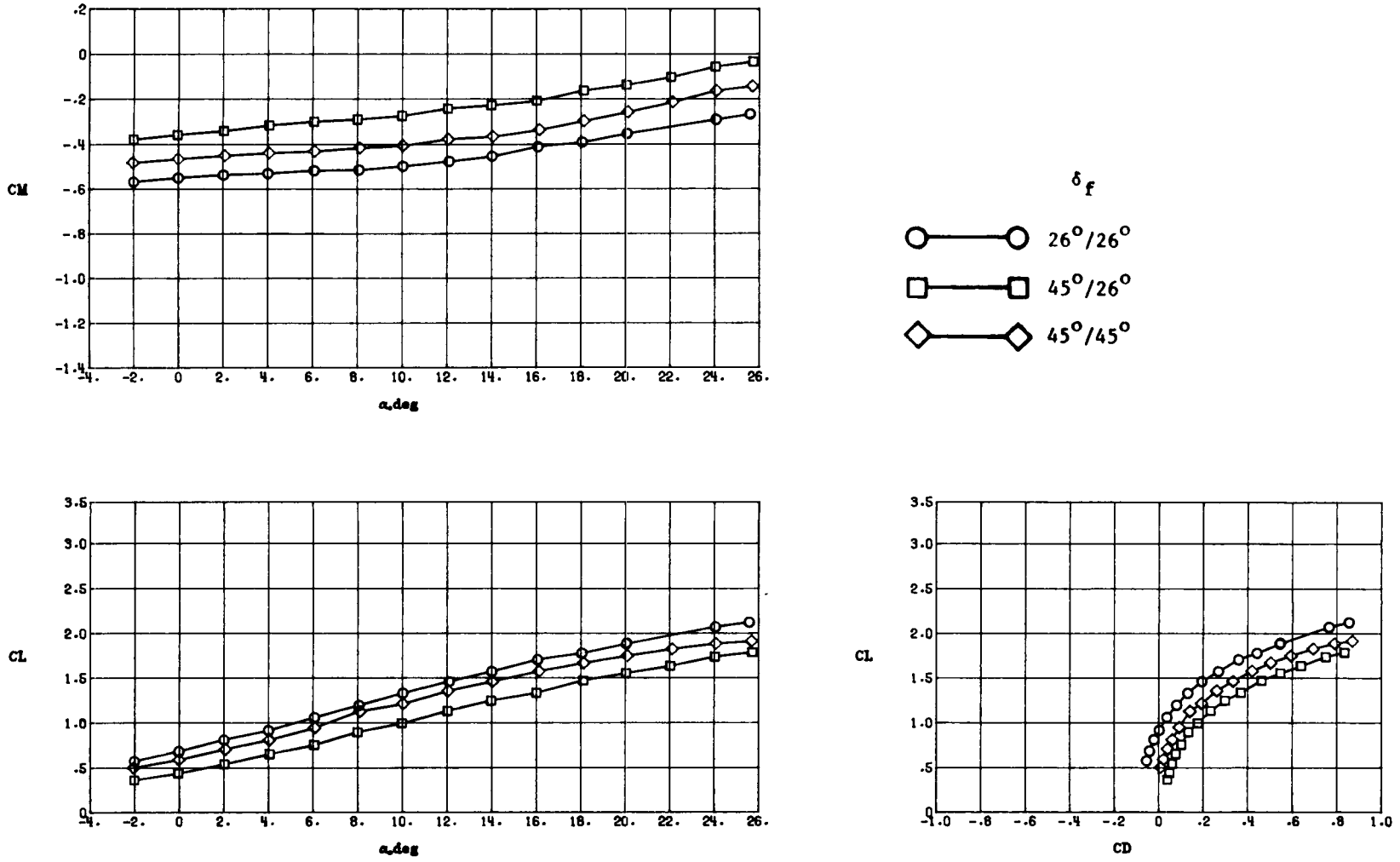

(a) Thrust included.

Figure 23.- Effect of flap deflection angle on longitudinal aerodynamic characteristics with $C_{\mu} = 0.19$ and $\Lambda_C = 60°$.

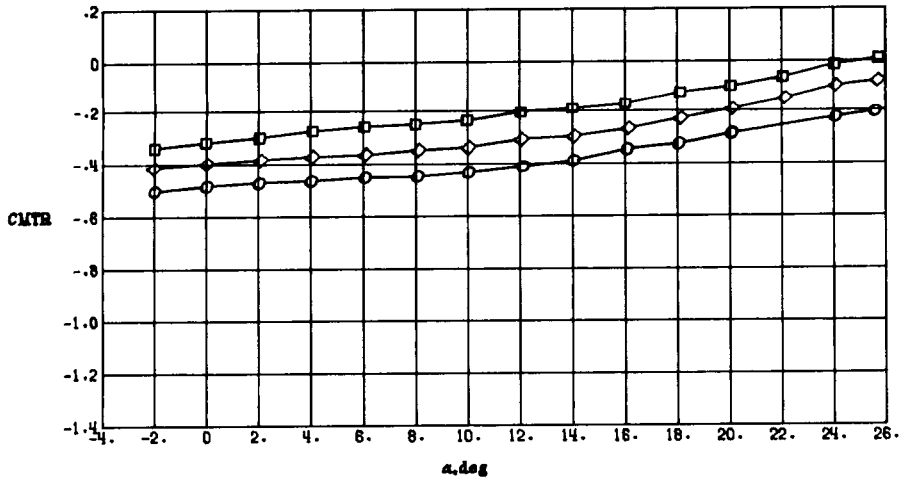

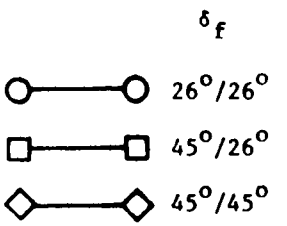

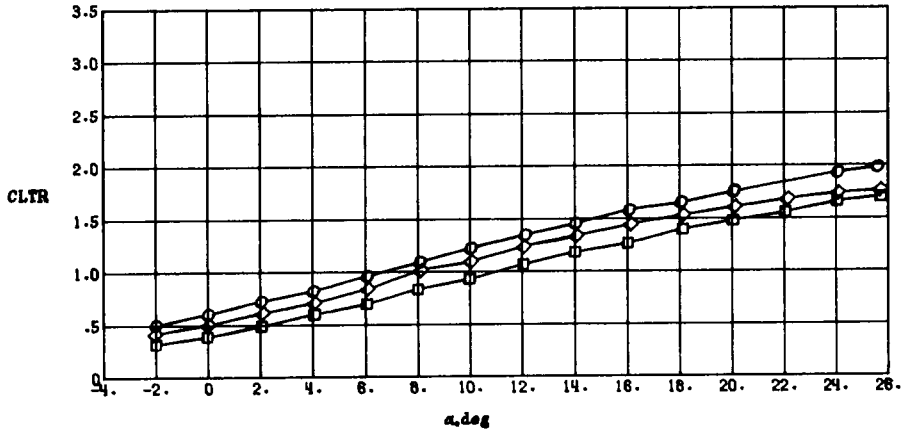

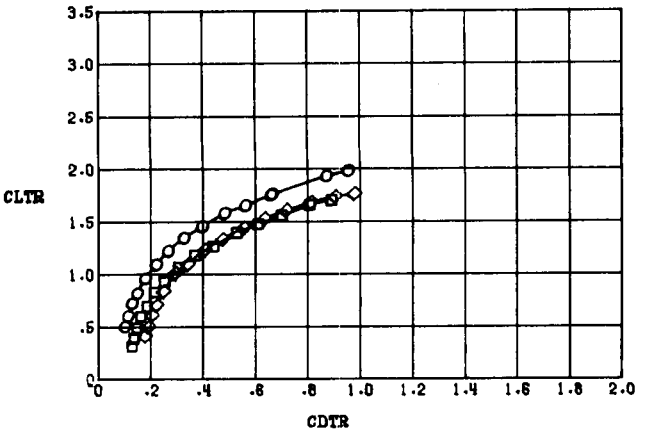

(b) Thrust removed.

Figure 23.- Concluded.

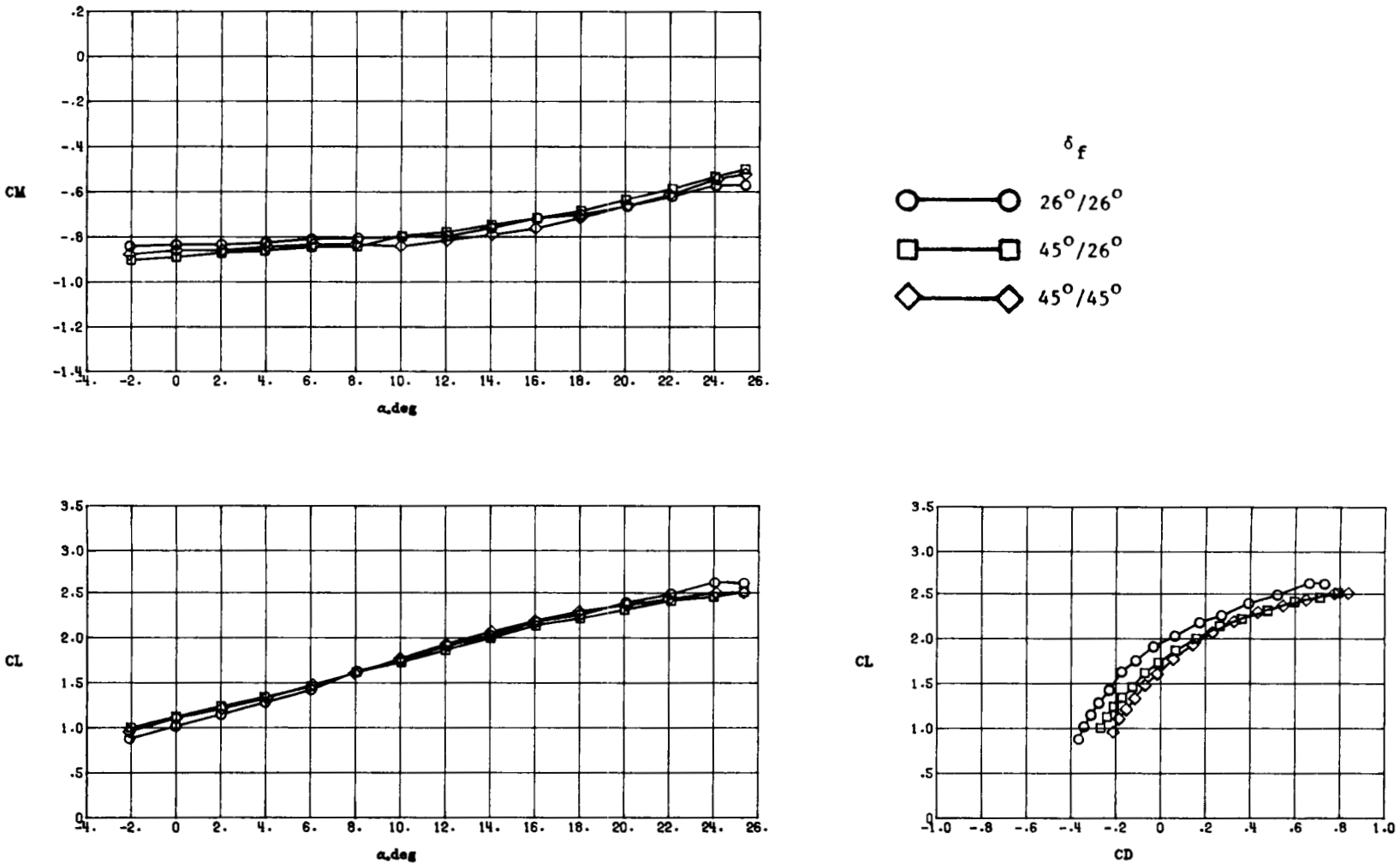

(a) Thrust included.

Figure 24.- Effect of flap deflection angle on longitudinal aerodynamic characteristics with $C_\mu = 0.60$ and $\Lambda_C = 60°$.

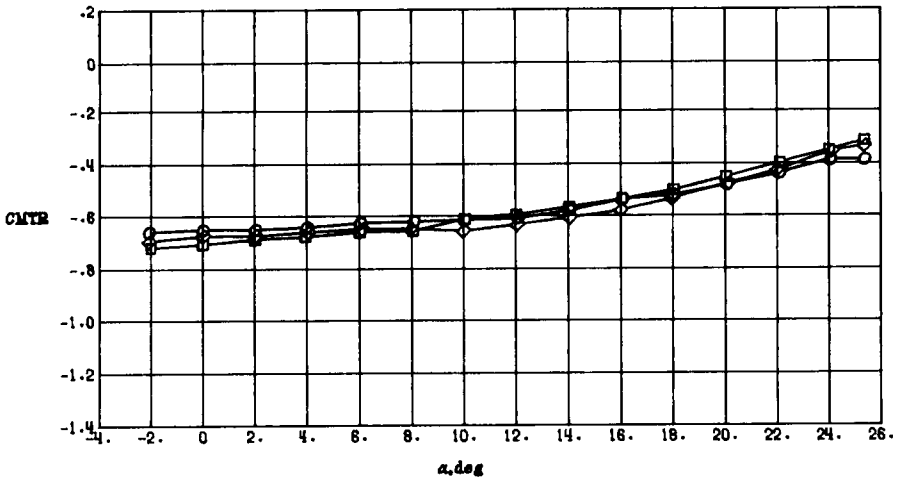

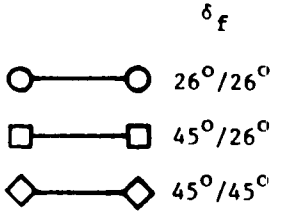

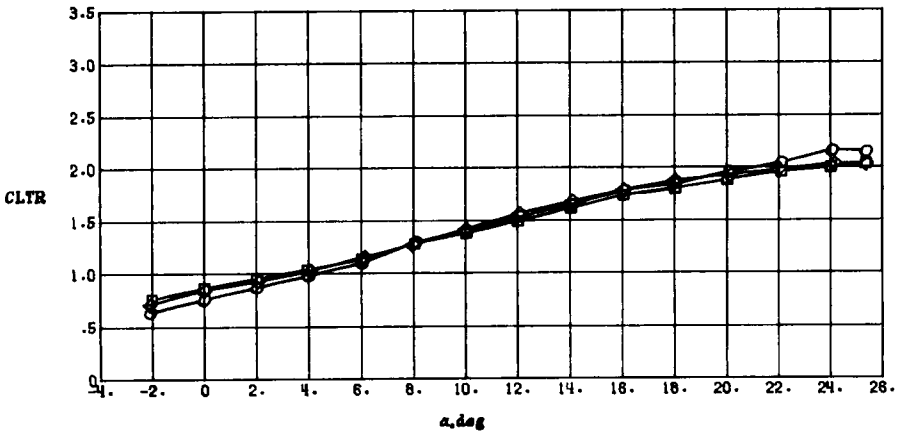

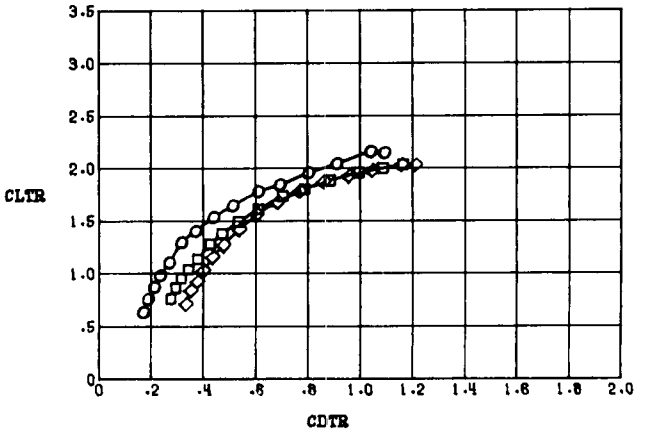

(b) Thrust removed.

Figure 24.- Concluded.

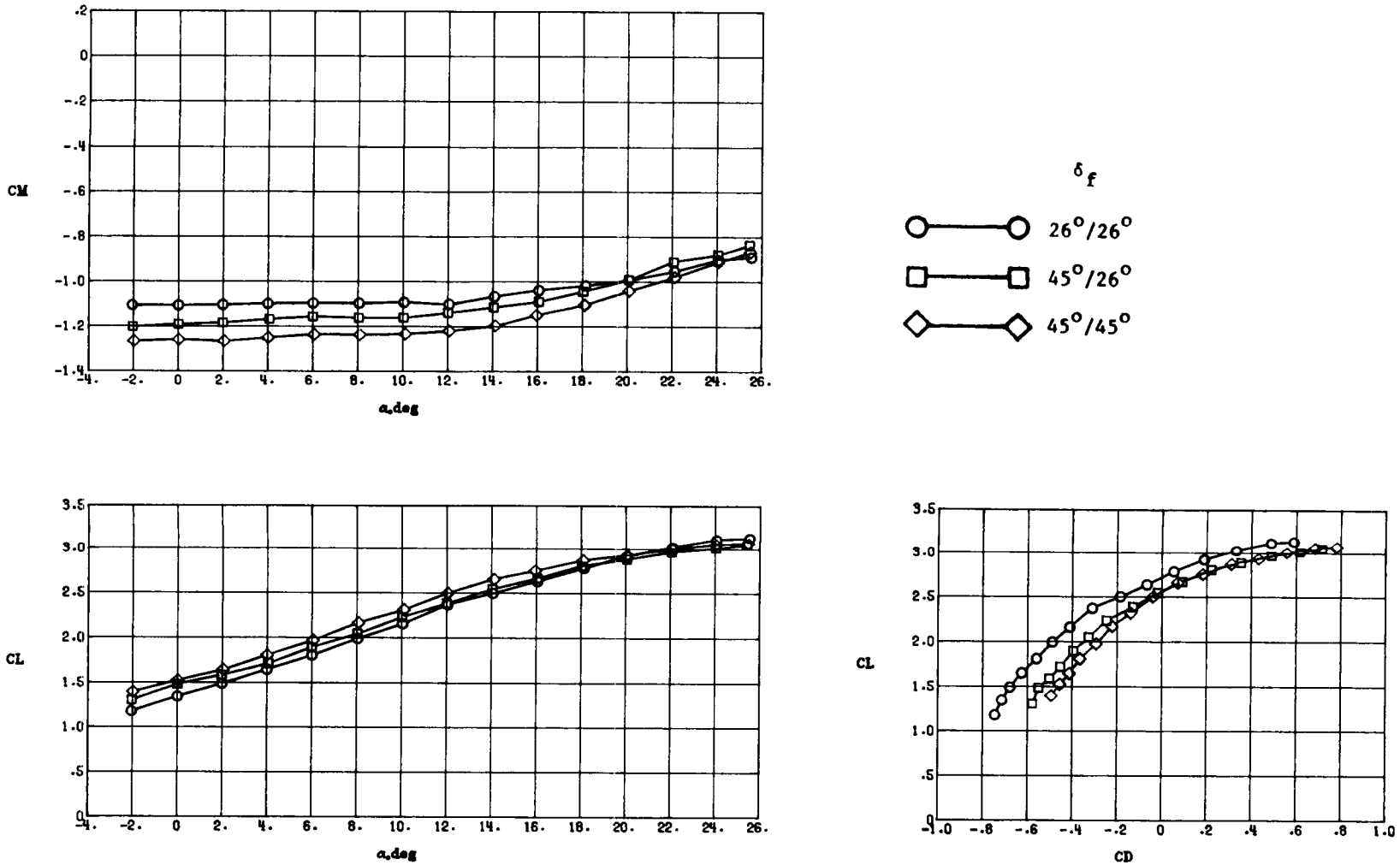

(a) Thrust included.

Figure 25.- Effect of flap deflection angle on longitudinal aerodynamic characteristics with $C_\mu = 1.07$ and $\Lambda_C = 60°$.

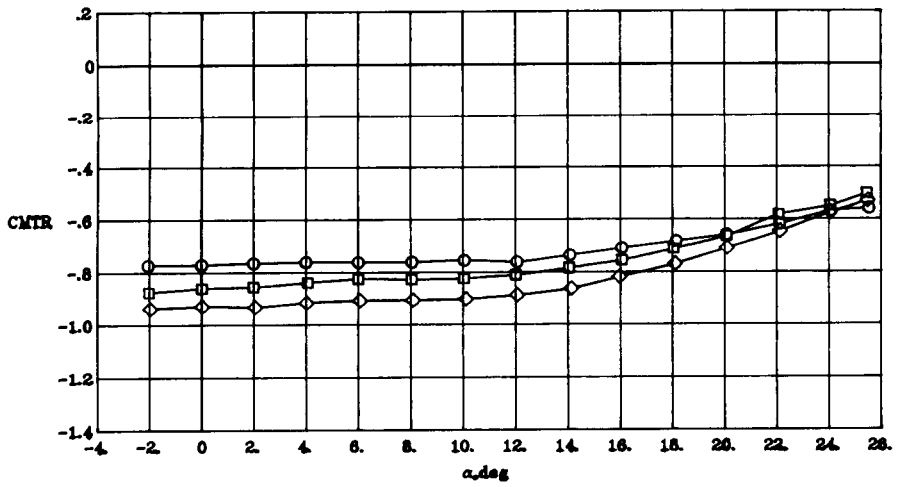

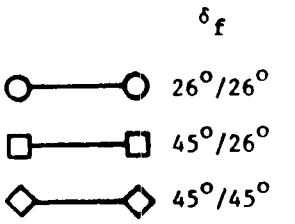

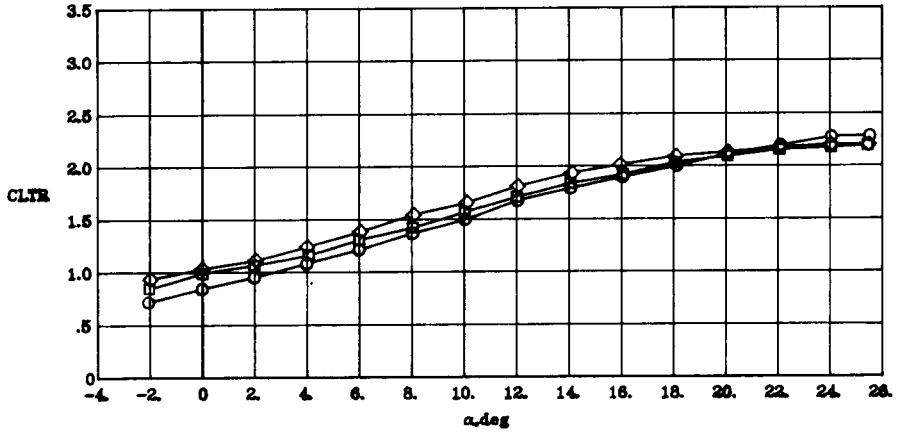

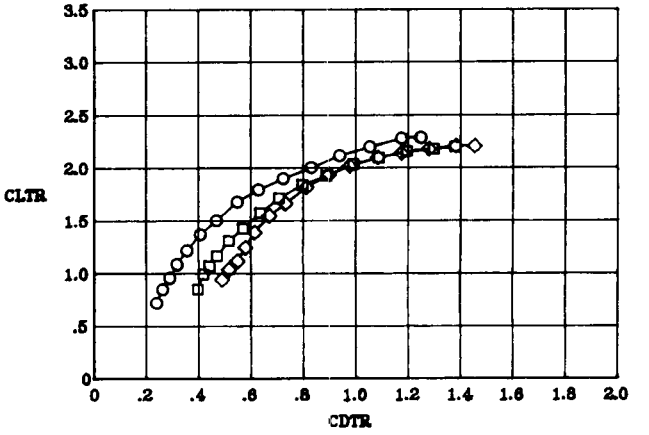

(b) Thrust removed.

Figure 25.- Concluded.

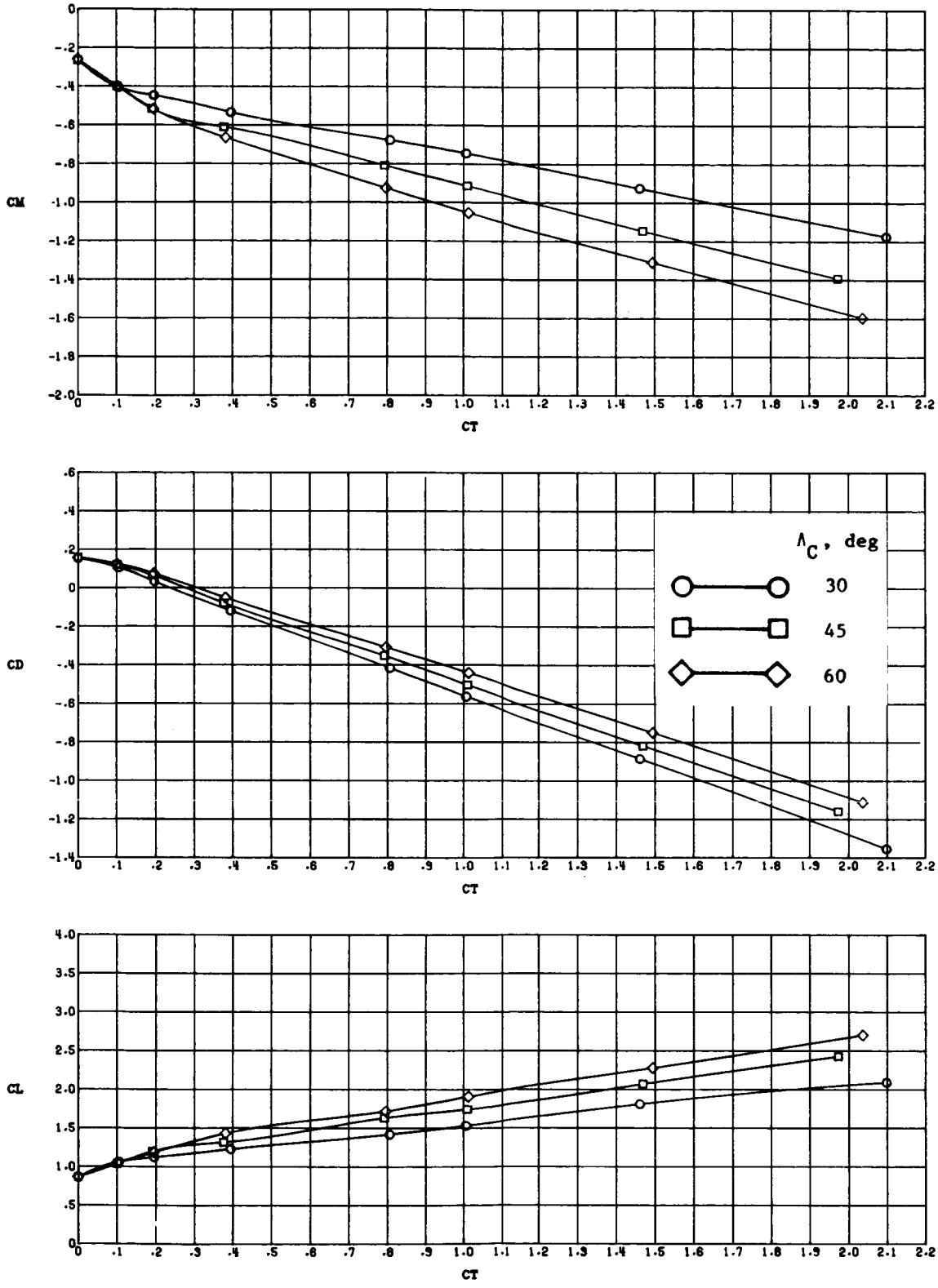

(a) Thrust included.

Figure 26.- Effect of cascade vector angle on longitudinal aerodynamic characteristics at various thrust coefficients with $\alpha = 8°$ and $\delta_f = 26°/26°$.

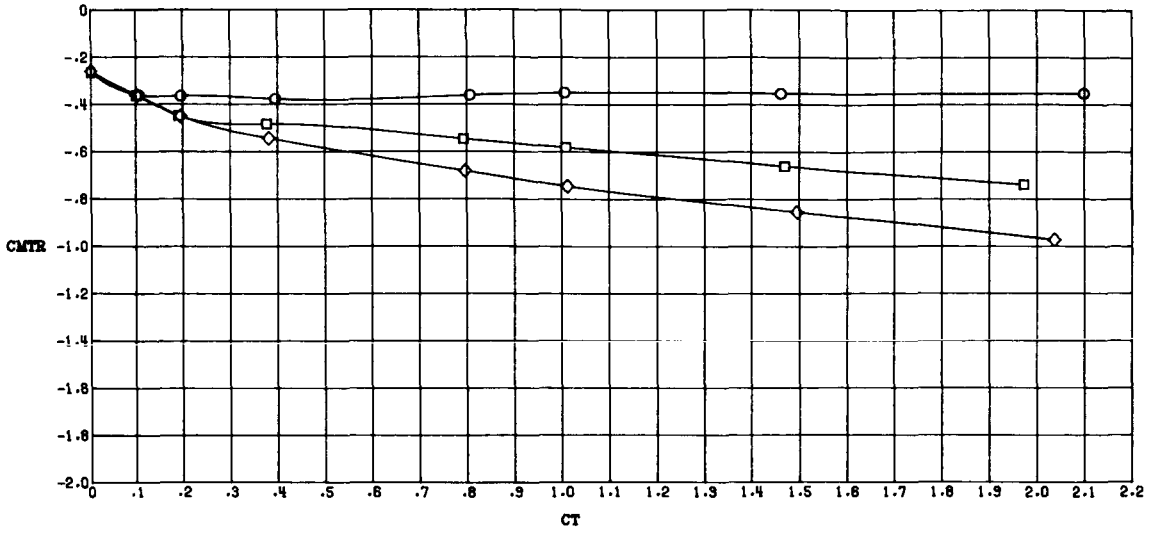

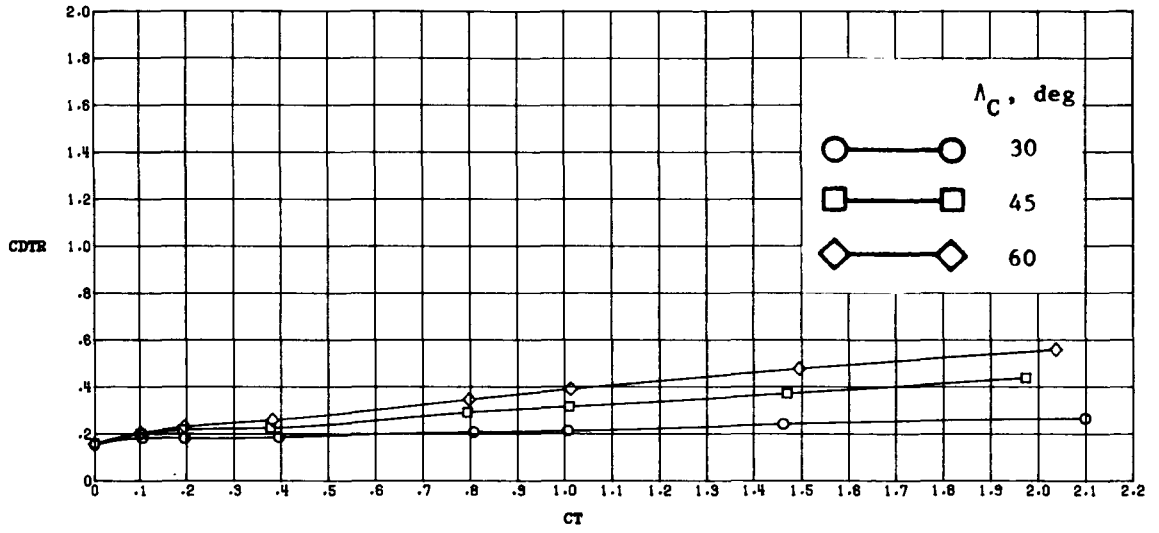

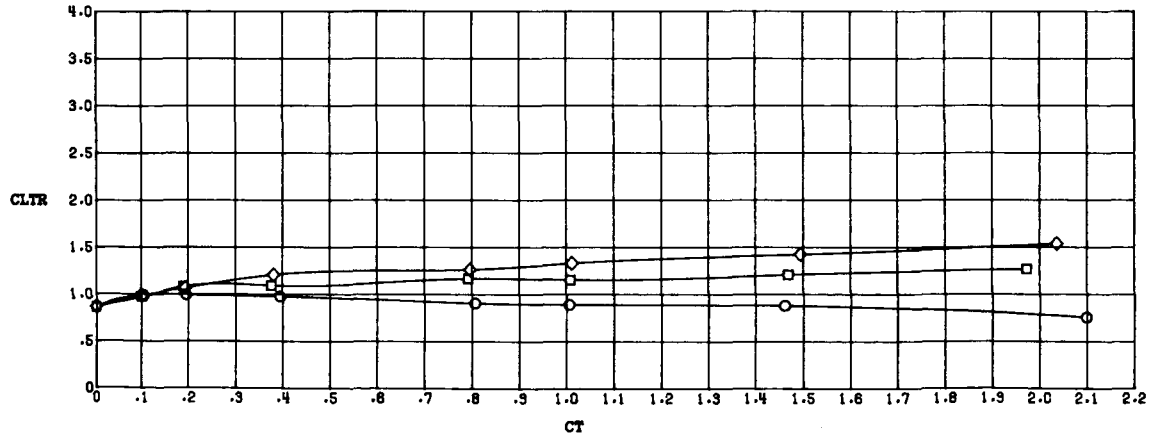

(b) Thrust removed.

Figure 26.- Concluded.

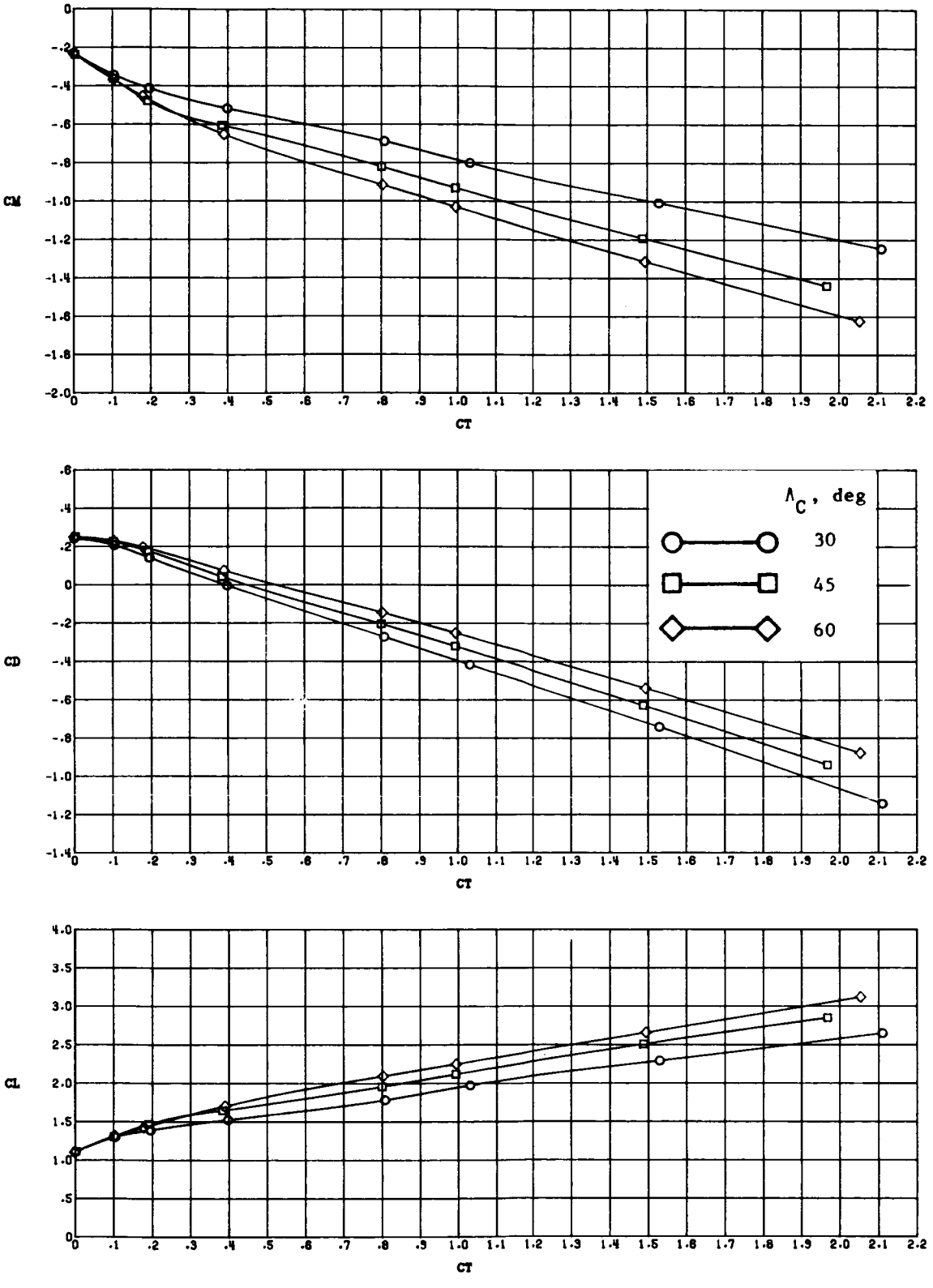

(a) Thrust included.

Figure 27.- Effect of cascade vector angle on longitudinal aerodynamic characteristics at various thrust coefficients with α = 12° and δ_f = 26°/26°.

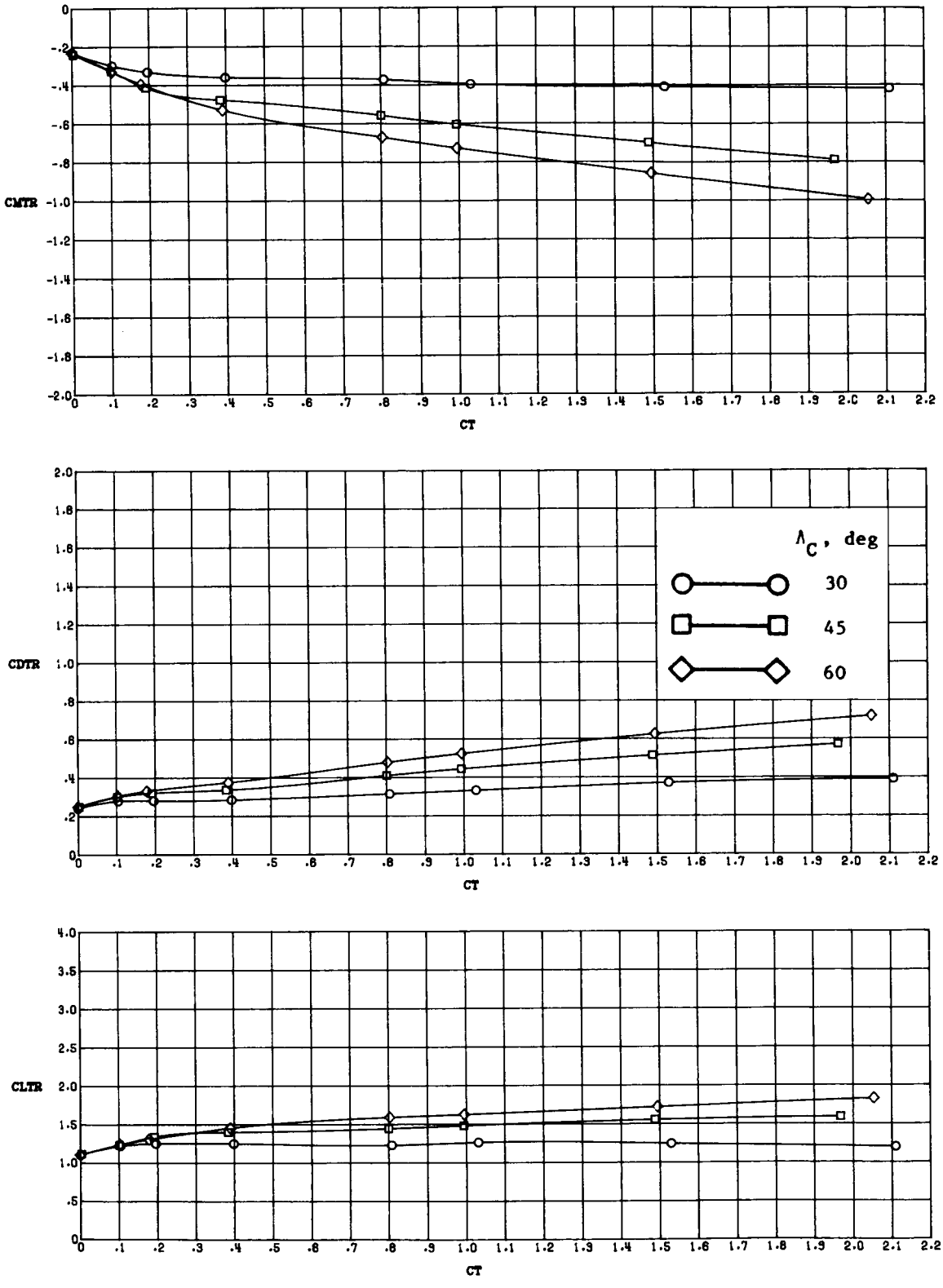

(b) Thrust removed.

Figure 27.- Concluded.

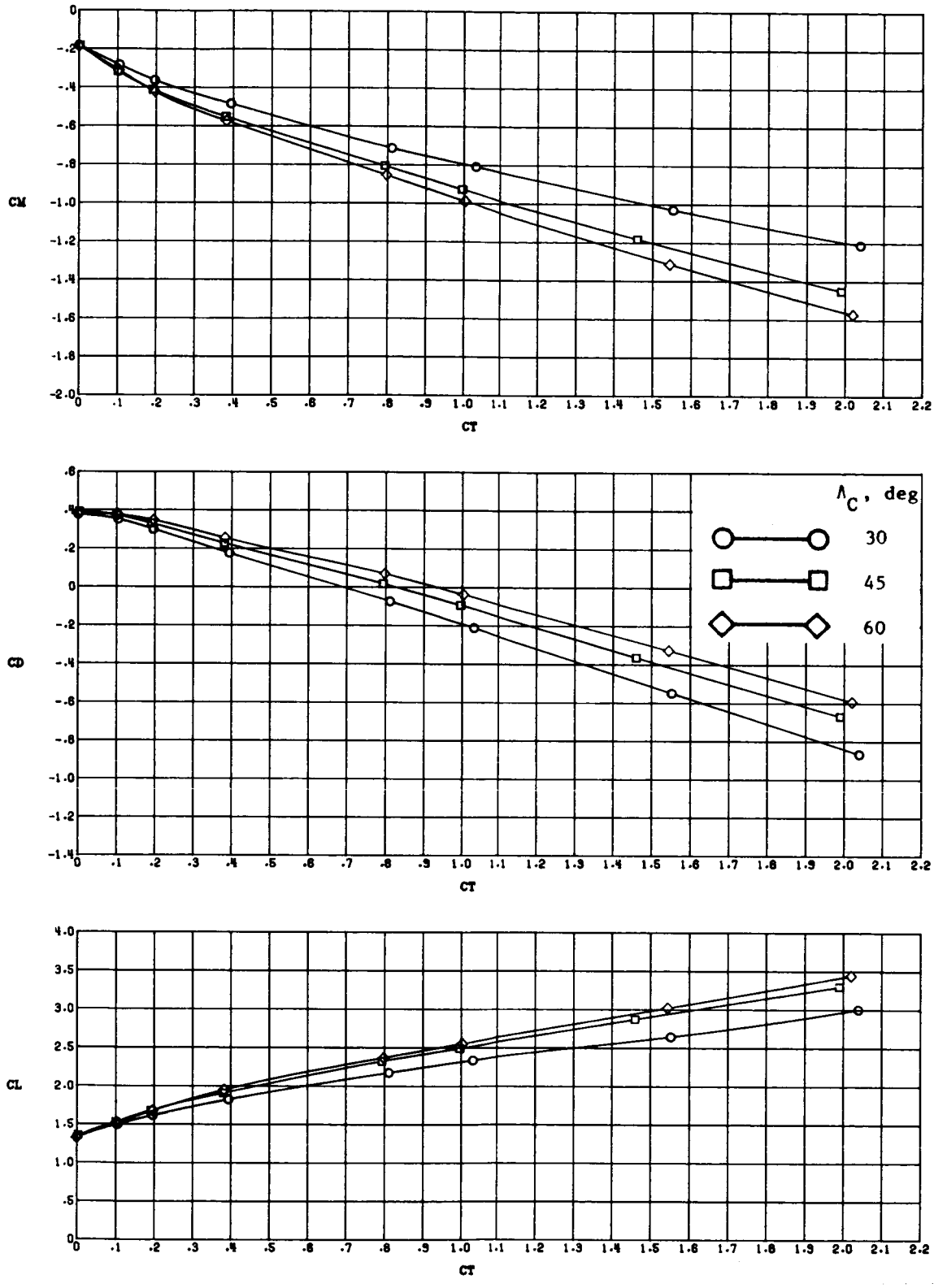

(a) Thrust included.

Figure 28.- Effect of cascade vector angle on longitudinal aerodynamic characteristics at various thrust coefficients with $\alpha = 16°$ and $\delta_f = 26°/26°$.

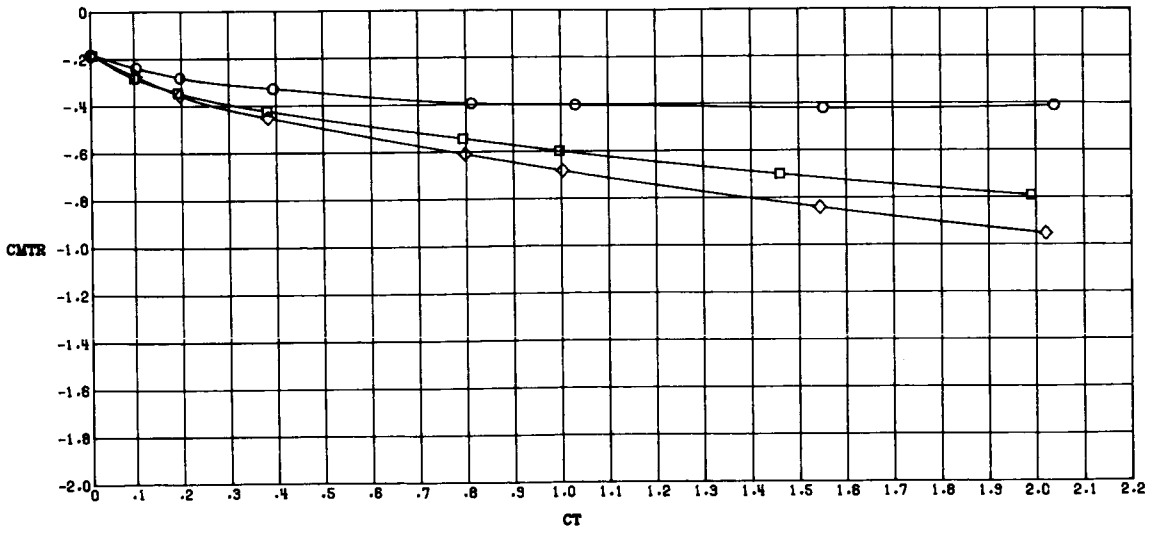

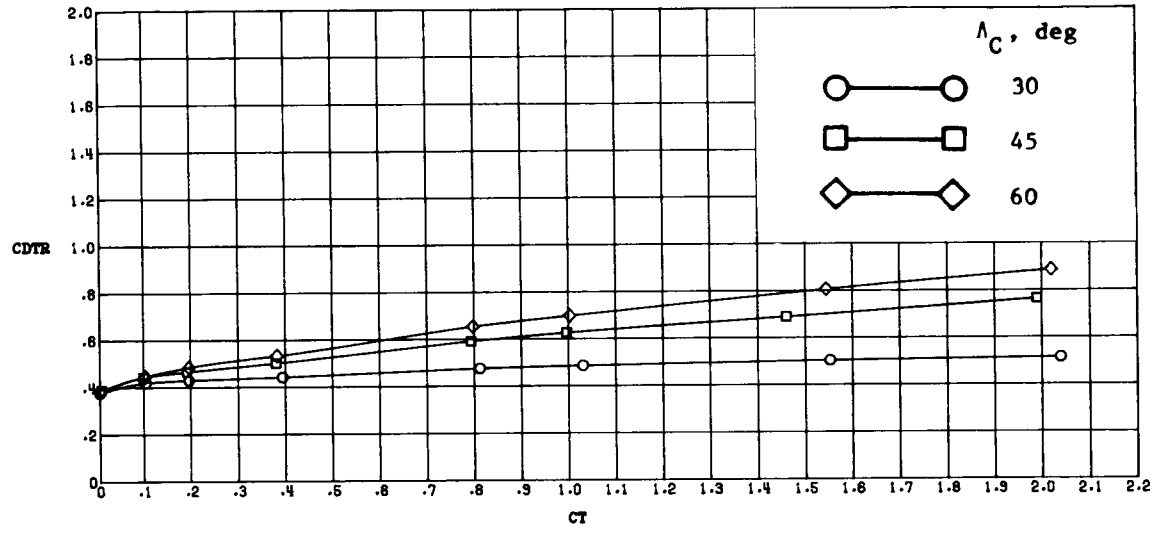

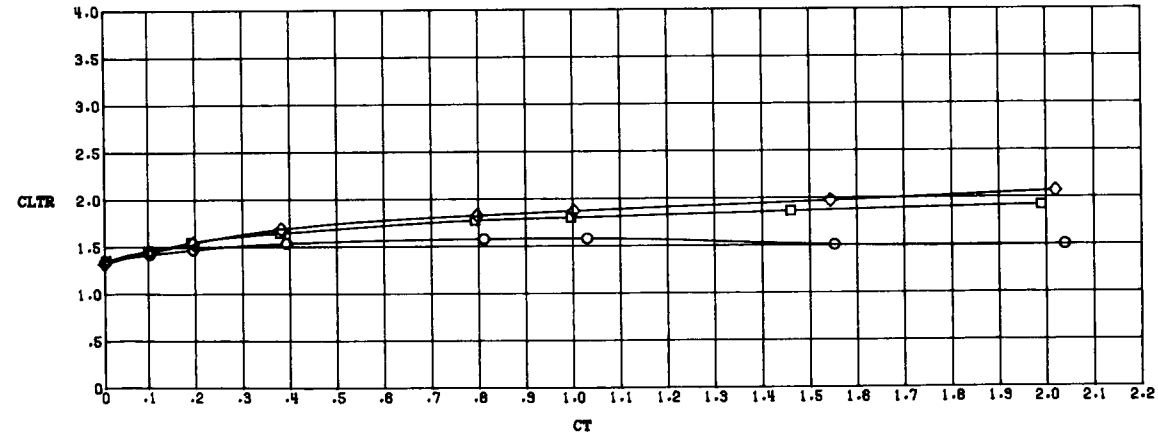

(b) Thrust removed.

Figure 28.- Concluded.

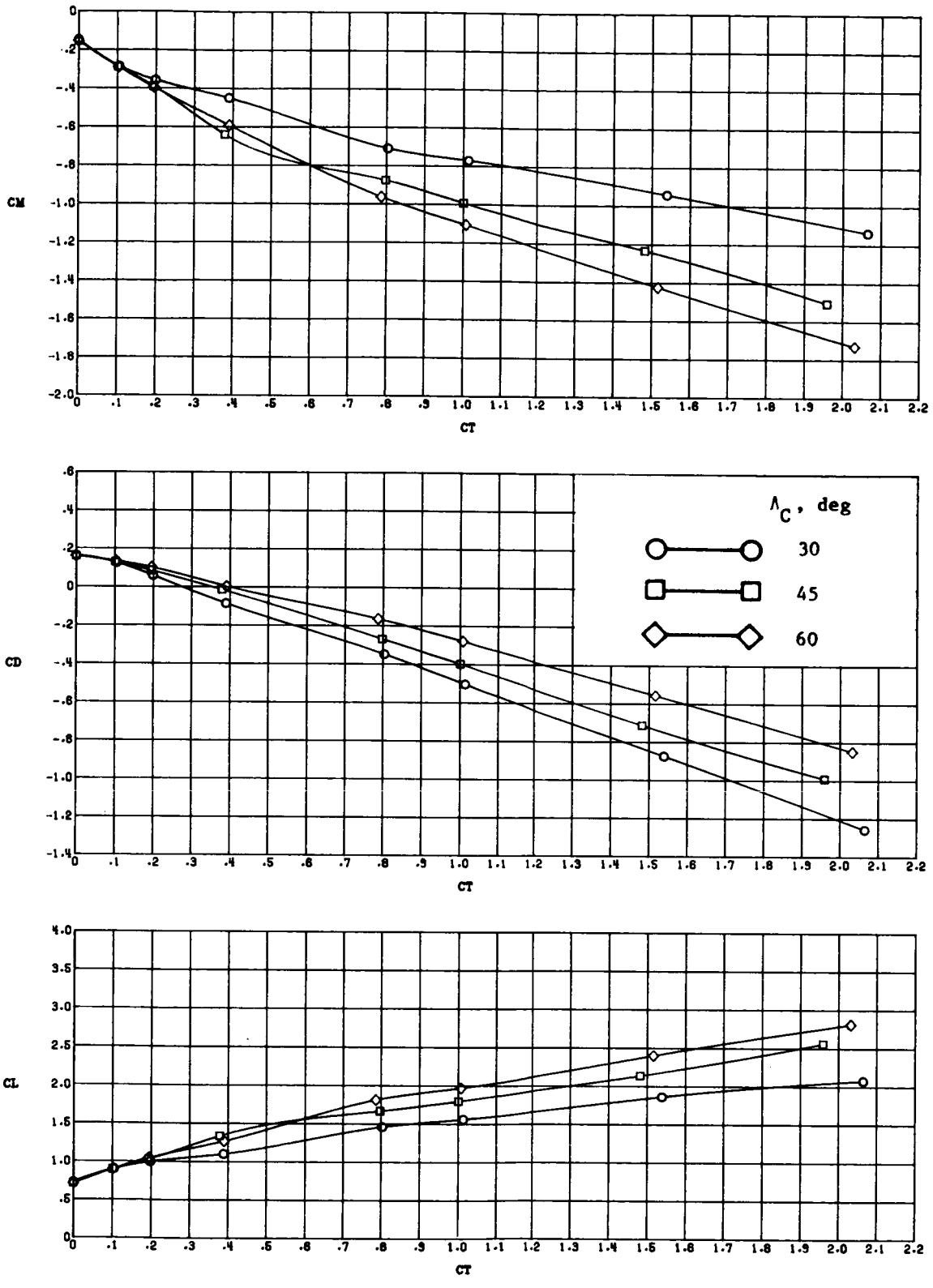

(a) Thrust included.

Figure 29.- Effect of cascade vector angle on longitudinal aerodynamic characteristics at various thrust coefficients with $\alpha = 8°$ and $\delta_f = 45°/26°$.

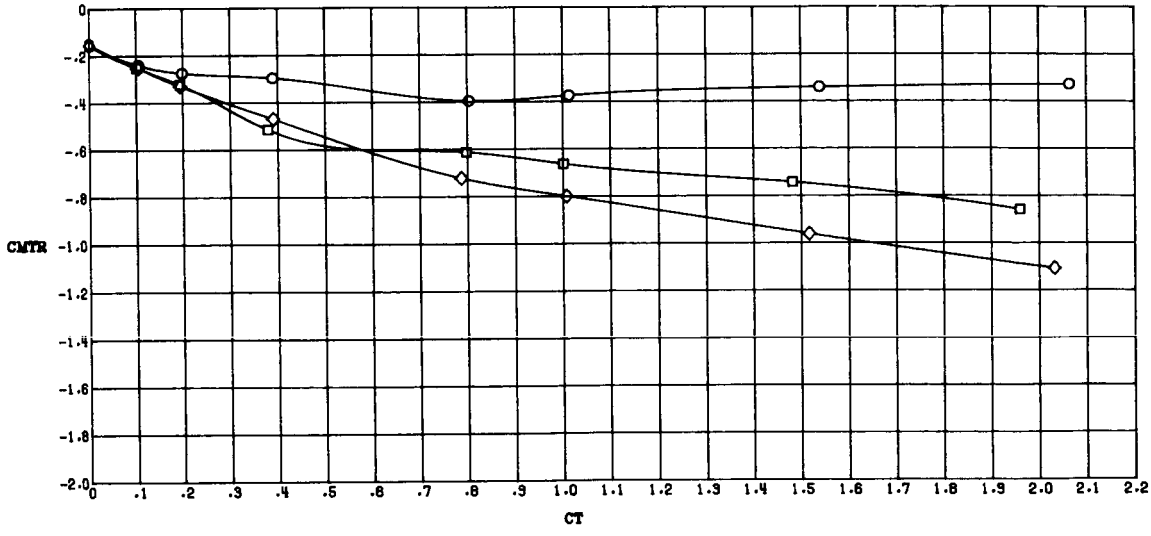

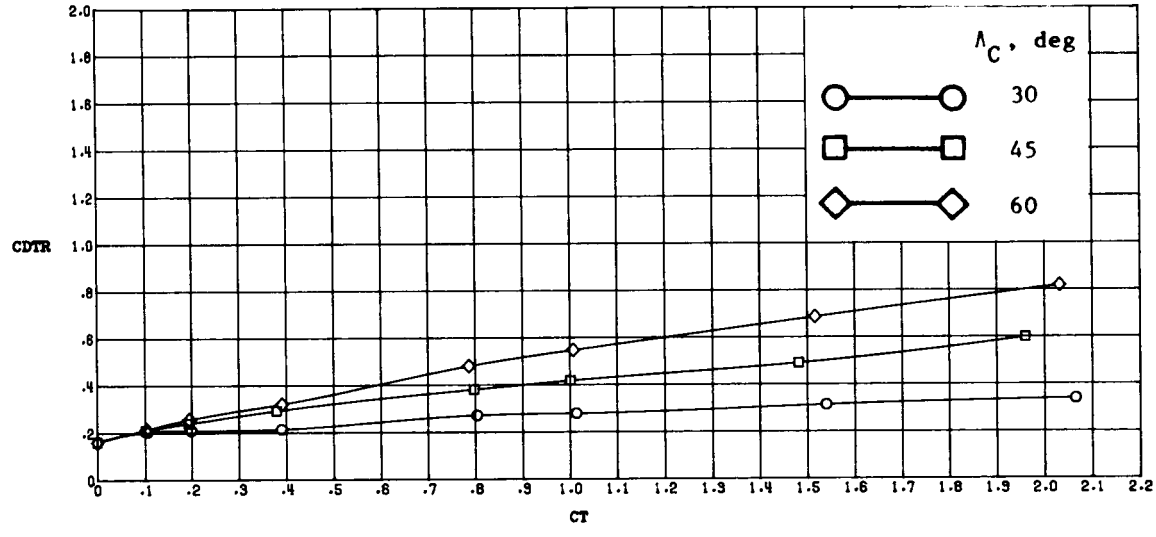

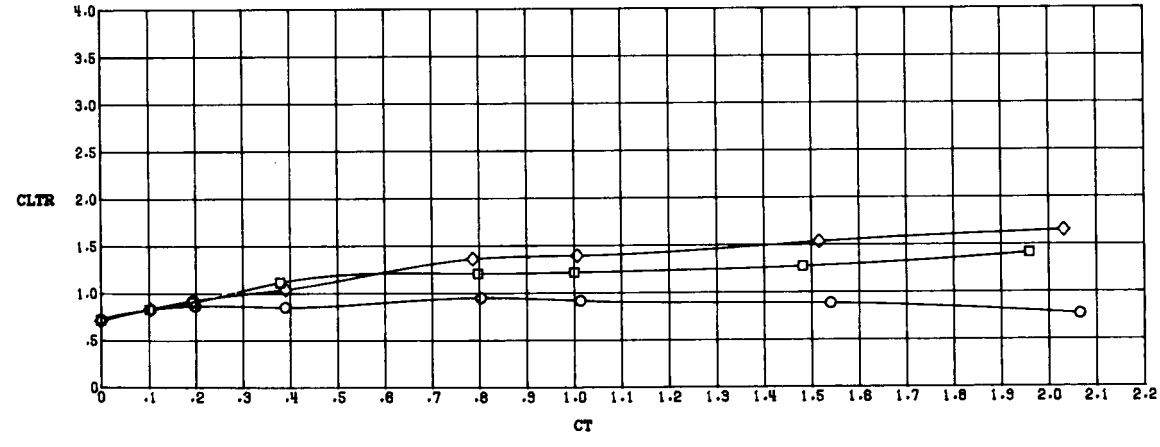

(b) Thrust removed.

Figure 29.- Concluded.

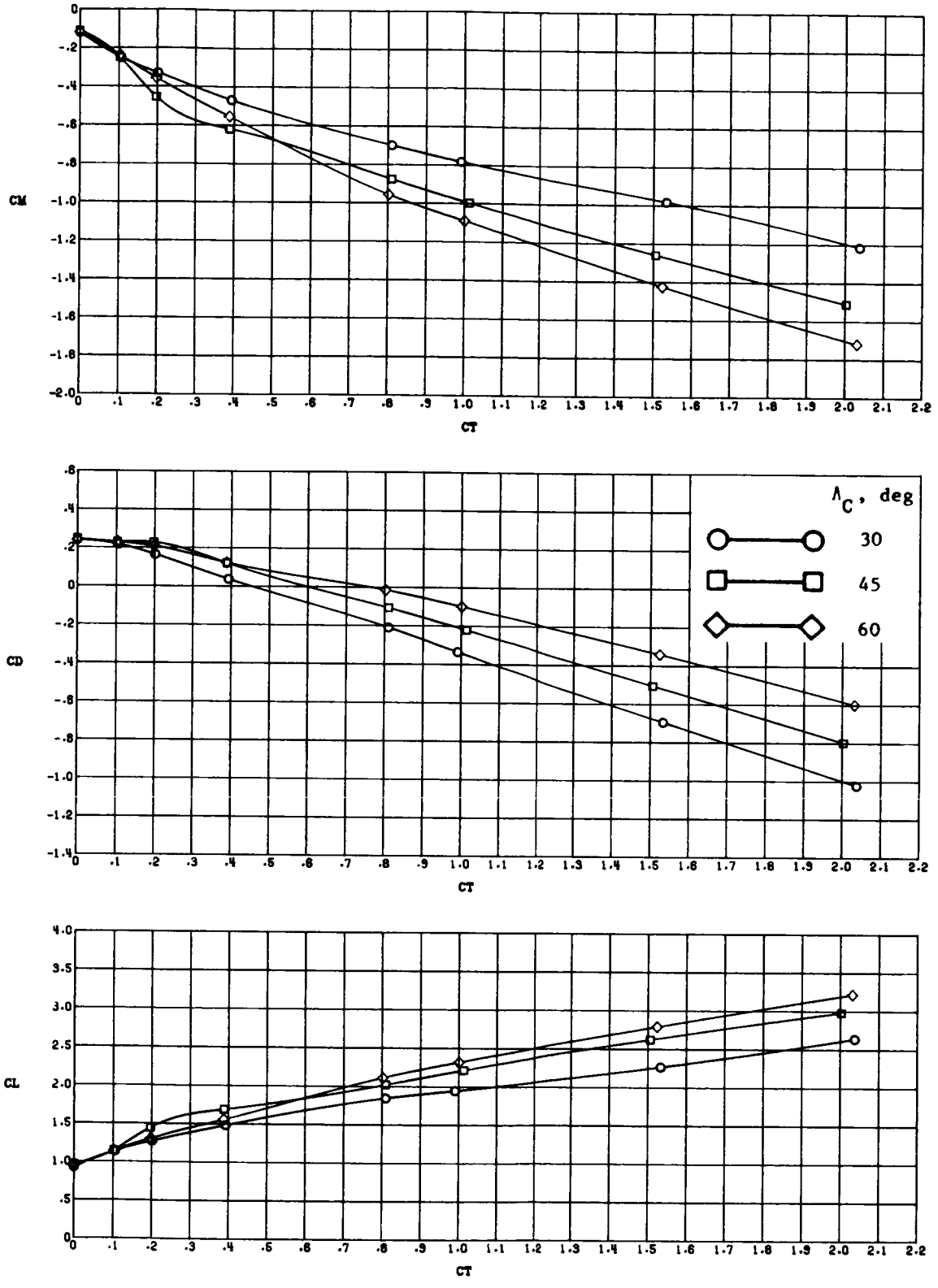

(a) Thrust included.

Figure 30.- Effect of cascade vector angle on longitudinal aerodynamic characteristics at various thrust coefficients with $\alpha = 12°$ and $\delta_f = 45°/26°$.

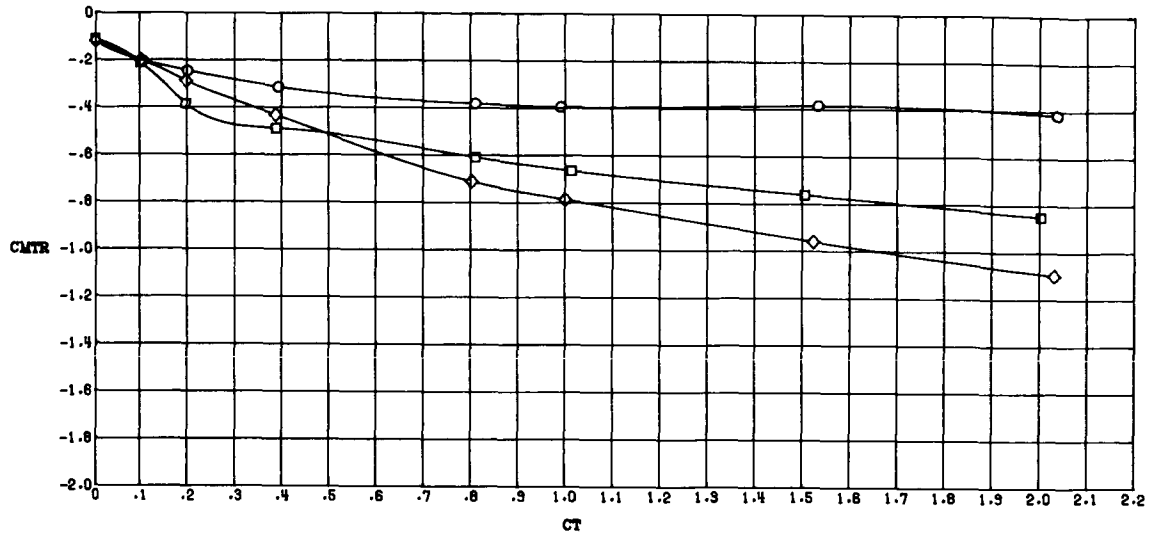

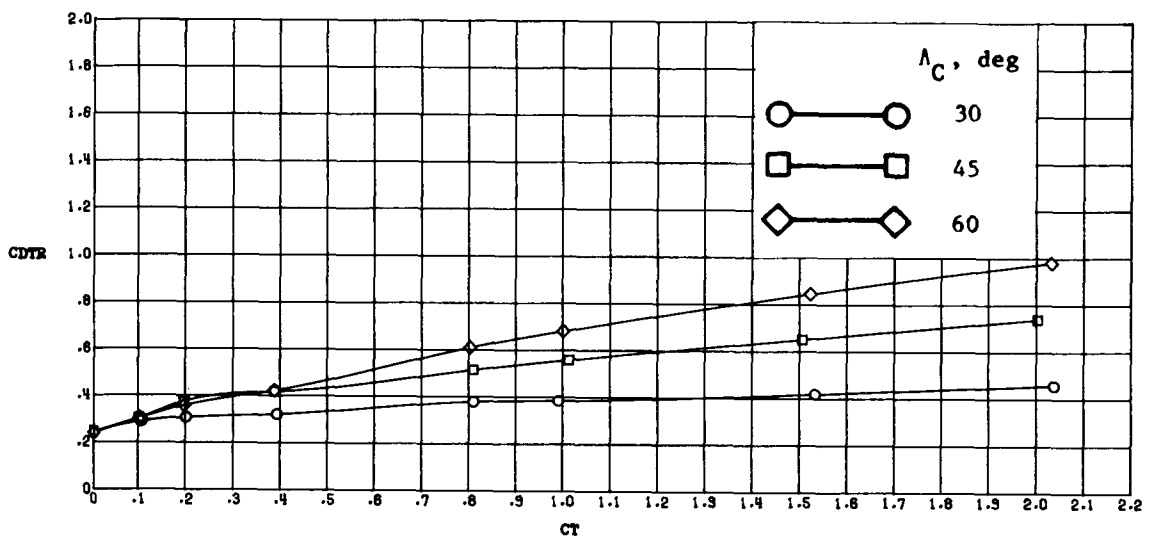

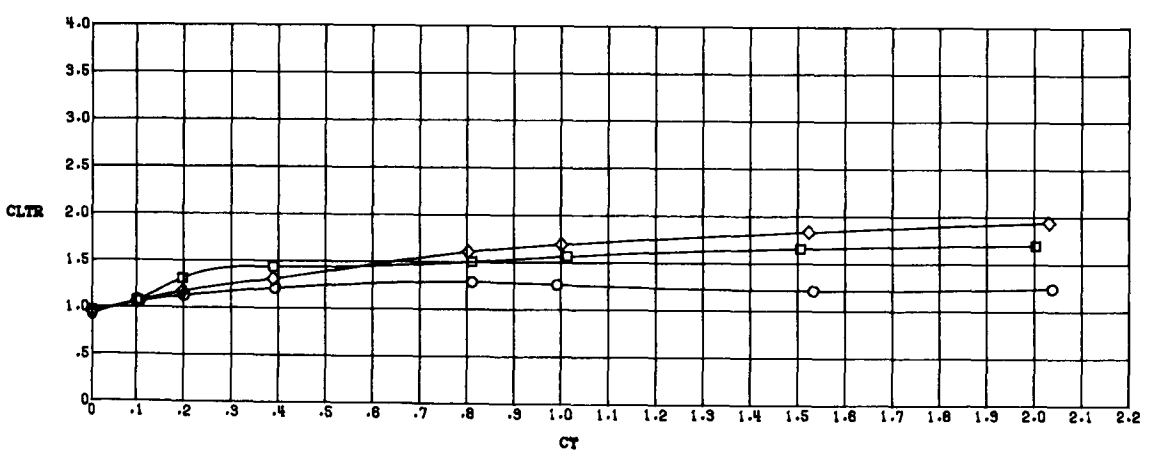

(b) Thrust removed.

Figure 30.- Concluded.

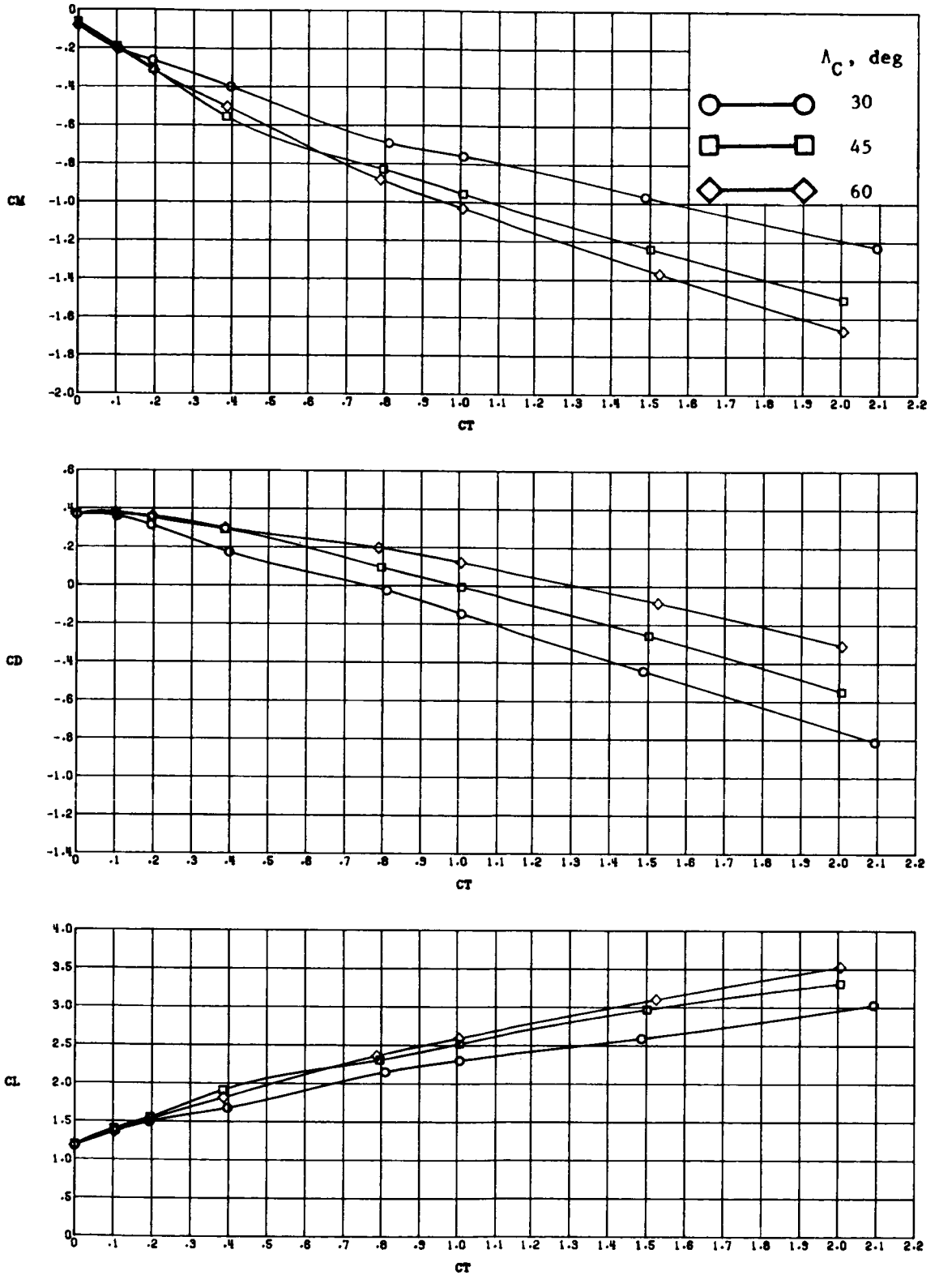

(a) Thrust included.

Figure 31.- Effect of cascade vector angle on longitudinal aerodynamic characteristics at various thrust coefficients with $\alpha = 16°$ and $\delta_f = 45°/26°$.

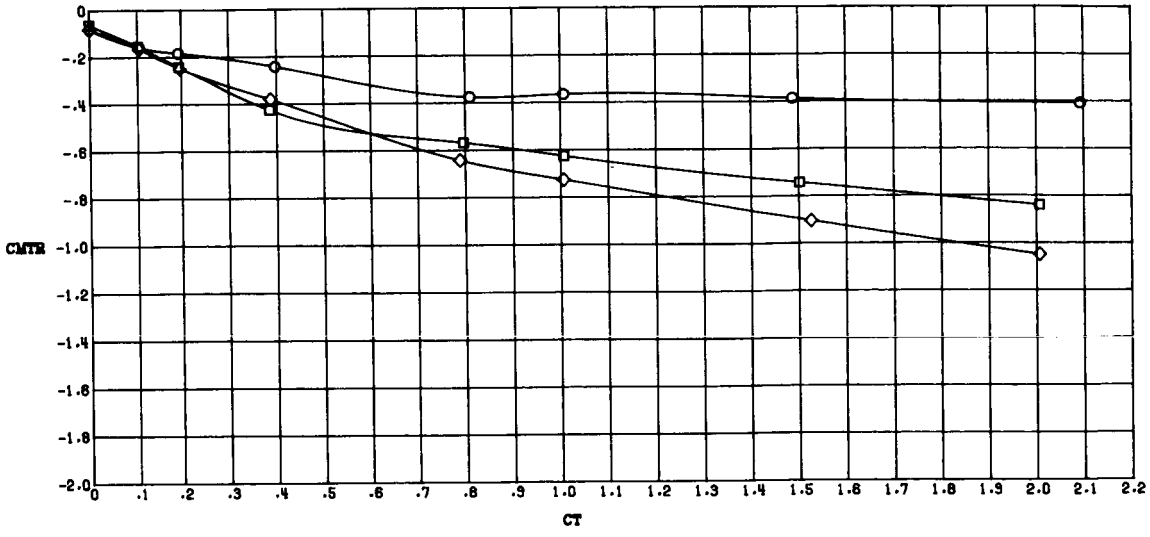

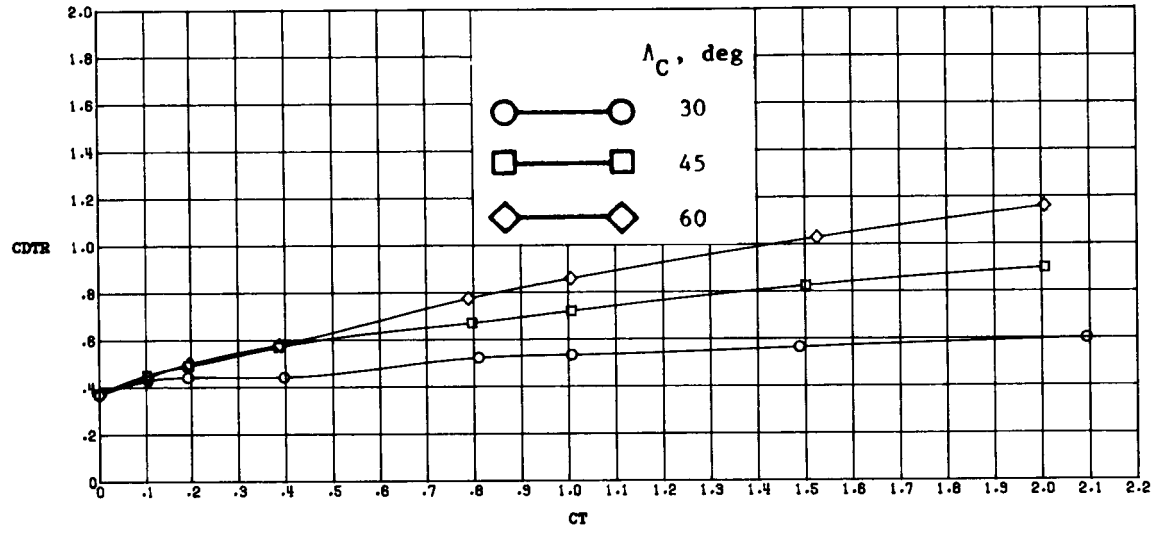

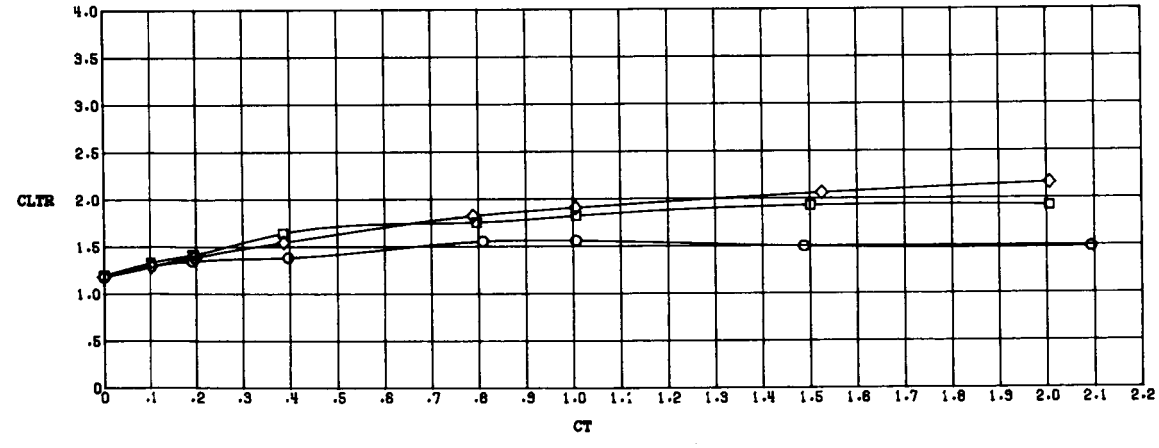

(b) Thrust removed.

Figure 31.- Concluded.

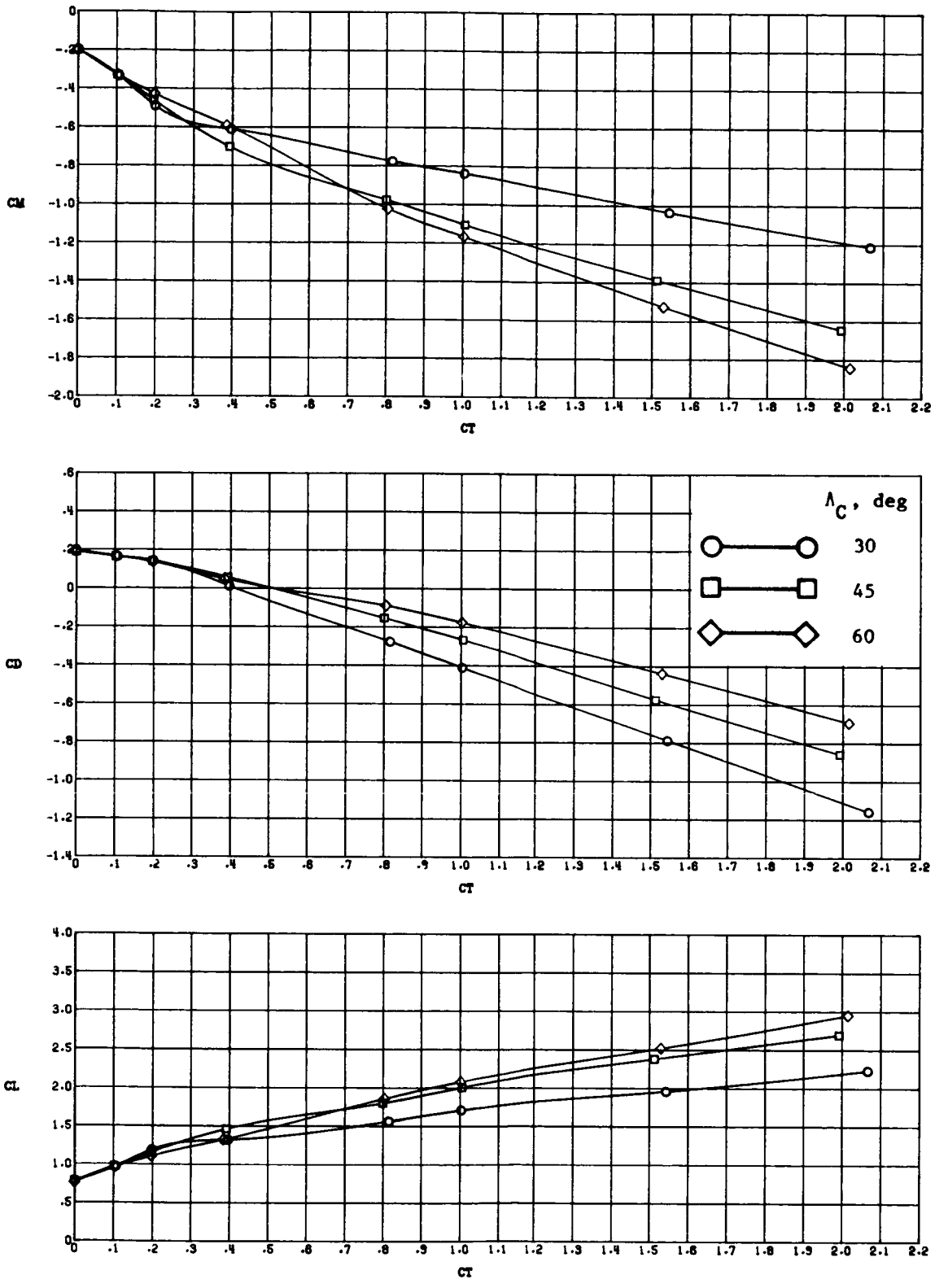

(a) Thrust included.

Figure 32.- Effect of cascade vector angle on longitudinal aerodynamic characteristics at various thrust coefficients with $\alpha = 8°$ and $\delta_f = 45°/45°$.

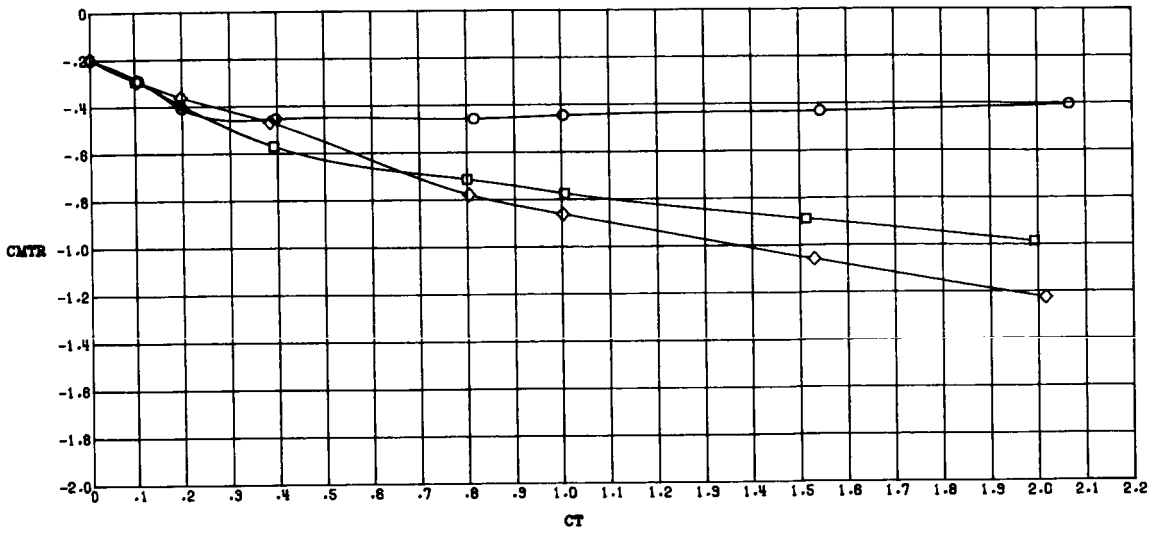

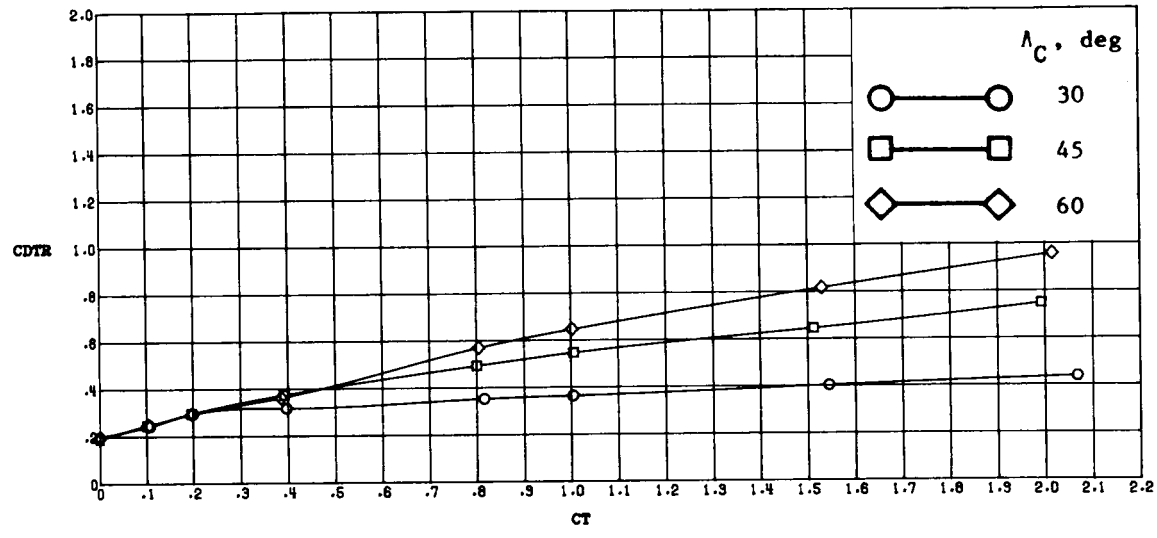

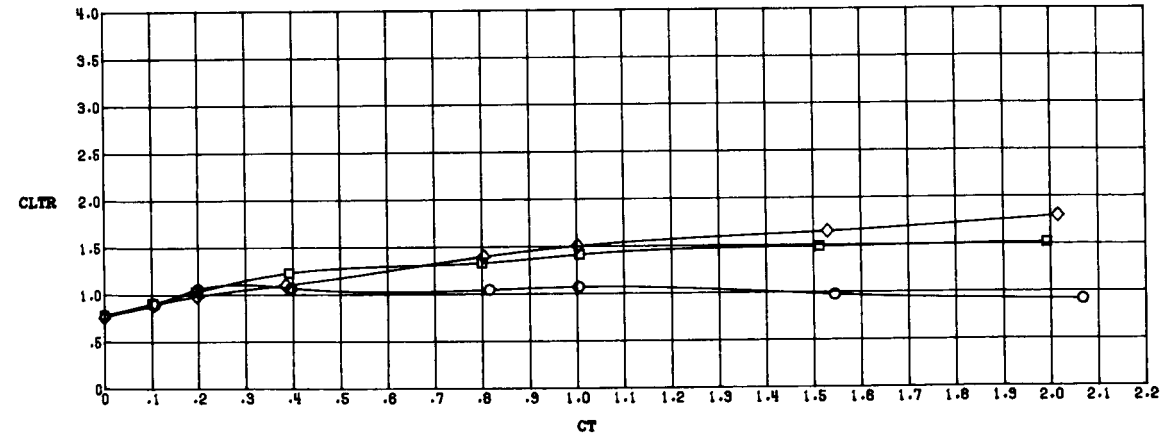

(b) Thrust removed.

Figure 32.- Concluded.

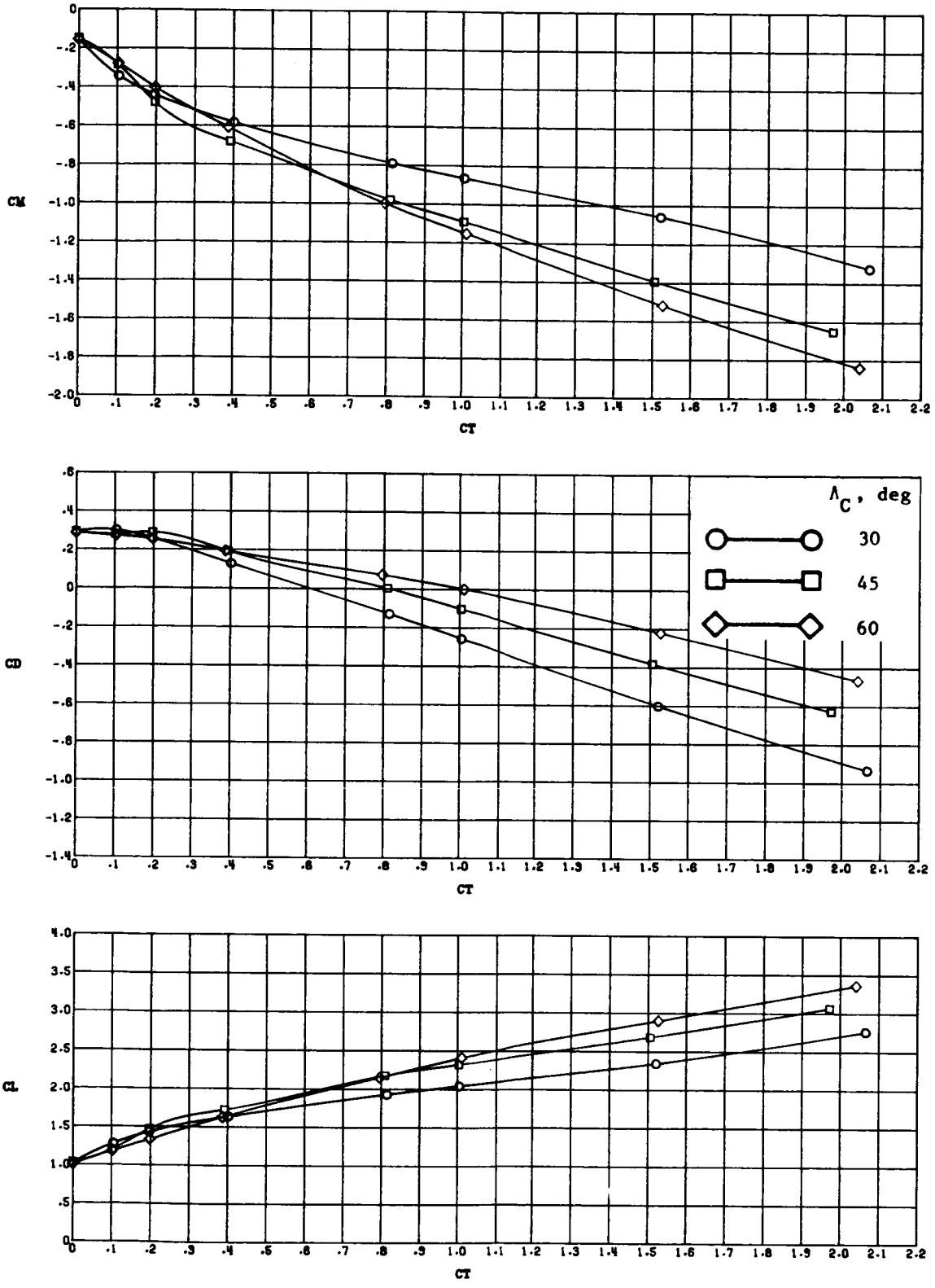

(a) Thrust included.

Figure 33.- Effect of cascade vector angle on longitudinal aerodynamic characteristics at various thrust coefficients with $\alpha = 12°$ and $\delta_f = 45°/45°$.

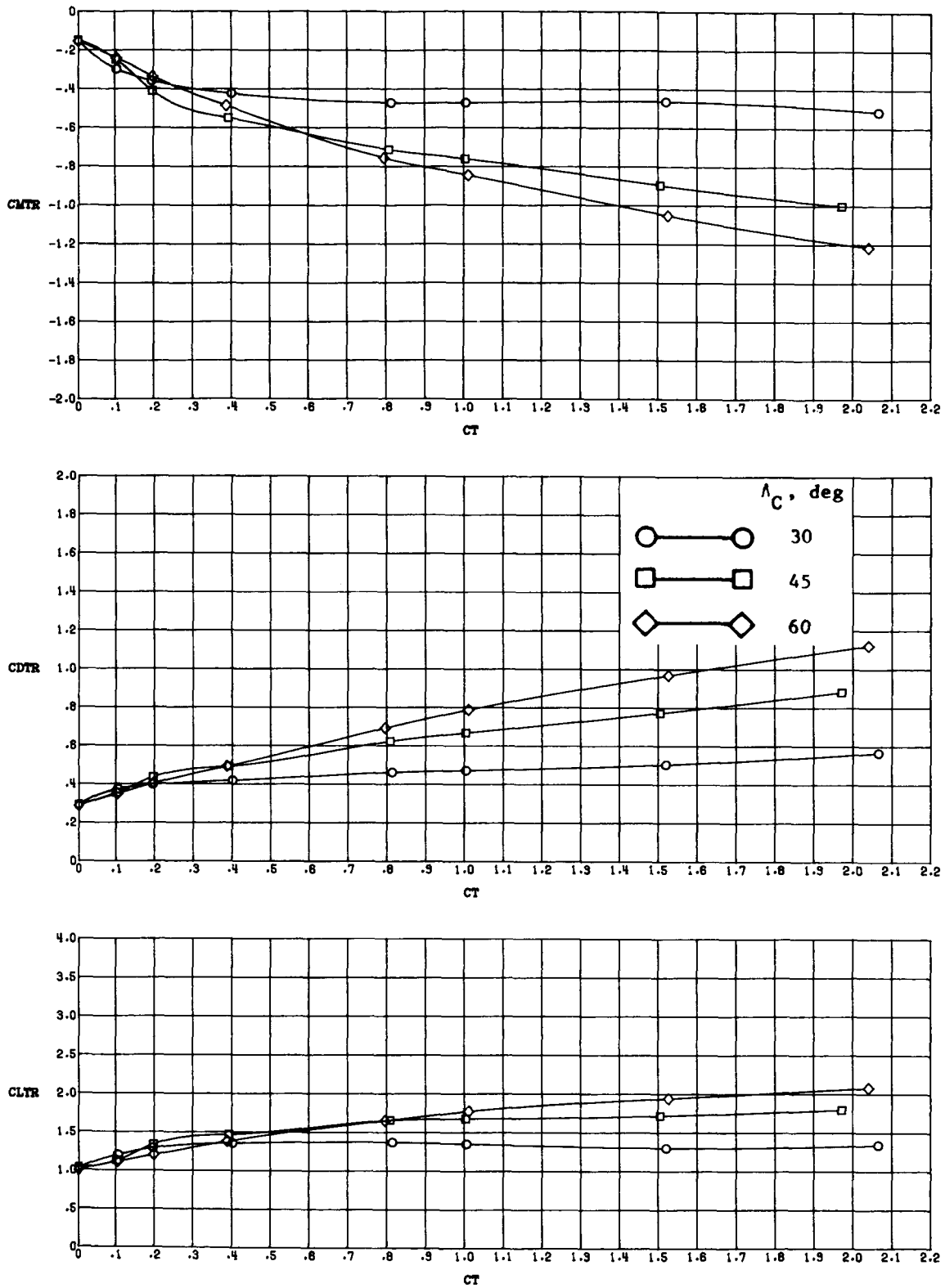

(b) Thrust removed.

Figure 33.- Concluded.

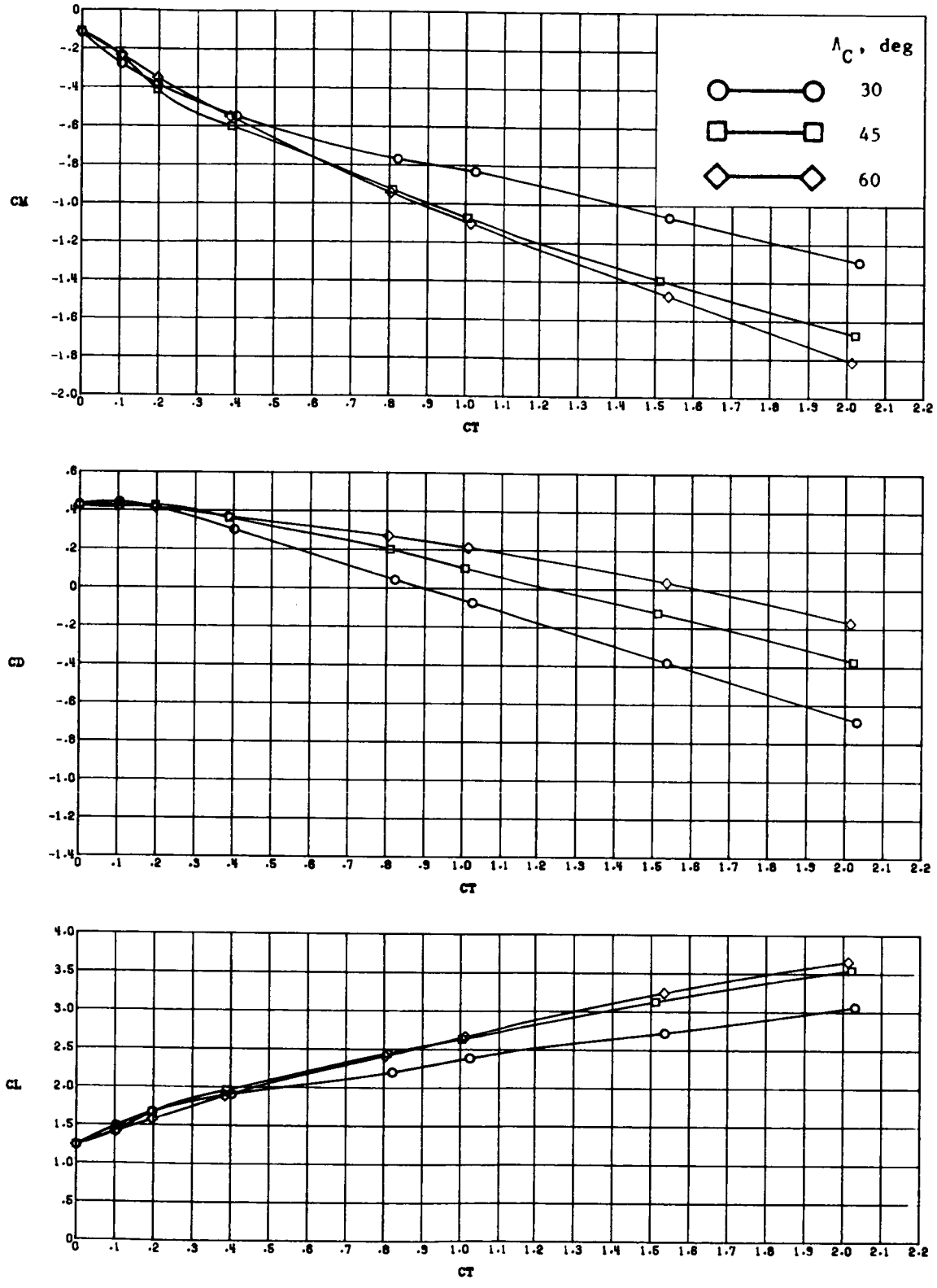

(a) Thrust included.

Figure 34.- Effect of cascade vector angle on longitudinal aerodynamic characteristics at various thrust coefficients with $\alpha = 16°$ and $\delta_f = 45°/45°$.

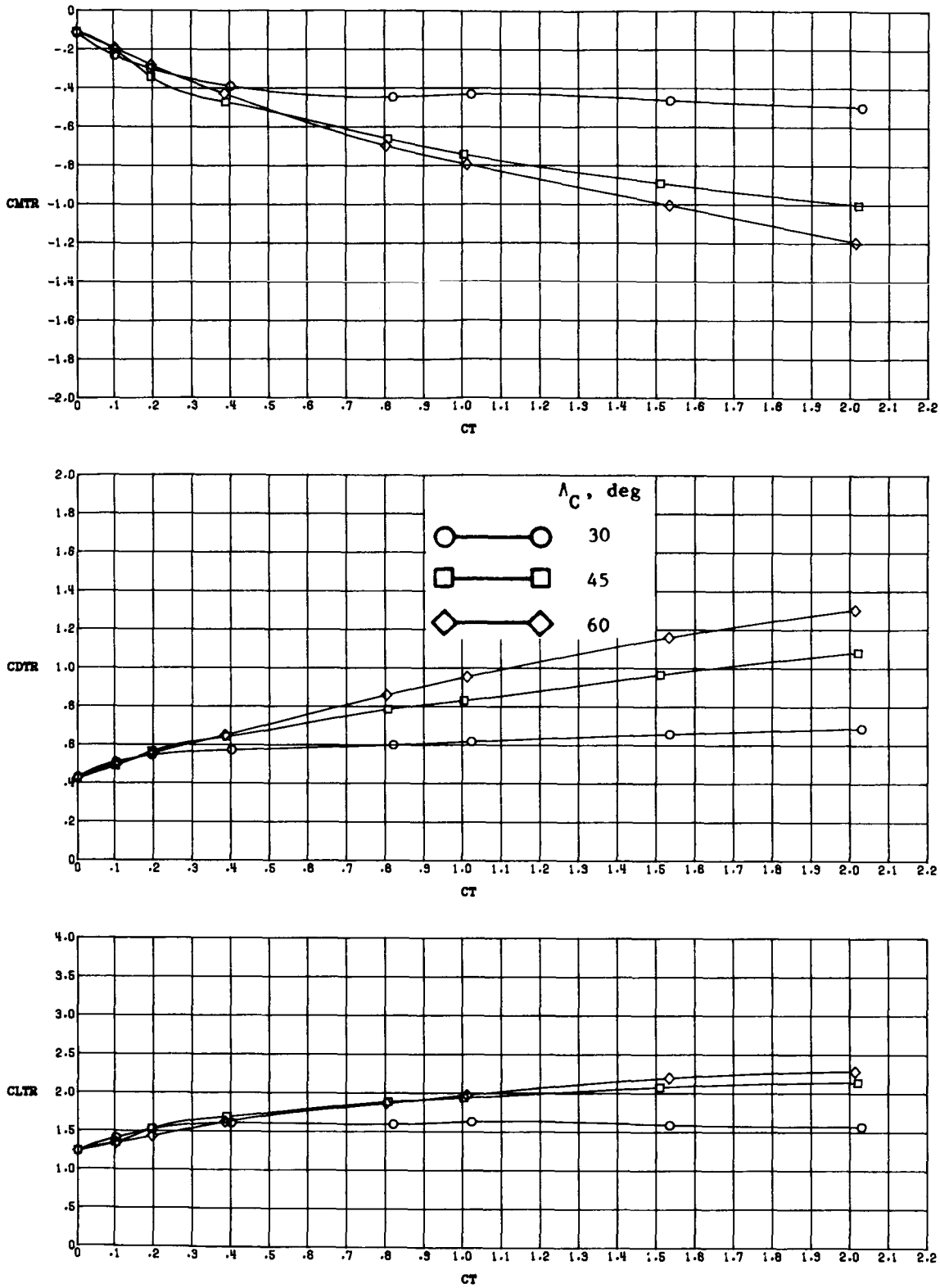

(b) Thrust removed.

Figure 34.- Concluded.

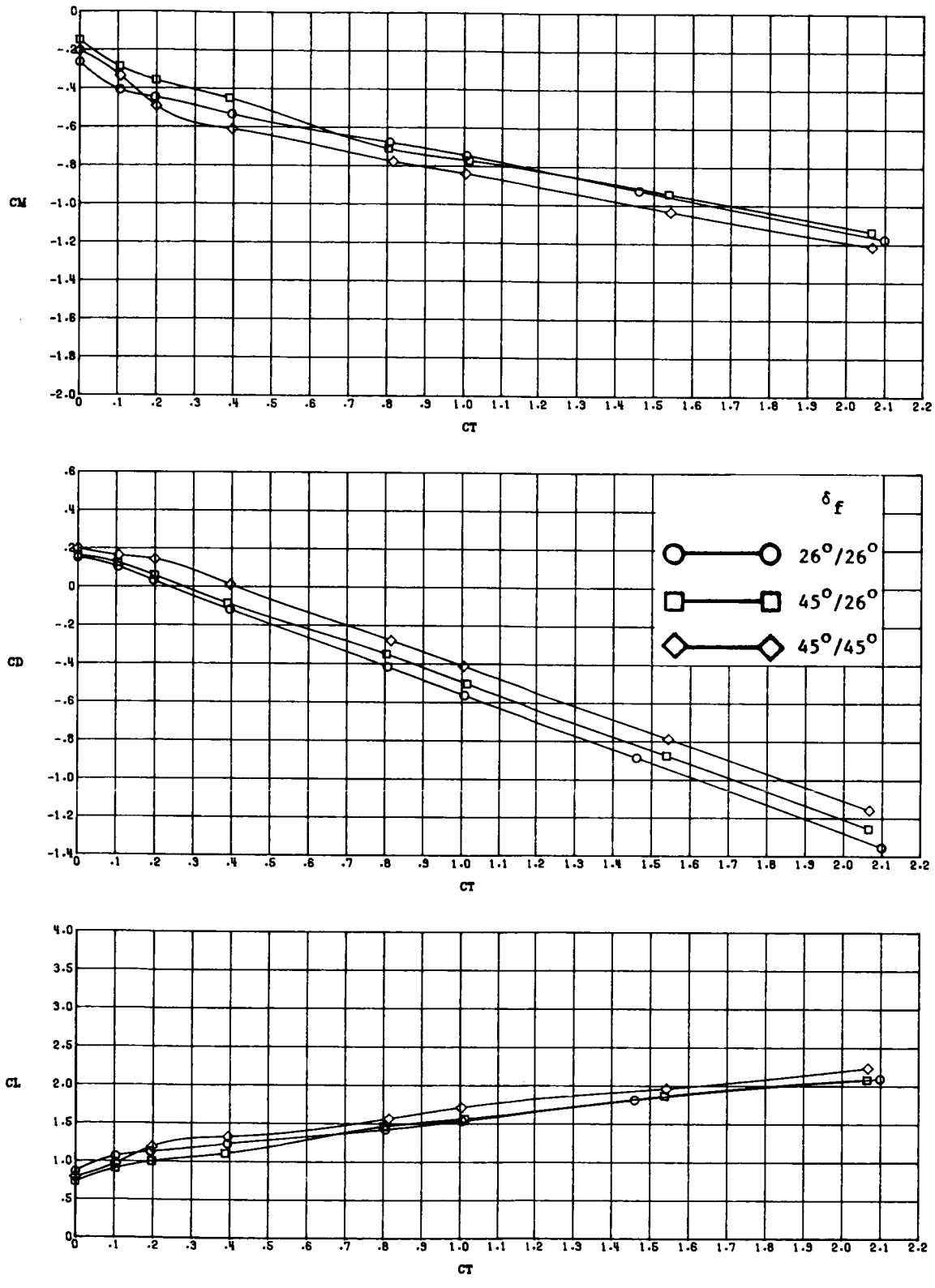

(a) Thrust included.

Figure 35.- Effect of flap deflection angle on longitudinal aerodynamic characteristics at various thrust coefficients with $\alpha = 8°$ and $\Lambda_C = 30°$.

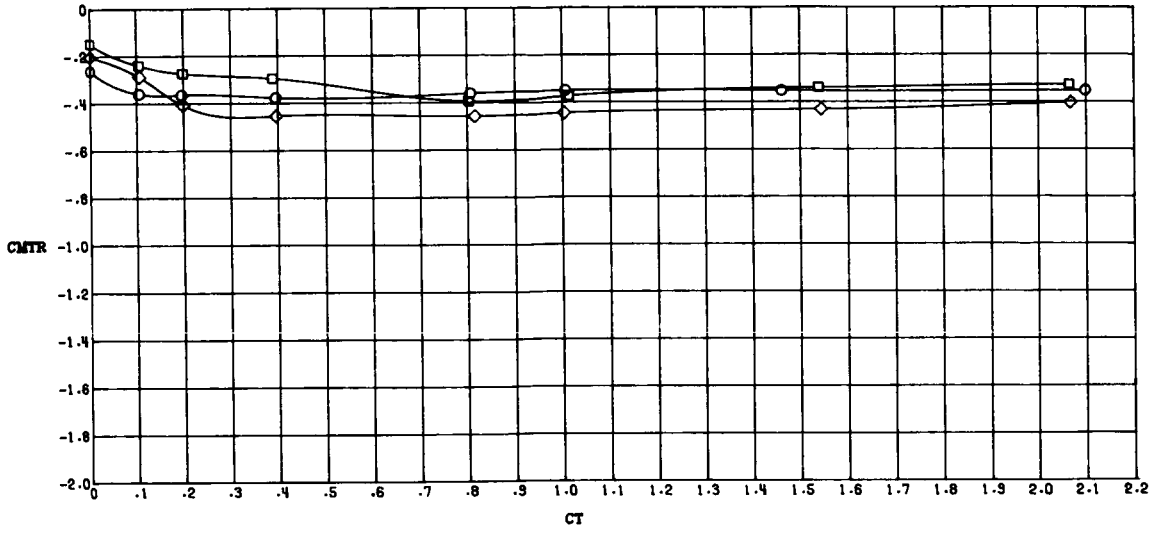

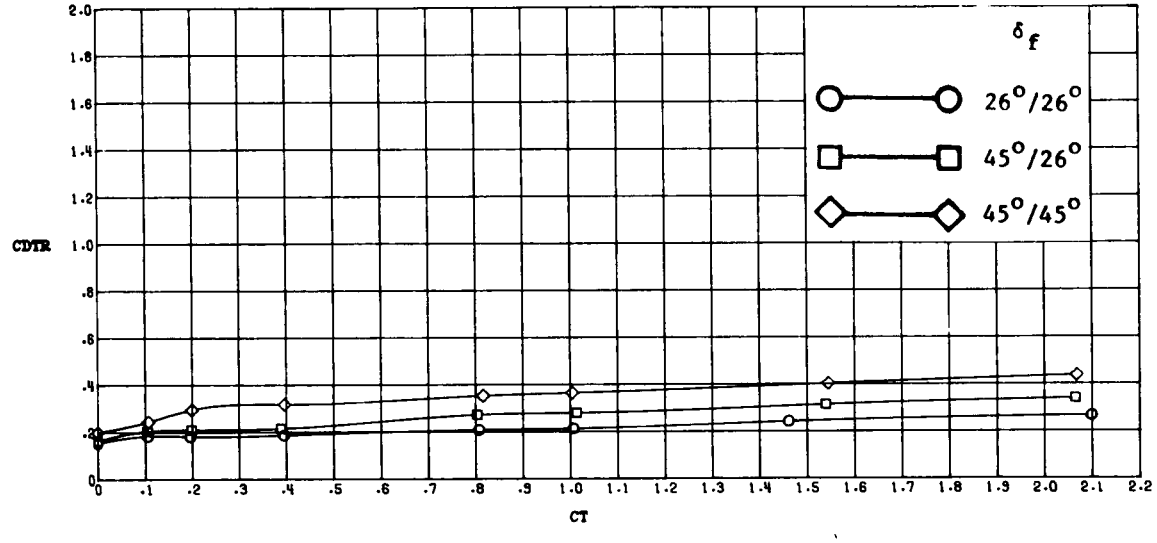

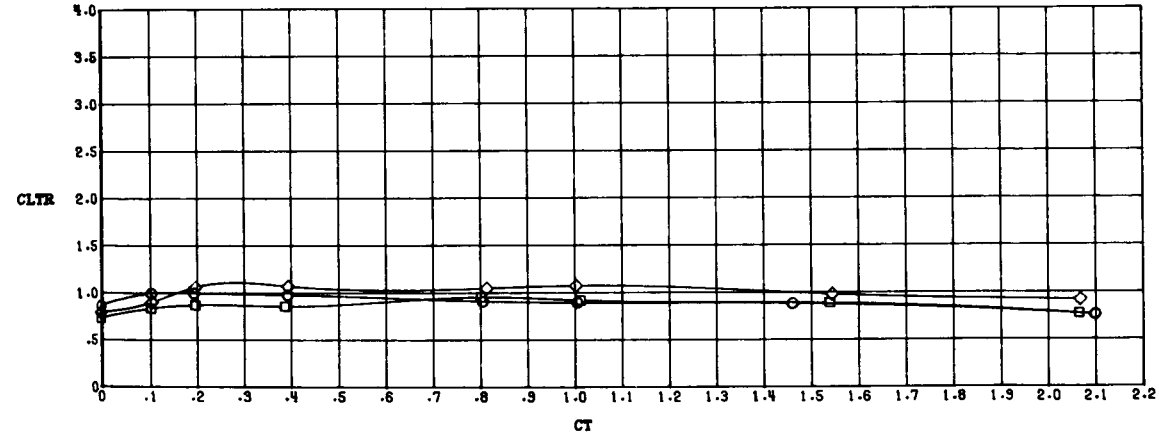

(b) Thrust removed.

Figure 35.- Concluded.

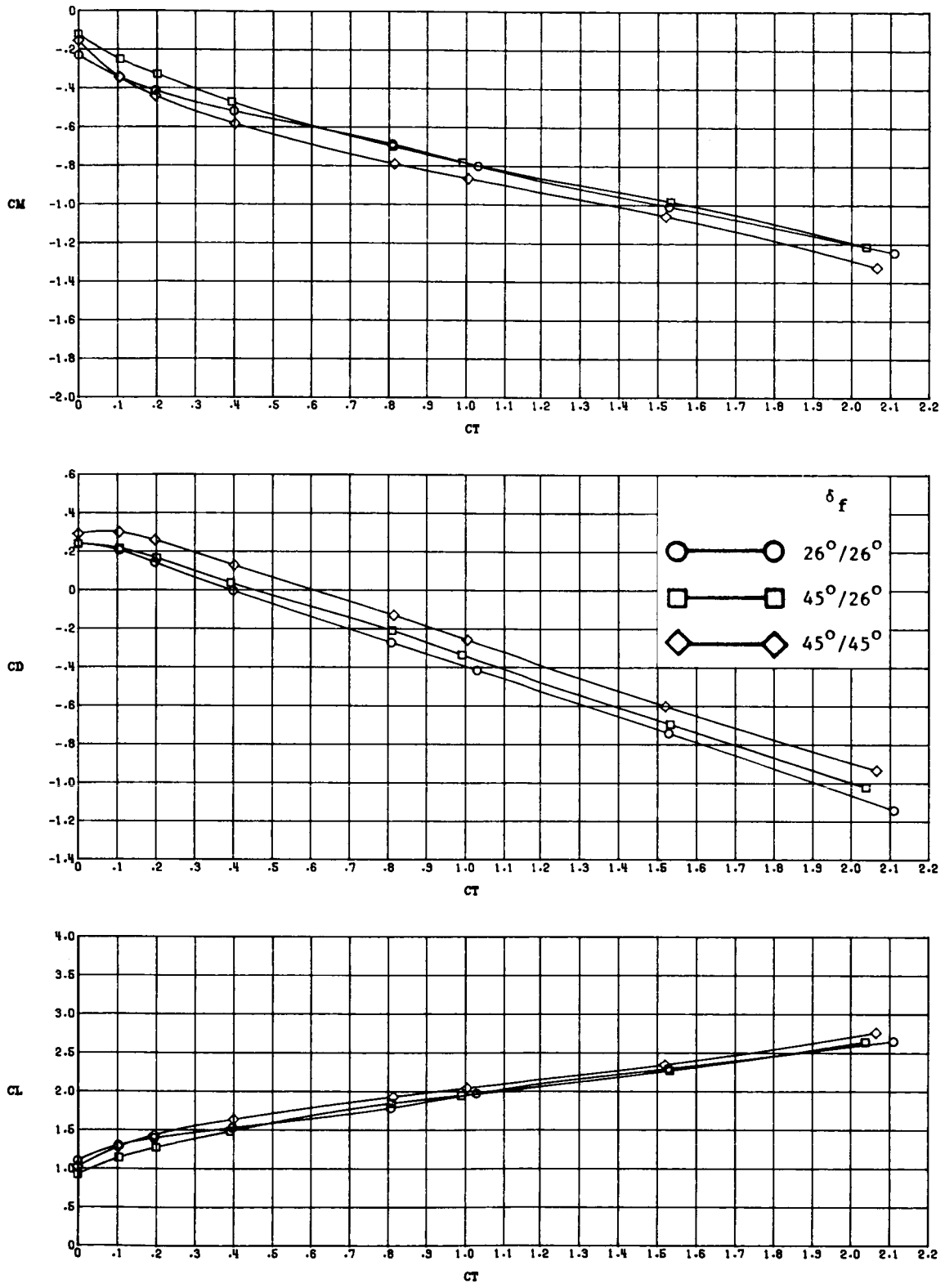

(a) Thrust included.

Figure 36.- Effect of flap deflection angle on longitudinal aerodynamic characteristics at various thrust coefficients with $\alpha = 12°$ and $\Lambda_C = 30°$.

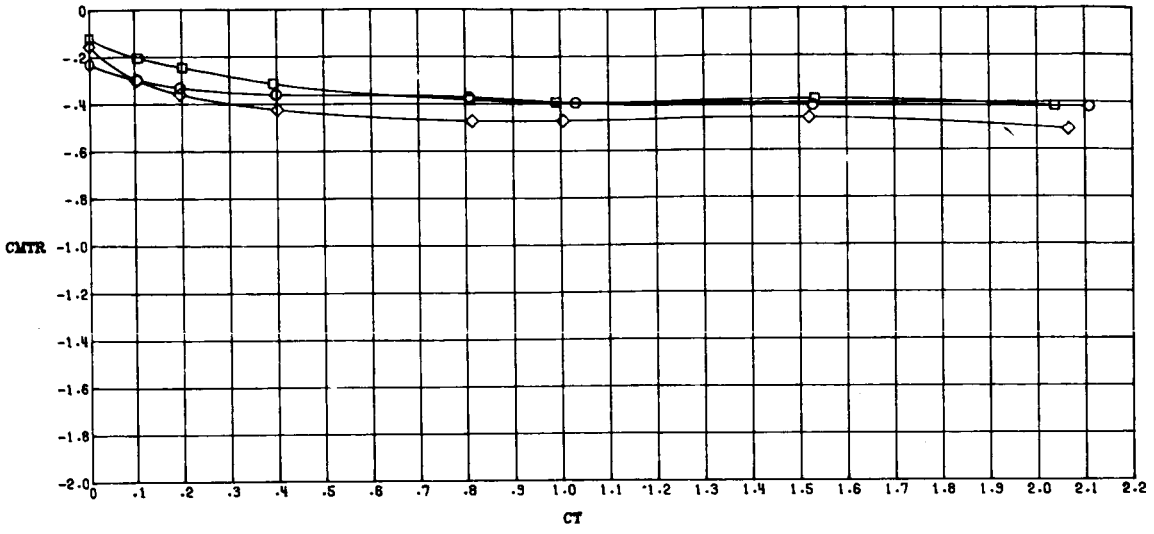

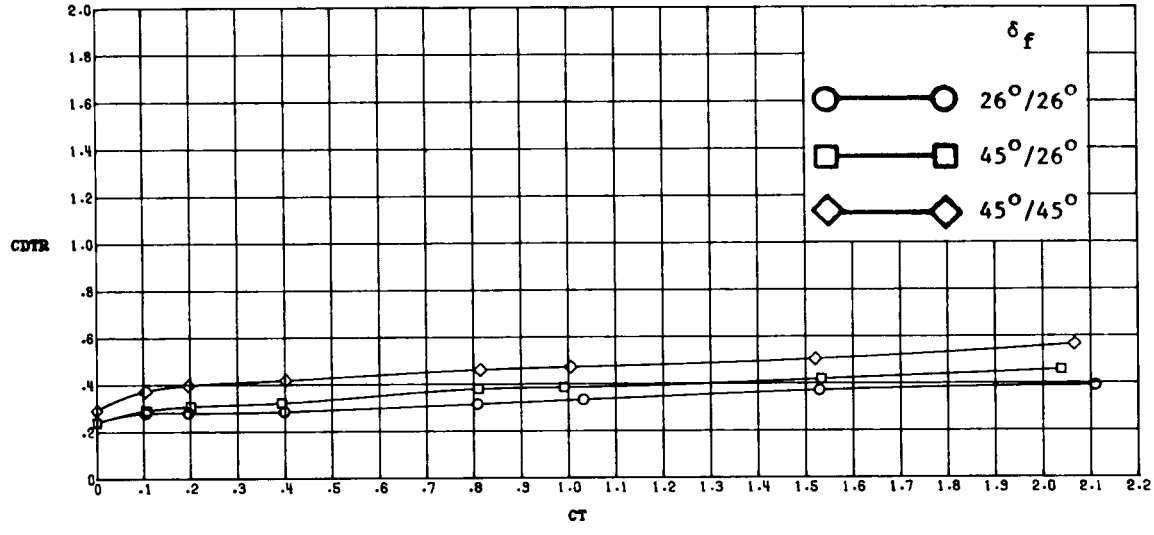

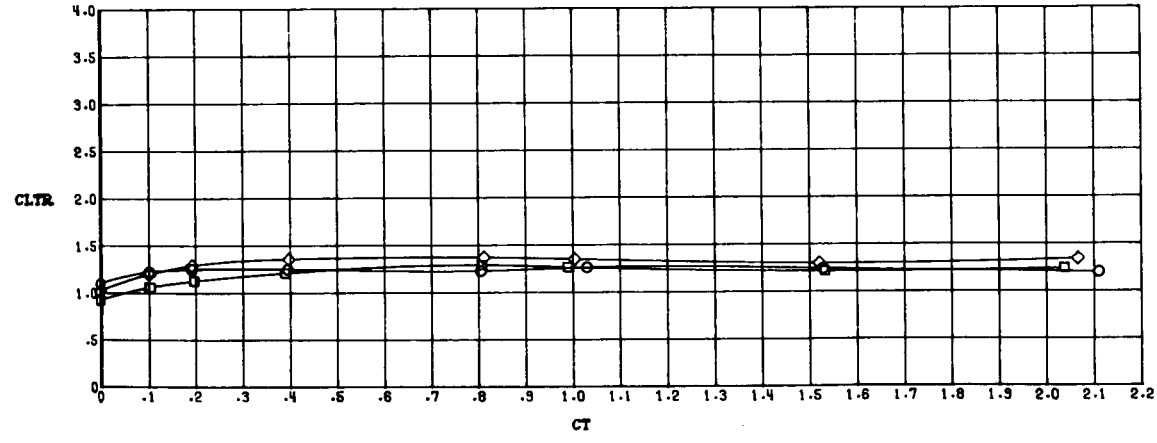

(b) Thrust removed.

Figure 36.- Concluded.

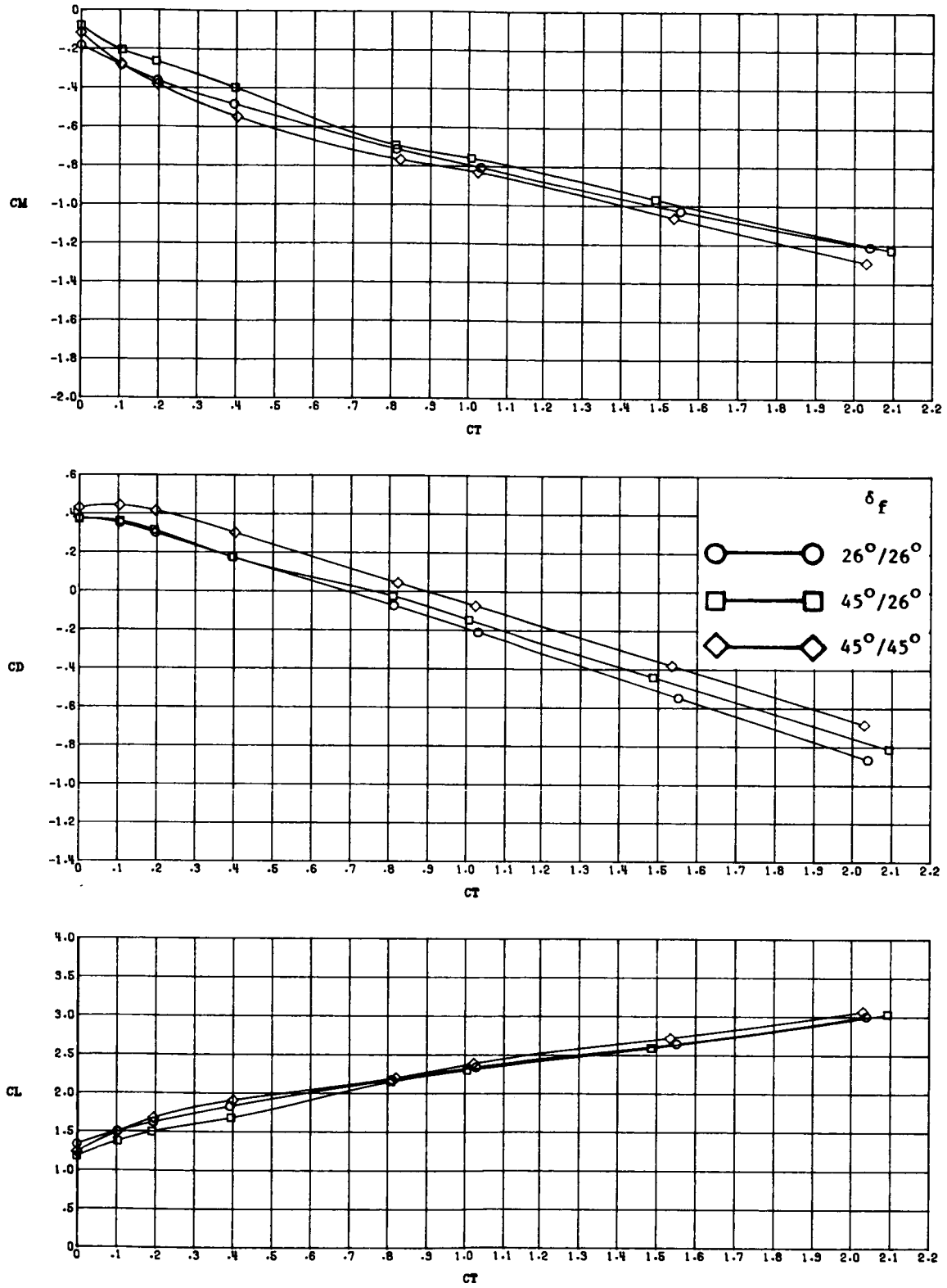

(a) Thrust included.

Figure 37.- Effect of flap deflection angle on longitudinal aerodynamic characteristics at various thrust coefficients with $\alpha = 16°$ and $\Lambda_C = 30°$.

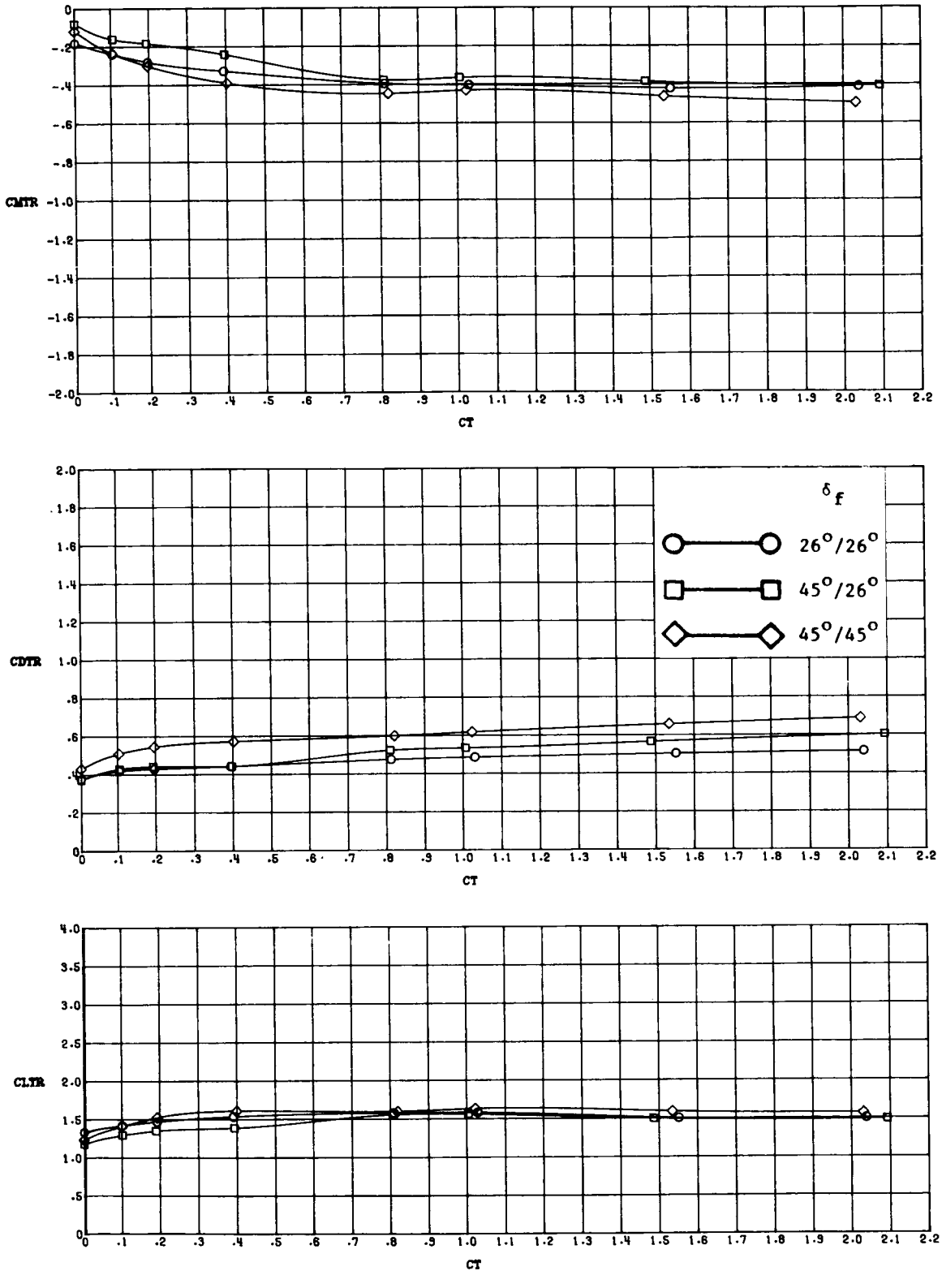

(b) Thrust removed.

Figure 37.- Concluded.

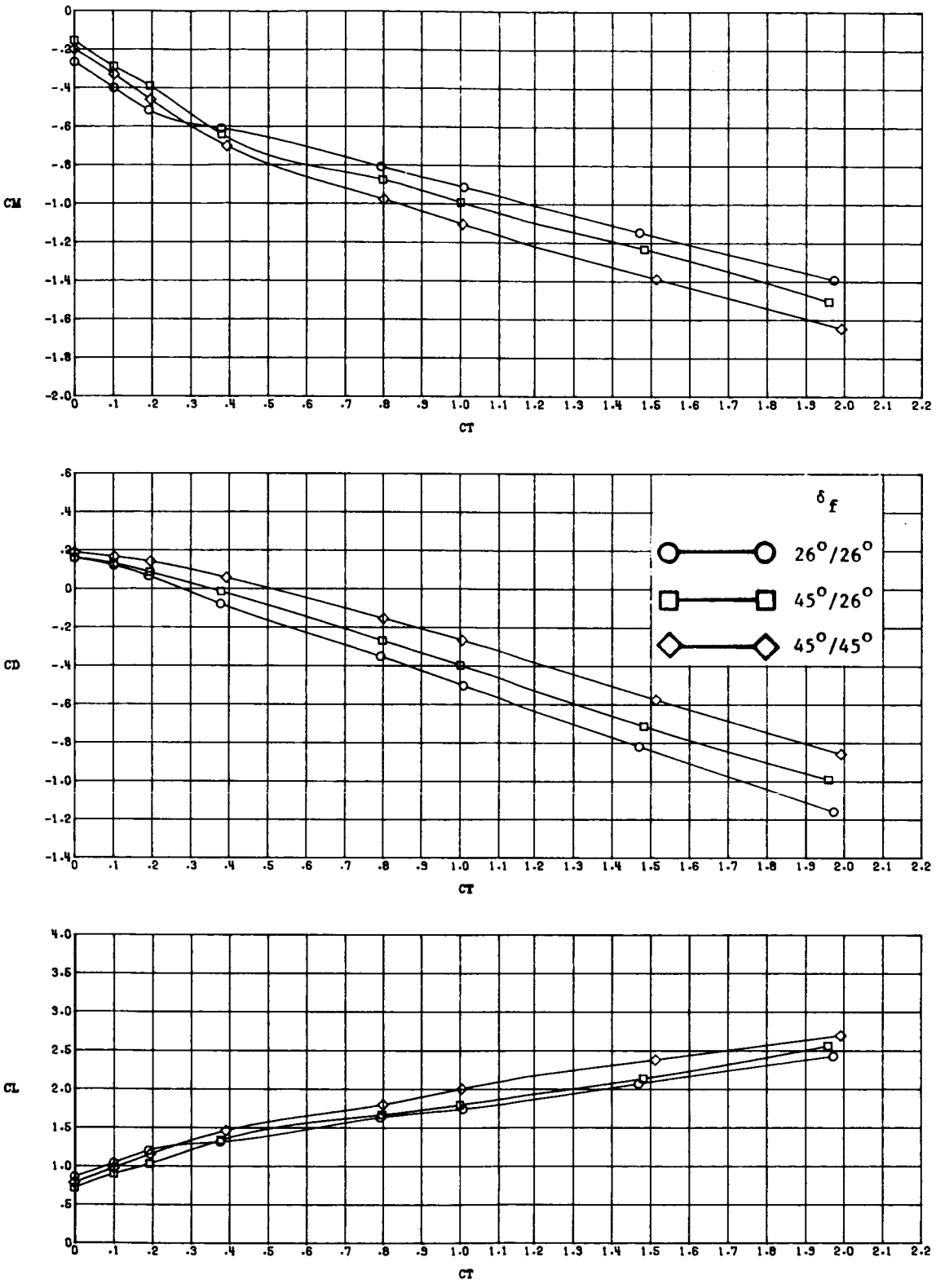

(a) Thrust included.

Figure 38.- Effect of flap deflection angle on longitudinal aerodynamic characteristics at various thrust coefficients with $\alpha = 8°$ and $\Lambda_C = 45°$.

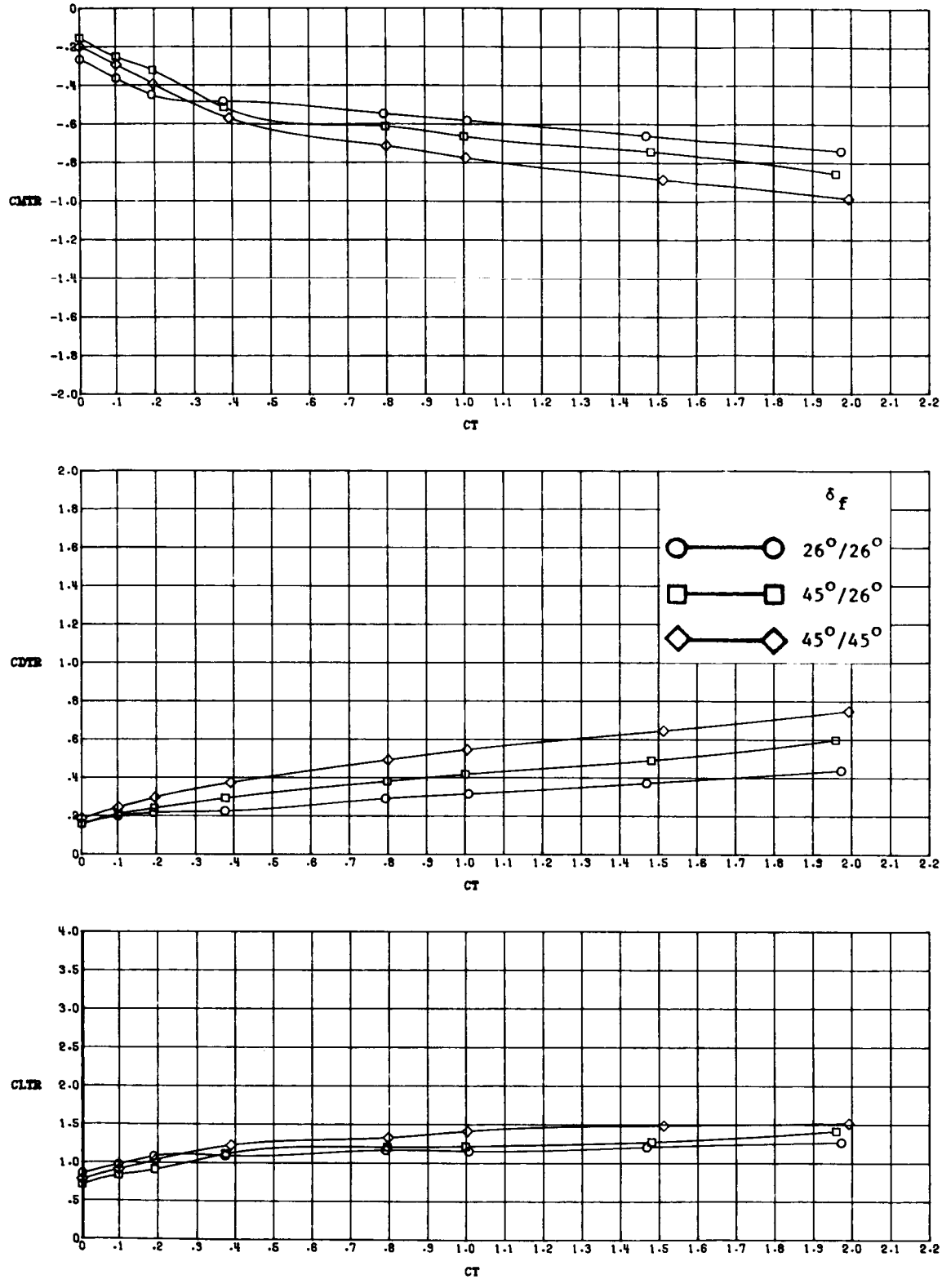

(b) Thrust removed.

Figure 38.- Concluded.

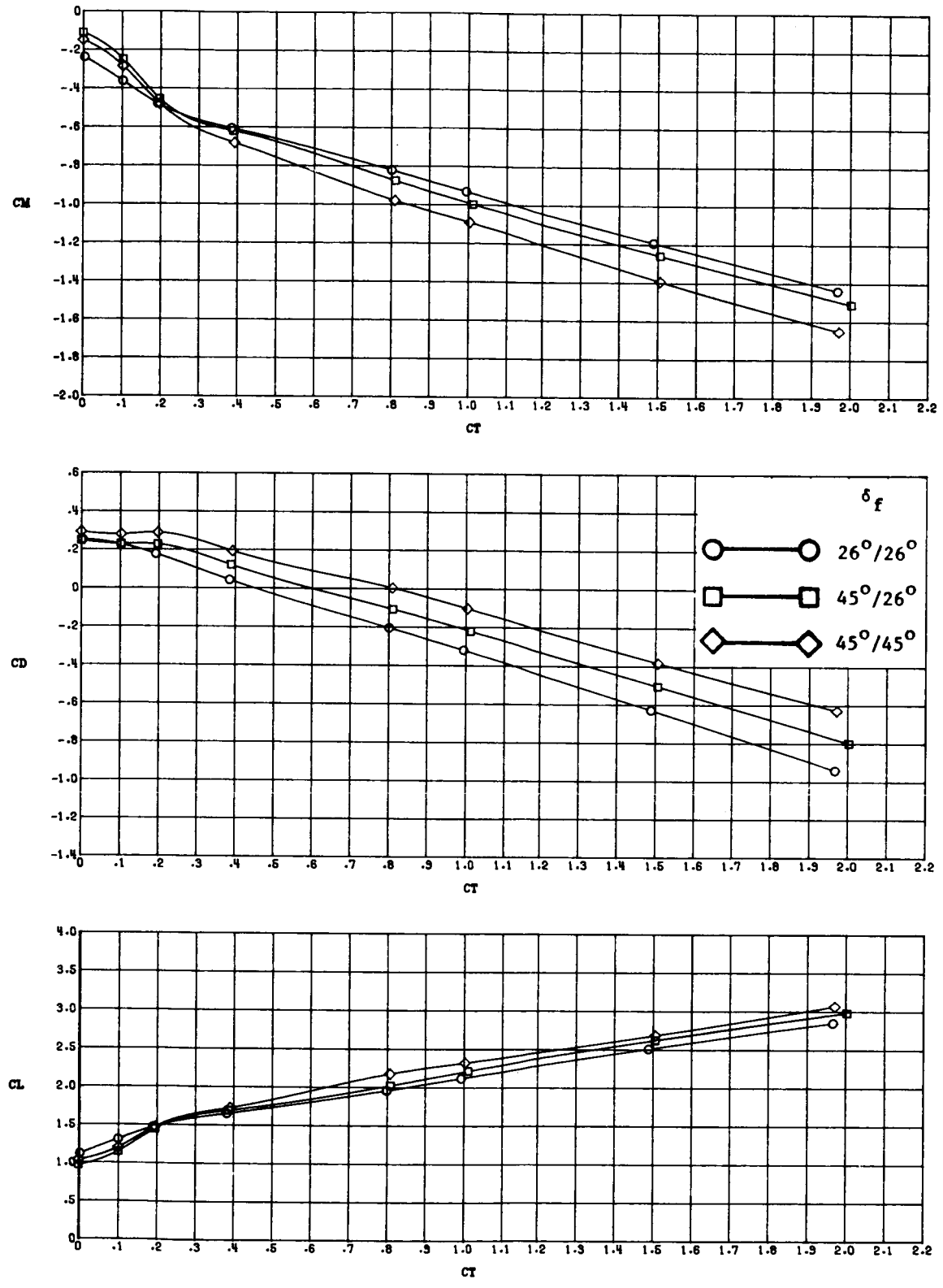

(a) Thrust included.

Figure 39.- Effect of flap deflection angle on longitudinal aerodynamic characteristics at various thrust coefficients with $\alpha = 12°$ and $\Lambda_C = 45°$.

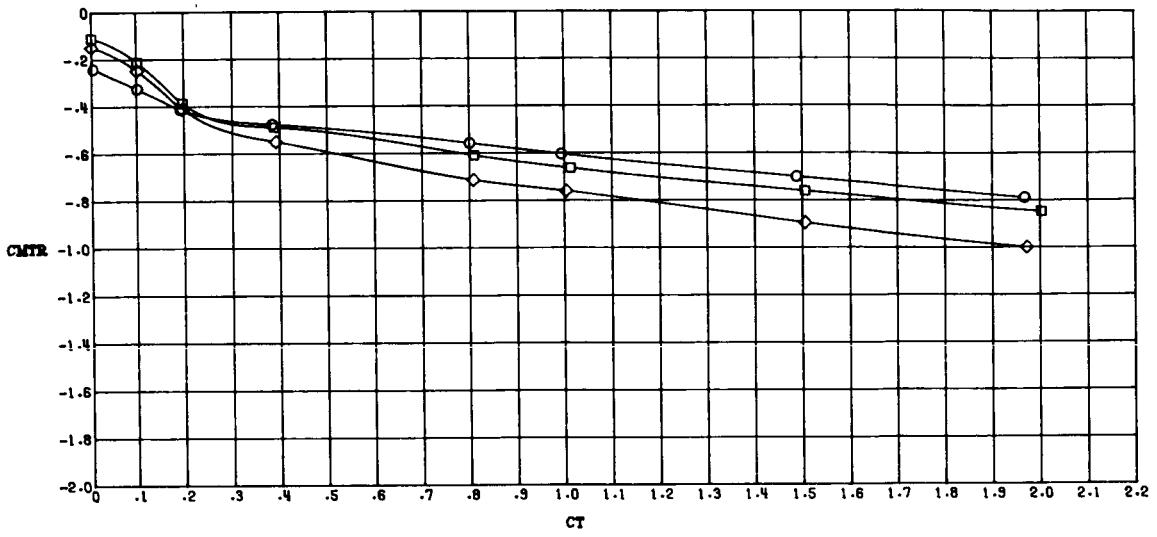

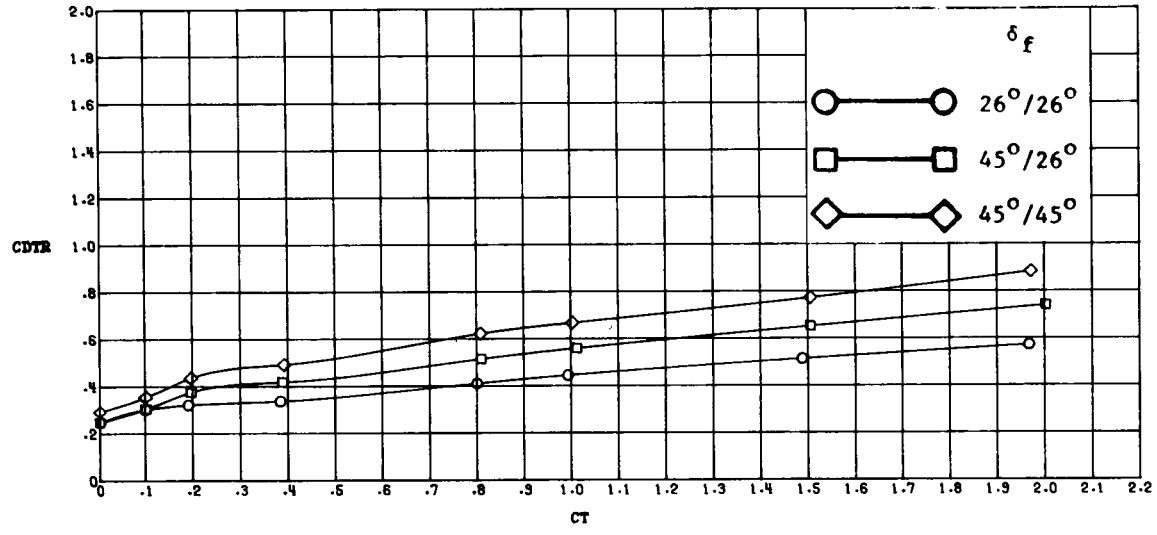

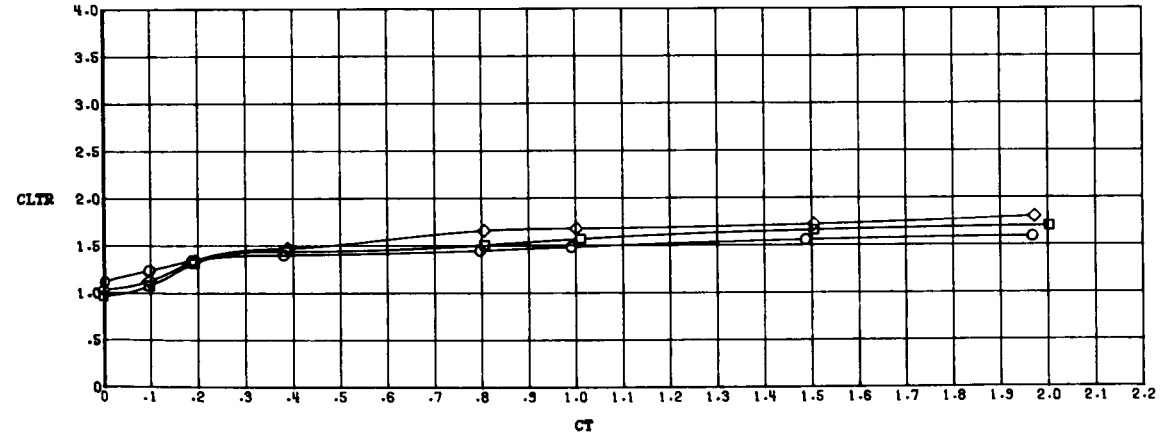

(b) Thrust removed.

Figure 39.- Concluded.

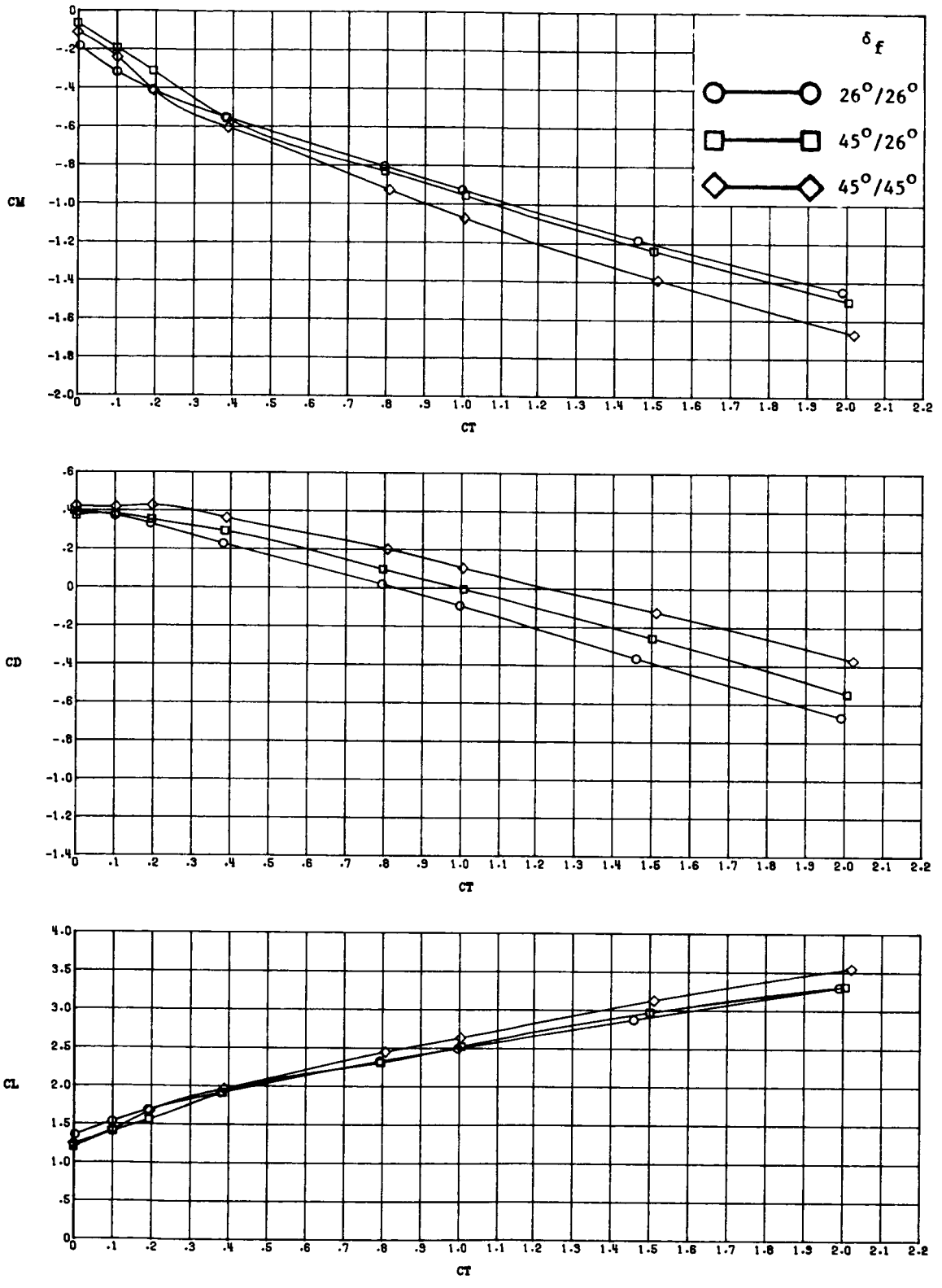

(a) Thrust included.

Figure 40.- Effect of flap deflection angle on longitudinal aerodynamic characteristics at various thrust coefficients with α = 16° and Λ_C = 45°.

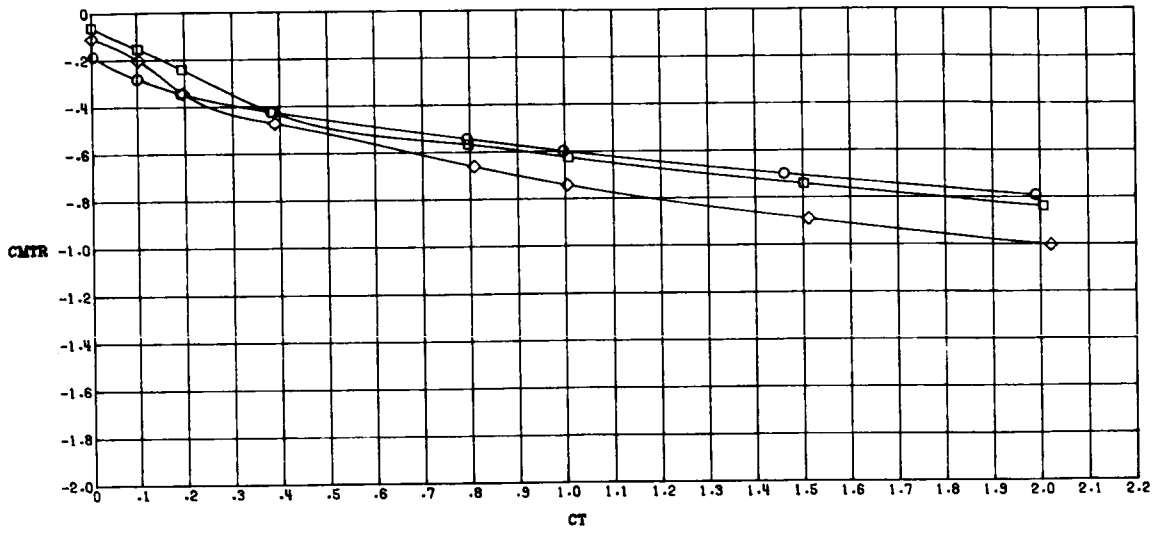

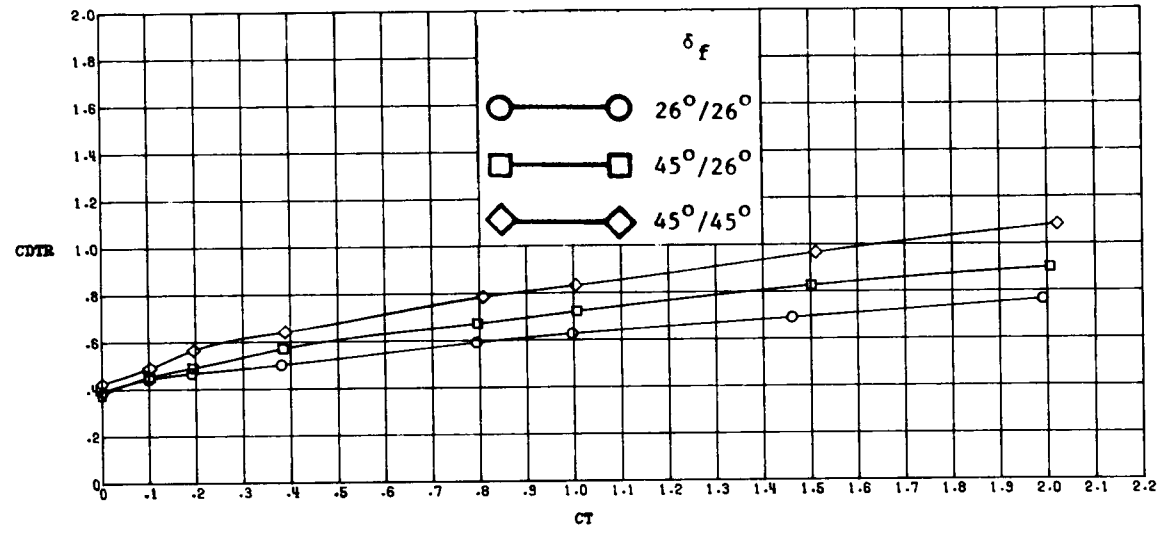

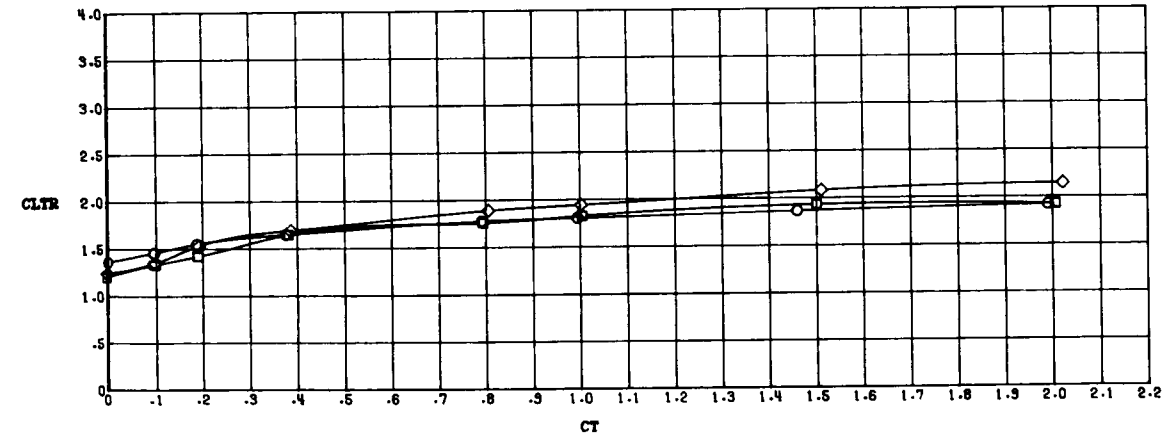

(b) Thrust removed.

Figure 40.- Concluded.

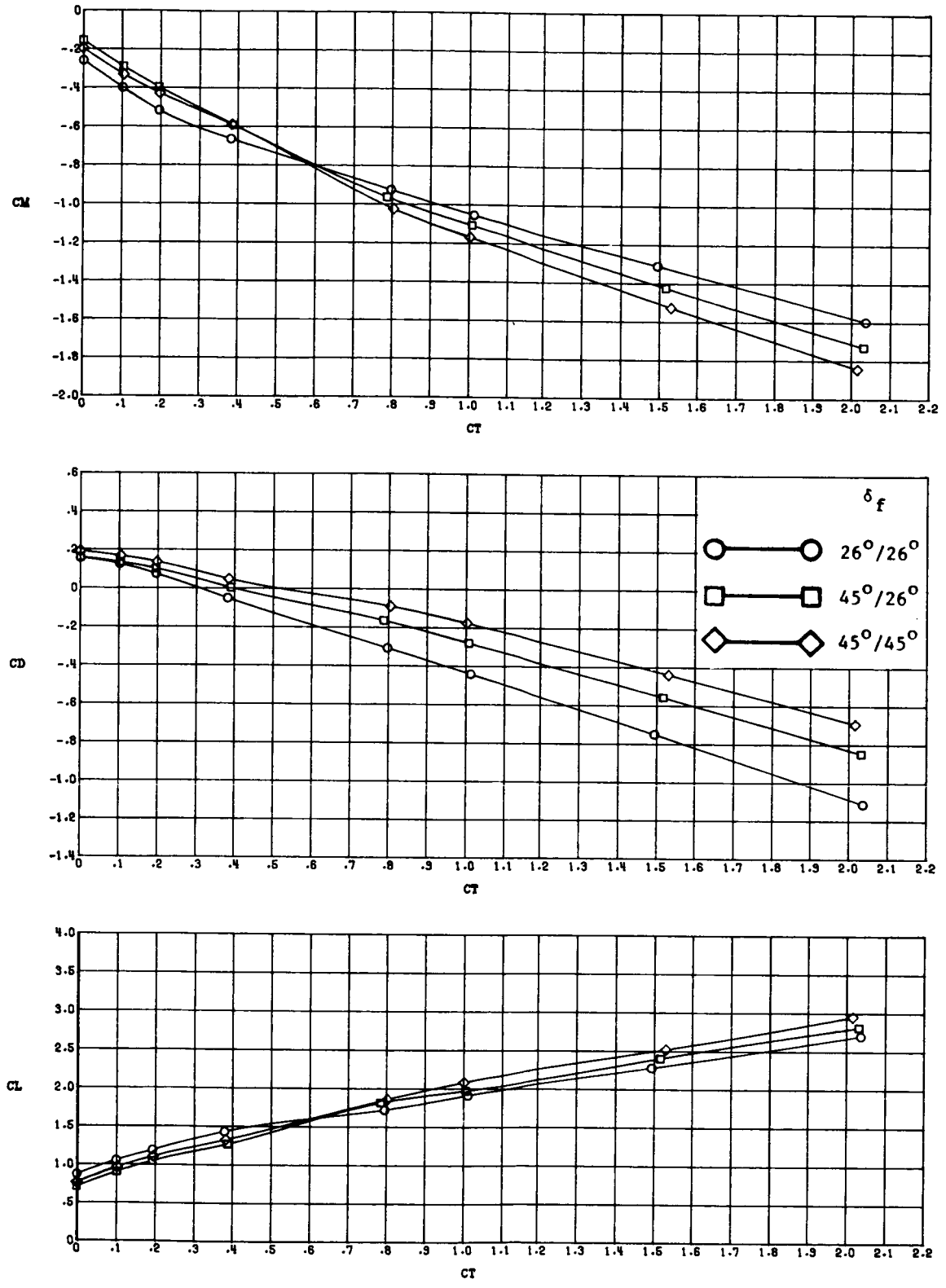

(a) Thrust included.

Figure 41.- Effect of flap deflection angle on longitudinal aerodynamic characteristics at various thrust coefficients with $\alpha = 8°$ and $\Lambda_C = 60°$.

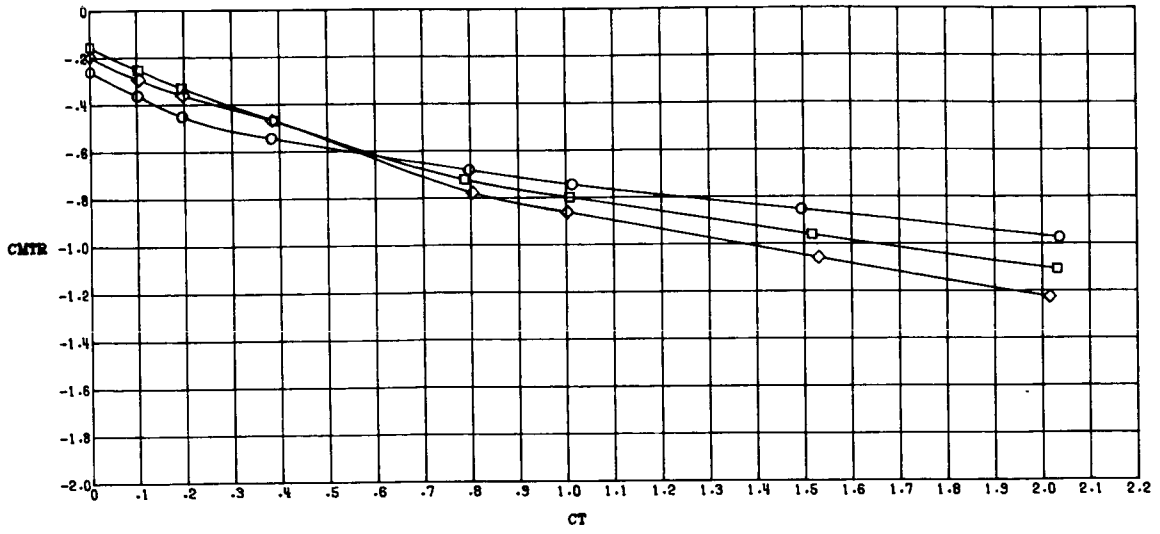

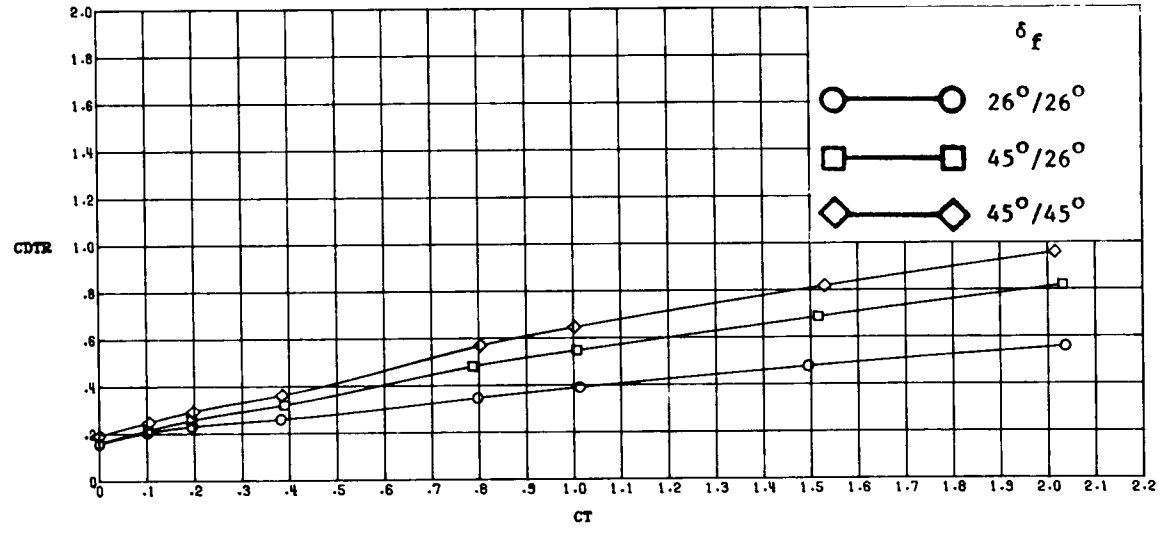

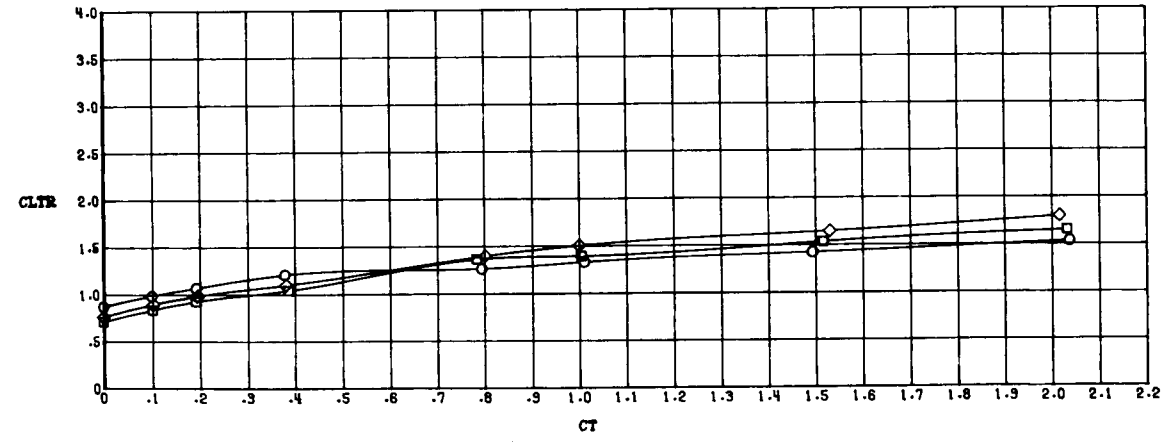

(b) Thrust removed.

Figure 41.- Concluded.

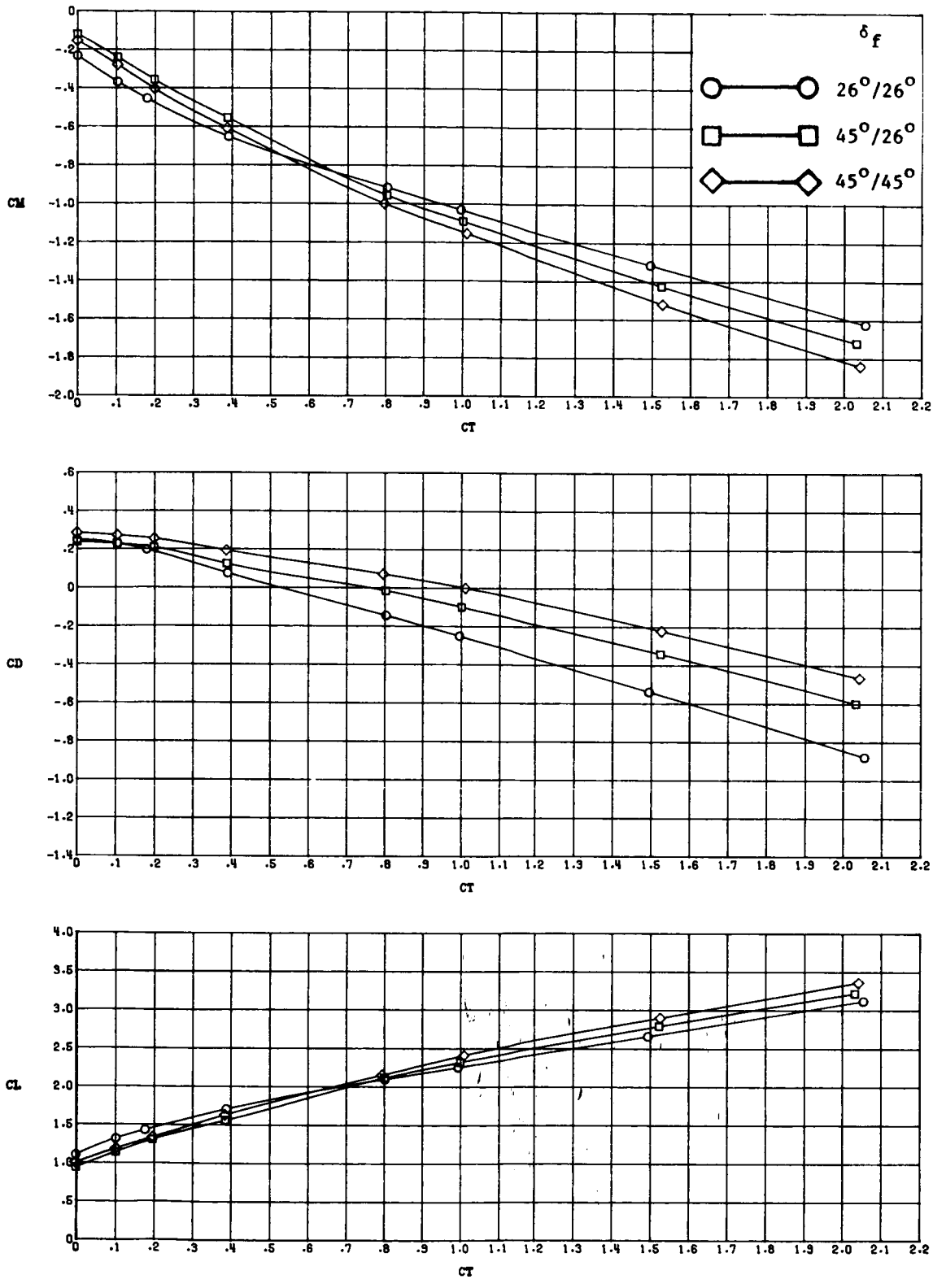

(a) Thrust included.

Figure 42.- Effect of flap deflection angle on longitudinal aerodynamic characteristics at various thrust coefficients with $\alpha = 12°$ and $\Lambda_C = 60°$.

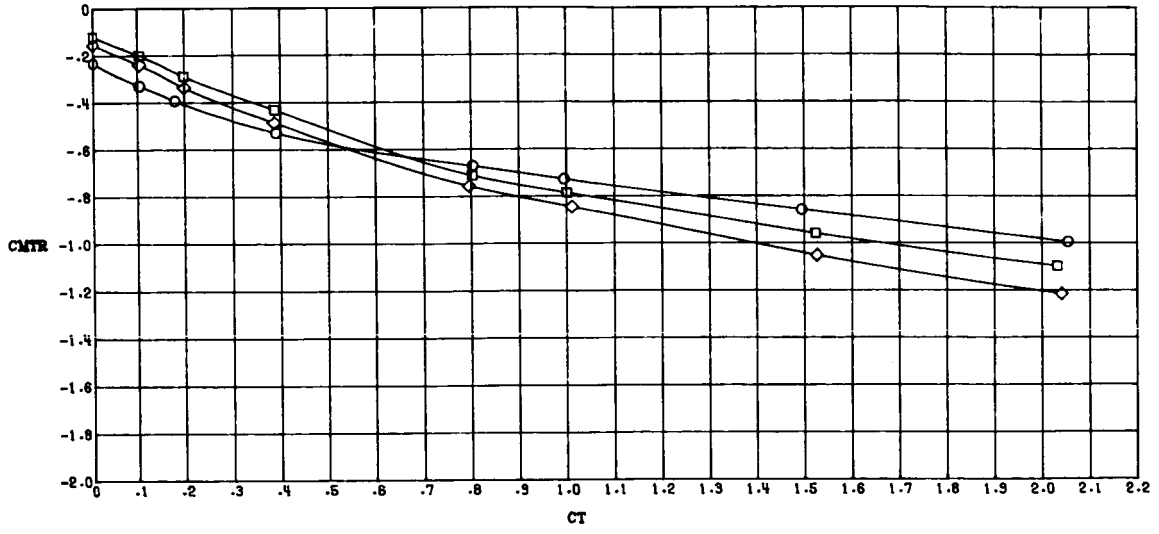

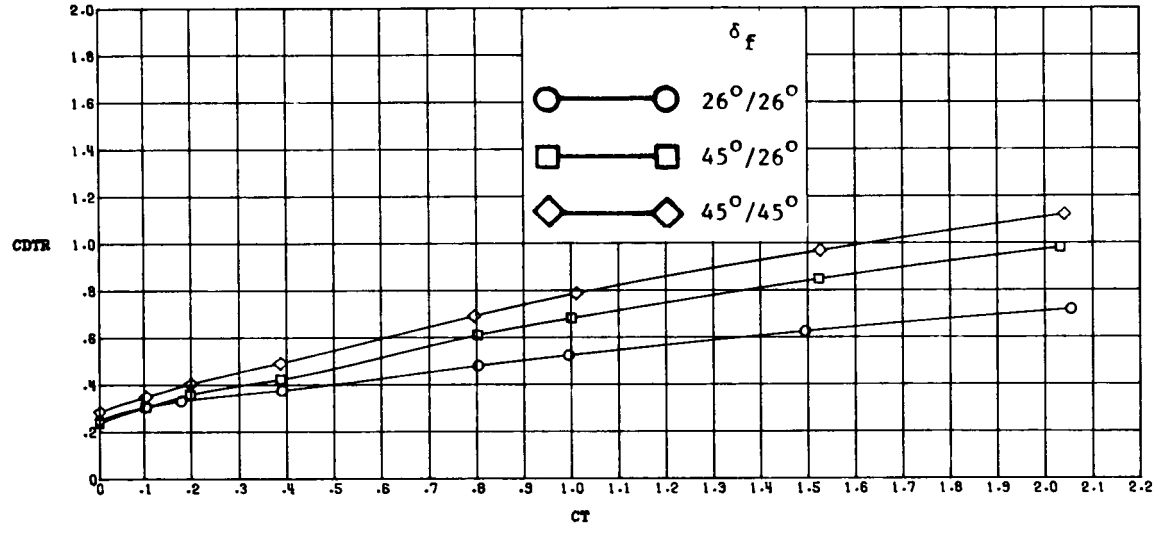

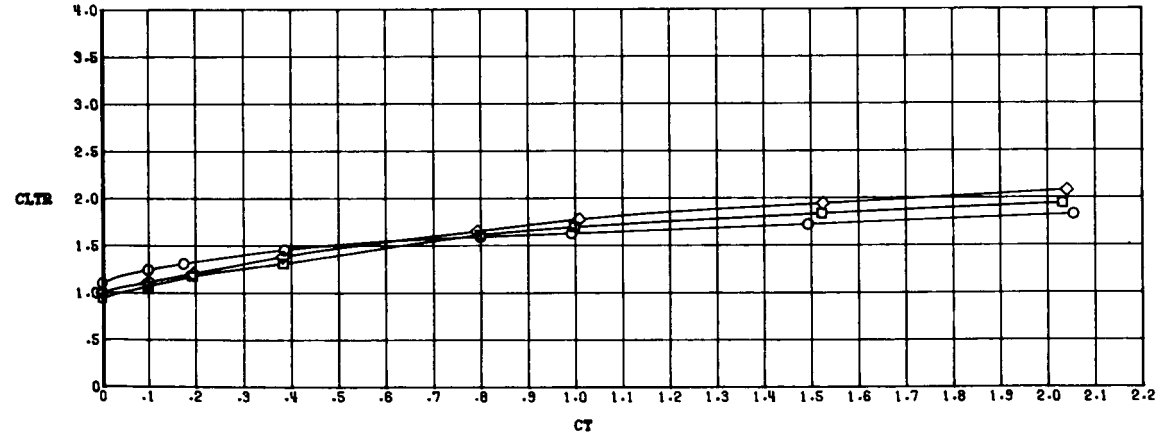

(b) Thrust removed.

Figure 42.- Concluded.

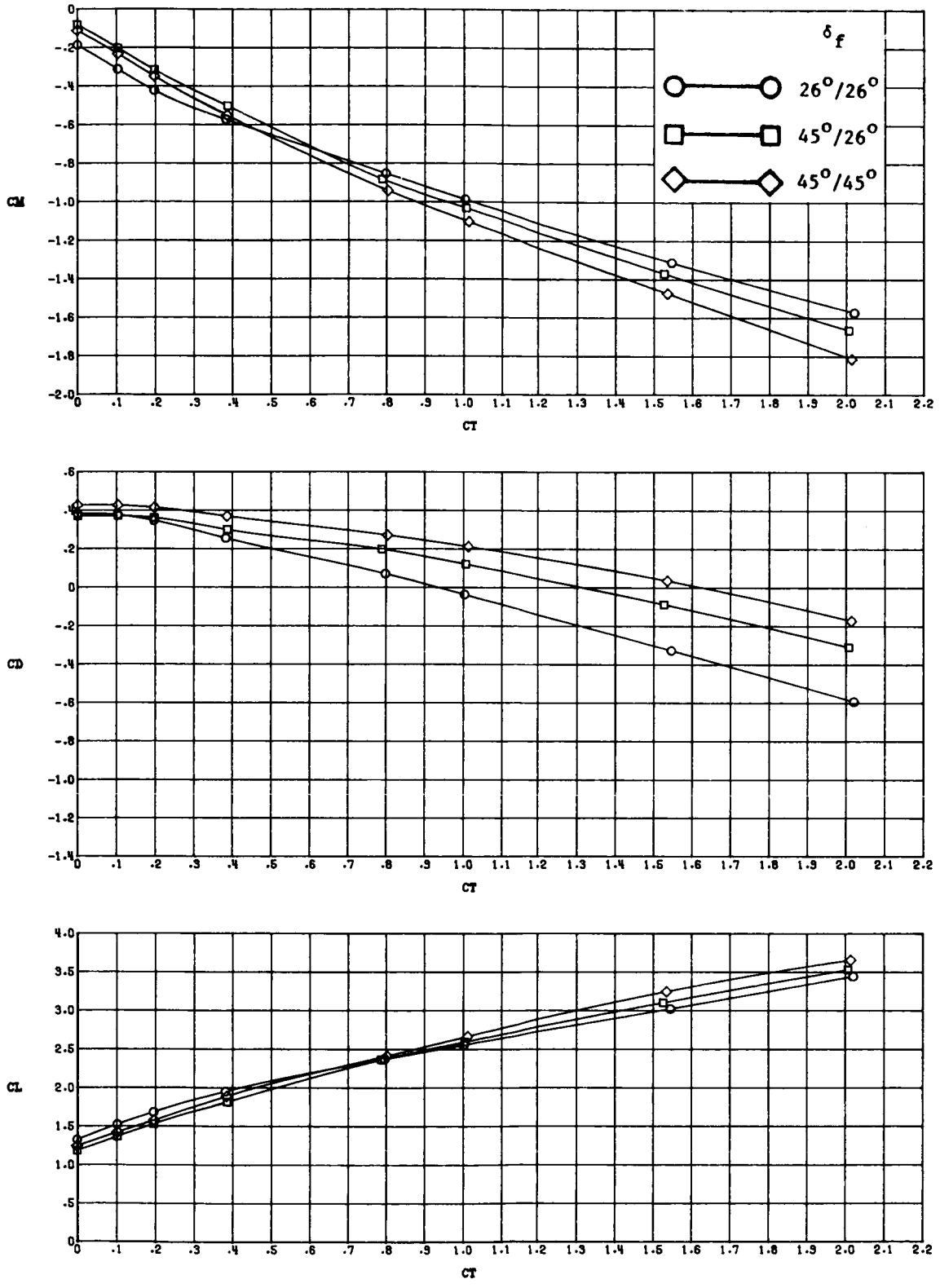

(a) Thrust included.

Figure 43.- Effect of flap deflection angle on longitudinal aerodynamic characteristics at various thrust coefficients with $\alpha = 16°$ and $\Lambda_C = 60°$.

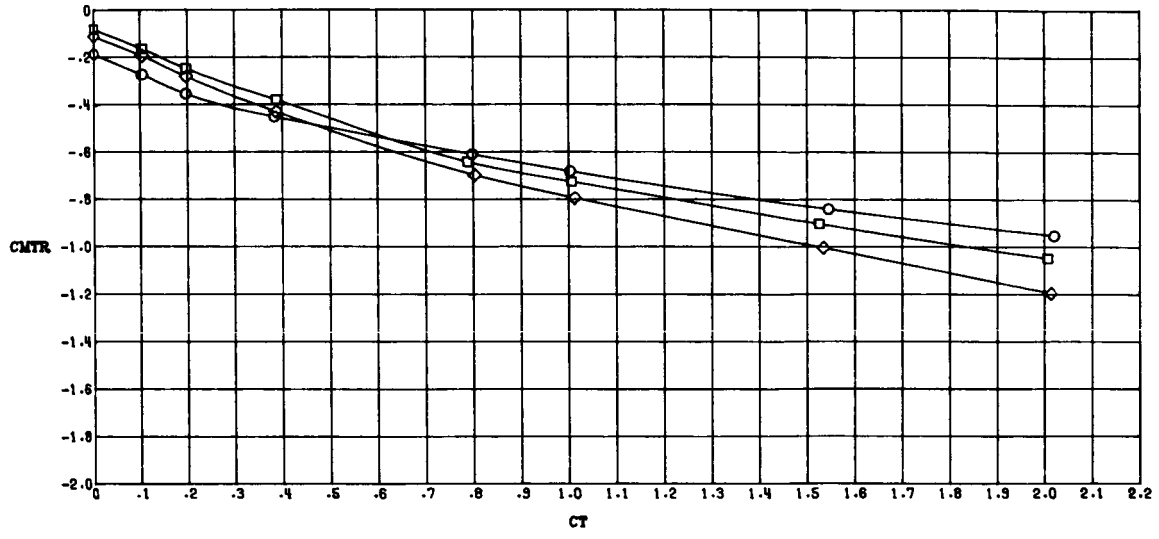

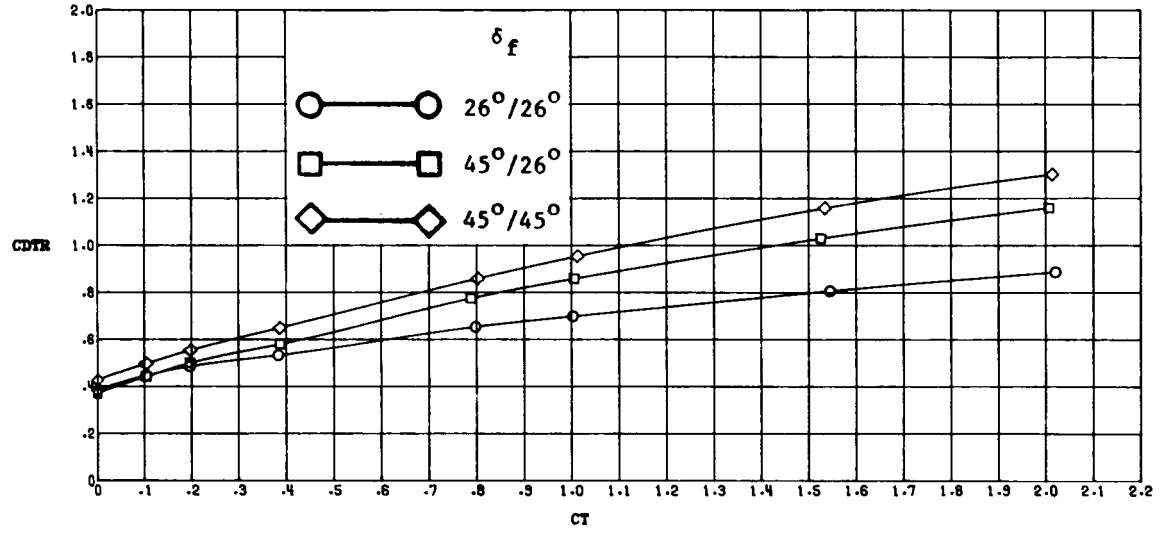

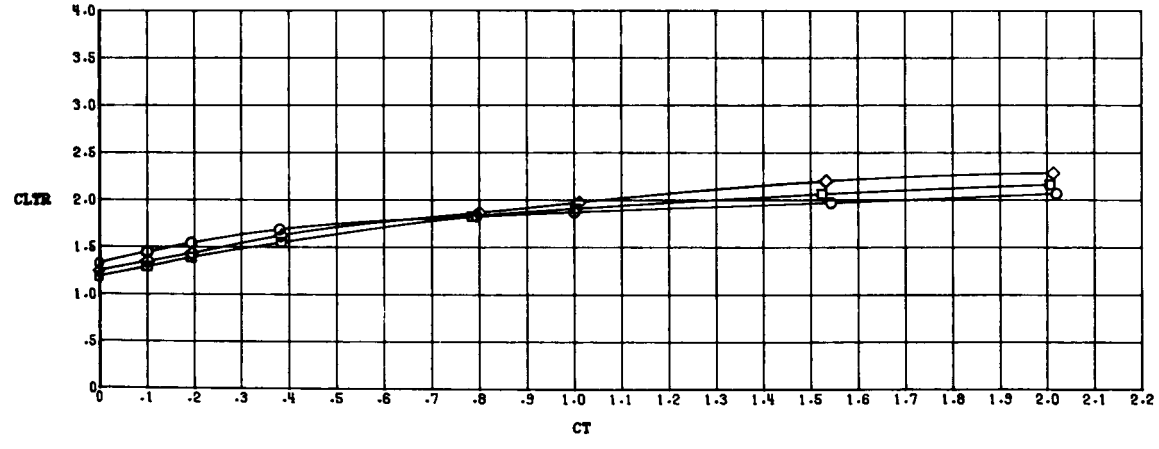

(b) Thrust removed.

Figure 43.- Concluded.

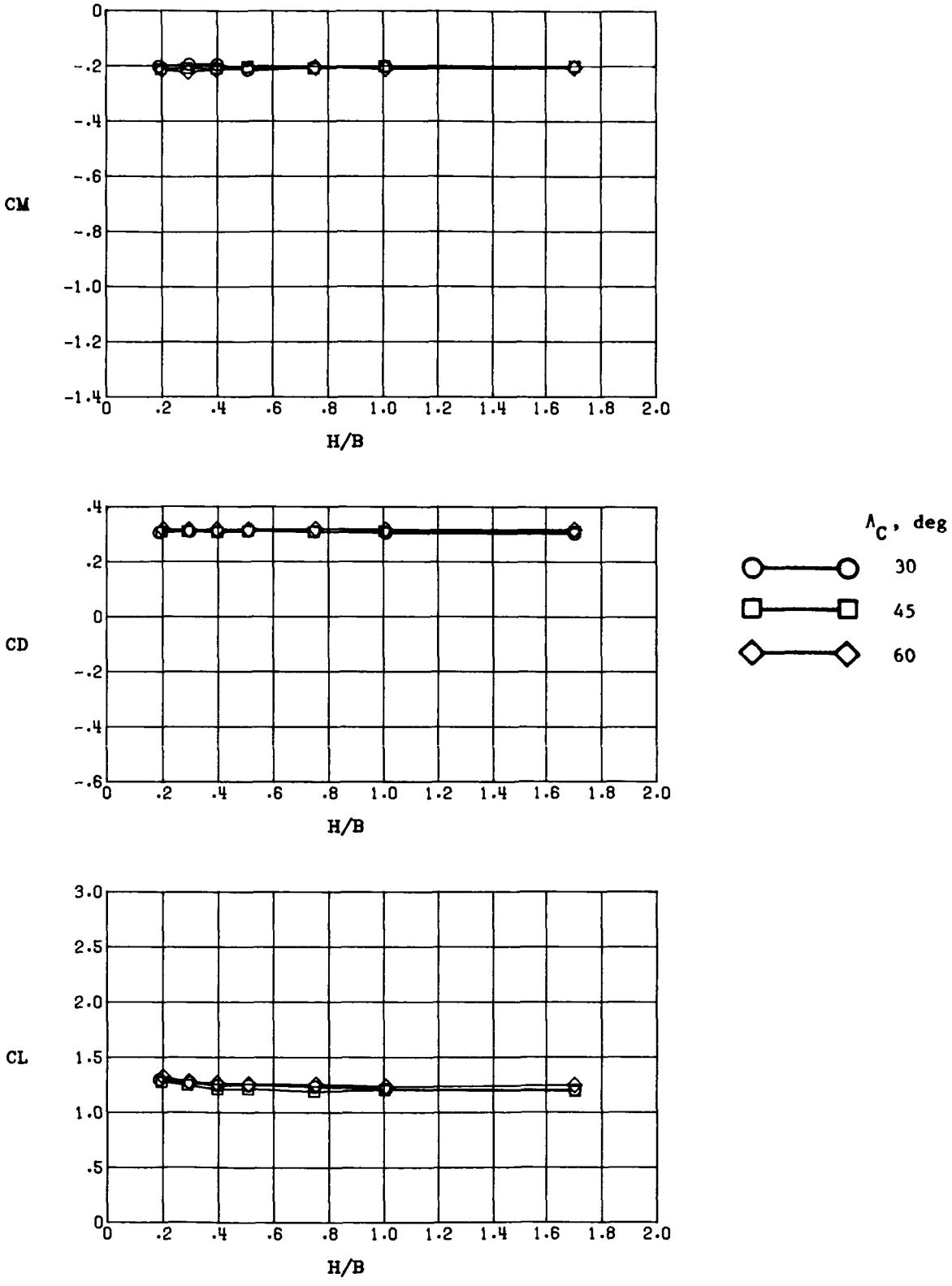

Figure 44.- Effect of cascade vector angle on longitudinal aerodynamic characteristics at various model heights with $C_\mu = 0$, $\delta_f = 26°/26°$, and $\alpha = 14°$.

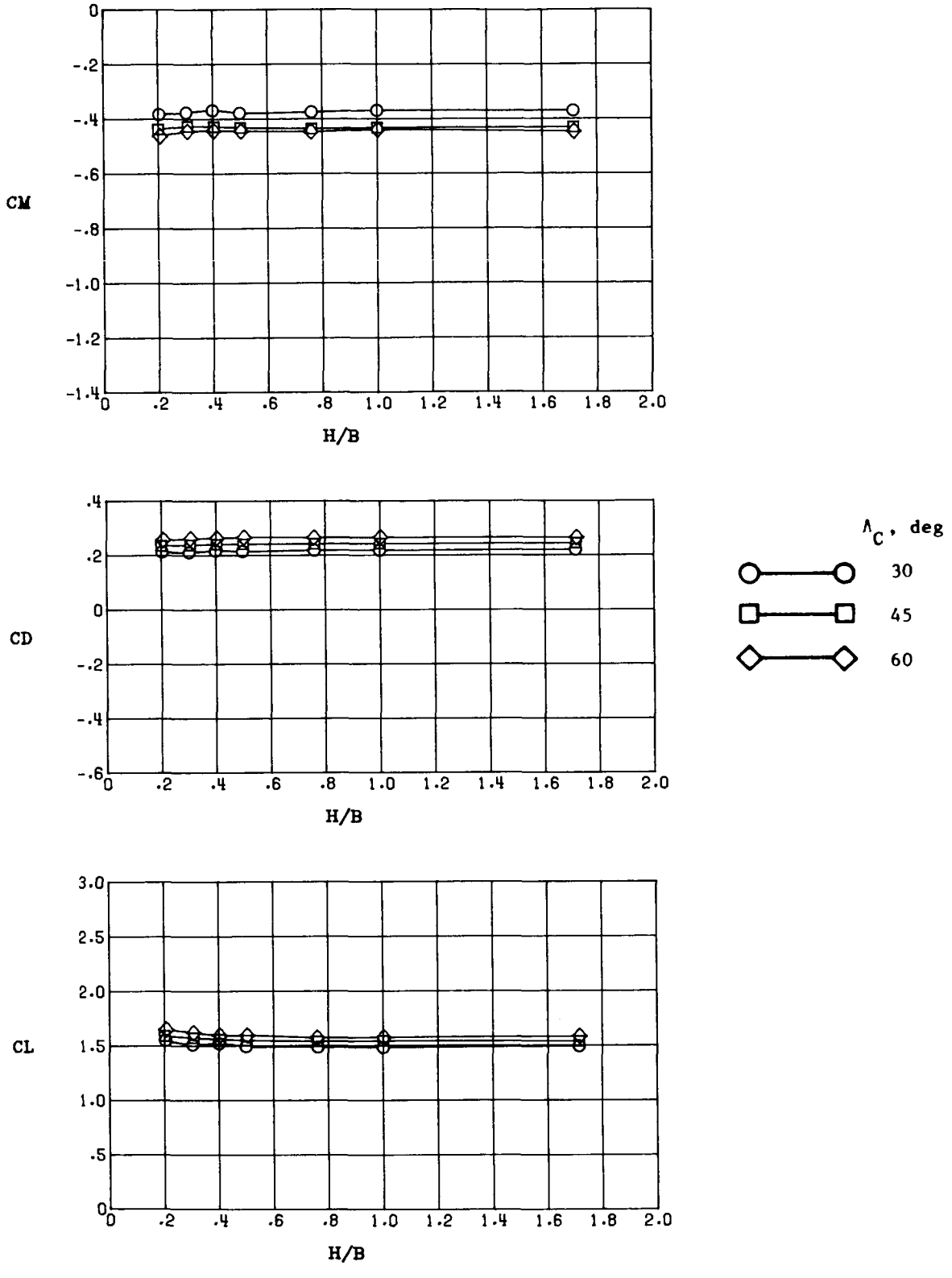

Figure 45.- Effect of cascade vector angle on longitudinal aerodynamic characteristics at various model heights with $C_\mu = 0.19$, $\delta_f = 26°/26°$, and $\alpha = 14°$.

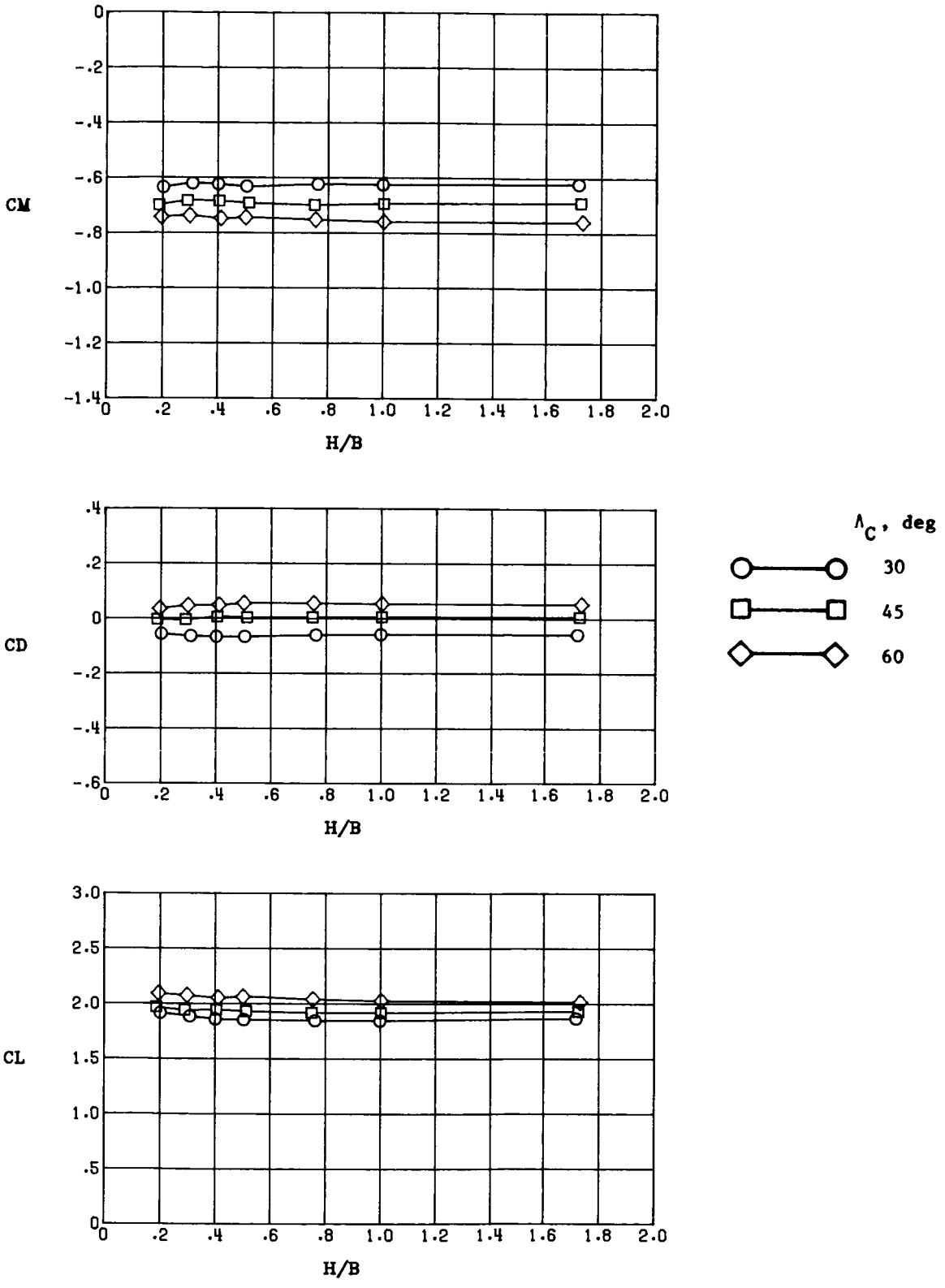

Figure 46.- Effect of cascade vector angle on longitudinal aerodynamic characteristics at various model heights with C_μ = 0.60, δ_f = 26°/26°, and α = 14°.

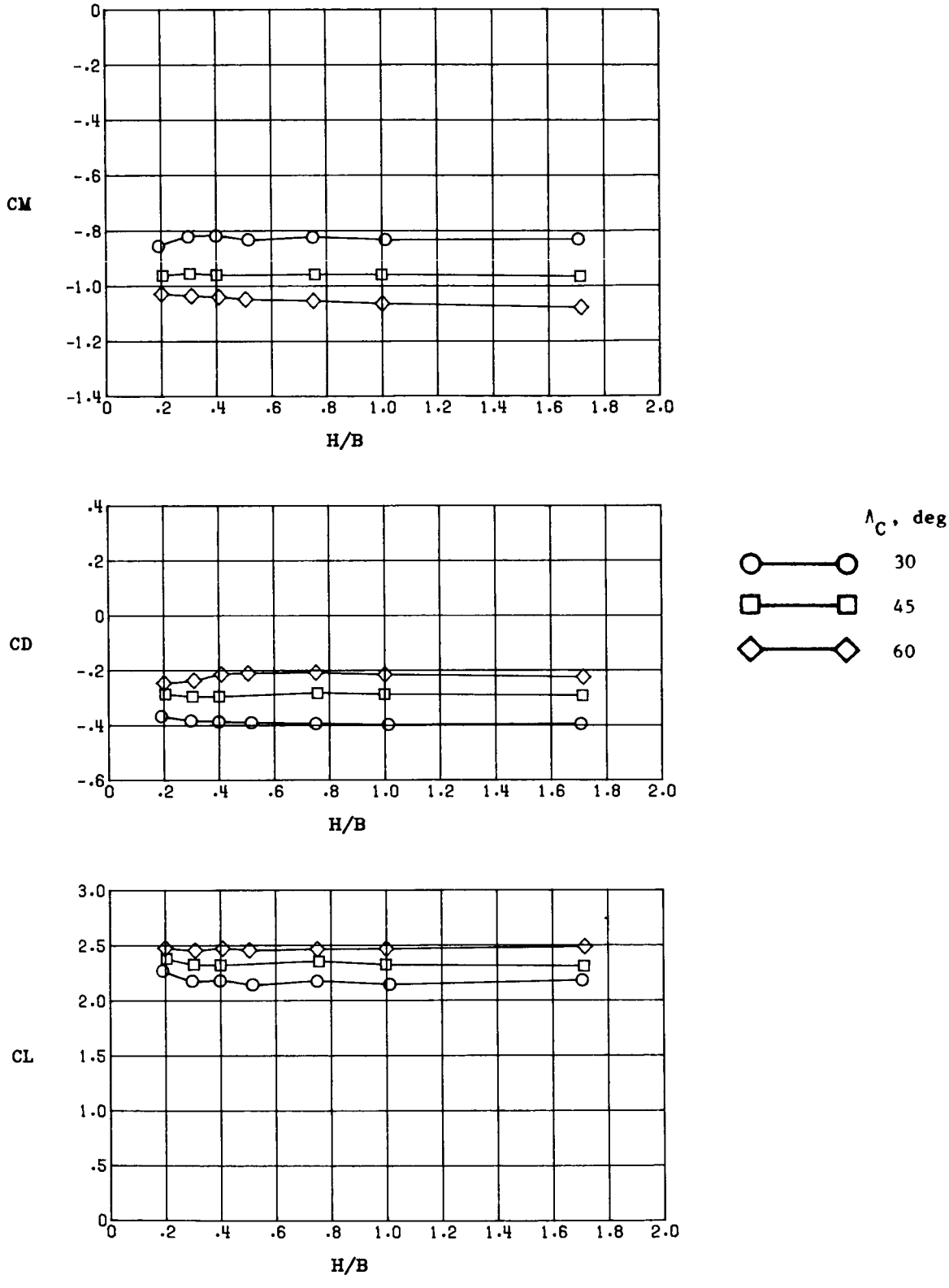

Figure 47.- Effect of cascade vector angle on longitudinal aerodynamic characteristics at various model heights with $C_\mu = 1.07$, $\delta_f = 26°/26°$, and $\alpha = 14°$.

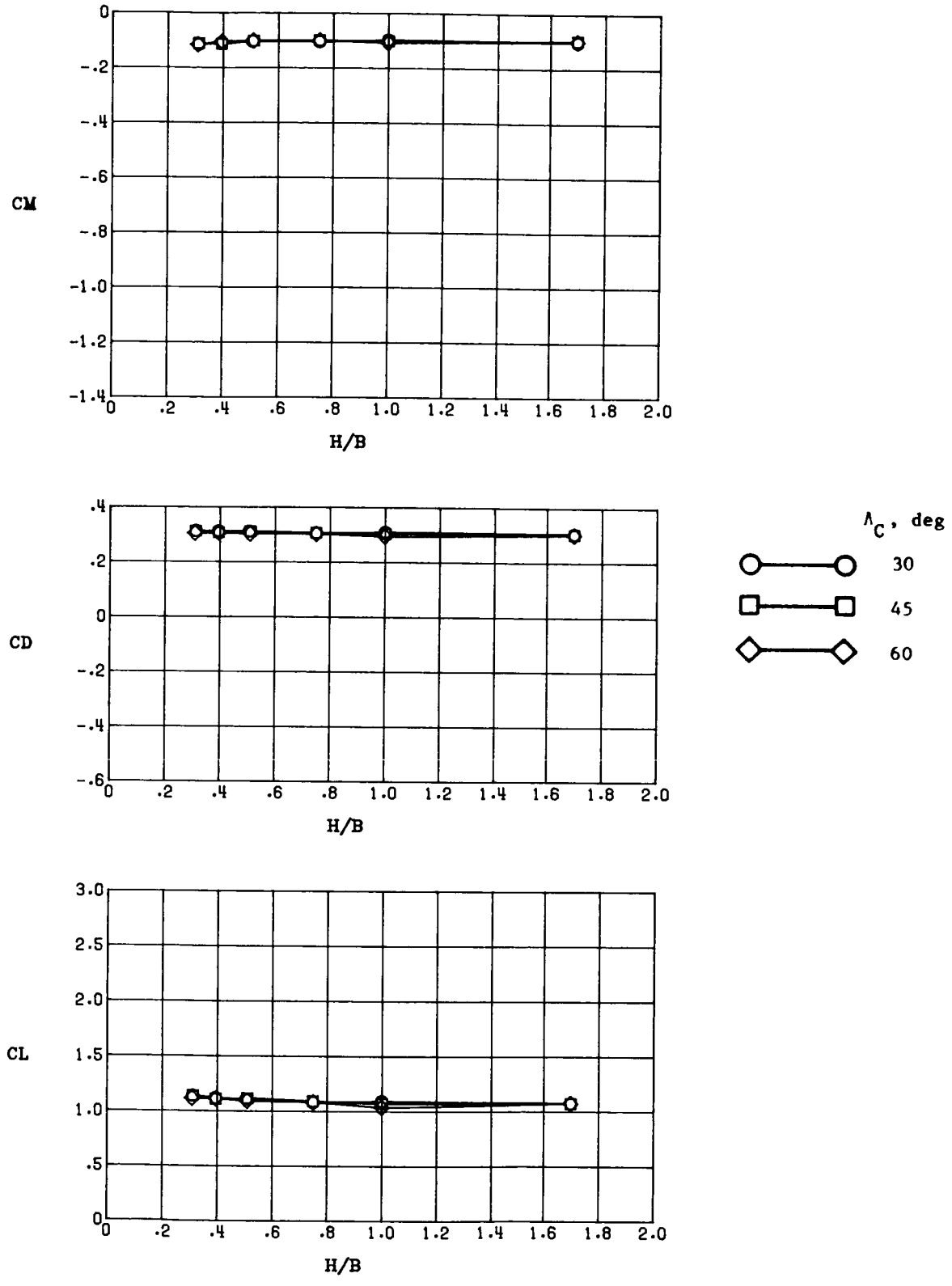

Figure 48.- Effect of cascade vector angle on longitudinal aerodynamic characteristics at various model heights with $C_\mu = 0$, $\delta_f = 45°/26°$, and $\alpha = 14°$.

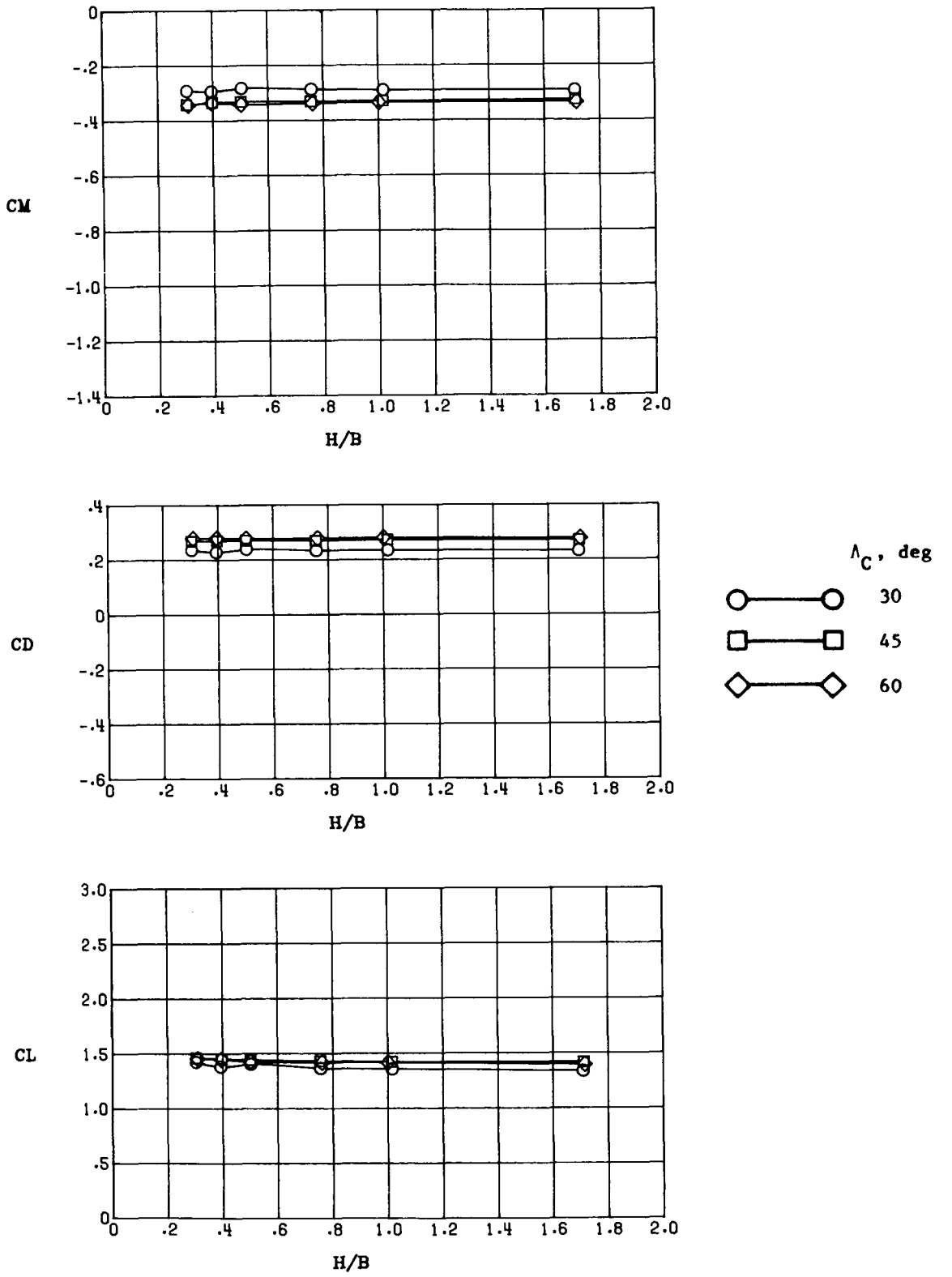

Figure 49.- Effect of cascade vector angle on longitudinal aerodynamic characteristics at various model heights with $C_\mu = 0.19$, $\delta_f = 45°/26°$, and $\alpha = 14°$.

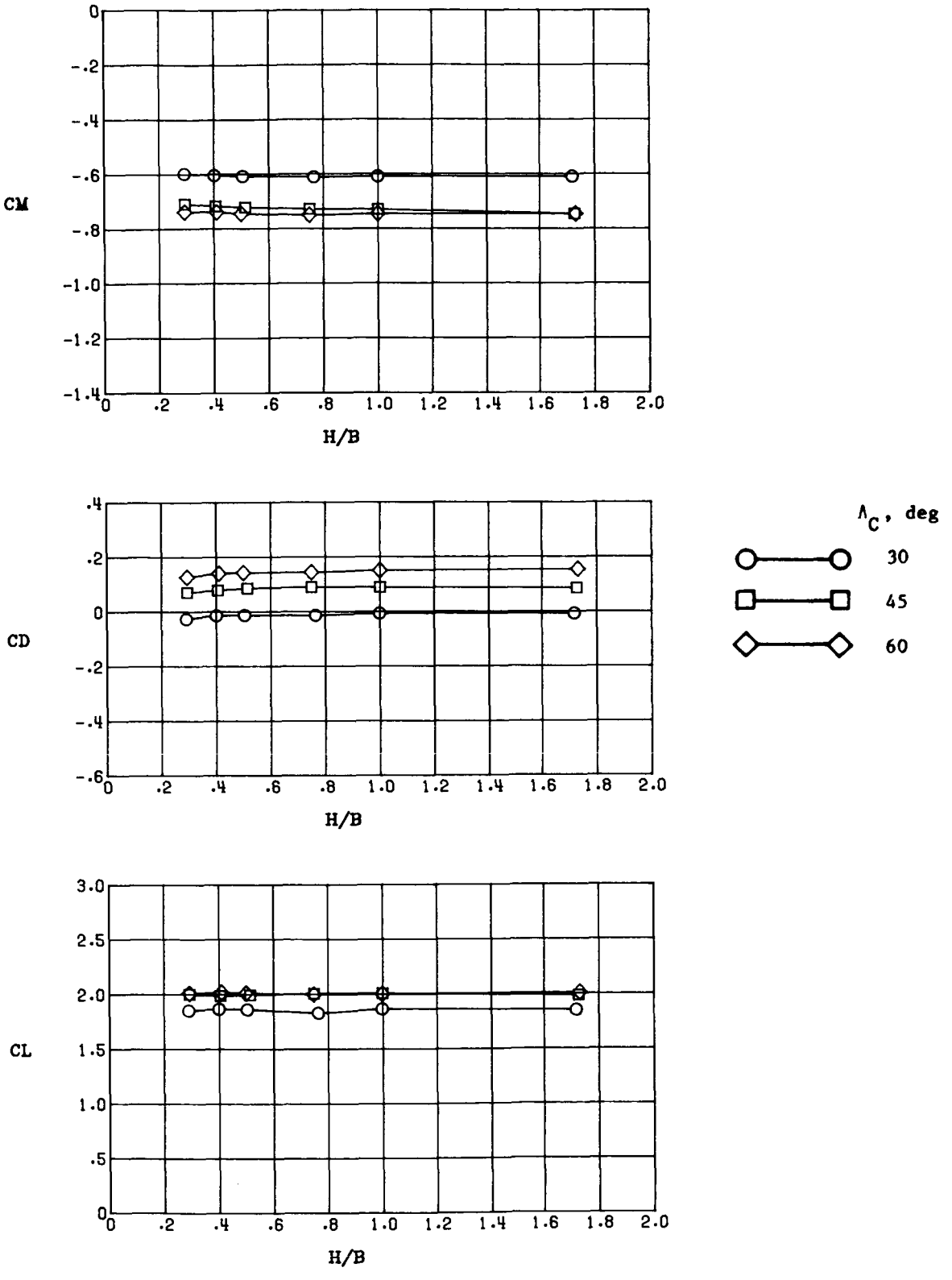

Figure 50.- Effect of cascade vector angle on longitudinal aerodynamic characteristics at various model heights with $C_\mu = 0.60$, $\delta_f = 45°/26°$, and $\alpha = 14°$.

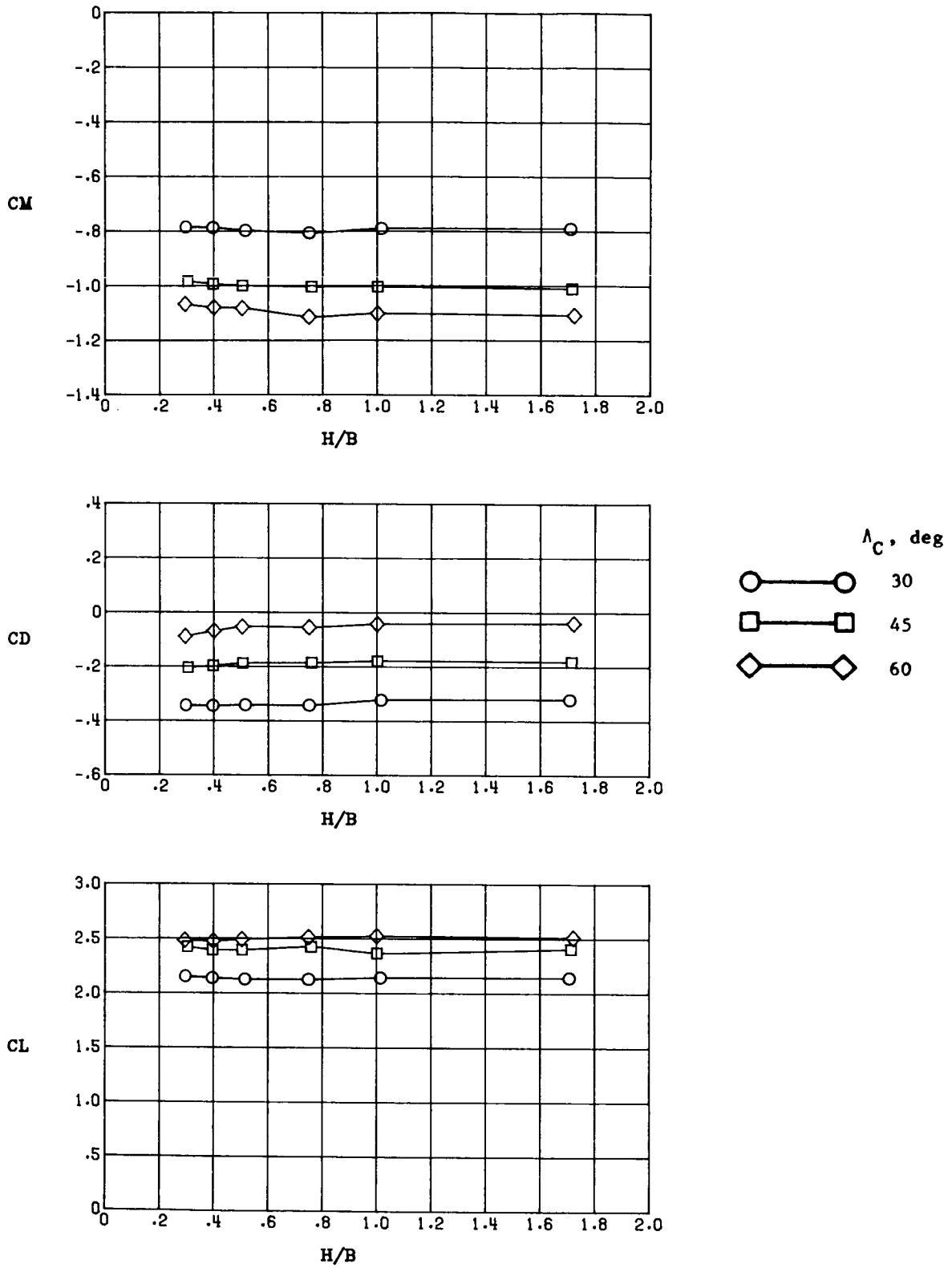

Figure 51.- Effect of cascade vector angle on longitudinal aerodynamic characteristics at various model heights with C_μ = 1.07, δ_f = 45°/26°, and α = 14°.

C-2

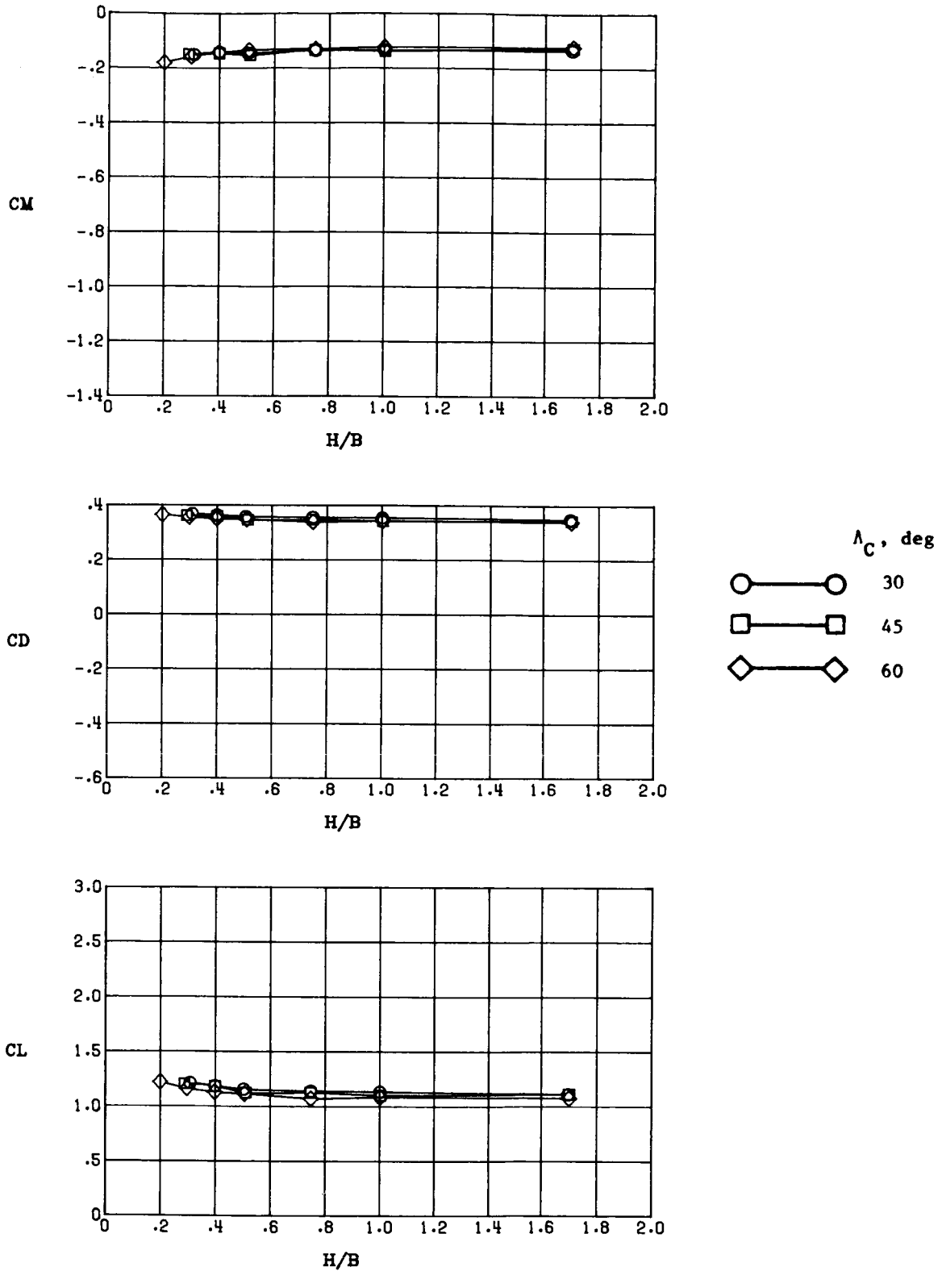

Figure 52.- Effect of cascade vector angle on longitudinal aerodynamic characteristics at various model heights with $C_\mu = 0$, $\delta_f = 45°/45°$, and $\alpha = 14°$.

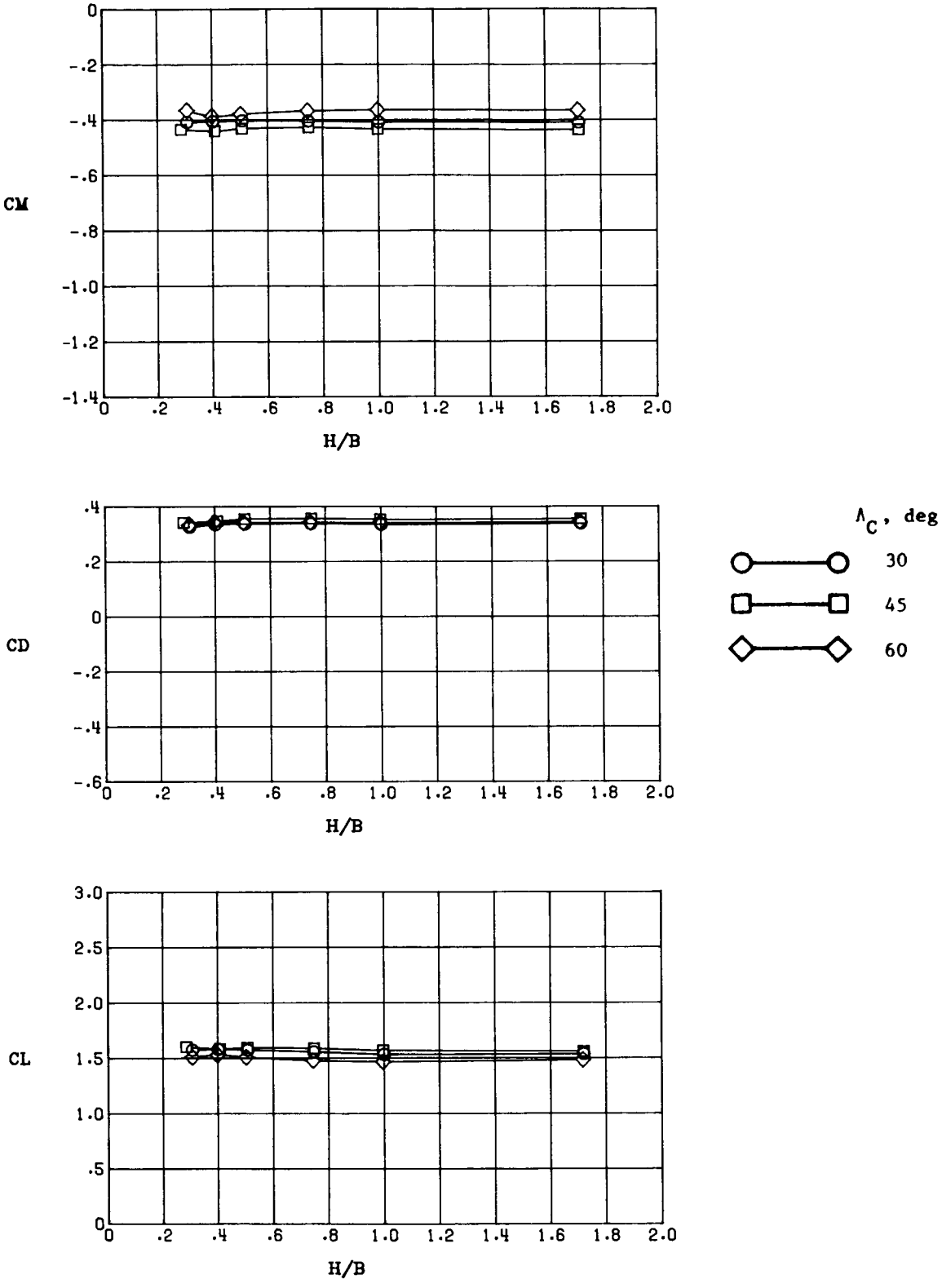

Figure 53.- Effect of cascade vector angle on longitudinal aerodynamic characteristics at various model heights with C_μ = 0.19, δ_f = 45°/45°, and α = 14°.

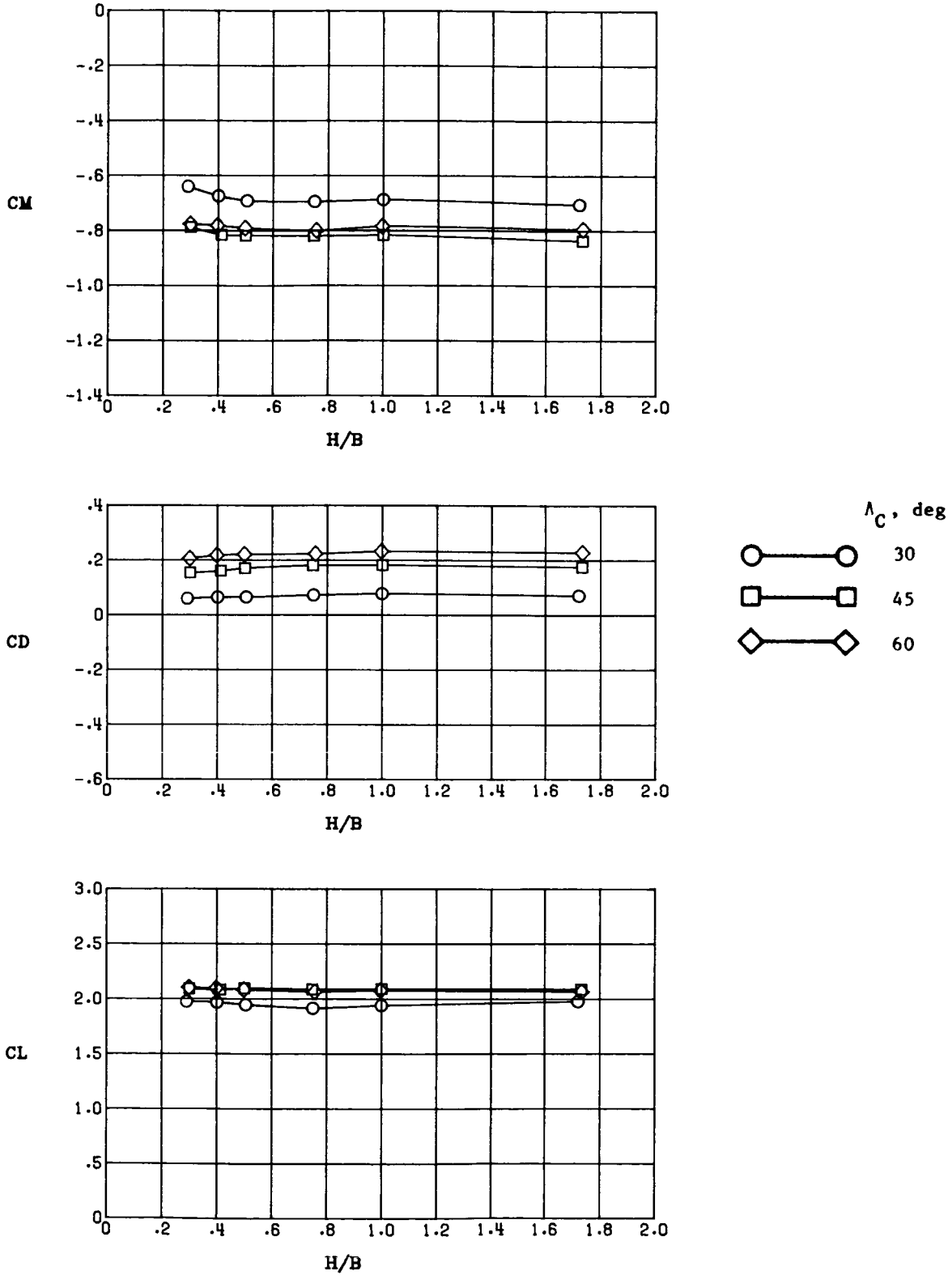

Figure 54.- Effect of cascade vector angle on longitudinal aerodynamic characteristics at various model heights with C_μ = 0.60, δ_f = 45°/45°, and α = 14°.

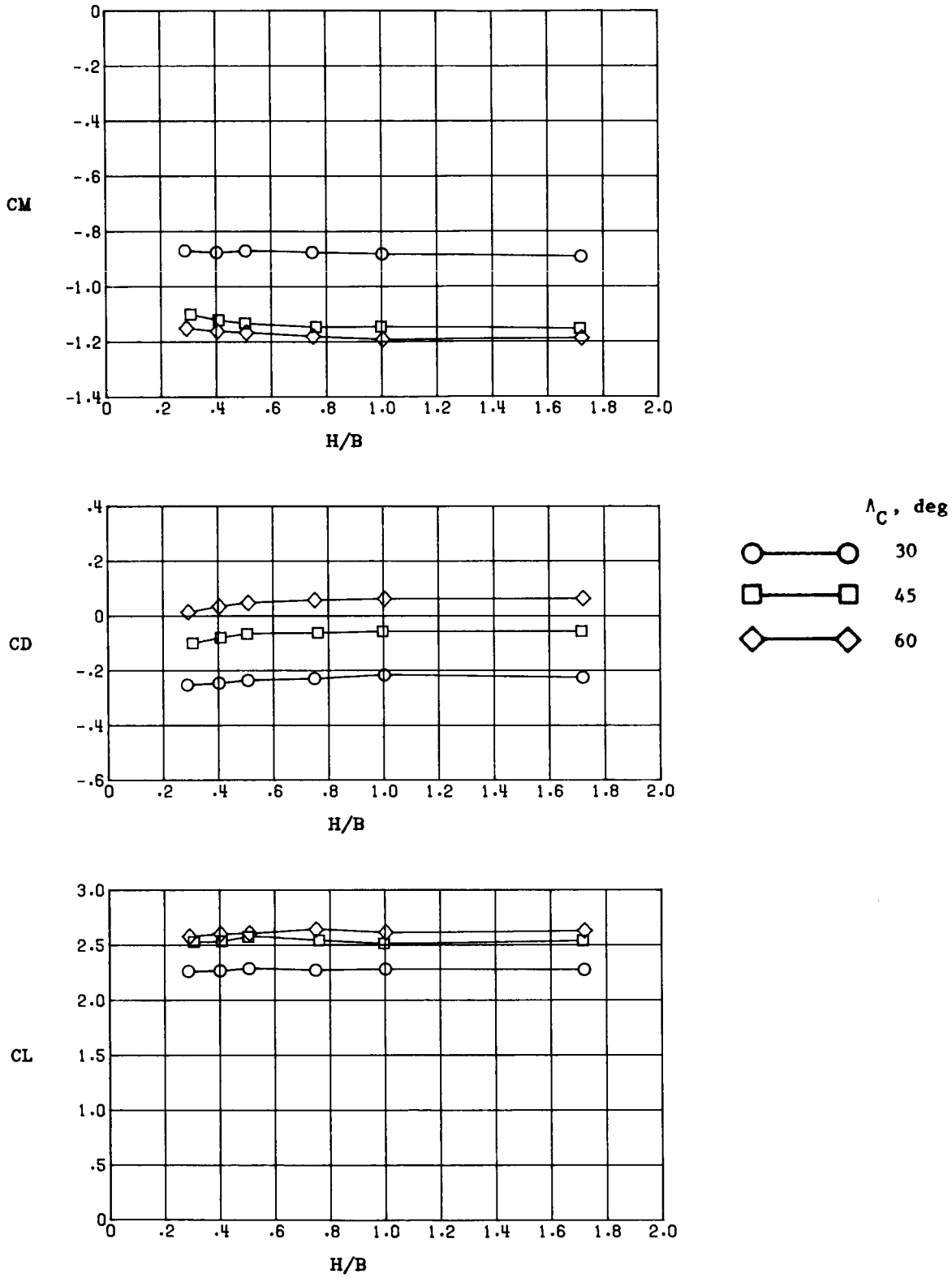

Figure 55.- Effect of cascade vector angle on longitudinal aerodynamic characteristics at various model heights with C_μ = 1.07, δ_f = 45°/45°, and α = 14°.

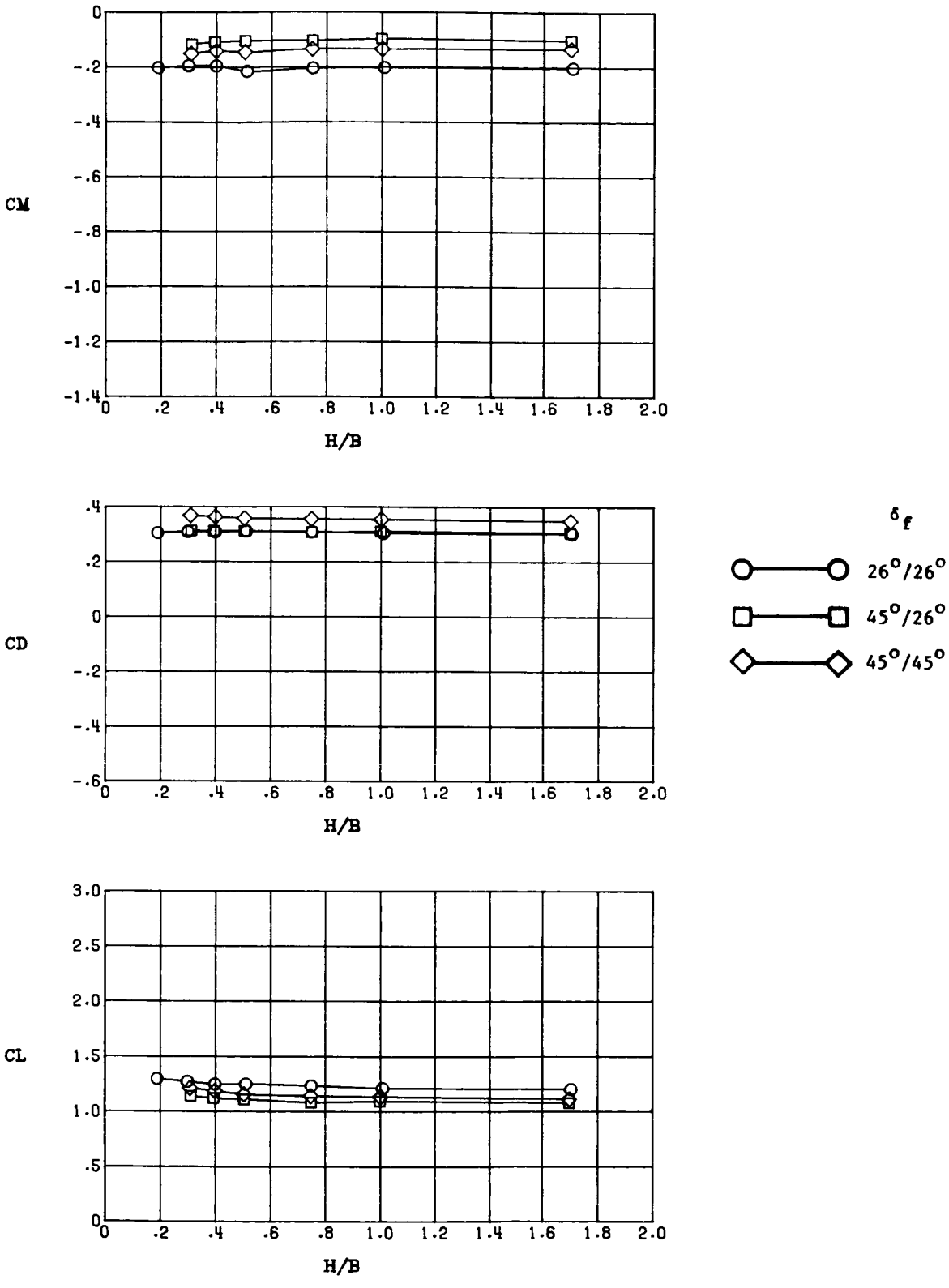

Figure 56.- Effect of flap deflection angle on longitudinal aerodynamic characteristics at various model heights with $C_\mu = 0$, $\Lambda_C = 30°$, and $\alpha = 14°$.

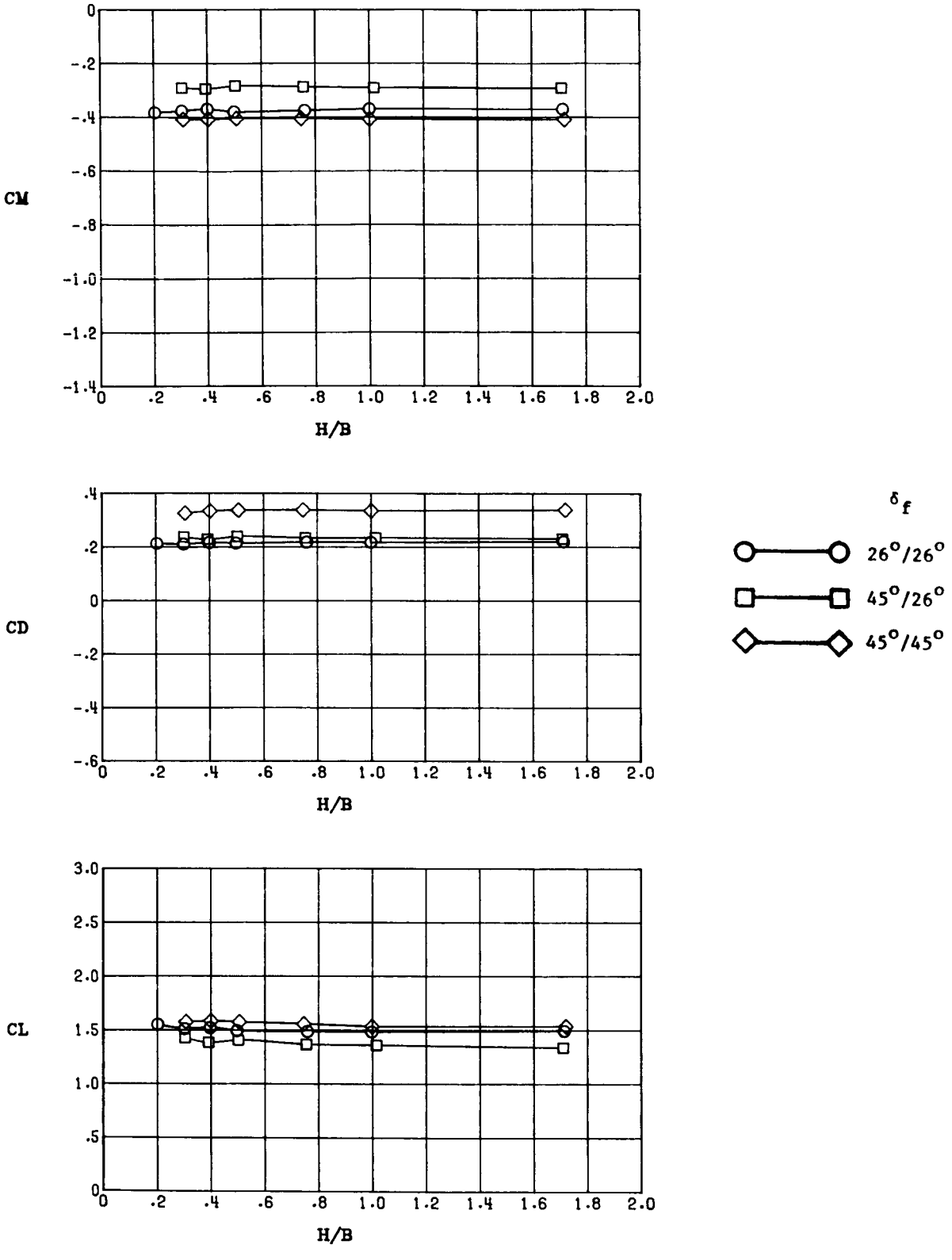

Figure 57.- Effect of flap deflection angle on longitudinal aerodynamic characteristics at various model heights with $C_\mu = 0.19$, $\Lambda_C = 30°$, and $\alpha = 14°$.

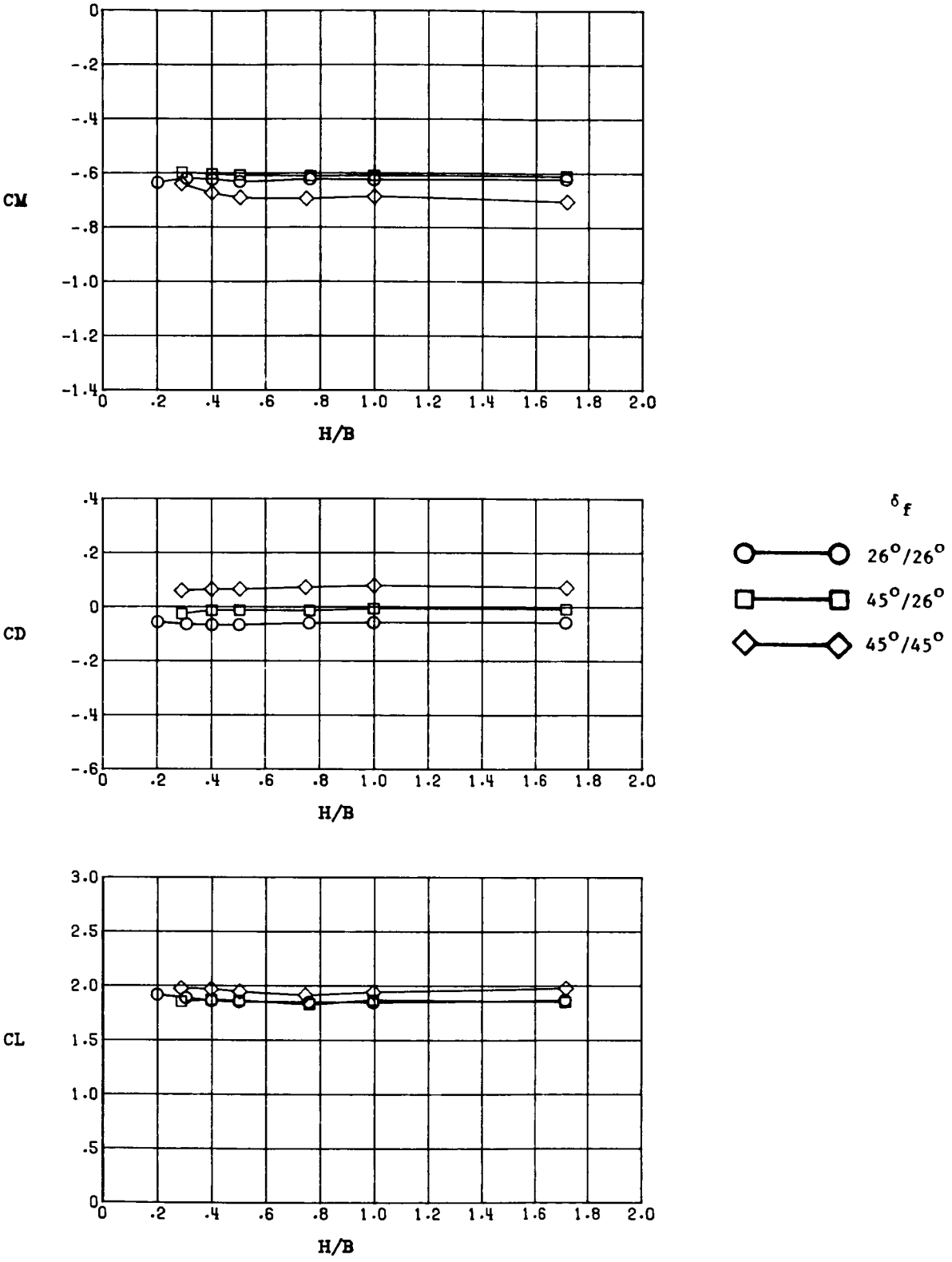

Figure 58.- Effect of flap deflection angle on longitudinal aerodynamic characteristics at various model heights with $C_{\mu} = 0.60$, $\Lambda_C = 30°$, and $\alpha = 14°$.

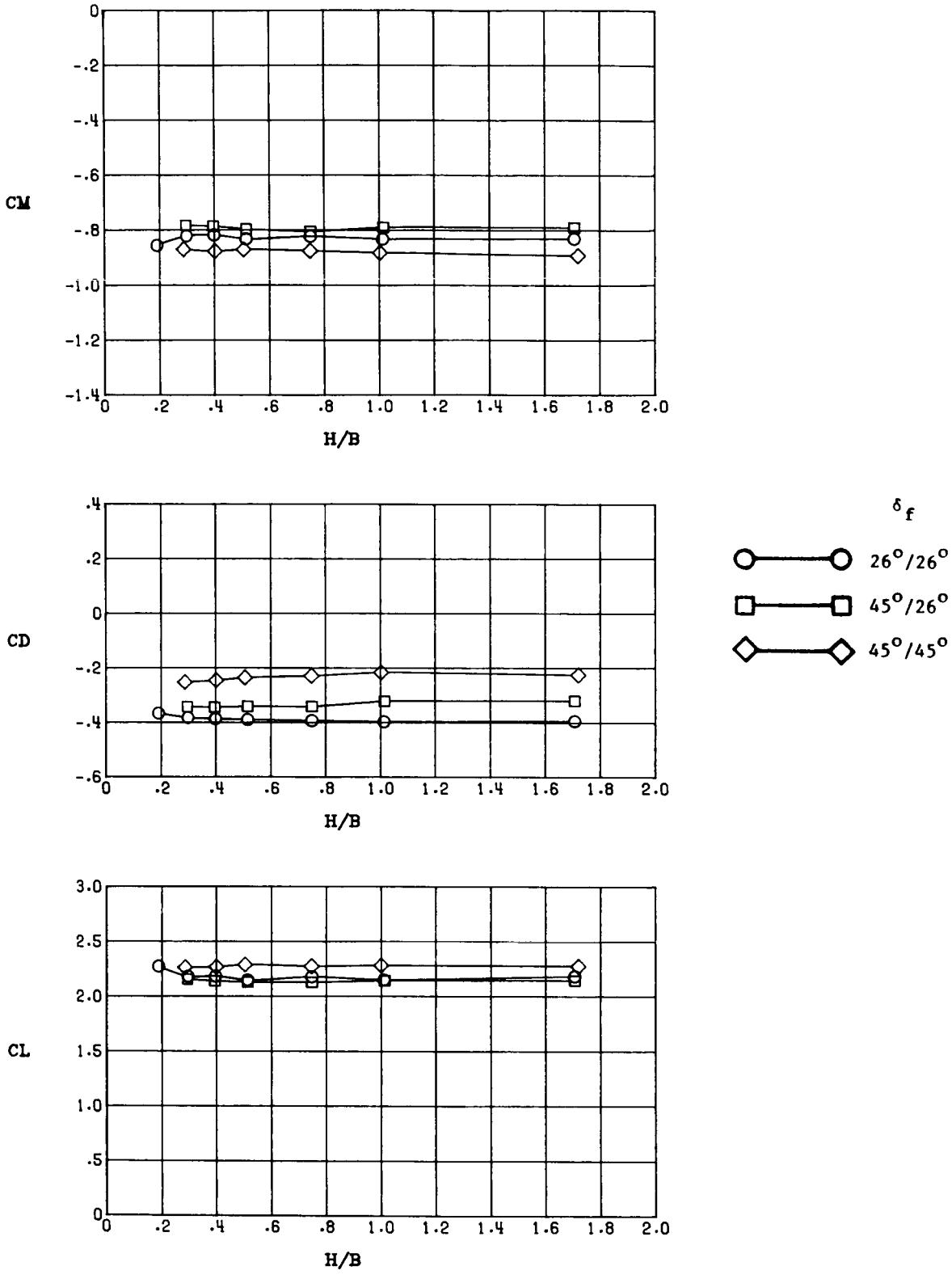

Figure 59.- Effect of flap deflection angle on longitudinal aerodynamic characteristics at various model heights with $C_\mu = 1.07$, $\Lambda_C = 30°$, and $\alpha = 14°$.

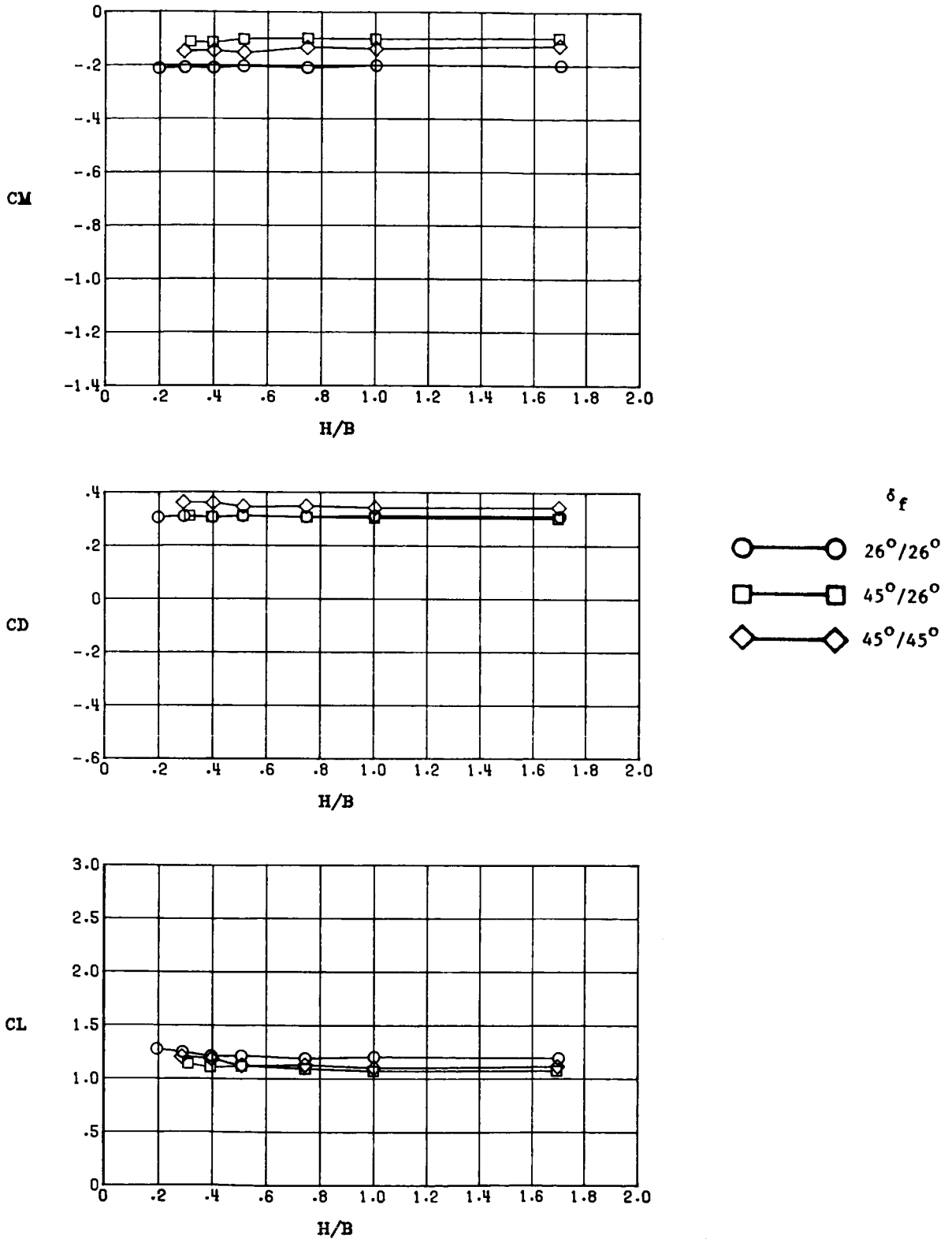

Figure 60.- Effect of flap deflection angle on longitudinal aerodynamic characteristics at various model heights with $C_\mu = 0$, $\Lambda_C = 45°$, and $\alpha = 14°$.

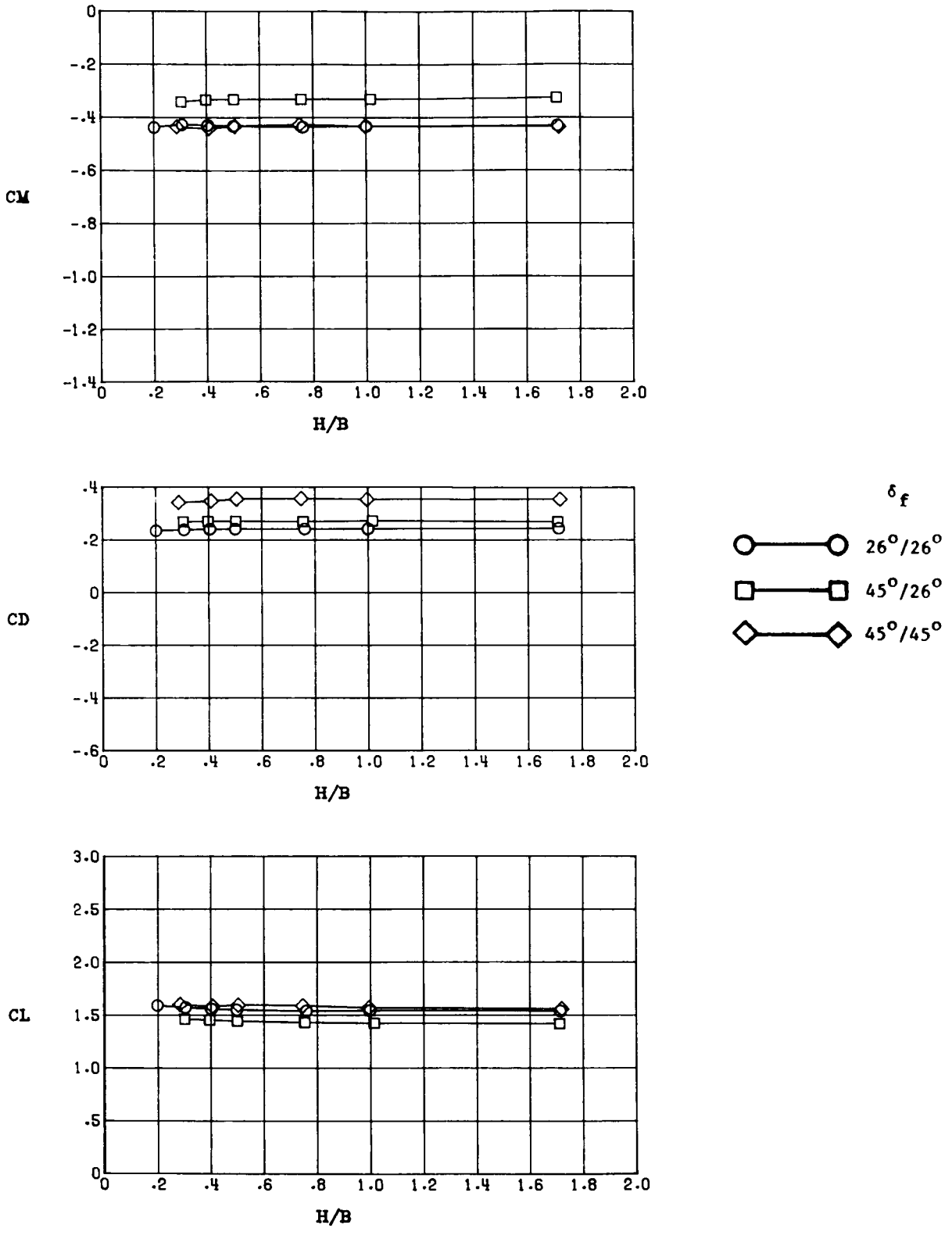

Figure 61.- Effect of flap deflection angle on longitudinal aerodynamic characteristics at various model heights with $C_\mu = 0.19$, $\Lambda_C = 45°$, and $\alpha = 14°$.

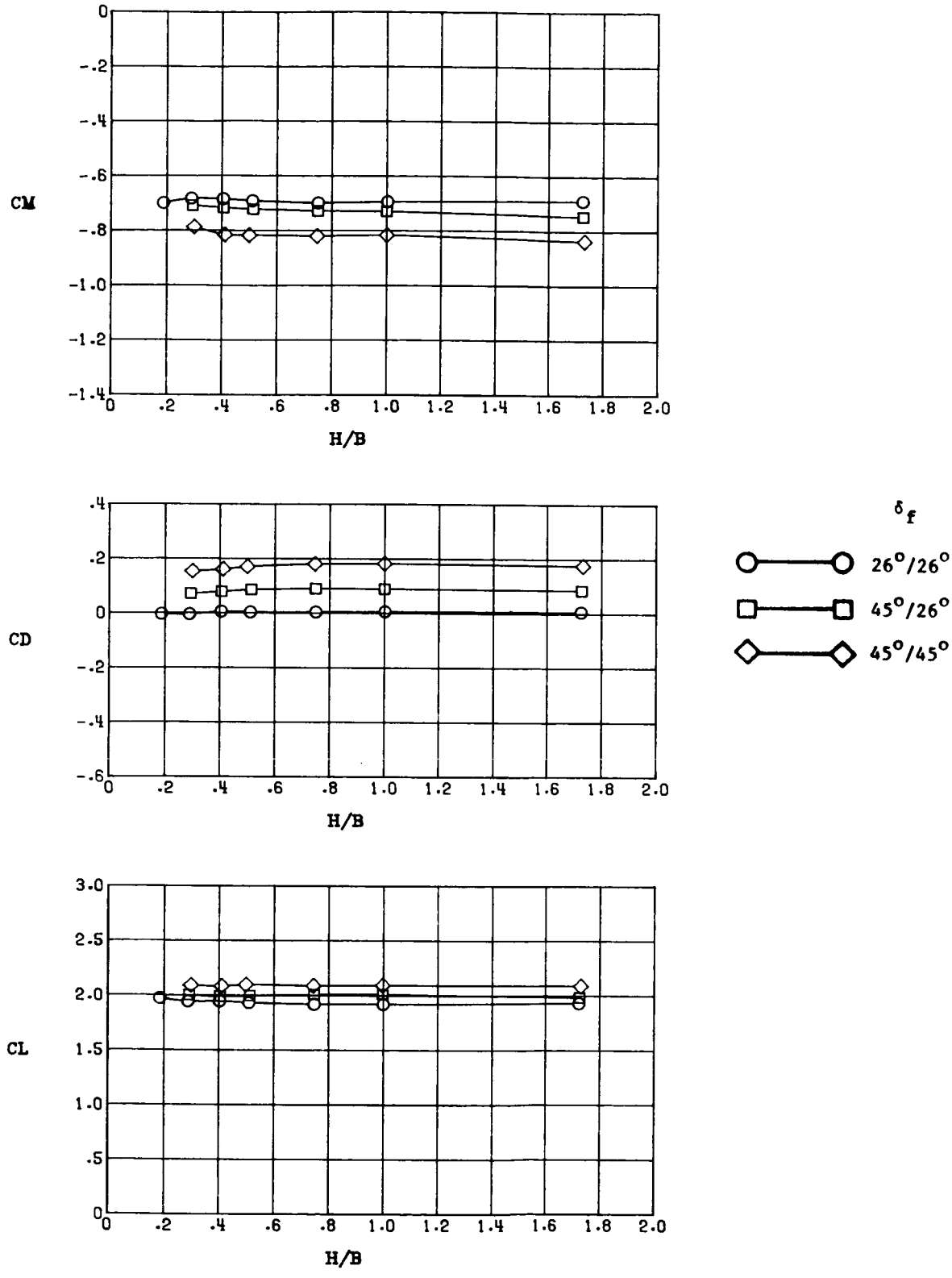

Figure 62.- Effect of flap deflection angle on longitudinal aerodynamic characteristics at various model heights with $C_\mu = 0.60$, $\Lambda_C = 45°$, and $\alpha = 14°$.

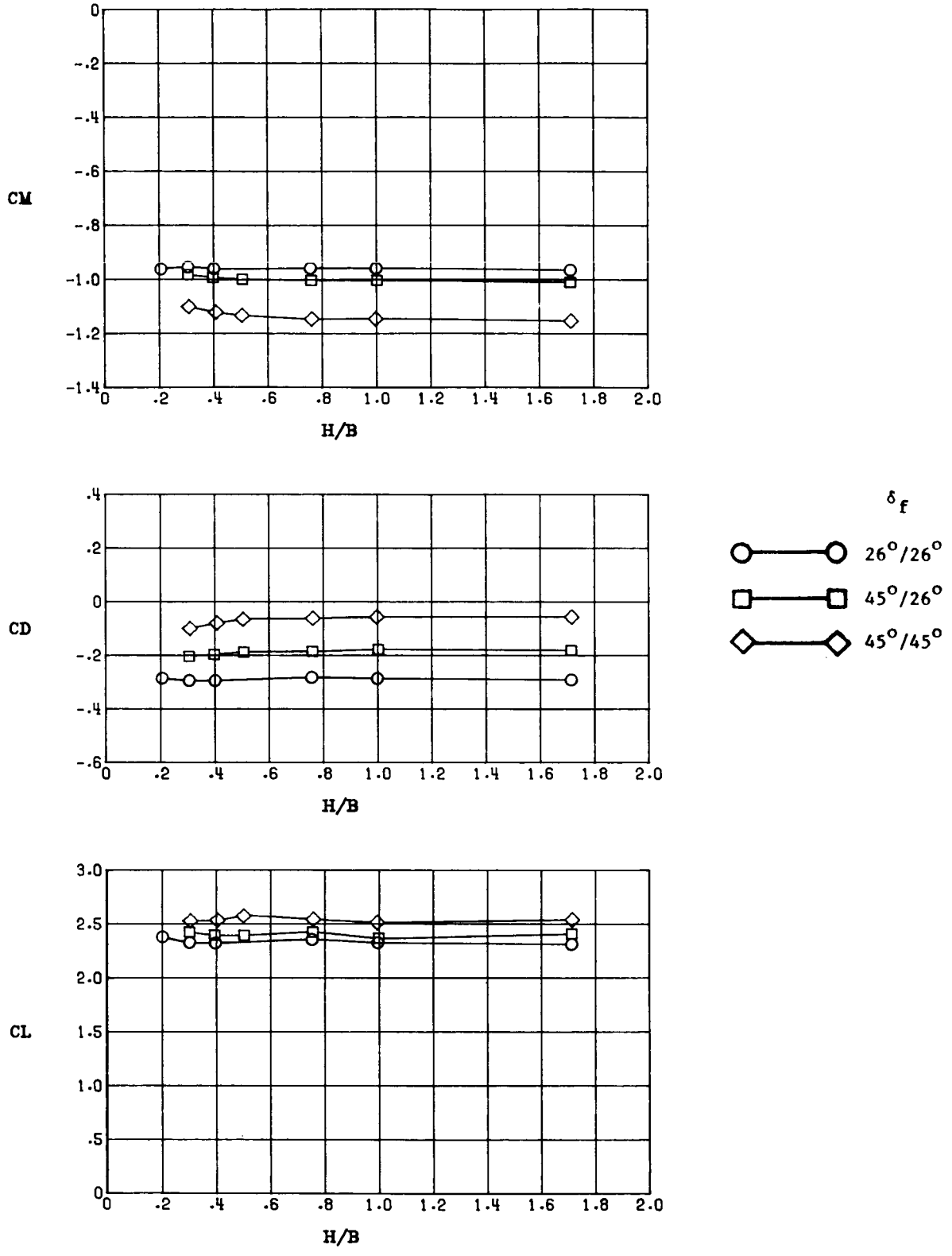

Figure 63.- Effect of flap deflection angle on longitudinal aerodynamic characteristics at various model heights with $C_\mu = 1.07$, $\Lambda_C = 45°$, and $\alpha = 14°$.

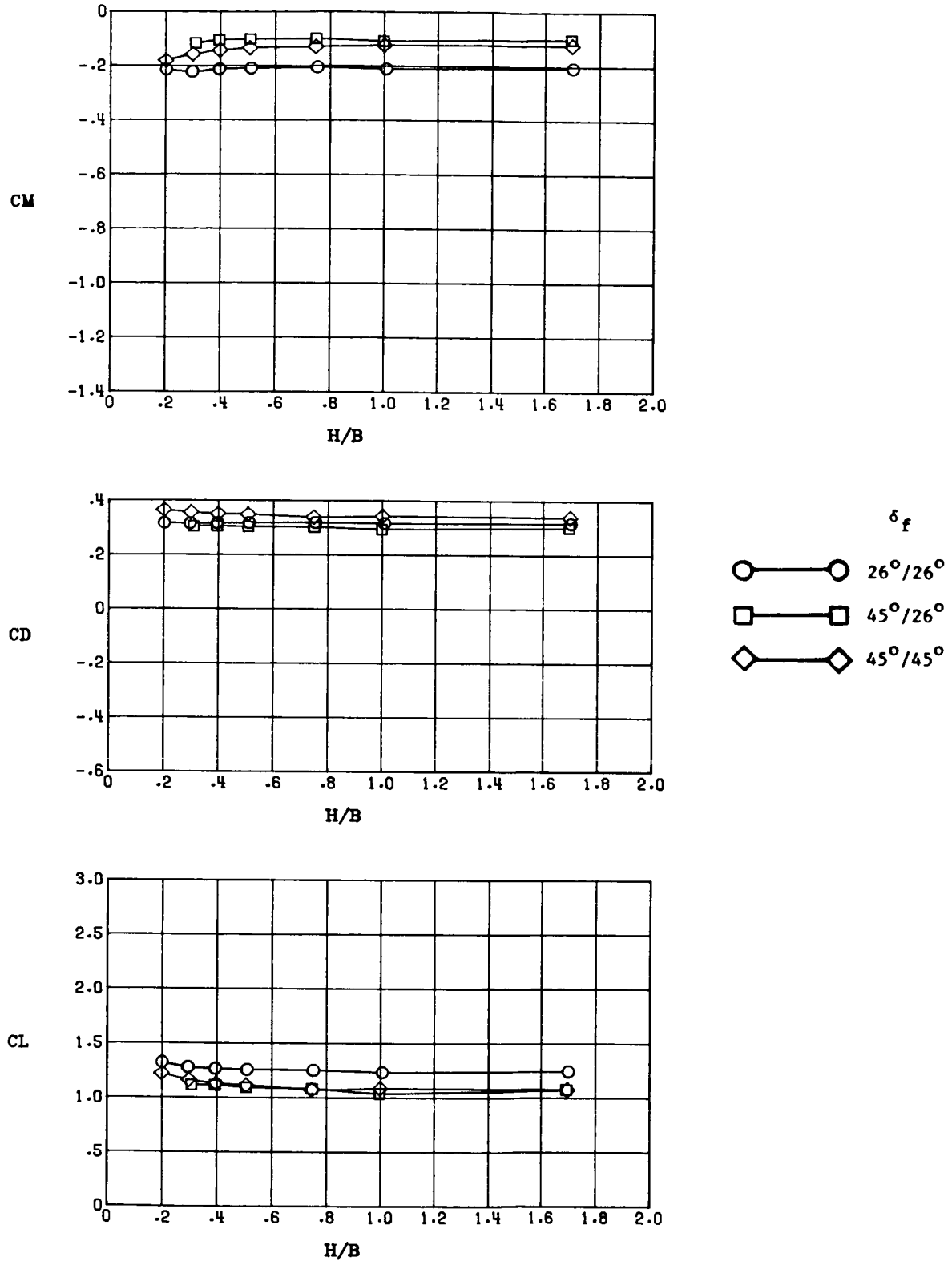

Figure 64.- Effect of flap deflection angle on longitudinal aerodynamic characteristics at various model heights with $C_{\mu} = 0$, $\Lambda_C = 60°$, and $\alpha = 14°$.

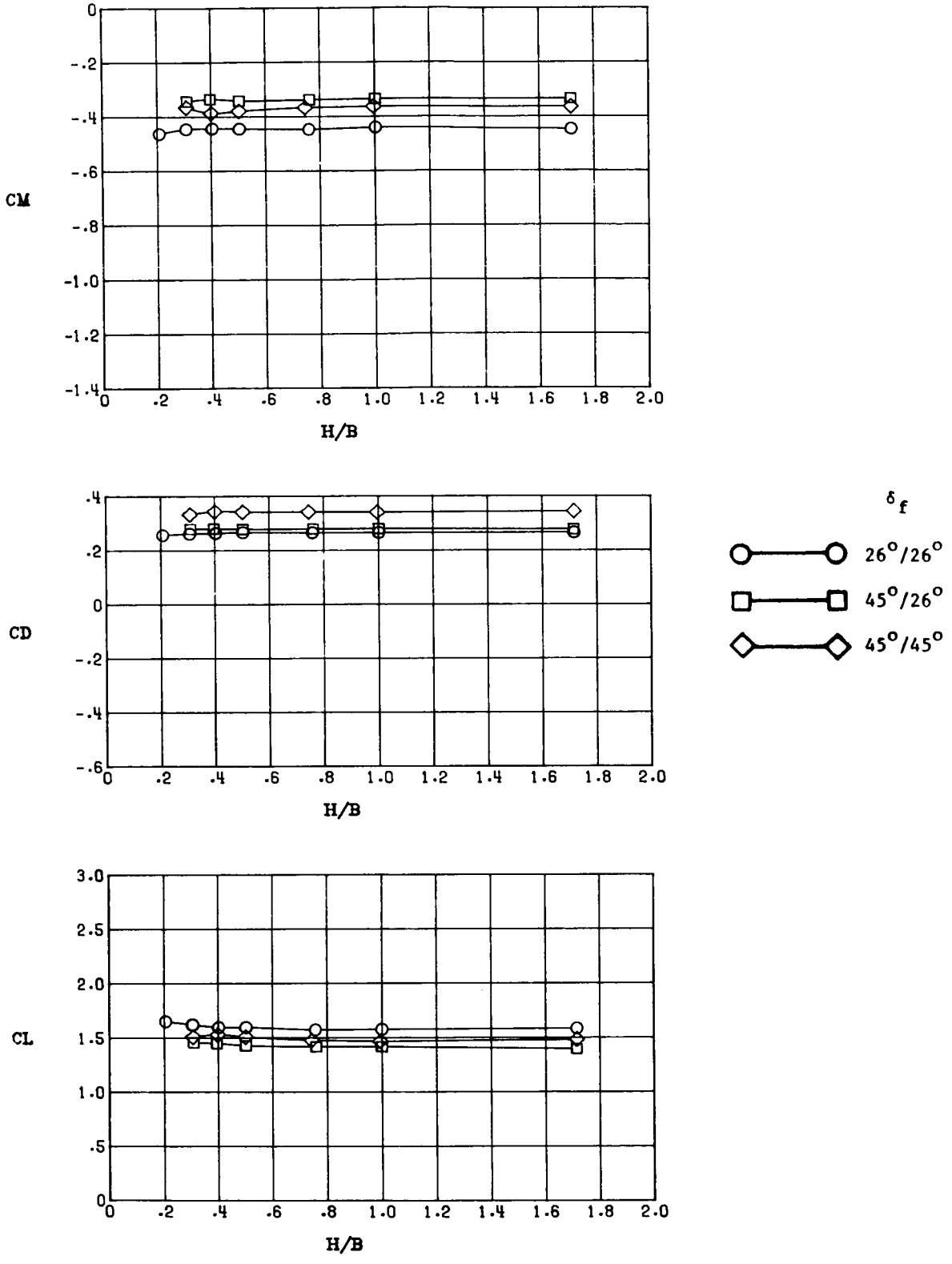

Figure 65.- Effect of flap deflection angle on longitudinal aerodynamic characteristics at various model heights with $C_\mu = 0.19$, $\Lambda_C = 60°$, and $\alpha = 14°$.

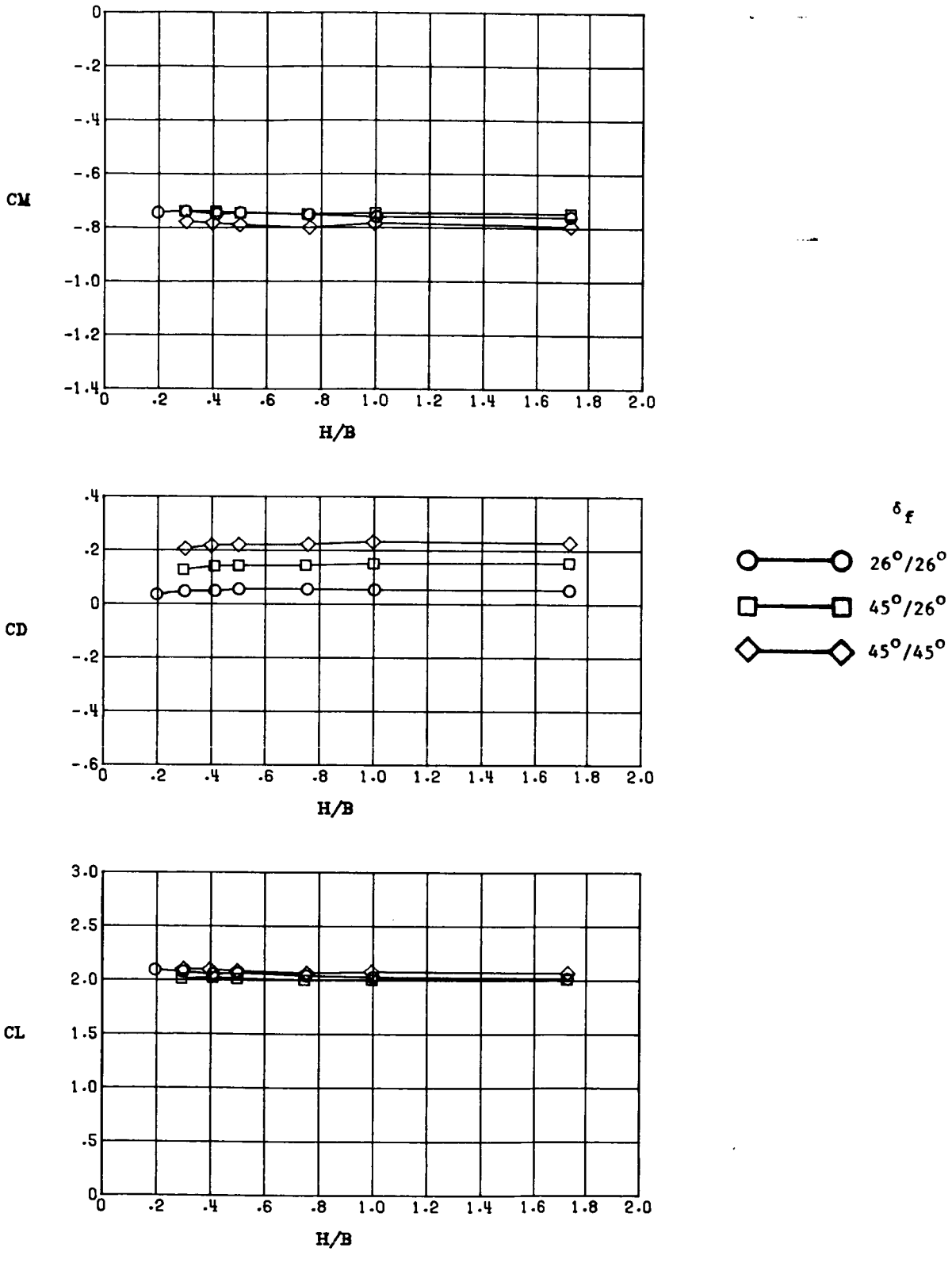

Figure 66.- Effect of flap deflection angle on longitudinal aerodynamic characteristics at various model heights with $C_\mu = 0.60$, $\Lambda_C = 60°$, and $\alpha = 14°$.

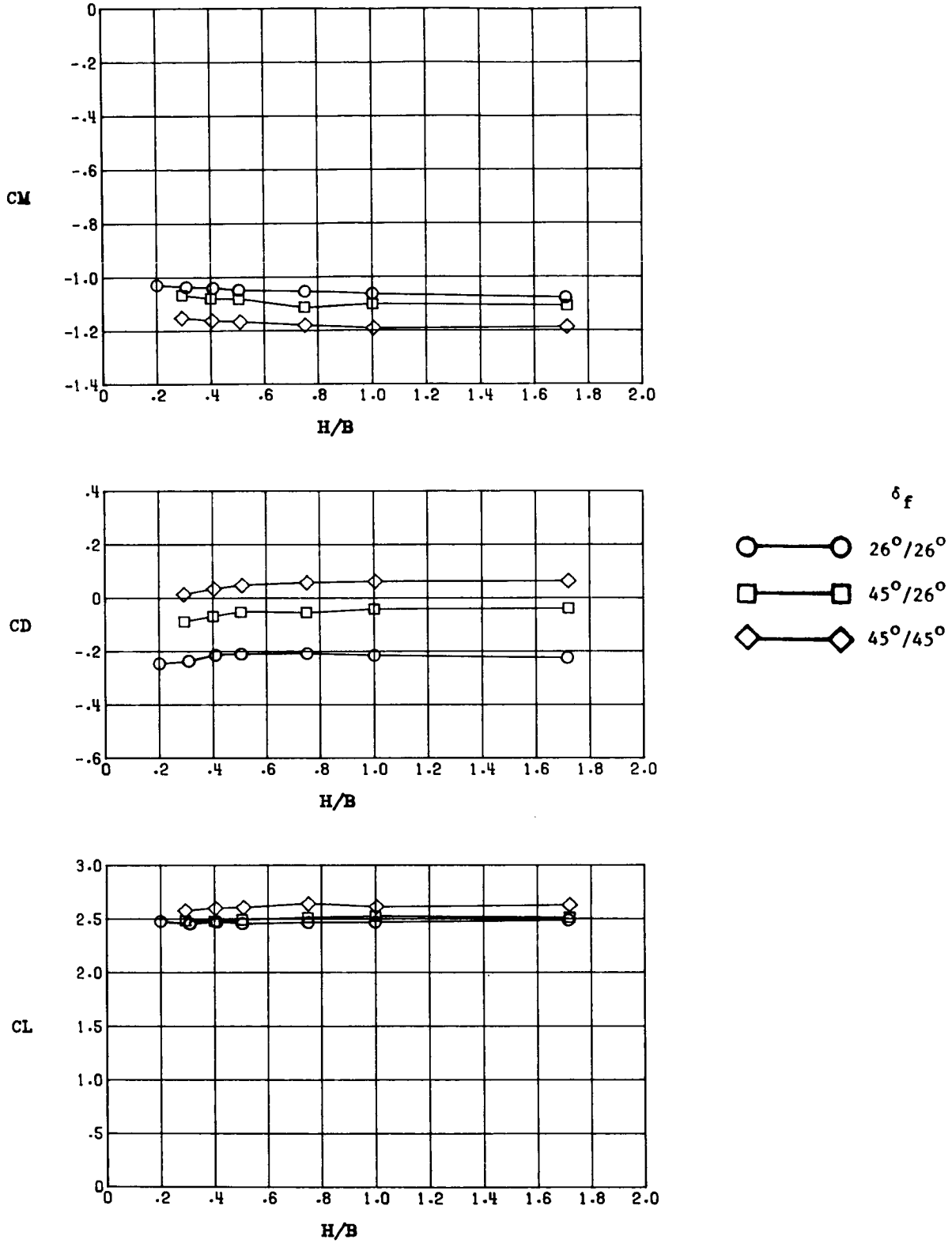

Figure 67.- Effect of flap deflection angle on longitudinal aerodynamic characteristics at various model heights with C_{μ} = 1.07, Λ_C = 60°, and α = 14°.

Standard Bibliographic Page

1. Report No.	2. Government Accession No.	3. Recipient's Catalog No.
NASA TM-89020		

4. Title and Subtitle	5. Report Date
Low-Speed Aerodynamic Characteristics of a Wing-Canard Configuration With Underwing Spanwise Blowing on the Trailing-Edge Flap System	January 1987
	6. Performing Organization Code: 505-61-71-02
7. Author(s): Daniel W. Banks and John W. Paulson, Jr.	8. Performing Organization Report No.: L-16161
9. Performing Organization Name and Address: NASA Langley Research Center, Hampton, VA 23665-5225	10. Work Unit No.
	11. Contract or Grant No.
12. Sponsoring Agency Name and Address: National Aeronautics and Space Administration, Washington, DC 20546-0001	13. Type of Report and Period Covered: Technical Memorandum
	14. Sponsoring Agency Code

15. Supplementary Notes

16. Abstract

An investigation of the effects of spanwise blowing applied to the lower surface of a trailing-edge flap system on a wing-canard configuration has been conducted in the Langley 4- by 7-Meter Tunnel. The investigation studied spanwise-blowing angles of 30°, 45°, and 60° measured from a perpendicular to the body center-line. The test conditions covered a range of free-stream dynamic pressures up to 50 psf for thrust coefficients up to 2.1 over a range of angles of attack from -2° to 26°. Model height above the wind tunnel floor was varied from a height-to-span ratio of 1.70 down to 0.20 (a representative wheel touchdown height). The results indicate that blowing angles of 30° and 45° increase the induced-lift increment produced by spanwise blowing on the lower surface of a trailing-edge flap system. Increasing the blowing angle to 60°, in general, produces little further improvement.

17. Key Words (Suggested by Authors(s))	18. Distribution Statement
Trailing-edge spanwise blowing Advanced wing-canard aircraft Cascade nozzle Thrust-induced aerodynamics Short take-off and landing	Unclassified - Unlimited Subject Category 02

19. Security Classif.(of this report)	20. Security Classif.(of this page)	21. No. of Pages	22. Price
Unclassified	Unclassified	113	A06

For sale by the National Technical Information Service, Springfield, Virginia 22161